INFN-LNL-220 (2007)

SPES

Advanced Exotic Ion Beam Facility at LNL

Technical Design

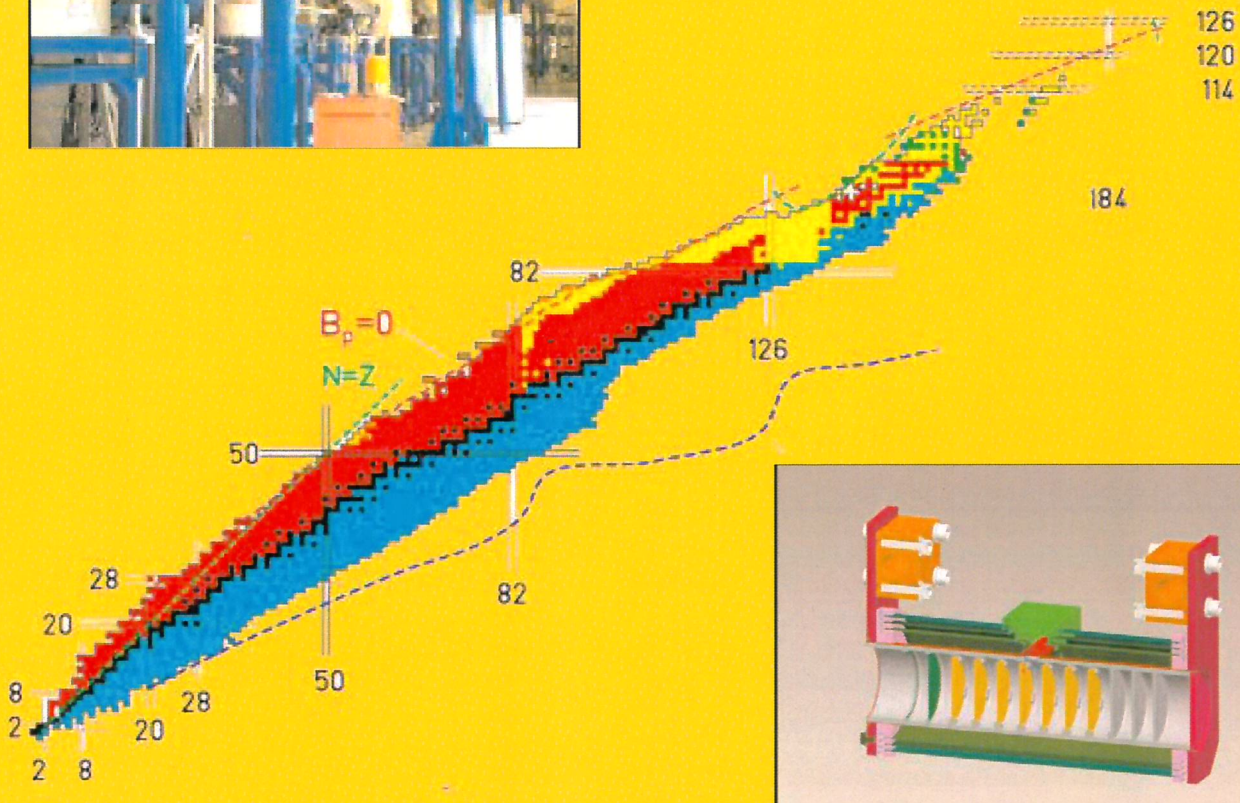

Editor Gianfranco Prete
Laboratori Nazionali di Legnaro

INFN-LNL-220(2007)

Istituto Nazionale di Fisica Nucleare
Laboratori Nazionali di Legnaro

SPES

Advanced Exotic Ion Beam Facility at LNL

Technical Design

Viale dell'Universitá, 2 - 35020 Legnaro (Pd) - Italia
phone: (+39)0498068311 Fax: (+39)049641925
http;//www.lnl.infn.it

Istituto Nazionale di Fisica Nucleare

Laboratori Nazionali di Legnaro

SPES

Advanced Exotic Ion Beam Facility at LNL

Technical Design

LNL Director: Gabriele Puglierin

LNS Director: Marcello Lattuada

Editor: Gianfranco Prete

Assistants to the editor: Anna D'Este
Paolo Schiavon

SPES

Technical Design for an Advanced Exotic Ion Beam Facility at LNL

Revised July, 2007

Editor: G. Prete

INFN-LNL-220 (2007)

Index

FOREWORD

SPES is an INFN project to develop a Radioactive Beam facility as an intermediate step toward EURISOL. The Laboratori Nazionali di Legnaro (LNL) was chosen as the site for the facility construction.

The LNL capability to play a role in this research field is related to the presence of the superconducting linac ALPI, able to re-accelerate exotic ions at 8÷13 MeV/u, the well consolidated know-how in linac construction, the existing detectors and the related know-how.

Moreover, the necessary real estate is available thanks to the extension of the Laboratory site (more than a factor two in area respect to actual size). Primary services and new infrastructures, like a 40 MW power station, are currently under implementation.

Here is outlined a revised form of the SPES project, already presented in the report LNL-INFN (REP)181/02 - June 2002. The major difference respect to the old project is related to the target concept that was changed from a Two Step to a Direct Target without changing the basic goal to have an ISOL facility for neutron-rich beams of fission fragments with a fission rate in the target of 10^{13} fissions per second.

This report comes after one year of R&D on the direct target concept which allowed verifying the feasibility of the target itself.

The new configuration reduces the complexity of the target structure and primary accelerator significantly. To produce a fission rate of 10^{13} fissions per second, the minimum requirements for the driver accelerator is to deliver a proton beam of 40 MeV energy and 0.2 mA current on a target of UCx (production target) made by 7 disks, each of 1 mm thickness and 4 cm diameter. These kinds of requirements for the proton driver accelerator could be met by commercial cyclotron accelerators but in this case no further improvement in the proton power beam is possible, nevertheless this solution will be taken into account for the final decision according to beam characteristics and cost. In this report we propose the use of a Linac accelerator to guarantee a future upgrade of the proton driver in energy and current. The proton driver is divided in two sections: the high current RFQ and the high energy DTL. It will supply a low energy proton beam of 5MeV with a current of 30 mA CW and 2 pulsed proton beams at 40 MeV, each one with a mean current of 0.3 mA and a repetition rate of 25Hz (or one beam at 50Hz).

This configuration allows a variety of solutions: two targets, both for radioactive beams or one for radioactive beam and the other for applied physics, can be operated at the same time; and the high current section allows the development of a neutron beam for medical applications and material studies.

The total amount of UCx requested in this project for the radioactive beam production is in the order of 30g. The specific power released by the proton beam in the target is 140W/gr a power density similar to that of HRIBF, the ISOL facility at Oak Ridge National Laboratory (USA).

INFN gains the expertise to operate an ISOL facility with the EXCYT project at LNS, where a direct target ISOL facility for the production of light exotic ions, based on the 500W ^{13}C beam of the CS superconductive cyclotron, is successfully operating at a primary beam power

density of 200-400 W/gr on a graphite target. The EXCYT expertise in designing and commissioning an ISOL facility will be a starting point for the SPES project.

The key feature of this new facility is to provide high intensity and high-quality beams of neutron rich nuclei to perform forefront research in nuclear structure, reaction dynamics and interdisciplinary fields like medical, biological and material sciences.

The exotic isotopes will be reaccelerated by the ALPI superconducting linac at energies of 10AMeV for masses in the region of A=130 amu.

The possibility to increase the energy sensibly beyond this limit requires a different approach as the lattice of the ALPI laboratory is approaching its limit. A possible upgrade toward exotic beams at Fermi energies can be a second step which may involve the development of SPES, with the construction of a new re-accelerator and EXCYT with the installation of a new primary beam driver allowing using the CS as high energy re-accelerator. It is to be stressed that the two options are not alternative but rather complementary, as the two facilities are designed for different regions of radioactive beam masses.

Most of the experiments made with the existing first-generation facilities are limited by the poor beam intensity. A real breakthrough in the field will be possible only with facilities like SPES producing both one order of magnitude higher beam intensities and much more exotic ion species than presently available.

The research goal for SPES is the study of the many-body aspects of the structure of nuclei by addressing important questions regarding nuclei far from stability as one gets closer and closer to the neutron drip line.

The exotic beams produced by SPES will open up new possibilities for experimental studies of neutron-rich nuclei employing different reaction mechanisms such as Coulomb excitation, inelastic scattering, single-and multiple-nucleon transfer, fusion reactions, etc. Such reactions not only provide invaluable nuclear structure information but they also allow reaching nuclei even further away from the stability line. Beams of neutron-rich nuclei offer better chances to synthesize heavy elements because the fused system will be less neutron deficient, therefore closer to the valley of stability and with better chances to survive.

Additional questions are related to areas of astrophysics and of nucleosynthesis in supernovae and other stellar processes and to tests of symmetries. Facilities of this type will allow learning much more about the origin of the elements in the cosmos and the limits of nuclear stability.

The SPES project is of great interest not only for Nuclear Physics but also for a direct application of nuclear physics techniques in medicine and in material science.

It is part of the project the development of a neutron facility operated by the high intense 5 MeV proton beam which allows the production of neutrons using a proper converter based on a high power beryllium target.

By using the neutron beam, the SPES project will develop a Boron Neutron Capture Therapy facility for cancer treatment, with the aim to produce the first facility of this kind based on accelerators instead of reactors and opening the way to the use of BNCT in hospital site.

The neutron beam will be used to study the neutron cross sections actually needed to take advances in several fields like nuclear astrophysics, nuclear waste transmutation, generation IV reactors, fusion reactors, decommissioning of first generation fission reactors, radioprotection, dosimetry and material science.

The proton beam at high energy can be directly used for the production of new radio isotopes for internal radio immunotherapy, a technique at the frontier of nuclear medicine.

With the SPES proposal, it is intended to fulfil the INFN-Community expectations: to exploit their expertise and capability in the fields of accelerators, radiation detectors and related technologies; to maintain and extend their substantial community of users; to preserve and

increase their internationally recognised reputation in nuclear structure and reaction mechanisms studies; to offer a neutron site for fundamental and applied physics, for applications in astrophysics, condensed matter, radiobiology and radiotherapy and to contribute to the design and test of high intensity proton beam of interest for other INFN communities and Government commitments (ADS, IFMIF).

Gabriele Puglierin
Director LNL

Marcello Lattuada
Director LNS

CHAPTER I

PHYSICS CASE

1.1 Introduction

A very large knowledge on the world of the nuclei has been acquired in the last 30 years thanks to many researches both experimental and theoretical. The nuclide chart has been widely explored by means of a variety of reactions from fusion-evaporation to direct reactions, from deep-inelastic collisions to central explosive interactions at high energies. All of this has given us access to a rather detailed description of the properties of atomic nuclei.

At rather low bombarding energies, fusion reactions opened the study of nuclei at high excitation, of both thermal and collective type, up to the maximum values of angular momentum that the system can sustain. At such high excitations it has been possible to discover and study very particular nuclear shapes with special attention to their decay and the coupling with the low-energy modes and with the Giant Dipole Resonance. By means of fusion processes, moreover, it has been possible to push the study of proton-rich nuclei towards the p-rich side of the stability valley. A part from nuclear physics, also astrophysics benefited of this investigation because many stellar processes and nucleosynthesis are based on nuclear reactions involving systems far from normal 'beta-stability line'. Coming to higher bombarding energies, many experiments have been performed to look at the behaviour of nuclei when produced at temperatures close to the nucleon binding energies: strange decays of nuclei in many pieces (multifragmentation decays) have been observed and studied, thus one could explore the Nuclear Equation of State (NEOS) far from equilibrium conditions; exciting scenarios well known on a macroscopic scale and with aspects important for general physics, such as phase transitions and liquid-gas phase coexistence, have been suggested and perhaps discovered.

Notwithstanding the enormous quantity of studies, till now it is impossible to predict, for example, the limits of nuclear stability or the behaviour of the NEOS at low and high barion densities. The asymmetry term in the NEOS is largely unknown but in the region close to saturation; however it is just this energy which plays an important role in setting the stability limits. For this reason many studies started worldwide to better investigate the behaviour of nuclear matter far from stability. There are of course many activities which can and must be pursued by means of conventional stable beams; however this is not sufficient to push the knowledge in the very far regions of the nuclide chart especially towards the n-drip line. Therefore many laboratories started a game to equip themselves with modern accelerator complexes to produce energetic high quality exotic (i.e. unstable) ion beams and to develop new generation detector devices.

Since years LNL represents a cornerstone for this type of physics at an European level as demonstrated by many recent activities, collaborations and initiatives which are in progress therein. Therefore, LNL endeavoured to upgrade the design of the SPES machine to match the request of the community of nuclear physics, both Italian and European. In this respect, it is important to note that the completion of the facility can be achieved in a reasonable time, quite competitive with the other European efforts in the direction of exotic ion beams.

In the following paragraphs we present some key experiments chosen among the wide research field addressable with SPES and extensively discussed in previous reports.

1.2 Spectroscopy of neutron rich nuclei

One of the most critical ingredient in determining the properties of a nucleus from a given effective interaction, is the overall number of nucleons and the ratio N/Z of neutrons to protons. One aspect which is presently strongly discussed concerns the modification of the average field experienced by a single nucleon due to the changes in size and diffusivity for nuclei with strong neutron excess. For large neutron excess the softening of the Woods-Saxon shape of the neutron potential is expected to cause a reduction of the spin-orbit interaction and therefore a migration of the high-l orbitals with a large impact on the shell structure of nuclei far from stability [1-5].

A different scenario has been recently suggested where the evolution of the shell structure in going from stable to exotic nuclei can be related to the effect of the tensor part of the nucleon-nucleon interaction. The tensor-force, one of the most direct manifestation of the meson exchange origin of the nucleon-nucleon interaction, is responsible of the strong attraction between a proton and a neutron in the spin-flip partner orbits. A recent generalization of such mechanism foresees a similar behaviour also for orbitals with non identical orbital angular momenta. It is expected an attraction for orbitals with antiparallel spin configuration and a repulsion for orbitals with parallel spin configuration. In most of the cases one is dealing with a combined effect of the attraction among orbitals with antiparallel spins and repulsion between orbitals with parallel spins [6-8].

Those effects become particularly visible when moving away from the line of stability. In such cases the proton-neutron interaction is changed by empting of the partner orbit causing a modification into the effective single particle energies (evolution of the shell structure).

The change of the shell structure based on such mechanism has been recently discussed in different mass regions of the nuclear chart. In such contest neutron-rich nuclei close to shell gaps are particularly interesting since, when compared with the shell model prediction, they allow to search for anomalies into the shell structure. It is predicted, for example, that the Z=28 gap for protons in the pf-shell becomes smaller moving from ^{68}Ni to ^{78}Ni as consequence of the attraction between the proton $f_{5/2}$ and neutron $g_{9/2}$ orbits and the repulsion between the proton $f_{7/2}$ and the neutron $g_{9/2}$ configurations. The same argument also predicts a weakening of the N=50 shell gap when approaching the ^{78}Ni nucleus due to the attraction between the neutron $g_{9/2}$ and $d_{5/2}$ configurations with the proton $f_{5/2}$ state and the repulsion between the neutron $g_{7/2}$ with the proton $f_{5/2}$ state.

Properties inconsistent with shell closure have been found in several neutron-rich systems around shell-model magic numbers [9, 10].

In the last few years, the use of binary reactions, quasi-elastic, multinucleon transfer or deep inelastic scattering, combined with modern γ - ray arrays (GASP, Gammasphere, Euroball, etc.) with or without efficient ancillary detectors, has increased substantially the amount of information available on the structure of previously inaccessible nuclei far from stability. An example is the neutron-rich nucleus ^{68}Ni, where investigation of the structure have revealed the doubly-magic character of N=40 Z=28 subshell closure.

The neighbouring ^{71}Cu nucleus has also been investigated that way. The knowledge of the determined residual interactions has opened the way for shell model calculations for nuclei in the region around N=40 Z=28 [11].

Deep-inelastic collisions have also been used to access different neutron rich nuclear regions at medium and high spin [12-14]. The Sn isotopes with N=72, 74 and 76 have been reached, allowing the identification of the 10^+ isomeric states with $\nu h_{11/2}^n$ configuration. In the region of doubly-magic ^{208}Pb, the two body, neutron-neutron residual interaction and the neutron single particle energies have been determined from the structure of the ^{210}Pb and ^{209}Pb nuclei, also populated in the afore-mentioned collisions. The information extracted on this nuclei is very

important for the understanding of the states in nuclei with valence neutrons above the shell closure at N=126.

In nuclear systems with quadrupole deformation, the coherent addition of the excitations induced by multinucleon transfer or deep-inelastic processes (and by Coulomb excitation) populates high angular momentum states. Some examples of this phenomenon are revealed in studies of the rotational bands and the alignment of $\nu h_{11/2}$ pairs in the ^{100}Mo region, or the investigation of rotational structures in the neutron-rich Dy, Yb and Sm isotopes.

The use of high resolution large acceptance spectrometer coupled to anti-Compton γ-ray detector array has marked a step forward with respect to the previous spectroscopy studies with deep inelastic or multinucleon transfer reactions. Examples are the PRISMA spectrometer of the LNL coupled to the CLARA detector array and the VAMOS spectrometer of GANIL coupled to the Exogam detector. They provide, for most of the reaction products, the full identification of mass and Z. This makes available information from reaction products of very low cross section and thus allows measurements on nuclei further away from stability.

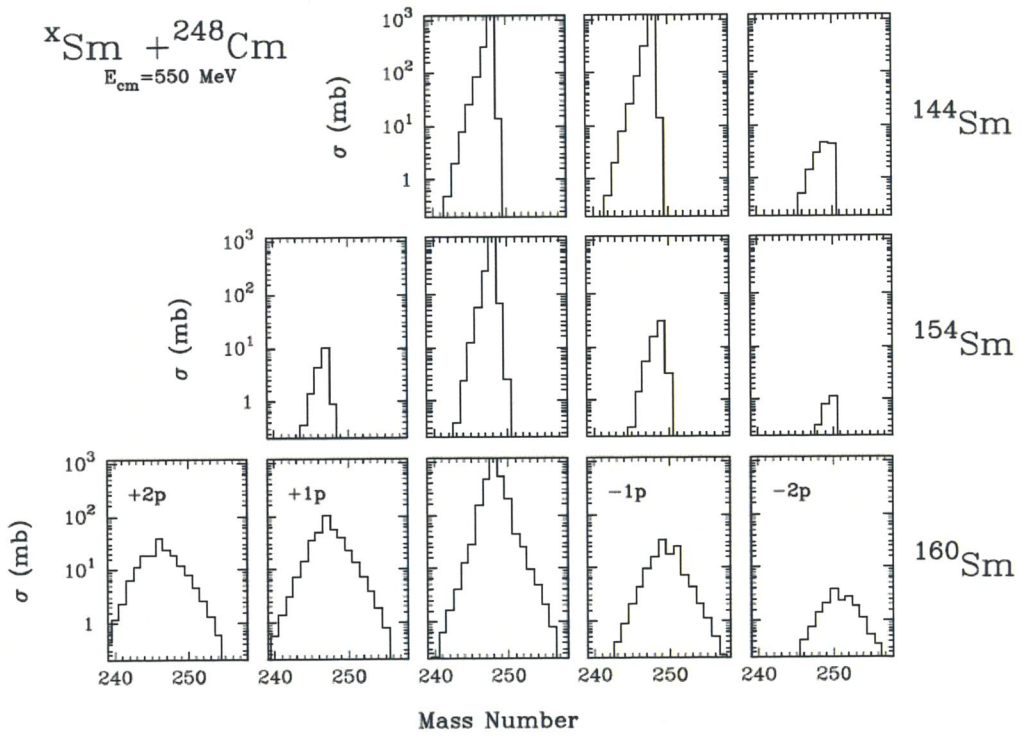

Fig. 2.1: *Coupled channel calculations performed with the program GRAZING. The production of neutron rich channels is strongly increased by the use of neutron rich beams.*

Beams of neutron rich radioactive nuclear beams of sufficient intensity offer the interesting possibility to further extend our knowledge of neutron rich nuclei.

Since, as already mentioned, the multinucleon flux moves from proton-stripping and neutron-pick up to vice-versa when going from proton-rich to neutron-rich beams, heavy neutron-rich projectiles can be used to populate the most exotic final products.

Figure 2.1 shows the production of neutron rich nuclei calculated using the program GRAZING [14a]. One should notice that the relative intensity of the neutron rich channels strongly increase when using an heavy neutron rich beam or a neutron rich radioactive nucleus.

Radioactive beams like ^{92}Kr, ^{94}Kr, ^{132}Sn and ^{134}Sn, when used with heavy targets like ^{208}Pb or ^{238}U, allow access to a range of neutron-rich nuclei of interest to address the following questions:

1. Study of the evolution or breakdown of shell gaps, resulting from the combined effects of the spin-isospin tensor interaction and of the density dependent terms of the nuclear force on single particle states. Of particular interest are the mass regions close to magic numbers far from stability like Z=28, N=50 or Z=50, N=82.
2. New region of deformation.
3. New nuclear symmetries (critical point symmetries, chirality). New critical point symmetries have been recently proposed and experimentally found. The new symmetries describe nuclei at the critical point respect to a shape/phase transition. Particularly interesting is here the N=90 mass region around Gd and Ce (X5 symmetry, spherical to prolate axial) as well as the ^{170}Er nucleus (Y5 symmetry, spherical to γ-soft). Chiral symmetry has also been suggested to be present in nuclear systems based on the energy degeneracy of the levels. A recent test of such symmetry based on the measurement of absolute transition matrix elements has shown that chirality does not appear in mass A=130. Of high interest is to check for existence of chirality in the A=106 mass region where almost complete energy degeneracy has been found.

1.3 Multiple particle transfer and sub-barrier fusion

Transfer reactions between heavy ions at Coulomb energies provide invaluable information for both nuclear structure and reaction dynamics studies. While from the stripping and pick-up of one neutron or proton one can deduce information about the shell structure of the two colliding nuclei, from the exchange of many nucleons one can study nuclear correlations, pairing in particular, in the nuclear medium. An important and highly debated item in the field of nuclear reactions, which is receiving new impulse in view of the future availability of intense radioactive beams like those produced by SPES, is the interplay between single particle and pair (or even cluster) transfer modes.

Extensive work, done in the past, with *(p,t)* and *(t,p)* reactions [15] stressed the ability of nucleons to correlate in pairs thus leading to the construction of the pairing vibrational and pairing rotational models correlating the spectra of neighboring nuclei. Later on, studies of inclusive cross sections for the transfer of one and two nucleon pairs in heavy ion collisions [16] suggested the presence of large enhancement and possibly the onset of a nuclear Josephson effect due to the coherence of the superconducting states involved in the transition [17].

More recently, several systems have been studied at LNL [18] and detailed experimental mass and nuclear charge yields were obtained together with angular and total kinetic energy loss distributions that allowed a good comparison with state-of-art theoretical models. In particular, interesting results were obtained for the ^{40}Ca+^{208}Pb system [19], where data have been compared with semi-classical models [20,21] where the surface modes of target and projectile, and the transfer channels are treated on the same footing. The transfer channels include the one- and pair-transfer modes (stripping and pick-up), and the multi-nucleon transfer that is treated in the sequential approximation of the fundamental modes.

Interesting hints for the possibility to observe multi pair-phonon excitations are coming from recent investigations on the ^{40}Ca+^{208}Pb [22], ^{40}Ca+^{96}Zr and ^{90}Zr+^{208}Pb [23-25] reactions where γ-particle coincidences have been performed with PRISMA+CLARA, which allowed the observation of weak γ decays from high-lying 0^+ states in ^{42}Ca in the excitation energy region expected for pairing vibrations.

It is very important to investigate the correlation properties far away from the stability, especially on the neutron rich side, since in this region the correlations, in particular the one due to the pairing interaction, should play a dominant role in defining the properties of these nuclei. A key point, yet unexplored, is whether transfer processes involving neutron-rich nuclei can lead to the onset of super-currents with very large number of neutrons transferred among the colliding nuclei. These super-currents, driven by the exchange of pairs, should allow an easy identification of the pair-modes, and they should alter in a very significant way the imaginary part of the optical potential with a polarization component that should be repulsive. The use of nuclei with an extended neutron distribution should allow to study in detail the density dependence of the pairing force, as well as to disentangle the role of the coupling to the continuum in the dissipation of energy and angular momentum, and in the formation of the compound nucleus (fusion). These effects are likely to be seen in the behavior of the yield distributions of the different multi-nucleon transfer channels as well as in the enhanced population of selected states with specific structure that reflect the transfer of correlated pairs. At variance with what happens with stable beams where the main transfer flux is along the pick-up of neutrons and stripping of protons, with radioactive beams one can populate nuclei along both the *pick-up and stripping of protons and neutrons* [26]. In this way not only the *(nn) and (pp)* correlations but also the (*np*) correlations can be studied at the same time looking at the population pattern of specific final states reached via addition and removal of pair-phonons. In Fig. 3.1 we show predicted cross sections in the reaction ^{44}Ar+^{208}Pb, from which one observes the "symmetric" population of transfer products [26].

Using the heavy neutron-rich beams, which will be provided by SPES, the reactions of ^{132}Sn beam on the ^{40,48}Ca,^{58}Ni, ^{90}Zr, and ^{112}Sn targets at energies close to the Coulomb barrier can be studied. In these reactions one aims at measuring the cross sections of different transfer channels, as well as the final state strength distribution. Studies should also be performed at sub-barrier energies [27,28], where only the tail of the wave functions enter into play and thus they should be of simpler analysis. To give a hint of why it is so, we recall that the nuclear part of the inelastic form factor is well described by the derivative of the optical potential and thus has a decay length of about half (~ 0.65 fm) of that of the transfer form factors (~ 1.3 fm). In this way, at sub-barrier energies the two ions probe their densities only at large distances. Here the nuclear couplings are dominated by transfer processes and the multi-nucleon transfer proceeds via a sequential mechanism.

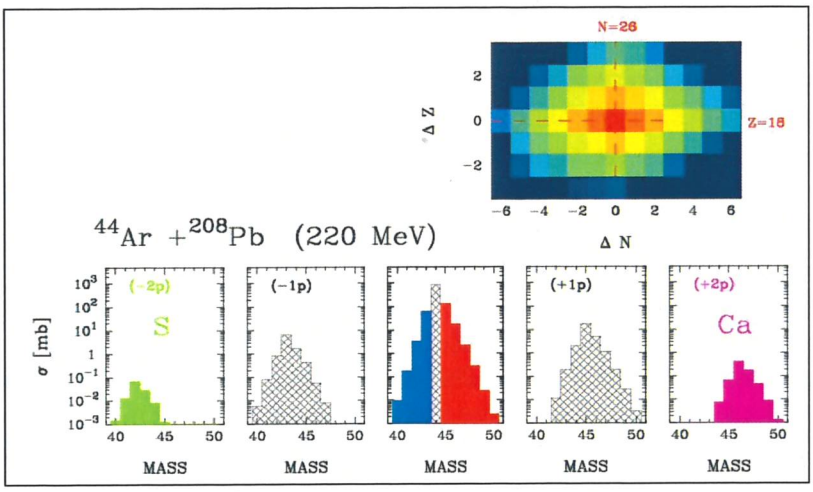

***Fig. 3.1**: Total cross sections for the indicated reaction calculated with the code GRAZING. ΔN and ΔZ represent the number of transferred neutrons and protons, respectively.*

The investigation of the transfer channels with very neutron rich beams may be also very useful to elucidate the role played by these different degrees of freedom in the fusion process. It has been shown that with stable beams fusion is generally dominated by strong couplings to nuclear shape vibrations and deformations [29] but the role of the nucleon transfer degrees of freedom has not been clarified yet. Fig. 3.2 shows the measured fusion cross sections [30] and the corresponding barrier distributions for the three cases $^{40}Ca + ^{90,94,96}Zr$, in a reduced energy scale. One notices the much faster decrease of the $^{40}Ca + ^{90}Zr$ cross sections below the barrier with respect to the other two systems, and the progressively wider and structureless barrier distribution when going from ^{90}Zr to ^{96}Zr. Whether these trends are due to the low-energy structure of the target isotopes (quadrupole and octupole vibrations) and/or to neutron transfer couplings, is a matter of current discussion.

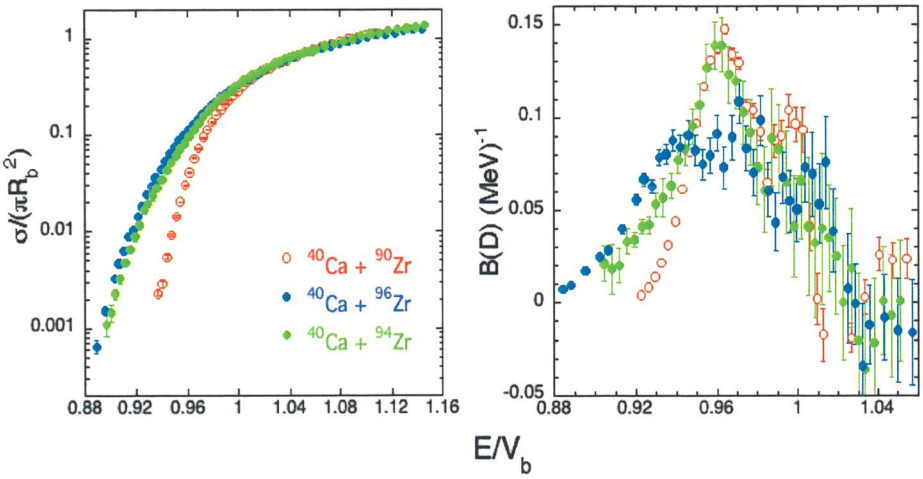

Fig. 3.2: *(left) Fusion excitation functions of the three systems $^{40}Ca + ^{90,94,96}Zr$, and (right) extracted barrier distributions. See text.*

In order to give just some examples, very neutron-rich RIB of $^{132\text{-}134}Sn$, $^{126,128}Cd$ might fruitfully be used on $^{40,44,48}Ca$ targets to measure fusion cross sections near and below the barrier, with the purpose of clarifying the situation, even if barrier distributions will be difficult to extract. In such cases the large neutron excess of the beam leads to huge and positive ground state Q-values for few- and multi-neutron transfer. These studies of near- and sub-barrier fusion reactions using the exotic beams from SPES will require the development of a new dedicated set-up with higher efficiency and background rejection capabilities than is available now at LNL.

At very low energies, fusion excitation functions usually show an exponential decrease [31]. For several systems, however, a different behaviour (called a "hindrance" effect) was found in recent years [32,33]. It was suggested [34] that fusion cross sections are sensible, at far subbarrier energies, to the nuclear potential in the inner side of the Coulomb barrier, in particular to a repulsive core [35] of the nuclear potential arising from nuclear incompressibility K. A good fit was obtained for $^{64}Ni + ^{64}Ni$ [35] using K=228 MeV, that is, the value extracted for cold nuclear matter in the "soft" equation of state [36]. Since K depends on the neutron excess, one expects the low-energy behaviour of the fusion excitation functions to be different in systems involving large number of neutrons especially near the nuclear surface. This would be very interesting to investigate with reactions like, e.g., $^{132,134}Sn$ beams on ^{48}Ca or ^{64}Ni.

1.4 Dynamics and Thermodynamics of exotic nuclear systems

Experiments performed with stable beams have produced hot nuclear systems and their decay modes have been extensively investigated. From the properties of the emitted particles (energy spectra, isotopic yields, multiplicity), information about the excitation energy and the temperature of these hot systems has been extracted [37] giving access to a detailed study of the evolution of NEOS up to non-equilibrium conditions. In particular, studies of the isospin degree of freedom in nuclear matter have already started in Italy at LNS with the CHIMERA detector and at LNL with the GARFIELD and 8πLP apparatuses. Important contributions of Italian groups has been also obtained from collaborations at GSI, at GANIL and at MSU, in particular in the study of the liquid-gas phase transition.
The n-rich ion beams of SPES will allow to further extend the investigation of the NEOS along the isospin coordinate, in a region where the it is largely unknown even at low excitation. In the following we focalize the discussion on two main topics that should be effectively investigated with the availability of the SPES beams.

1.4.1 Limiting temperatures in hot N/Z asymmetric nuclear systems

Theoretical calculations have predicted and experiments have observed the existence of a *limiting temperature*, T_{lim} [38-46]. Below this temperature, the nuclear system can be described as a nuclear drop evaporating light particles, whereas above T_{lim}, the thermodynamically equilibrated nuclear drop cannot survive anymore and breaks up.
From a theoretical standpoint, calculations based on Skyrme-type nucleon-nucleon interactions and other parameterizations have predicted mass-dependent limiting temperatures [41, 43, 44], with heavier nuclear systems being characterized by a lower T_{lim} value. Such A-dependence of T_{lim} is predicted to provide important information about the critical temperature, T_C, of infinite nuclear matter and about the isoscalar part of the nucleon-nucleon effective interaction [41, 43, 44]. Experimentally, a systematic study of limiting temperatures has been performed by J. Natowitz et al. [47]. By collecting all the available data on nuclear caloric curves (i.e. the correlation between measurements of excitation energy and temperature), a decreasing limiting temperature with increasing mass of the hot nuclear system has been experimentally observed. The mass-scaling of T_{lim} has been associated to an effect of Coulomb instabilities becoming more and more important as the number of protons is increased [47]. These studies were performed with stable beams leading to the production of hot nuclear systems with small N/Z asymmetries. Systems close to the stability line are characterized by high limiting temperatures (T_{lim}~6-9 MeV) [47,48]. However, theoretical calculations predict that T_{lim} decreases significantly as one moves away from stability. The authors of Refs. [39, 48] have mapped T_{lim} as a function of N and Z, predicting that very N/Z asymmetric nuclear systems are expected to be characterized by a significantly lower limiting temperature. The attenuation of T_{lim} away from stability is predicted to be induced by a combined effect of Coulomb instabilities and the symmetry energy [39, 48]. These predictions suggest that it will be possible to achieve and explore the limiting temperature regime of exotic nuclei with large N/Z asymmetries even at the relatively low incident energies available with SPES. By populating compound nuclei with the same mass number, A, and different N/Z asymmetries, the effects of the symmetry energy is enhanced as one moves towards more neutron rich species, on the other hand the effects of the Coulomb instabilities are evidenced approaching the proton-rich side of the nuclear chart.
A list of key projectile/target combination populating medium mass systems should be:
^{64}Ni +^{78}Zn, ^{94}Kr +^{50}Ti, ^{96}Sr + ^{48}Ca, ^{72}Kr + ^{50}Ti. A similar list for heavier masses should include the reactions: $^{114\text{-}145}$Xe +^{40,48}Ca, ^{122}Cd + ^{58}Ni and ^{90}Kr + ^{90}Zr.

With these reactions one can produce chains of isotopes as compound nuclei all with the same Z and different mass number A. Furthermore, reactions such as ^{72}Kr,^{78}Kr + ^{28}Si and ^{74}Zn, ^{80}Zn + ^{26}Mg allow to produce compound nuclei with the same mass but with different Z-values. This is particularly useful to isolate mass and isospin effects in limiting temperature measurements [47].

1.4.2 N/Z dependence of nuclear level densities

The density of nuclear levels is a fundamental quantity in nuclear physics which plays an essential role in understanding compound nuclear reactions. It is also a basic ingredient for the determination of thermonuclear rates for astrophysics, with applications both in nucleosynthesis and supernovae dynamics [49,50]. While the level density around the Fermi surface depends critically on nuclear structure details [51], at higher energy it can be effectively parameterized via a mass (A), isospin (T_3=(N-Z)/2) and temperature (T) dependent level density parameter a(A,T_3,T) and possibly a backshift Δ accounting for pairing effects [52, 53]. Recently, it has been shown [54] that an isospin dependence of the level density from the quantity (Z-Zo), where Zo is the atomic number of the beta stable isotope with the same mass, should be more adequate at least for low excitation energies. Furthermore, the variation with temperature of the effective nucleon mass *m**, which is responsible for the level density parameter variation, contribute also to the change of the symmetry energy term in the nuclear binding energy through the dependence on the isospin component: $E_{sym}(T)=b_{sym}(T)\cdot 4.T_3^2/A$.
Variations of the nuclear symmetry energy affects the rate of electron capture in a collapsing star, changing the energy of the supernova explosion. It has been shown in Ref. [49] that the dependence of the symmetry energy on the temperature would produce a gain in the explosion energy of the order of ΔE_k~0.5-0.7 x10^{51} erg, value comparable to the explosion energy itself (E_k~1.5 x10^{51} erg for the case of the SN1987 supernova). Therefore, the experimental confirmation of this isospin effect would be of great interest in the astrophysical context.

On the basis of the statistical model, the effect of the isospin term on particle evaporation is expected to be relevant in the first steps of the de-excitation chain, where the nuclei involved are relatively far from the stability valley. Therefore, decay channels involving a small number of particles are more effective for this study. This also provides a stringent test of the statistical model, the decay not being integrated on many decay steps. As far as the symmetry energy in concerned, it affects the binding energy of particles involved in the evaporative process, the correction term reaching values up to ~ 10 MeV for temperature T~1 MeV [49], for the most neutron-rich nuclei. Owing to these predictions, the best condition to observe these effects is to produce composite systems at relatively low excitation energy (~20 MeV).

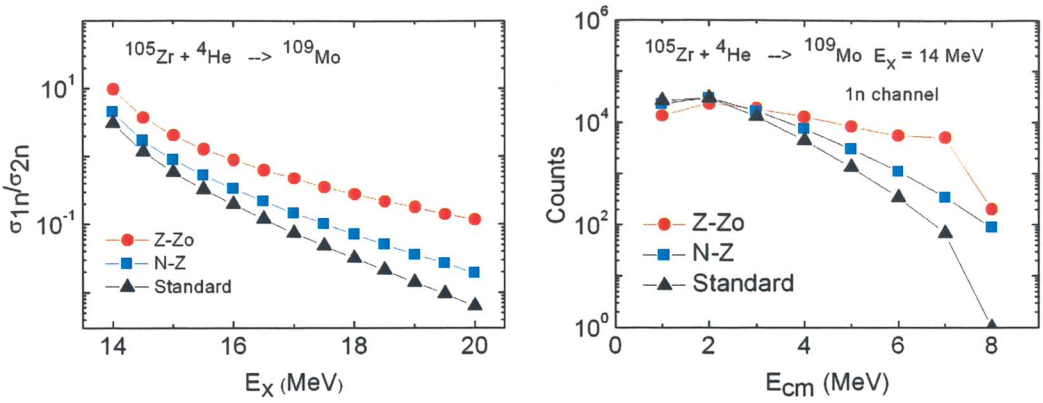

Fig. 4.1: *(left) Ratio between 1n and 2n channel cross sections for the composite system ^{109}Mo as a function of the excitation energy; (right) neutron energy spectra in the c.m. system for the 1n channel, for the same nucleus at E_x=14 MeV. Calculations have been carried out by Lilita_N97 code: i) including in the level density the (Z-Zo) (circles) and (N-Z) dependence (square); ii) using standard parameters (triangles). Lines are drawn to guide the eye.*

In order to evaluate these effects, statistical model calculations using the code Lilita_N97 have been carried out , for neutron-rich Mo isotopes, whose study is relevant, as they represent an important fraction of the chemical composition of the crust of a collapsing star .
In Fig. 4.1 (left) the calculated ratio between 1n and 2n channel cross sections is shown as a function of the excitation energy for the ^{109}Mo, taking into account for the Z-Zo and N-Z dependence in the level density. The standard (i.e. isospin-independent) calculation is also reported for comparison. The corresponding neutron spectra at E_x=14 MeV are reported in Fig.4.1 (right). Significant effects are observed. Furthermore, the xn channels for this system are predicted to be strongly affected also by the symmetry energy. These results indicate that the evaporative neutrons are a powerful tool for such a study. This composite system could be formed in the reaction ^{105}Zr + ^{4}He at E_{lab}=192-330 MeV. These reactions meet the conditions of providing a high fusion cross section with low excitation energy (15-30 MeV) of the composite systems. Furthermore, the relatively low angular momenta and excitation energies involved in these reactions are expected to enhance the effects of the isospin on the level density.
Studies of Mo nuclei at higher excitation energies (50-100 MeV) could be carried out with reactions on heavier targets as for example the ^{98}Kr + ^{12}C → ^{110}Mo. As a general behaviour, also for this reaction the statistical model predicts significant effects on the evaporation process.

---

[1] G.A. Lalazissis et al., Phys. Lett. B 418 (1998) 7.
[2] B. Blank, P.H. Regan, Nucl. Pohys. News Internat. 11 (1) (2001) 15.
[3] J. Dobaczewski et al., Phys. Scr. T56 (1995) 15.
[4] R.C. Nayak, Phys. Rev. C 60 (1999) 064305.
[5] X. Campi et al., Nuclear Phys. A 251 (1975) 193.
[6] T. Otsuka et al., Phys. Rev. Lett. 11 (1964) 145
[7] T. Otsuka et al., Phys.Rev.Lett. 97, 162501 (2006).
[8] T. Otsuka et al., Phys.Rev.Lett. 95, 232502 (2005).
[9] H. Grawe, Springer Lect. Notes in Phys. 651 (2004) 33.
[10] A. Gadea et al., Eur. Phys. J. A20 (2004) 193.
[11] R. Broda, J.Phys.(London) G32, R151 (2006)
[12] Y.H. Zhang et al., Phys. Rev. C 70 (2004) 024301.
[13] G. de Angelis Nucl.Phys. A751, 533c (2005)
[14] G. de Angelis Progress in Particle and Nuclear Physics 3113 in press.
[15] D.R. Bes et al, Phys. Rep. 34(1977)1
[16] C.Y. Wu et al., Ann. Rev.Nucl.Part.Sci.40(1990)285

[17] M. Kleber and H. Schmidt, Z.Phys. 245(1971)68; H.Weiss, Phys.Rev.C19,834(1979)
[18] L. Corradi and G. Pollarolo, Nucl.Phys.News, Vol. 15, N.4 (2006)
[19] S. Szilner et al., Phys.Rev.C71(2005)044610
[20] A. Winther, Nucl. Phys. A572, 191 (1994); Nucl. Phys. A594, 203 (1995), Program GRAZING, htpp:/www.to.infn.it/~nanni/grazing
[21] E. Vigezzi and A. Winther, Ann.Phys. (N.Y.) 192 (1989) 432; D.R. Napoli et al., Nucl.Phys.A559(1993)443
[22] S. Szilner et al., Eur.Phys.J A21(2004)87
[23] *Fusion06 : International Conference on Reaction Mechanisms and Nuclear Structure at the Coulomb Barrier*, S.Servolo, Venezia (Italy), 19-23 March, 2006, AIP Conference Series Vol.853, Melville (New York), L.Corradi et al. eds.
[24] A.M. Stefanini et al., Proposta di esperimento PRISMA, LNL-INFN, (Rep)-120/97 (1997); Nucl.Phys. A701(2002)217c
[25] A. Gadea et al., Eur.Phys.J.A20(2004)193
[26] C.H. Dasso, G.Pollarolo and A.Winther, Phys.Rev.Lett.73(1994)1907
[27] R.R. Betts et al., Phys.Rev.Lett.59(1987)978
[28] R.B. Roberts et al., Phys.Rev.C47(1993)R1831
[29] M. Dasgupta et al., Annu.Rev.Nucl.Part.Sci., 48(1998)401
[30] A.M. Stefanini et al., Phys.Rev. C73 (2006) 034606
[31] C.Y. Wong, Phys.Rev.Lett. 31 (1973) 766
[32] C.L. Jiang et al., Phys.Rev.Lett. 89 (2001) 052701
[33] C.L. Jiang et al., Phys.Lett. B640 (2006) 18
[34] C.H. Dasso and G.Pollarolo, Phys.Rev. C68 (2003) 054604
[35] S. Misicu and H. Esbensen, Phys.Rev.Lett. 96 (2006) 112701
[36] W.D. Myers and W.J. Swiatecki, Phys.Rev. C57 (1998) 3020
[37] E. Suraud et al., Progr. Part. Nucl. Phys. 23, 357 (1989) and Refs. therein
[38] P. Bonche et al., Nucl. Phys. A427, 278 (1984)
[39] J. Besprosvany et al., Phys. Lett. B217 (1989)
[40] H.Q. Song et al., Phys. Rev. C47, 2001 (1993)
[41] H.Q. Song et al., Phys. Rev. C44, 2505 (1991)
[42] H.Q. Song et al., Phys. Rev. C49, 2924 (1994)
[43] Y. Zhang et al., Phys. Rev. C54, 1137 (1996)
[44] M. Baldo et al., Phys. Rev. C59, 682 (1999)
[45] J.N. De et al., Phys. Rev. C55, R1641 (1997)
[46] P. Wang et al., Nucl. Phys. A748 (2005)
[47] J. Natowitz et al., Phys. Rev. C65, 034618 (2002)
[48] Z. Li et al. Phys. Rev. C69, 034615 (2004)
[49] P. Donati et al., Phys. Rev. Lett. 72 2835 (1994)
[50] T. Rauscher et al., Phys. Rev. C 56, 1613 (1997)
[51] W.E. Ormand et al, Phys. Rev. C 40, 1510 (1989)
[52] W.E. Ormand, Phys. Rev. C 56, R1678 (1997)
[53] D. Bucurescu et al, J. Phys. G: Nucl. Part. Phys. 31 S1675 (2005)
[54] S.I. Al-Quraishi et al., Phys. Rev. C 63, 065803 (2001)

CHAPTER II

FACILITY CONCEPT AND OVERVIEW

The main goal of the proposed facility is to provide an accelerator system to perform forefront research in nuclear physics by studying nuclei far from stability. The SPES project is concentrating on the production of neutron-rich radioactive nuclei with mass in the range 80-160.. The emphasis to neutron-rich isotopes is justified by the fact that this vast territory has been little explored, at exceptions of some decay and in-beam spectroscopy following fission. Therefore, reactions in inverse kinematics will allow a new class of data to be obtained.

The high proton current produced by the TRASCO injector is useful for the development of a Neutron Facility with two main applications: the development of a Boron Neutron Capture Therapy (BNCT) installation to perform research in the treatment of cancer and an irradiation-Time Of Flight facility (LENOS) for material research and cross section measurements

The feasibility of the SPES project has been positively analyzed both from the point of view of the production target and of the proton driver.

The most critical element of the SPES project is the Direct Target. Up to day the proposed target represent an innovation in term of capability to sustain the primary beam power. The design is carefully oriented to optimise the radiative cooling taking advantage of the high operating temperature of 2000°C.

An extensive simulation of the target behaviour has been performed to characterize the thermal properties and the release process. Experimental work to bench mark the simulations was carried out at HRIBF, the Oak Ridge National Laboratory ISOL facility (USA).

The design of the proton driver will take advantage from the TRASCO project using the high current proton source TRIPS, developed at LNS and transferred at LNL where it is now in operation, and the RFQ able to deliver a proton beam of 30mA 5MeV.

The high energy part of the driver will follow the design of the Drift Tube Linac (DTL) under construction for the Linac4 project at CERN.

The low energy, high current proton beam will be used to feed the Neutron Facility devoted to the Boron Neutron Capture Therapy (BNCT) and to produce a neutron beam for cross section measurement of astrophysical interest and material irradiation (LENOS).

The high energy DTL will be designed with the aim to extend its capability to produce a 50Hz pulsed proton beam up to 1 mA and100 MeV. A switching system will allow the operation of two beams with a repetition rate of 25Hz each.

The production target will be designed following the ISOLDE and EXCYT projects and special care will be devoted to the safety and radioprotection of the system. According to the estimated level of activation in the production target area of 10^{13} Bq a special infrastructure will be designed. The use of up-to-date techniques of nuclear engineering will result in a high security level of the installation. The radiation management and the control system will be integrated and redundancies will be adopted in the design.

The isotopes will be extracted and ionized at +1 with a source directly connected with the production target. Several kinds of sources will be used according to the beam of interest. A laser source will be implemented in collaboration with INFN-Pavia with the aim to produce a beam as pure as possible.

The selection and the transport of the exotic beam at low energy and low intensity is a challenging task. Techniques applied for the EXCYT beam will be of reference for the beam diagnostic and an online identification station will be part of the diagnostic system.

To optimize the reacceleration, a Charge Breeder will be developed to increase the charge state to +N before to inject the exotic beam in the Bunching RFQ and PIAVE Superconductive RFQ which represents the first re-acceleration stage before the injection in ALPI.

The expected beam on experimental target will have a rate on the order of 10^8-10^9 pps for ^{132}Sn, ^{90}Kr, ^{94}Kr and 10^7-10^8 pps for ^{134}Sn, ^{95}Kr with energies of 9-13 MeV/u.
The SPES lay-out is shown in fig.3.1.

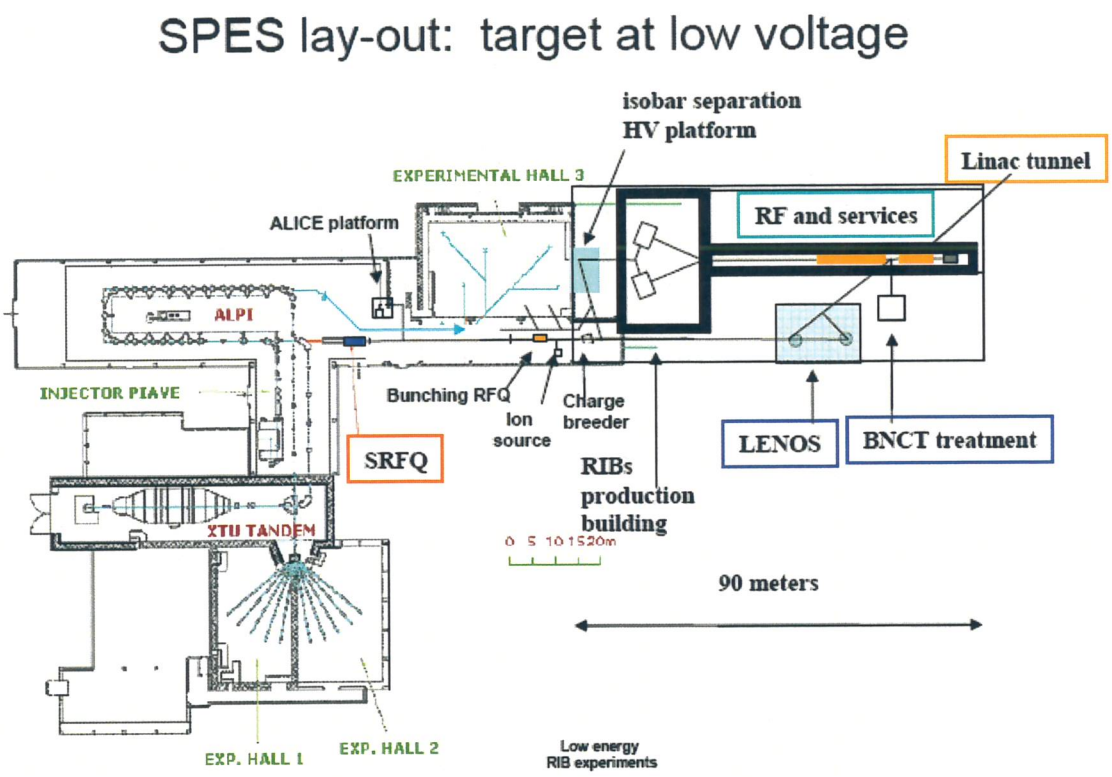

***Fig. 2.1** SPES lay-out.*

The final lay out of the facility will be defined after a detailed analysis of risk and safety aspects. The study will be carried out by nuclear engineering company with the support of ENEA and Politecnico di Milano. According to the results of these studies some aspects of the lay out can be upgraded.

CHAPTER III

PERFORMANCES

3.1 Exotic beam production by Direct Target

The evaluation of the in target Yield for physics experiment at SPES has been determined starting from the production yield (fission fragment distribution), which was calculated mainly through a Monte Carlo simulation based on transportation model MCNPX [1]. This simulation allows a detailed 3D definition of the system to be analysed and a full transport calculation starting from the proton distribution [3]. The proton fission cross-section, is obtained from the experimental data and from the MCNPX calculations using the Bertini model [2], and benchmarked with others models (CEM2k, ISALBEL). The target is designed with the aim to reach a fission rate of about 10^{13} fission/s, considering this number a challenge.

As far as the final beam current is considered, a very crucial point is linked to short-life time of radioactive isotopes which are produced in the target: the target plus ion source system have to be built considering with a great care the properties related to the release and the efficiency of the system.

The important step for a radioactive beam is the overall efficiency of the target-source system plus the efficiency linked to the post-accelerator configuration: the evaluation of the intensity of some radioactive beam species, interesting for the nuclear physics community, has been performed and validated through the existing experimental data.

The production yields in the present design of the facility, together with the evaluation of the final beam current on target, have been compared with that one predicted in the case of a double step target, which was considered in the previous configuration of SPES [4].

The intensity I of an exotic beam available for an experiment is determined by the following factors:,

$$I = \Phi \cdot N \cdot \sigma \cdot E_r \cdot Ei \cdot E_s \cdot E_t \cdot E_p$$

σ: is the cross section of the production reaction,
Φ: the primary beam intensity;
N: the thickness of the production target,
E_r the efficiency of release of the target and transfer
E_i the efficiency of ion source,
E_s the efficiency of the separator,
E_t the delay transfer efficiency due to radioactive decay losses
E_p the efficiency of the post-accelerator.

So the final radioactive beam current depends on the efficiencies of several chemical - physical processes and beam transport elements For ISOL facilities, the total efficiency is extremely case dependent and lies between 10^{-2} to 10^{-6}. To give an evaluation of the final beam the exotic species must be followed all along their path.

The exotic species are produced inside the target as neutral atoms and are extracted in a gas fase due to the high operating temperature of the target (2000°C). This process is governed by the release efficiency: that is the diffusion process in the uranium carbide grains, the effusion in the container and the injection in the ion source. As soon as the atoms are in the ion source they

should be ionized +1 to be extracted and injected in the transport system; this process is controlled by the source ionization efficiency. For an efficient reacceleration it is necessary to increase the charge state of the ions. This is done by the Charge Breeder which increases the charge state from +1 to +N with a breeding efficiency. Finally the overall efficiency of the transport and post-accelerator system (the efficiency of the separator and finally the transport efficiency through the post accelerator up to the experimental set up) must be considered.

All these parameters strongly affect the final current, but the target efficiency itself is a very complicated stuff.

The diffusion in the material is a complicated phenomenon, which is not completely known especially when the material is at high temperature: it strictly depends on the material structure and on the temperature at which the material is maintained. [5]

A statistical approach is used to describe the effusion of atoms inside the target powder. After the diffusion the atoms follow a random walk up to exit the container following the effusion process. The effusion time depends on the time spent colliding between the grains (*inter-grain effusion*) and the time spent colliding on the target and container surfaces before to reach the ionization source volume (*free effusion)*. Three parameters dominate the process: the number of bumps, the average flight time between one collision and the subsequent (*time of flight* or alternatively the *flight path*) and the average trapping time at each collision (*sticking time*).

The *sticking time* is the time during which the radioactive atom remain trapped in the surrounding material (target itself or material of the container, transfer tube etc) and can drastically influence the effusion time.

The effusion time is in fact the result of the multiplication of the number of collisions by *sticking time + tof.*

In the case of radioactive isotopes the decaying properties are also included.

We performed Monte Carlo simulations to get information on these effects and we compared, when possible, our results to experimental values for validation. Two main codes are presently available: the GEANT4 toolkit [6] and the RIBO [7] (Radioactive Ion Beam Optimization) codes. Both codes can evaluate the effusion time, RIBO gives also the diffusion time. Experimental data available from ISOLDE-CERN [9], ORNL [10] and Gatchina [11, 12] have been used.

The final results of our calculation indicate a release time of 1s for Sn isotopes and 10s for Kr for the chosen target configuration, mainly due to the diffusion time, as reported in table 3.1.

Table 3.1

element	diffusion time (s)	Nr of collisions	Effusion Time (s)	Release Time (s)	T1/2 (s)	TRF (%)
132Sn	1	10^5	0.2	1.2	40	98
133Sn	1	10^5	0.2	1.2	1	40
Kr	10	10^5	0.1	10	1	15

Calculations of the Total Release Fraction for Tin isotopes were performed considering different release times, as a function of the half life of the isotope, and are reported in Fig.3.1.

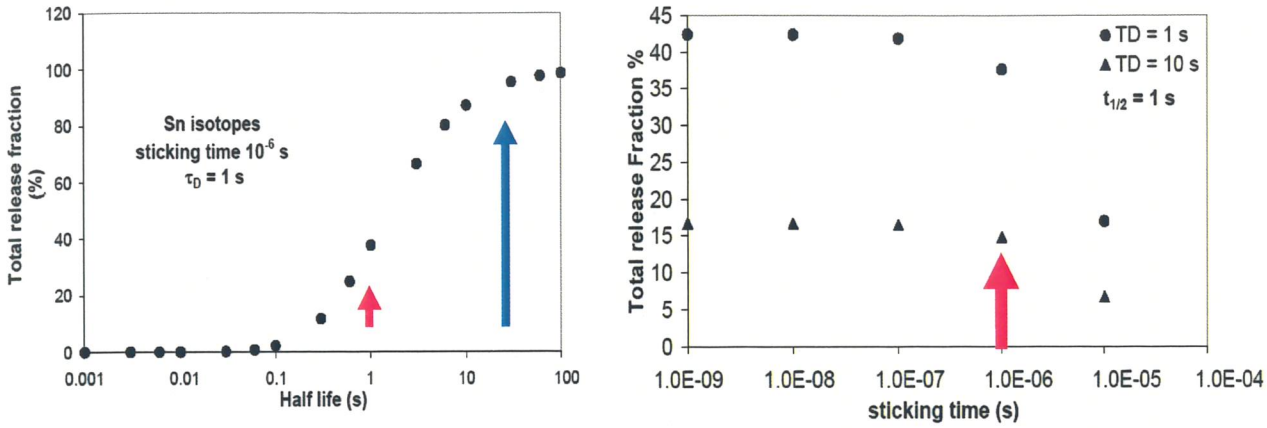

Fig 3.1: *Left panel: Total release time calculated for the Sn isotopes in the SPES –DT configuration as a function of the life time $T_{1/2}$. Arrows relates to ^{132}Sn and ^{133}Sn time-lives. Right panel: Total release fraction of an isotope of $T_{1/2}$=1s (short living) as a function of the sticking time.Arrows refer to the sticking time for Sn isotopes in UCx as obtained from Isolde data.*

Of course the release time has a large influence on the final production as shown in fig.3.3 which compare the expected beam of Sn isotopes in the case of the present target configuration (one step) and the old one (massive two step target).

As shown in Table 3.1 the diffusion time gives an important contribution to the total release time; therefore it is very important to optimize the material structure of the target disks. To this purpose, an extensive study on the target materials is in progress at LNL.

For sake of comparison between the 2 steps target of the old version and the Direct Target of the new project, some calculations were performed starting from the in-target production of 1E13 fissions per second induced by neutrons and protons respectively for the two configurations.

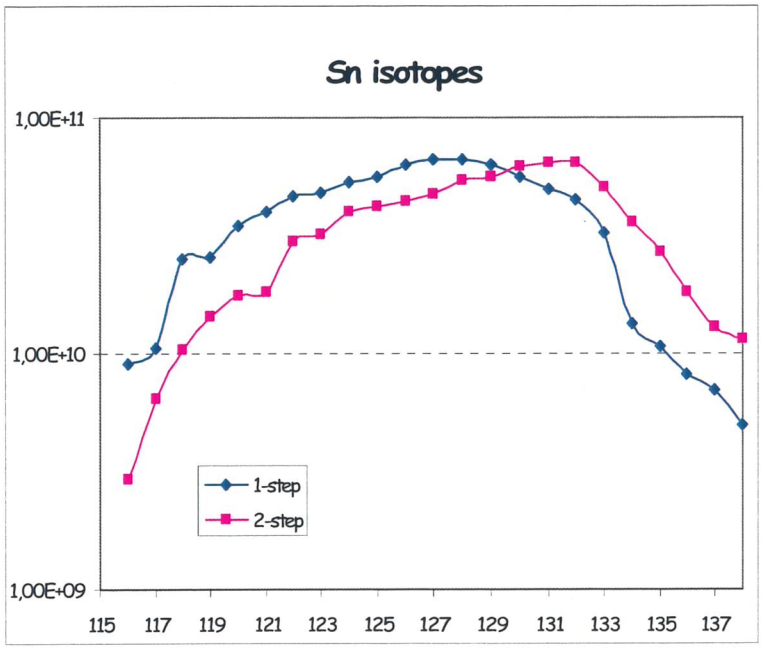

Fig. 3.2: *In target production yield in the case of one-step target (SPES –DT) compared to the 2-step target of the previous project.*

Fig. 3.2 shows the result of the in target production for the Sn isotopes following a Monte Carlo calculation (MCNPX code with ORNL model). To evaluate the isotope's yield injected in the +1 source we considered the composition of two exponentials: the release $R(t)=\exp(-t / t_{release})$ and the isotope decay $D(t)=\exp(-t / t)$. A release time of 2s (up to 5s) and 40 s were used for SPES-DT and SPES – old project respectively.

In the hypothesis of a saturated source, the % of extracted isotope was evaluated as the maximum of: $E(t) = (1 - R(t)) * D(t)$.

The fission fragments transported inside the source are ionized and extracted with a charge state +1.

A Charge Breeder section is then supposed to bring the charge state to +N.

The assumed +1 and +1/+N ionization efficiencies are 90% (+1) and 12% (+1/+N) respectively for Kr and Xe, but only 30% (1+) and 4% (1+/n+) respectively for Zn, Sr, Sn, I and Cd. These values are obtained by the SPIRAL2 project and are expected for an optimized extraction in which the source is specifically designed for each beam. In some case the use of an ECR source is required.

The Linac ALPI transmission efficiency is considered 50%.

Using these quantities an evaluation of the beam current on target, which can be obtained with the new SPES facility, are then shown in Fig.3.4 for some isotopes.

Fig. 3.3 shows the effect induced by the low release time of the Direct Target on the production of Sn beams.

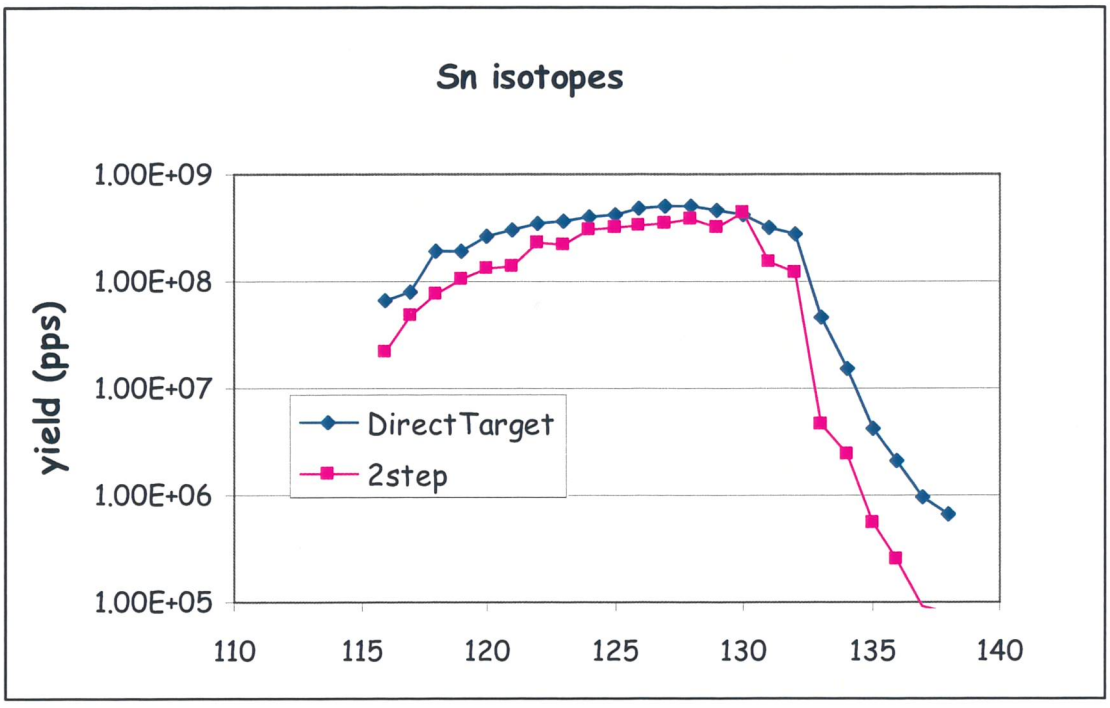

***Fig. 3.3**: Sn beam on experimentt: intensities calculate considering release, ionization and acceleration efficiencies (see text).*

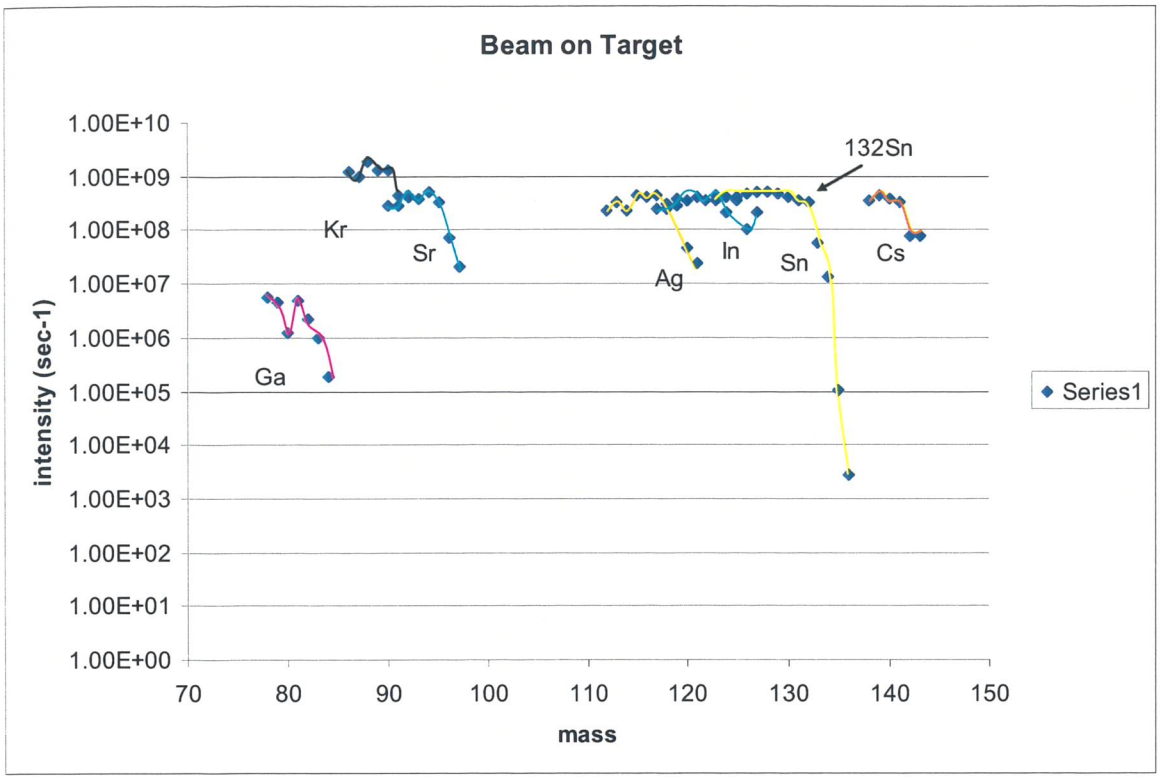

Fig. 3.4: *Beam on target: Intensities calculates considering emission, ionization and acceleration efficiencies (see text) for different isotopes.*

The comparison with others facilities is a complicated task due to the different production methods and the different transport line and re-accelerator machine used.

The ion charge at the output of the production target is positive (+1). Due to this the facilities based on Tandem re-accelerator need a charge exchange device; on the contrary if a Linac or a Cyclotron is used a charge breeder to increase the positive charge is usually implemented. These two devices have different efficiencies depending on the isotope of interest. Another critical part is the source coupled to the production target, as several kinds of sources can be used, each one with different extraction and ionization efficiencies; also in this case the performances are related to the isotope species.

Finally the useful beam for nuclear physics experiment is extremely related not only on the kind and intensity of isotope produced but also on its purity and energy.

In the following table we report, for sake of comparison, some world-wide facilities looking to the fission rate and to the power deposited in the production target.

Table 3.2

	Primary beam	Power on target	target	Fissions per sec
ISOLDE	p 1GeV 2 microA	0.4 KW	Direct Convert.	$4\cdot 10^{12}$ spallation
HRIBF	p 40MeV 10 microA Up-grade: 20 microA	0.4 KW	Direct	$4\cdot 10^{11}$
TRIUMF	p 450MeV (250 MeV in target) 40 microA Up-grade: 70 microA	10 KW 17 KW	Direct	spallation
EXCYT	^{13}C 45AMeV	0.5 KW	Direct	Light ions by direct reactions $4\ 10^8$ ^{8}Li ($9\cdot 10^6$ extracted)
SPIRAL2	d 40 MeV 5 mA	200 KW	Convert.	10^{13}- 10^{14}
SPES-DirectTarget	p 40 MeV 200 microA	8 KW	Direct	10^{13}

SPES is located to a high production rate of fission fragments similar to Spiral2. Nevertheless a comparison with Spiral2, from the point of view of driver, layout and cost, is doubtful as the driver of the Spiral2 facility is oriented to the production of high intensity stable beams and in this sense the two facilities cannot be compared at all.

In fig. 3.5 is reported the physics topics which may be addressed by an ISOL facility according to their beam intensity and energy. The expected beams of SPES cover an interesting region where large perspectives in nuclear physics research are possible.

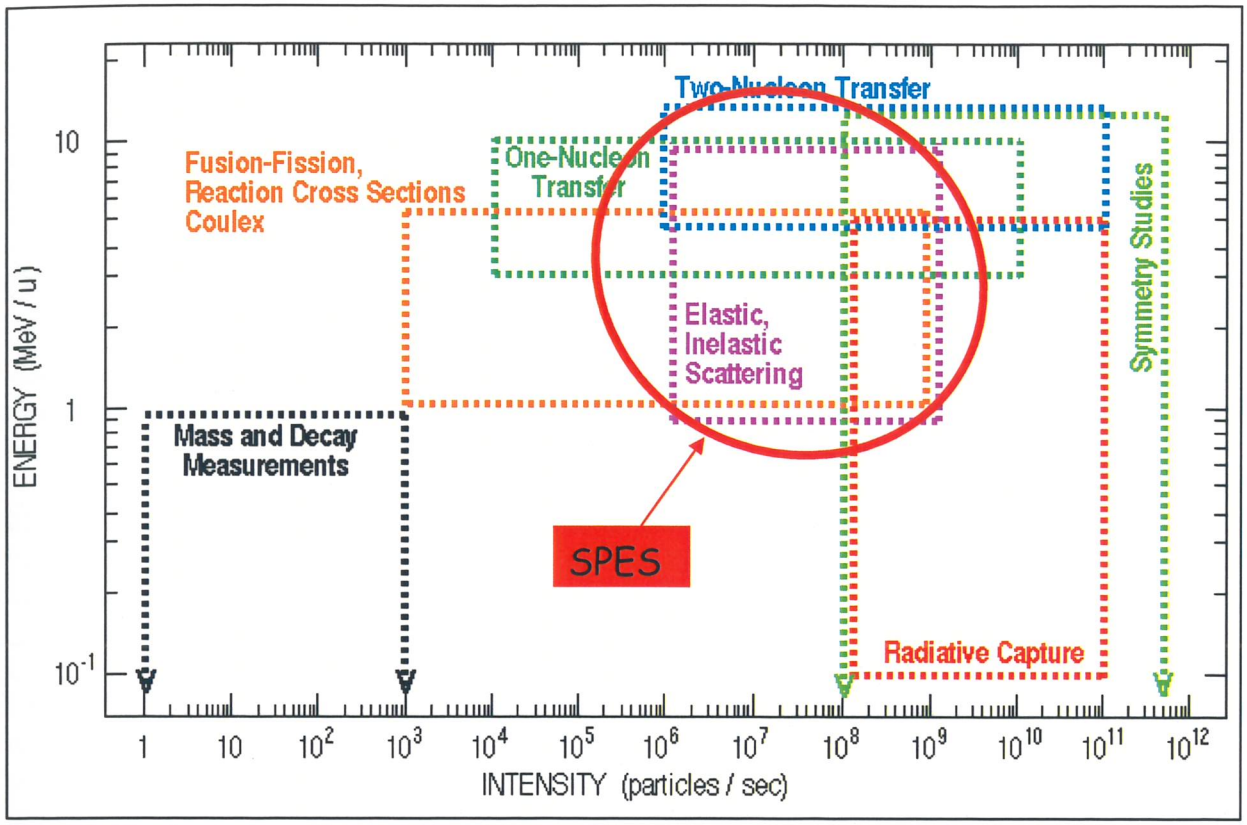

Fig. 3.5: *Physics topics addressed by an ISOL facility according to intensity and energy [13].*

[1] J.S. Hendricks et al., MCNPX vers. 2.5.e – LA-UR-04-0569 (2004)
[2] A. Andrighetto, S. Cevolani, C. Petrovich – Europ. Journal of Physics A25(2005) 41-47
[3] A. Andrighetto, S. Cevolani and C. Petrovich proceedings of 5th Italy- Japan Symposium - nov '04- pag 409
[4] LNL-INFN (REP)181/02 - June 2002
[5] J. Crank, The Mathematics of Diffusion, Clarendon Press (1956).
[6] GEANT4: Geant_detector description and simulation tool CERN Program Library W5013
[7] RIBO: http://ribo.web.cern.ch/rib
[8] J. C. Bilheux - Effusive flow characterization of arbitrary size and geometry target/vapour transport systems: radioactive ion beam applications – Paper 11.25
[9] Isolde data
[10] Oak Ridge data –WATD Triumf – Carter presentation
[11] M.Barbui at al. LNL Annual report 2006, 182
[12] M.Barbui at al. LNL Annual report 2006, 184
[13] http://www.ganil.fr/eurisol/TOWNMEETINGORSAY3/SydneyGales.pdf (2003)

CHAPTER IV

PROTON DRIVER

4.1 Introduction

The proposed driver, composed by RFQ-DTL, generates a low emittance and high intensity beam, for an average current of 1.5 mA and an energy of 43 MeV, upgradable to 95 MeV, for an optimal illumination of the uranium carbide target under development for SPES project, keeping the operative margins necessary for future developments.

The high rep rate frequency beam structure of the linac does not show substantial differences respect to cw structure for the mechanical beahavior of the target. The low emittance, typical of the linac solution, offers some advantages in the beam losses control in along the accelerator and in the transfer lines, and a better definition of the beam spot on the target.

In this configuration the linac uses the same injector (up to 5 MeV) both as neutron source (BNCT) and for the production of RNB. While this represents a clear rationalization in the development of the high intensity accelerator, respect to the development of two independent injectors, it has to checked if this implies limitations respect to the actual beam time requirements by the two users. The complete independence of the two users may anyway be implemented in a second time, developing a fast beam switch in the MEBT or building a dedicated pulsed RFQ.

The proposed accelerator is composed by the source TRIPS, built at LNS and now in operation at LNL, by the RFQ of TRASCO research program (5 MeV 30 mA), very advanced in the construction, and by a normal conducting Drift Tube Linac (DTL). This last accelerating structure is the same proposed for LINAC4 at CERN (recently approved for the consolidation of LHC injectors). A prototype of this structure, of interest for both projects, is in construction (with the joint effort of CERN and LNL) at Cinel company and will be tested at full power next year at CERN.

The RFQ and the two tanks of the DTL are fed by 3 klystrons; the first one, with a power of 1.3 MW, is already at LNL, while the other two with a power of 2.5 MW each are the same adopted for LINAC4. The power supply of the RF system (50 Hz 600 μs) has been evaluated in details on the bases of the system in operation for the Japanese project JPARC (four 2.5 MW klystrons per power supply).

The development of the high power RF system represents the most relevant future development in the construction of the RFQ: The extension of the same RF system from the RFQ to the DTL can be implemented with a relatively small effort by the same team.

The proposed linac, partially already in construction phase, represents therefore an accelerator at the technological frontier. On the other hand for all the components the performances required have already been demonstrated. It is therefore an accelerator that makes full use of the experience matured at LNL and of what has already been built, of the synergy with CERN and with other international laboratories. The engineering made in common with CERN allows to be competitive in costs and realization schedule with more conventional commercial accelerators.

4.2 Linac architecture

The proposed driver is a 43 MeV proton linac, operating at 352 MHz, pulsed at high repetition rate, composed by a room temperature radiofrequency quadrupole (RFQ) and a drift tube linac (DTL) with permanent magnet quadrupole focusing (Fig. 4.1). This last structure replaces the superconducting linac foreseen in the TDR, allowing a good saving in capital and running costs for the nominal current of 0.5 mA [1]. The klystron and the power supply are dimensioned for a maximum current of 1.5 mA, while the possibility of an upgrade in the final energy is maintained. The main linac parameters are:

- Beam energy: ~43 MeV
- Average beam current : up to 1.5 mA
- Beam pulse length up to 600 μs
- Repetition rate 50 Hz
- RF frequency: 352.2 MHz
- Possible upgrade to 95 MeV

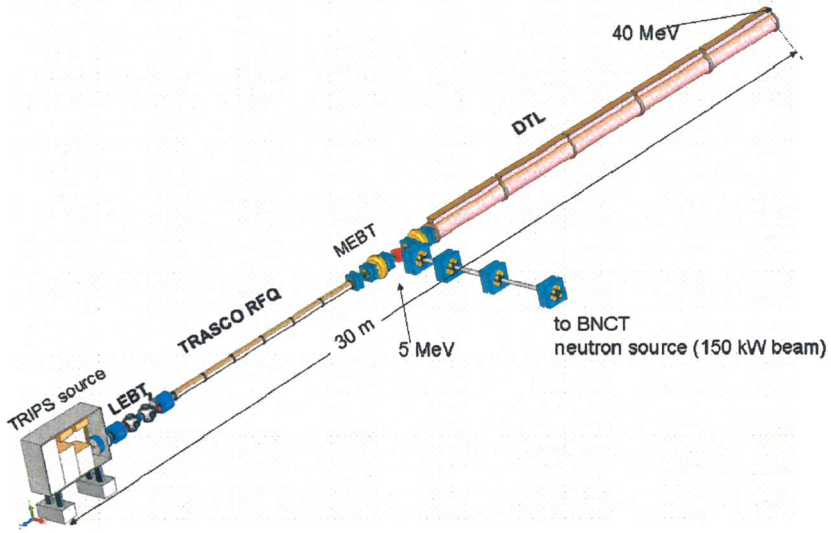

Fig. 4.1: *Spes driver layout*

The maximum energy for the possible energy upgrade is determined by the available space in the building.

The linac pulsing is necessary to decrease the power dissipation in the copper of the structure. As in any normal conducting linac the power consumption reduction is reached by decreasing the duty cycle (pulse length * repetition rate), keeping the peak current such that during the RF pulse the beam loading is comparable with the RF dissipation. A peak current of 50 mA and a beam duty cycle of about 1.0% are good figures for this case. A specific requirement for SPES rises from the thermal behavior of the production target, that is heated up to more than 2200 deg to enhance the release of fission fragments and has to withstand the beam power deposition of about 10 kW. The linac pulsing adds a time dependent transient to the target temperature distribution that could increase the stresses on the disks; indeed with a linac repetition rate >10 Hz this effect is negligible (Fig. 4.2). At the nominal rep rate of 50 Hz the transient temperature ripple is more than 10 times lower than the maximum temperature non-homogeneity in the target and would not influence the target performances and lifetime [2].

The layout of the LINAC is presented in Fig.4.1.; the main elements are the off resonance ECR source (TRIPS), the Low Energy Beam Transport (LEBT), the radio frequency quadrupole (RFQ), the Medium Energy Beam Transport (MEBT) and the Drift Tube Linac (DTL).

After the linac a High Energy Beam Transport (HEBT) line will deliver the beam to two different RIB production target and possibly to other lines for different operations like neutron production. The pulsed structure of the beam allows the distribution of the beam between the various users switching a dipole magnet from pulse to pulse (20 ms). It is for example possible in this way to operate simultaneously two RIB production targets at 0.25 mA and 25 Hz .

The beam is produced by an off resonance ECR source, and accelerated up to 5 MeV by a high current RFQ. The injector, beside the pulsed beam, is also able to deliver the more demanding beam characteristics

- Beam energy: 5 MeV
- Beam current : up to 35 mA
- Beam duty cycle: cw

necessary for the operation of the 150 kW beryllium target of the neutron source of the BNCT facility. Other neutron production targets could be operated in alternative.

In summary for BNCT the RFQ works alone in cw mode, for RIB production both the RFQ and the DTL operate in pulsed mode.

The simultaneous operation of the two facilities (BNCT and RIB), making full use of the cw capabilities of the RFQ is possible in principle, but requires the development of a fast beam switching system in the MEBT, presently under evaluation, and not included in this proposal. On the other hand due to the low number of equipments to be set the switch between the cw low energy mode (BNCT) and pulsed high energy mode will be possible in less than one hour. This allows to have and optimum sharing between different users, and potentially to analyze with the neutron beam radioactive samples produced with the RIB facility.

The performances of the linac can evolve in future, for the use of new generation fission targets, or for the production of neutrons. In the following section we considered the possible upgrade in energy (95 MeV); in this way the original SPES linac requirements (>100 kW for neutron converter operation) can be met.

Table 4.1: main parameters of linac structures

	RFQ	DTL	
Energy	5	43	MeV
Frequency	352,2	352,2	MHz
Ave. Acceleration	0,7	2,5	MeV/m
Max Field	1,8	1,6	Ekp
RF Power	0,8	4,03	MW
Nb. of Klystrons	1	2	
length	7,13	15,2	m

Concerning the building, the linac footprint has been chosen considering this 100 MeV linac. In a first moment the HEBT from the 43 MeV linac to the beam distribution dipoles will be longer; the quadrupole available from the dismantling of some of the beam lines in ALPI vault will be used.

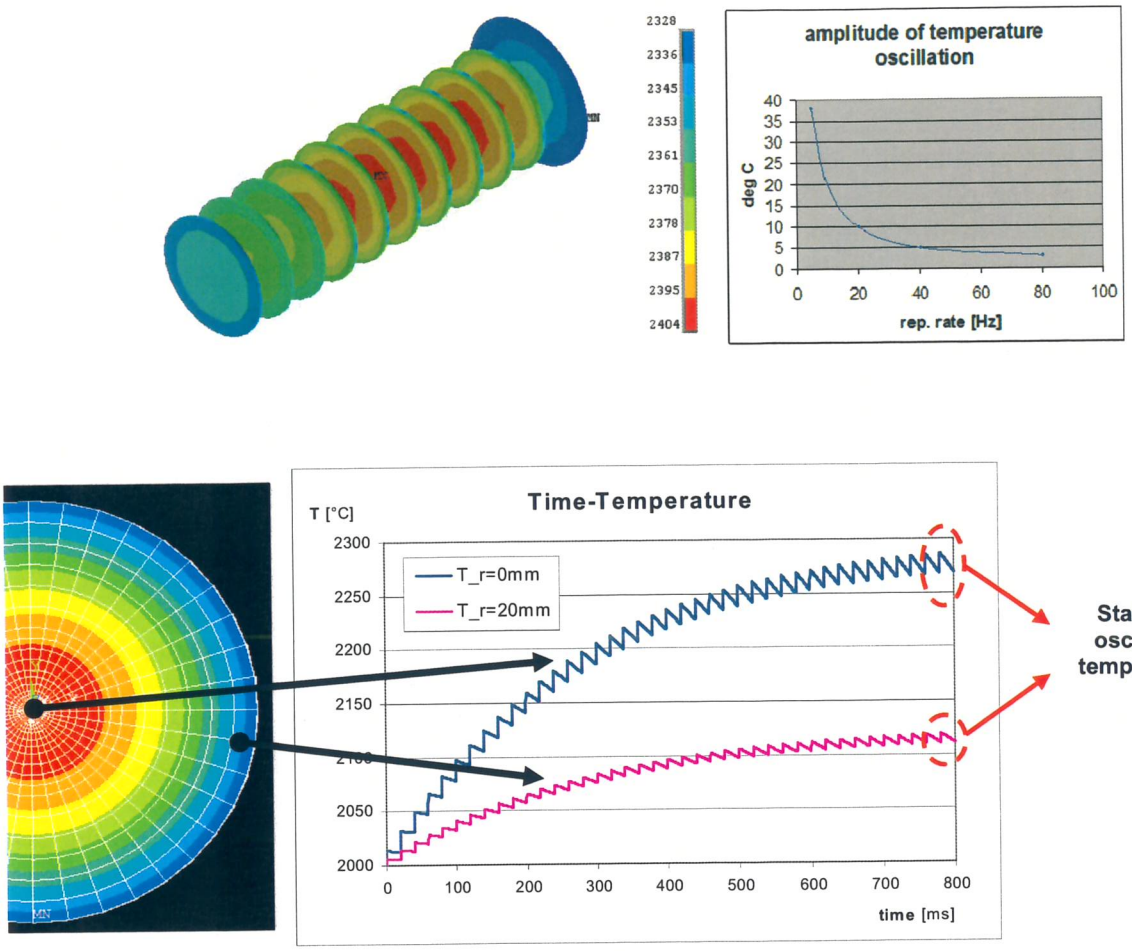

Fig. 4.2: *Temperature distribution in the steady state and temperature ripple amplitude as function of pulsing frequency (upper figure); evolution of the temperature for the inner and outer part of the central disk in the case of 50 Hz pulsing (lower figure).*

4.3 Source and RFQ

The front end of the linac has to deliver two very different beams, a 2.5 kW pulsed beam for the DTL and the RIB production, and a 150 kW cw beam for the 5 MeV neutron source.

The second application corresponds exactly to the beam requirements originally given for research program TRASCO (and its continuation ADS) where the main components of the injector of a high intensity linac for Nuclear Waste Transmutation were studied and prototyped. The ion source, built and commissioned with beam at LNS, has been now installed at LNL. Concerning the RFQ, two of the six modules are completed, for the other four the high precision machining is completed and they are waiting for the brazing to be done at CERN. The main components of the RF system, part of the former LEP RF system, are already stored at LNL.

For the first application the source and the RFQ have to be pulsed at 50 Hz with 1.0% beam duty cycle. The RF system for RFQ pulsed operation is identical to one of the 5 DTL units, based on a LEP klystron, described in the DTL section. The RFQ structure, with the cooling capability necessary for cw operation, can be pulsed with a large margin of redundancy. The

water circuit has to be designed so to be used for frequency stabilization with both pulsed and cw operation.

The beam pulse shape is formed in the source by pulsing the RF and installing pre-chopper in the LEBT; the performances of this system, that has unknowns related to the source behavior and beam neutralization in the LEBT during the transient, are part of the experimental test program at LNL test bench.

4.3.1 Source and Low-Energy Beam Transport

The main requirements for extracted beam are:

- Energy: 80 keV
- Extracted Current: 65 mA (pulsed mode), 46 mA (cw)
- Proton Fraction: $\geq$90 %
- Normalized RMS emittance: <0.2 π mm.mrad
- Intensity stability: ±1% to ±2% depending on the target requirements
- Pulsed mode characteristics:
    - Repetition Rate: 50 Hz
    - Pulse Length: 600 μs

The cw mode requirements are fulfilled by the TRIPS source which was developed in the framework of the TRASCO project. The source is a high current microwave discharge ion source [3]. Its goal is the injection of a minimum proton current of 35 mA for an operating voltage of 80 kV in the following RFQ, with a rms normalized emittance lower than 0.2 π-mm-mrad and with a reliability close to 100 % (few failures per year).

The pulsed mode beam is prepared by pulsing the source RF generator; a sharper beam pulse rise time, for a further reduction of beam losses, can be reached with a relatively slow beam chopper in the LEBT (about 1 μs rise time; a very similar device will be installed for CNAO linac).

4.3.2 Design

The plasma chamber (Fig.4.3) is cylindrical, 90 mm in diameter, and 100 mm in length. The microwave pressure window is placed behind a water-cooled bend in order to avoid any damage due to back-streaming electrons. The microwave power produced by a 1.2 kW 2.45 GHz magnetron is coupled with the plasma chamber through a circulator, a directional coupler, a four-stub automatic tuning unit and a four section ridged waveguide transition. The magnetic field is produced by two coils on line movable and independently energized. The position of the electron cyclotron resonance (ECR) zones plays an important role in the behavior of the source. For this reason the source works with two ECR zones located at both ends of the chamber, where two boron nitride disks are placed [4]. The five-electrode extraction system has been simulated with the AXCEL code [5] and the results have been crosschecked with the IGUN code [6].

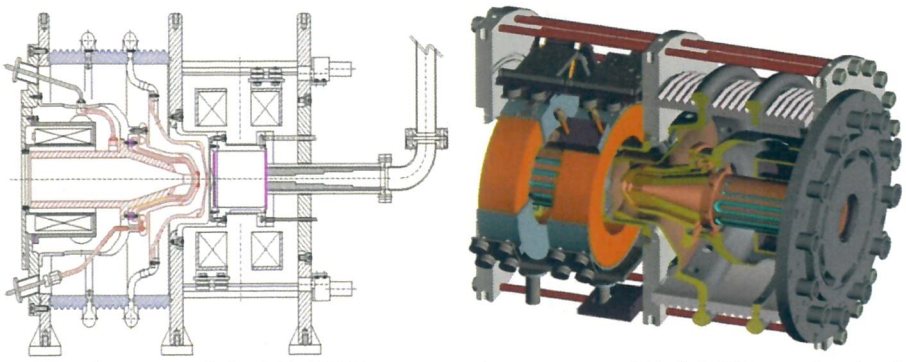

Fig. 4.3: *(Left) Line drawing of the TRASCO injector ion source. (Right) 3D mechanical representation. It is also visible the cooling system of ground electrodes and of the plasma chamber inside solenoid coils.*

It consists of a plasma electrode made of molybdenum, a puller electrode, two water-cooled grounded electrodes, and a negatively biased screening electrode, inserted between the grounded electrodes in order to avoid secondary electrons due to residual gas ionization going up to the extraction area. Each electrode, except for the plasma one, is divided into two parts: the first, close to the beam, is made of molybdenum and the other is copper. This choice increases the electrode power dissipation and allows easy replacement of the first part without machining the entire electrode.

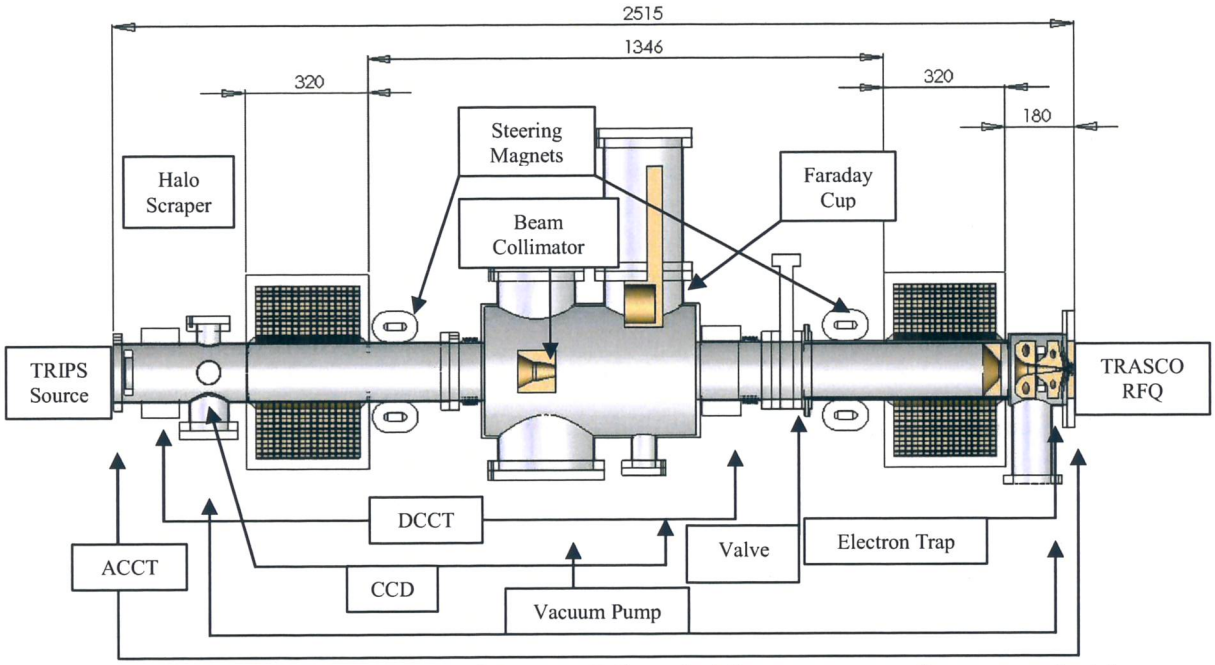

Fig. 4.4: *LEBT design. The location of Bergoz DC and AC current transformers and video camera diagnostics are indicated.*

The Low-Energy Beam Transport (LEBT) line [7] provides the beam matching from the source to the RFQ and contains the diagnostics to monitor the source (Fig.4.4). It is a neutralized magnetic line and its functions include beam focusing and steering, dc and ac beam current diagnosis and beam profile measurement through CCD monitors located at two stations along the beam line. An insertable plunging beam stop is planned to stop the 65 mA-80 KeV beam. Two water-cooled collimators and an electron trap at the RFQ entrance completes the line.

4.3.3 *Beam Dynamics*

Extraction and transport up to RFQ has been studied with AXCEL and PARMELA code [8] taking into account the partial neutralization and the presence of contaminant species such as H^{2+} and H^{3+}. Full proton transmission and a proton fraction as high as 99.5% may be reached at RFQ input through selective loss of the contaminants in the LEBT. Non linear phenomena are strongly reduced using neutralization [9] and limiting beam radius inside solenoids. Rms normalized emittance at match point may be reduced to 0.08 mm-mrad.

4.3.4 *Pulsed Mode Operation*

The major problem concerning beam pulsing in the LEBT is neutralization. Electrons needed for beam neutralization are generated through ionization of the residual gas with proton beam. Tens of microseconds are needed to reach neutralization equilibrium. During this time Twiss parameters at the RFQ match point vary converging toward optimum values. During this variation, source beam is not well-matched to RFQ. Plasma ignition experiences a similar evolution toward equilibrium. Transient time is in the range of hundreds of microseconds. The solution of the problem is pulsing the source rf generator with a repetition rate of 50 Hz and an overall pulse length of 1.35 ms chopping the first part of pulse with a pre-chopper in the LEBT line (Fig.4.5). Magnetron pulsing guarantees the first raw reduction of beam power from 5.2 kW to 254 W. Chopper removes 98 W while collimators chain eliminates beam spurious components and reduce the power at RFQ entrance at 140 W at maximum. For optimum pulsing it is necessary to know neutralization rise time and plasma ignition. Residual Twiss parameters time-variation due to neutralization rise-time after chopper must be investigated.

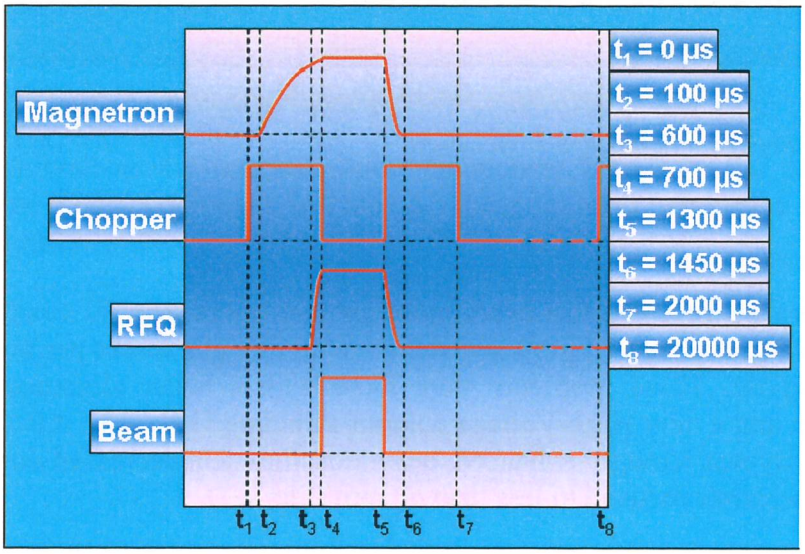

Fig. 4.5: *Timing for beam pulsing.*

4.3.5 *Status*

Source was transferred from LNS to LNL at the end of 2005 [10]. Installation was completed in late July 2006 and beam extraction was succesfully tested in September 2006 [11]. Source performances are presented in Table 4.2. The current installation and a picture of the beam extracted in September 2006 are presented in Fig.4.6.

Table 4.2: TRIPS main working parameters

	Requirement	**Status**
Beam energy	80 keV	80 keV
Total current	70 mA	60 mA
Proton fraction	90 %	≈85 %
Microwave power frequency	<2 kW at 2.45 GHz	0.3-1kW at 2.45 GHz
Duty factor	100 % (dc)	100 % (dc)
Beam emittance	≤0.2 π mm mrad	~0.07 π mm mrad
Reliability	~100 %	90 % at 30 mA
Gas flow	<2 sccm	0.4-0.6 sccm

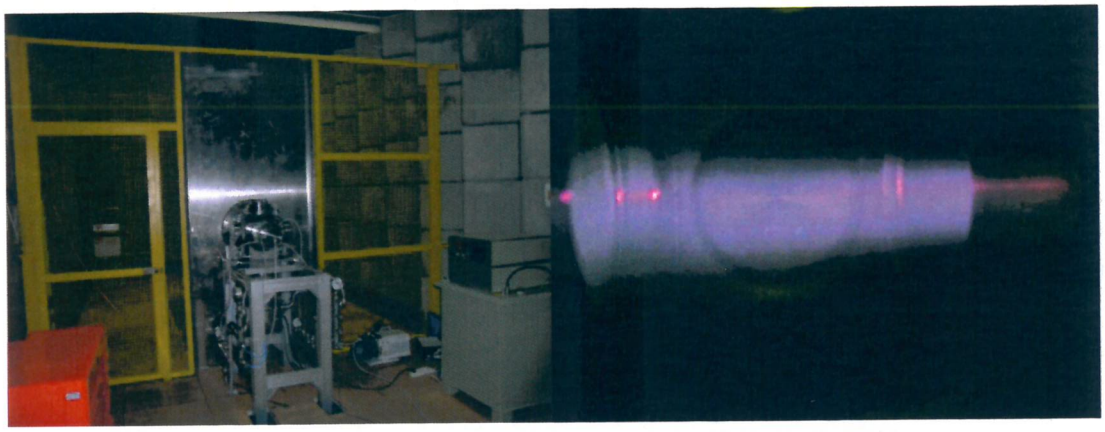

Fig. 4.6: *(Left) SPES source installation. (Right) Beam extracted from the source in September 2006 photographed through diagnostic box viewport.*

4.3.6 Source Upgrades

Measurements revealed that beam misalignment (more than 60 mrad), beam dimensions at LEBT entrance (more than 75 mm) and source reliability (10 sparks per hour) were not adequate for SPES purpose. These problems were fixed with a better alignment, an optimization of extraction gap and a new High-Voltage column shielding [12], [13]. After improvements, beam source reliability was strongly enhanced, beam misalignment decreased down to less than 6 mrad and beam dimensions reduced to less than 40 mm (Fig. 4.7).

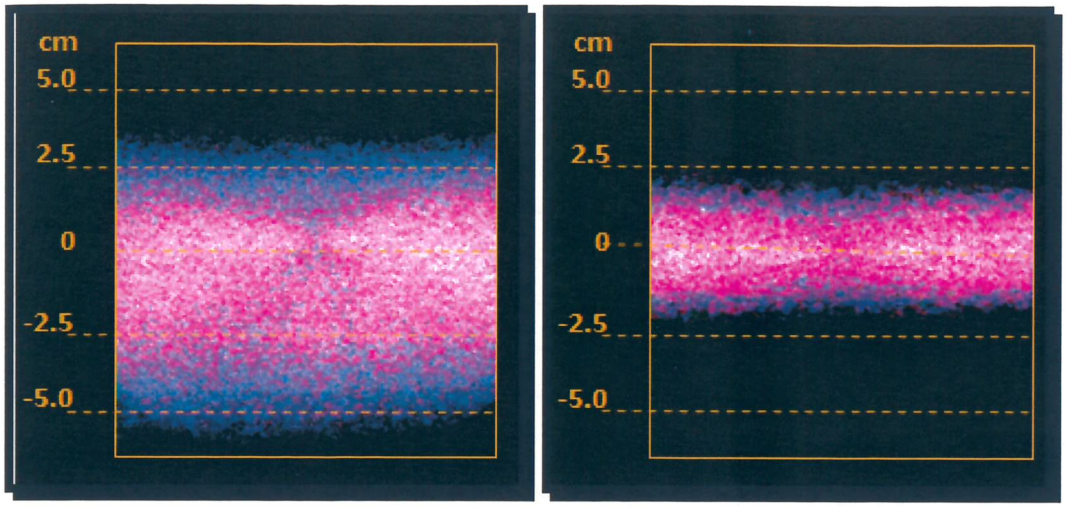

Fig. 4.7: *Comparison of the measured beam profiles at LEBT entrance before (left) and after (right) source improvements. Reduction of beam misalignment and dimensions is evident.*

4.4 The RFQ

The RFQ, initially developed for the TRASCO project, has two working regimes, pulsed and cw; the operating frequency is 352.2 MHz, with the design choice of using a single 1.3 MW klystron already used at LEP. The RF power will be fed by means of eight high power loops. The achievement of the longitudinal field stabilization for the operating mode will be achieved with two coupling cells in order to reduce the effect of perturbating quadrupole modes and with 24 dipole stabilizing rods in order to reduce the effect of perturbating dipole modes. Indeed, 104 slug tuners will keep the quadrupole mode longitudinal ripple below 1% of the useful value ($|\Delta V_q/V_q| \leq 0.01$), as well as the residual dipole component below 2% of the longitudinally uniform quadruople mode component. In Table 4.3 the main RFQ parameters are listed for both CW and pulsed regimes.

Table 4.3: Physical RFQ parameters

Energy Range	0.08-5	MeV
Frequency	352.2	MHz
Beam Duty cycle	Up to 100	%
Maximum Surf. Field	33	MV/m (1.8 Kilp.)
Emittance T RMS in/out	0.2/0.2	mm mrad norm.
Emittance L RMS	0.18	MeV deg
RFQ length	7.13	m (8.4 λ)
Intervane voltage	68	kV
Transmission	96	%
Modulation	1-1.94	
Average Aperture R_0	2.9-3.2	mm
Synchronous Phase	-90÷-29	Deg
Dissipated Peak Power SF*1.2	0.579	MW
Q (SF/1.2)	8261	
Peak Beam Loading	0.1476	MW
Peak RF Power	0.726	MW

4.4.1 Beam dynamics studies

The RFQ beam dynamics was designed following well-consolidated techniques and the Losa Alamos simulation codes (CURLI, RFQUICK, PARI, PARMTEQM). The optimization of the beam transport along the structure was carried out with the aim of keeping beam losses principally below 2 MeV, thus minimizing activation problems. A particularity of this study was the choice of imposing a constant longitudinal voltage profile, to keep the pole tip radius ρ constant and to increase the average aperture R_0. The choice of a constant value of ρ allows a relatively easier and cost-effective machining of the electrode modulation, while the increase of R_0 permits to keep the power losses well below 1 MW, thus permitting the usage of a single klystron. The gentle buncher section is the most critical part, mainly because the end of this section is the transverse bottleneck and the main parameters were chosen with the aim of getting a beam transmission of at least 95%. Moreover particular care has been put in the optimization of the accelerator section that corresponds to more than ¾ of the total structure length.

The main beam dynamics parameters obtained are shown in Fig. 4.8.

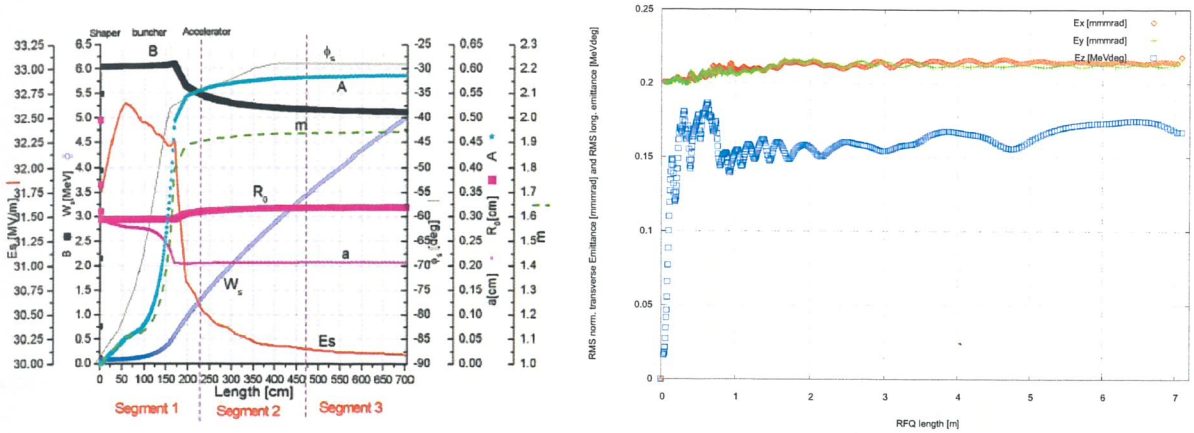

Fig. 4.8: *(Left) RFQ parameters as function of length. (Right) Beam Emittance transverse and longitudinal as function of length including the rfq gaps, calculate by TOUTATIS.*

The beam transmission (calculated with 100000 macro-particles) is equal to about 97.7% @ 50 mA. This result was confirmed after checks performed with LIDOS and TOUTATIS codes including the vanes gaps at 1/3 and 2/3 of the structure.

The error study was performed by taking into account the following factors: input mismatch, voltage ripples, beam misalignments and dipole perturbations. The related results furnished the acceptable margins for such parameters and are the following:

- **Input mismatch**: the transmission is kept higher than 95% for an input β Twiss Parameter variation of ±5% with respect to its nominal value.
- **Voltage ripple**: the transmission is kept higher than 95% for a quadrupole voltage ripple ΔVq within ±1% with respect to the nominal voltage.
- **Beam misalignment**: the transmission is kept higher than 95% for a beam misalignment within ±0.1 mm.
- **Dipole perturbation**: the transmission drop with respect to its nominal value is within 1% for a dipole components within ±2% of the quadrupole nominal electric field.

4.4.2 Construction and testing

The schematic layout of the RFQ is shown in Fig.4.9. The structure consists of six modules 1.18 m long each made of OFHC copper. The vacuum ports are on the first and fourth segments and the couplers on the other four. Particularly challenging are the very tight mechanical tolerances (20 μm) necessary for the purity of the accelerating mode (as required by beam dynamics) that have to be kept in presence of a large power density.

The RFQ consists of three segments 2.4 meters long each, resonantly coupled via two coupling cells in order to reduce sensitivity to machining errors. Each segment consists of two 1.18 meters long modules, which are the basic construction units. Each module is built in OFHC copper and is made of four main parts. The head flanges between segments and the rectangular vacuum flanges are made of SS (LN316). To reduce the number of brazing joints, the longitudinal cooling passages are deep-hole drilled from one side and closed with brazed plugs on the flat surfaces of the RFQ segment (opposite to the coupling or end cells). Moreover, the vacuum grids with their cooling channels are directly machined on the copper bulk [14].

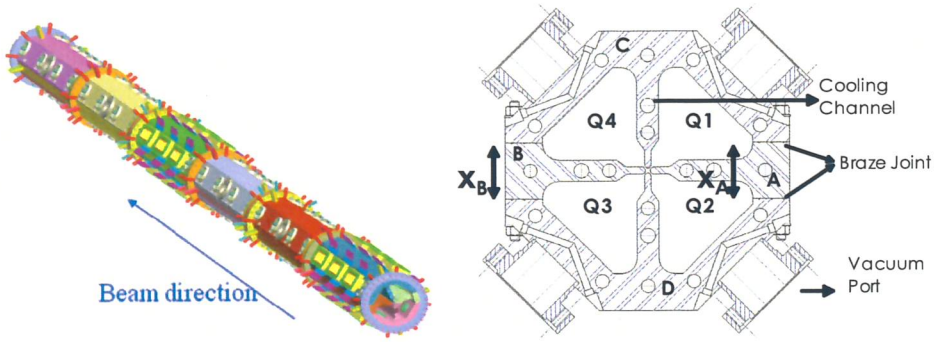

Fig. 4.9: *(Left) 3D view of the RFQ (Right) Transverse section of the RFQ with the indication of quadrants and braze joints.*

Two brazing steps occur. In the first the four main parts (A, B, C and D in Figure) are brazed in horizontal position in a horizontal vacuum furnace, as well as the OFE plugs for the cooling channels. After first brazing, the housing for the head flanges and the flat end surfaces (where the cooling channel plugs are located) are machined. In the second brazing cycle the head SS flanges, the inlet and outlet cooling water SS tubes and the SS flanges for vacuum ports or couplers are brazed in vertical position in a vertical vacuum furnace. The whole machining of the cavity is made by CINEL Strumenti Scientifici at Vigonza (PD), Italy, and the vacuum brazing as well as the copper heat treatment are made at CERN. RF and mechanical measurements allow to check the correctness of each step. To date, the first two modules (RFQ1 and RFQ2) underwent the complete construction cycle and the remaining four modules (RFQ3, RFQ4, RFQ5 and RFQ6) were pre-braze assembled and RF characterized and are ready for brazing at CERN [[15]].

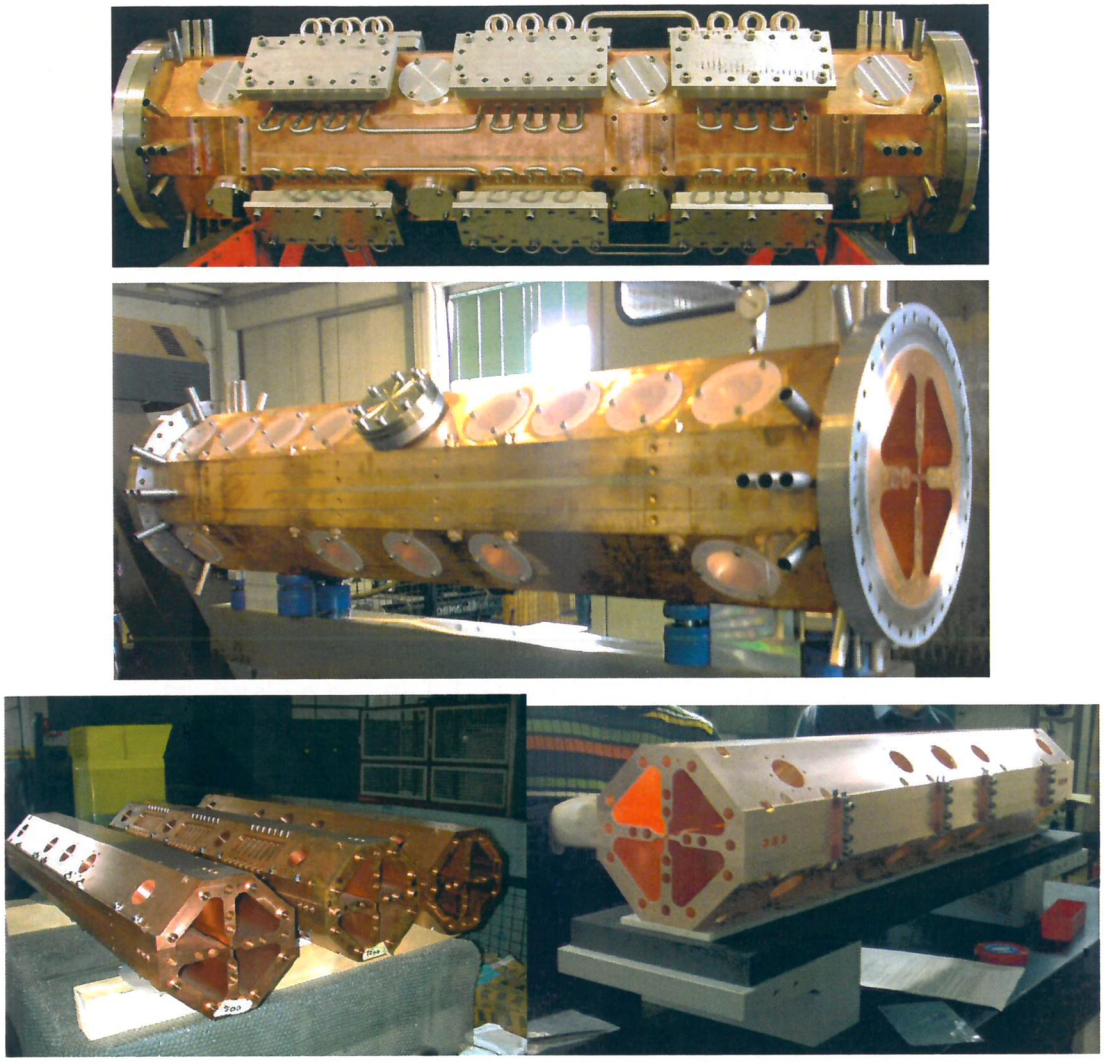

Fig. 4.10: *RFQ1 (top) and RFQ2 (center) after completing construction; the remaining four modules ready for brazing (bottom).*

After the completion of all the modules, the final tuning of the whole cavity will be performed, by using the tuning algorithms for the case of coupled RFQ developed at LNL and based on Transmission-Line modeling and Perturbation Theory. They were already tested on the aluminum model and their effectiveness in meeting the field specification was demonstrated [16]. In this framework, a complete characterization of the Dipole Stabilizing Rods (DSR) was given, through both their modeling in the equivalent transmission line model of the RFQ and simulations and measurements performed on the aluminum model of the RFQ. In particular, the reducing of dipole perturbation upon operational mode due to DSR's insertion was demonstrated via bead pull measurements [17]. The final step of the overall tuning procedure will be the removal of the temporary brass tuner and the insertion of the copper slug tuners, each of them to be machined at the penetration indicated by the procedure itself.

4.4.3 Thermo-Structural design

Once the RFQ is tuned at room temperature, it will be required to match the operating frequency under high power operations. This will be accomplished by varying the water temperature in the main cooling channels of each modules, named as in Fig. 4.9. The radii of the channels are equal to 6 mm, except C2, whose radius is 6.5 mm. The related calculation of water

temperatures and velocities were carried out with HFSS and SUPERFISH for RF power deposition on the cavity walls (with 1.44=1.2 * 1.2 margin, see 4.6) and with ANSYS for the subsequent copper deformations and bulk temperatures. Then, by direct use of Slater theorem and perturbation theory, the local and global frequency variations were calculated. It has to be pointed out that, for a given set of temperatures and velocities for each channel, there are two frequency variations to be taken into account: In fact, the resonant frequency of the structure is different whether the RFQ is "cold" (i.e. power and cooling system off) or "hot" (i.e. power and cooling system on). Let Δf_1 be such difference. Indeed, the temperature increase between the inlet and the outlet of the channels provokes a local deformation and therefore a variation $\Delta f_2(z)$ of the local frequency, so that the total frequency perturbation is equal to: $\Delta f(z) = \Delta f_1 + \Delta f_2(z)$. The most convenient choice is to arrange the water temperatures and velocities in such a way that $\Delta f(z)$ averages to zero along each RFQ module. Moreover, each module having its separate cooling circuit, the arrangement of Fig. 4.11 (with water flow in opposite direction for adjacent modules) allows having a local frequency perturbation which couples with a high-order mode, thus reducing its effect on quadrupole field under high power.

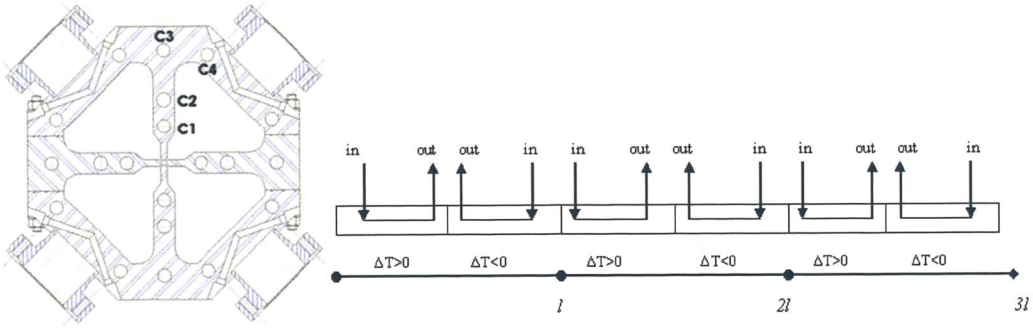

Fig. 4.11: *RFQ cooling channel and longitudinal channel layout.*

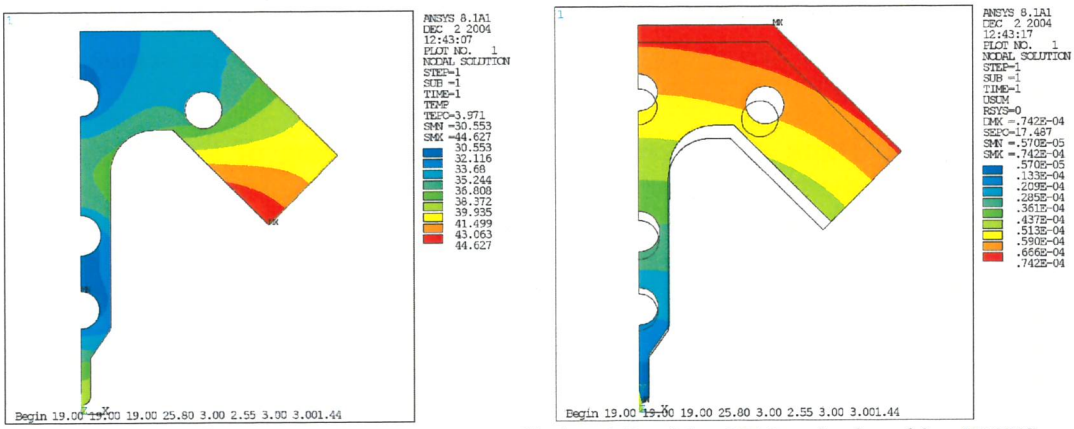

Fig. 4.12: *Inlet temperature and deformation profiles in 1/8 of the RFQ calculated by ANSYS.*

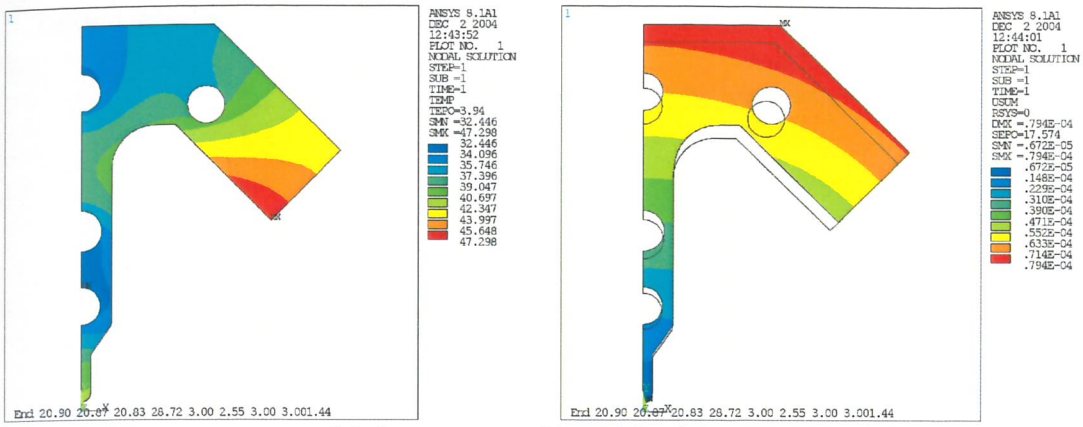

Fig. 4.13: *Outlet temperature and deformation profile in 1/8 of the RFQ calculated by ANSYS.*

Though there are several cooling arrangements that meet the above mentioned specifications, it has been chosen not to exceed ±20 kHz (roughly corresponding to the 3dB RFQ bandwidth), as maximum detuning. For instance (Figs.4.12-4.13), if the inlet temperature of the channels C1, C2 and C3 is set to 19 °C and the temperature of C4 is set to 25.8 °C, with velocities v1=v3=v4=3 m/s and v2=2.55 m/s, the overall detuning is less than 3 kHz, corresponding to a temperature rise of 1.9 °C in C1 and C2, 1.8°C in C3 and 2.9°C in C4. The frequency variation with temperature is $\left.\frac{\partial f}{\partial T4}\right|_{T1,T2,T3=19C,T4=25.8C}$ =-38kHz/°C. Therefore, the regulation of water temperature within ±0.1°C permits to remain with comfortable margin in the RFQ bandwidth. The overall water flow of the RFQ operating in CW mode is equal to about 4500 l/min for a pressure drop of 1 bar between inlet and outlet. The water channels interconnections are schematically indicated in Fig.4.14.

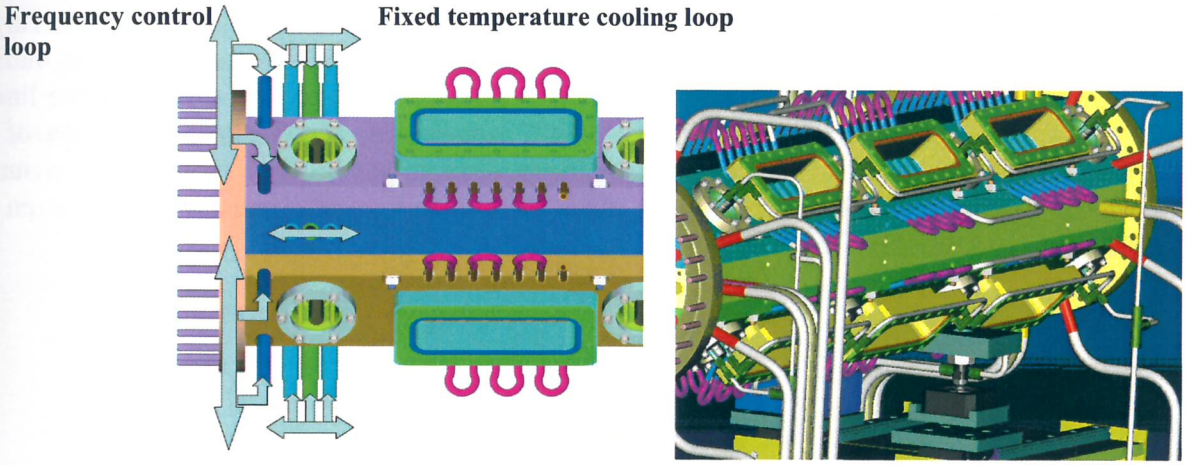

Fig. 4.14: *RFQ cooling channel layout. (left) Frequency control loop and fixed temperature water loop. (right) Cooling pipes layout.*

The cooling system is also able to stabilize the RFQ under pulsed operation, but in this case, due to the much lower power level, the water temperatures on the main channel as well as the water flow need to be adjusted accordingly.

The power coupler design is inspired to the LEP NC cavities couplers and is composed of a waveguide-to-coax transition, a RF alumina window and a water-cooled drive loop. The alumina windows are of the same type of those used for LEP NC cavities and will be brazed on a kovar welding lip to be TIG welded onto the copper bulk of the coupler, according to the scheme of Fig.4.15.

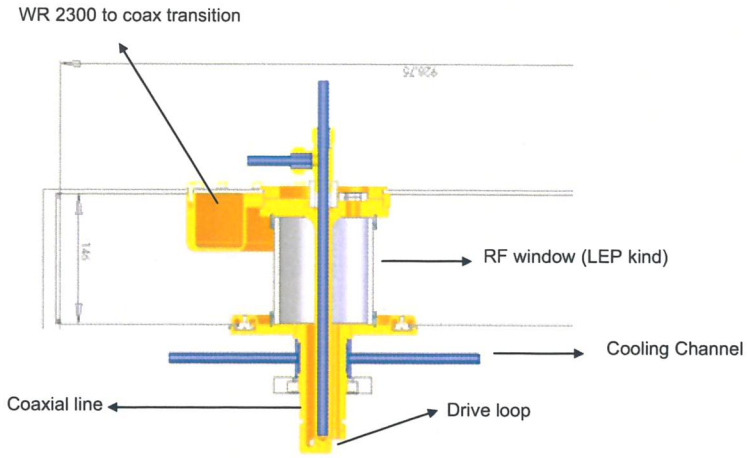

Fig. 4.15: *The RFQ power coupler, including WR2300 to coax transition.*

The RF coupler design was performed with the aim of keeping the VSWR below 1.05:1 even with full power operation. Therefore, in the thermo-structural simulations, the coaxial cooling channels were set at the inlet temperature of 19°C with a maximum value of power density of 25 W/cm2 (with 1.44 margin). The maximum temperature is reached in lower part of the drive loop and is equal to 95°C, with a corresponding maximum deformation of 0.1 mm [18] .

4.5 MEBT and DTL

4.5.1 MEBT Design

The MEBT line has been design with the aim of either matching the 50 mA (peak current) pulsed beam from the RFQ to the DTL and transport the 30 mA dc beam to the BNCT Target. The chosen lattice is as simple as possible: five nc magnetic doublets and two longitudinal focusing pill-box bunchers for the line to the DTL and four nc magnetic doublets for the line to BNCT. As shown in Fig.4.16, the line to the BNCT target starts almost from the centre of the MEBT with a 90° degree bend: this choice is made in order to have a very short MEBT ensuring a high beam quality to the DTL and, at the same time, to restrict the interferences between the BNCT facility and the RFQ-DTL building.

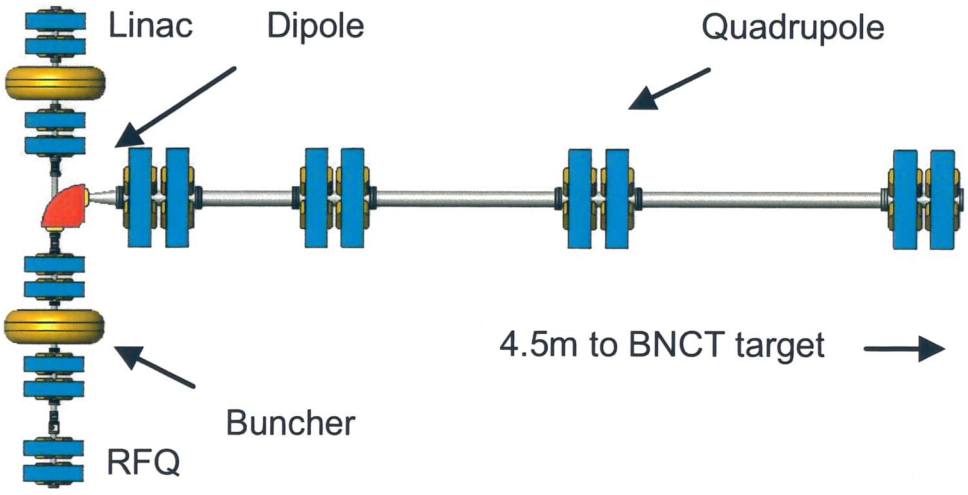

Fig. 4.16: *MEBT and BNCT line overview.*

Table 4.4: MEBT characteristics (line to BNCT from the dipole to the last doublet).

Line to		DTL (50 mA peak)		BNCT (30 mA dc)	
Total length (m)		3.15		5.9	
No. Doublets		5		4	
Length (mm)		100-70-100		150-100-150	
Bore radius (mm)		20		50	
Max env. (mm)		7.5		20	
Max gradient (T/m)		25		10	
		In	*Out*	*In*	*Out*
$\varepsilon_{n,RMS}$	x (mm.mrad)	0.204	0.208	0.217	0.709
	y (mm.mrad)	0.201	0.204	0.212	0.215
*ΔE/E	z (deg.MeV)	0.253	0.240	*0.83%	*1.9%

4.5.2 *Line to DTL*

The flexibility needed for the two current (and purposes) regimes is obtained using normal conducting doublets with independent power supply for each magnet. The bunchers position has been carefully chosen looking at either the matching capability and the safest operating condition from the phase envelope point of view, since the longer is the distance between the bunchers, the longer is the resulting focusing effect but the wider is the maximum phase width at the second cavity location.

The beam simulations have been carried out transporting the RFQ out distribution through the line monitoring envelope width, emittances and halo. After a deep optimization we obtained:

- a bore over RMS ratio greater than 9 inside the buncher and greater than 10 elsewhere (Fig.4.17);
- the transverse RMS emittances growth contained in 2% of the initial value;
- a redistribution of the longitudinal plane that reduces the RMS emittance of 5.5%.
- negligible transverse beam halo increase.

A preliminary error study shows no beam losses up to 0.5 mm of uniformly random off axis displacement of the line magnets.

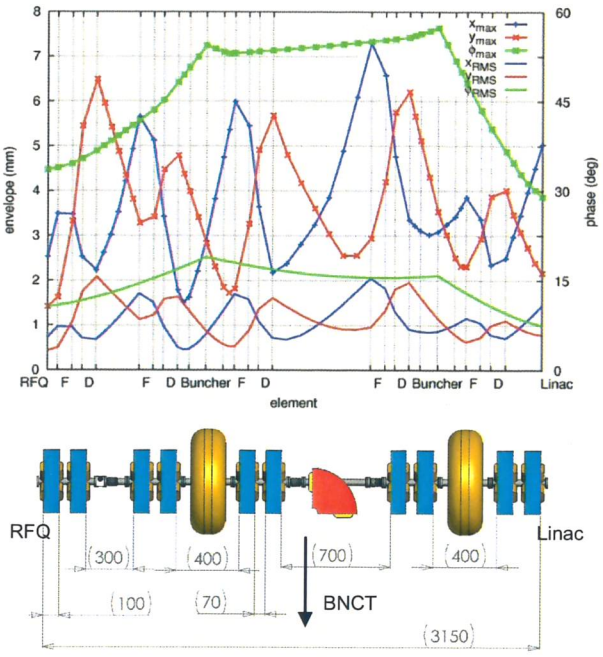

Fig. 4.17: *The beam envelopes (RMS and max) and some line specifications in mm.*

4.5.3 *Line to BNCT*

The full current beam to BNCT has to reach the high power (150 kW) Be target for neutron production under development at the Efremov Institute [19]. Due to the limitation on the power density on the target, the beam has to arrive with a large spot and a well determined distribution. Therefore the solution is to have a waist of the beam after the last magnetic doublet and consequently a large magnification on the target.

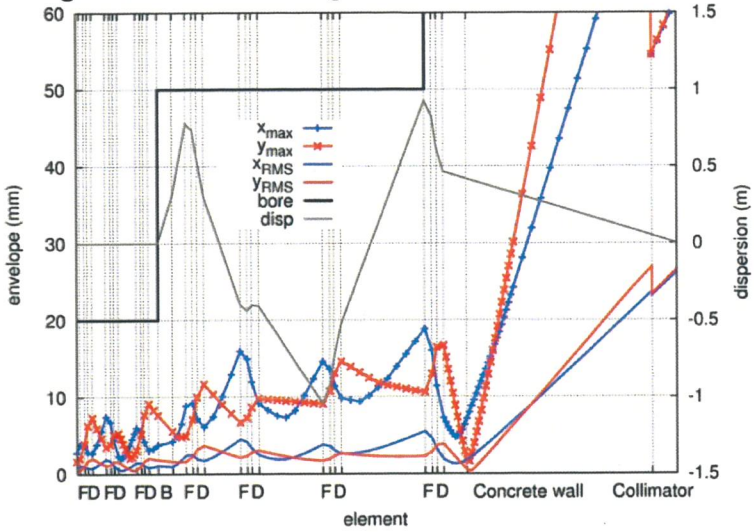

Fig. 4.18: *The envelopes and the dispersion function for the line to BNCT.*

To avoid for the energy distribution of the beam to have a broadening effect on the horizontal profile at the target, the energy dispersion is forced to vanish on the target. As shown in a very low dispersion angle (-92 mrad) and a small dispersion envelope were obtained, ensuring small coupling between longitudinal and transverse phase planes. Therefore, there is a very low probability of undesired beam loss along pipe.

Simulating the line with the RFQ output distribution as input, the choice of the last two doublets has been made in order to have a beam spot on target with axial symmetry, with a maximum width of 62 mm and a RMS radius of 26.5 mm and with the aim of keeping the losses on the collimator as low as possible.

4.5.4 *The Drift Tube Linac*

The proposed structure for the main linac is a Drift Tube Linac of Alvarez type, operating in TM_{010} mode. Pulsed DTL are operating in most of the main high energy Physics, Nuclear physics and neutron science laboratories; the latest linacs built are characterized, as for SPES, by an operating frequency above 300 MHz and a duty cycle exceeding 3%.

The beam focusing in SPES DTL is guaranteed by permanent quadrupole magnets with alternated polarity (FFDD scheme) hosted in the accelerating tubes. The use of permanent magnets, besides reducing number of power supplies and the complexity of the control of the machine, allows the use of smaller drift tubes and the achievement of a higher shunt impedance; the beam has to be matched to the periodic focusing channel operating on the electromagnetic quadrupoles of the MEBT.

The cooling system of the resonator is dimensioned for a duty cycle of 10%, so to leave open the development toward a higher power linac. The cooling water temperature is used for the tuning of the resonant frequency.

In the first column of Table 4.5 the main characteristics of the linac up to 43 MeV are listed, while detailed parameters of the first five tanks are listed in Table 4.6. This linac fulfils the requirement of the direct target, with a large margin in beam current. Moreover in the third and

forth column the possible upgrade of the linac in energy (up to 95 MeV) are considered; in this way the original SPES linac requirements (>100 kW for neutron converter operation) can be met.

Table 4.5: Main DTL parameters

RF frequency	352.2	MHz
Repetition rate	50	Hz
Pulse length	0.600	ms
Beam duty cycle	3	%
Average current	1.5	mA

	RFQ	**DTL**	**DTL upgrades**		
Energy	5	43	60,8	95,5	MeV
Frequency	352,2	352,2	352,2	352,2	MHz
Ave. Acceleration	0,7	2,5	2,3	2,1	MeV/m
Max Field	1,8	1,6	1,3	1,3	Ekp
RF Power	0,8	4,03	2	4,1	MW
Nb. of Klystrons	1	2	1	2	
length	7,13	15,2	7,6	16,3	m

Table 4.6: Parameters of the first five DTL Tanks up to 61 MeV.

	Tank 1	**Tank 2**	**Tank 3**
Output energy [MeV]	23.82	43	60.76
Frequency [MHz]	352.2		
Gradient E_0 [MV/m]	3.10	3.10	3.10
Synchronous phase [deg]	-35/-20	-20	-20
Lattice	FFDD		
Aperture radius [mm]	10		
Diameter [m]	0.52		
Drift tube diameter [mm]	90		
Length [m]	7.53	7.68	7.59
Max surface field [kilp.]	1.6	1.23	1.15
Peak RF power [MW]	2	2	2
N. of klystrons	1	1	1
Quadrupole length [mm]	45		
N. of gaps	55	35	28
Stem diameter [mm]	28		
N. of post-couplers	27	17	14
Post coupler diameter [mm]	20		
Frequency tuning	Water temperature		
Fixed tuner diameter [mm]	90		
N. of fixed tuners	10	10	10

4.5.5 Mechanical design

The design of the cavity takes advantage from the experience and the studies done at CERN in the last years for LINAC4[20]. Indeed the main requirements of this linac (like the operating

frequency, the duty cycle) are in common with LINAC4; the different input energy (3 MeV for CERN and 5 MeV for LNL) allows avoiding the most demanding part for focusing strength and peak electric field. Therefore, except for the details in the dimensions and position of drift tube, the cavity design can be the same for CERN and LNL.

In particular the power couples developed for CERN, based on slot coupling and planar RF window are adopted. These devices have been already tested at full power for the CCDTL cavity model.

Concerning the mechanical design of the accelerating structure, the original CERN proposal is based on the results of the ISTC research program with two Russian Laboratories, ITEP and Sarov. At the same time CERN and LNL experts we have jointly investigated the possibility of an industrial production in EU. The main choices of SNS DTL [21] (operating at 402.5 MHz with energy range 2.5-86.8 MeV) have been used to verify the feasibility of such industrial production in Europe and to obtain a first construction time and budget estimate.

More recently in the frame of the R&D programme for the Linac4 project, a novel mechanical design for a Drift Tube Linac (DTL) at 352 MHz has been developed. The advantages of this new design are simpler assembling, better long term stability and lower cost as compared with other DTL designs.

LNL participates directly to this R&D effort, contributing to the construction of the high-power prototype required to validate the new design. CERN will provide the mechanical drawings, the raw material, the weldings and surface treatments and the final testing at the CERN test stand, while LNL is taking care of the mechanical construction.

In Fig. 4.19 the DTL prototype construction is shown. The drift tubes are in bulk copper, with e-beam welded water channels to allow full power RF tests. The rigidity of the system is guaranteed by the thick iron tube (copper plated) of the tank structure. The precision of the alignment of the drift tubes (about 0.1 mm) is reached with the machining of the aluminium drift tube girder on the top. Concerning the permanent magnets installation in the drift tubes a first prototype has been developed in the framework of ISTC programme. In this construction the magnet is in air and the drift tube is closed using laser welding. This approach minimises the possibility of trapped volumes in vacuum. As an alternative a simpler construction will be developed leaving the permanent magnets in vacuum, as successfully in operation for SNS Linac.

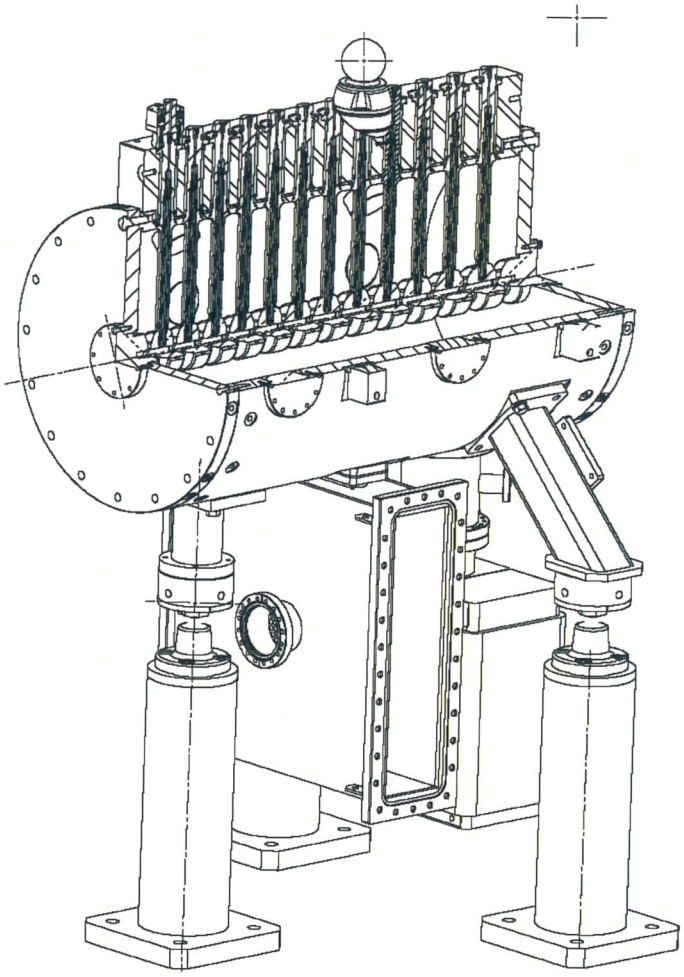

Fig. 4.19: *High power prototype of the DTL structure under construction for SPES and Linac4 linacs.*

4.5.6 Beam dynamics

The beam dynamics design and simulation of the DTL is an integrated process done by using a specific Excel sheet with macros [22], SuperFish, Toutatis and Parmela.

Beam dynamics considerations influenced the choice of the structure parameters from the first conception stage. The main guidelines were the control of losses, the minimization of the emittance growth as well as the minimization of the halo development. In order to achieve this, much care was put in keeping the following constraints :

1. a zero-current phase advance always below 90, for stability;
2. a longitudinal to transverse phase advance ratio (with current) between 0.5 and 0.8 in order to avoid emittance exchange
3. a smooth variation of the transverse and longitudinal phase advance per meter.

The continuity of phase advance for meter is kept to avoid creation of transverse mismatch. This continuity can be achieved by the Excel macros or directly by the simulation code TRACEWIN.

The longitudinal beam dynamics is done ramping the synchronous phase from -35 deg to -20 deg at the end of the first tank. The larger (in module) initial phase is needed in order to accommodate the input beam. In all other tanks the phase is kept constant at -20 deg.

The Excel file also creates the 34 geometry files of drift tubes for SuperFish, in order to calculate the TTF, shunt impedance and the peak surface fields for the range of energy from 5 to

100 MeV (Fig.4.20). The maximum surface Electric field is 1.6 kilpatrick. The input files for the simulation codes TRACEWIN and PARMELA are also created by Excel. Calculations performed with PARMELA make use of the complete electric fields given by SuperFish. They agree quite well with the corresponding TRACEWIN calculations in which a thin gap in the center of drift tube was used to simulate the fields. In all case the simulations were done with 10000 macroparticles, and no losses where observed

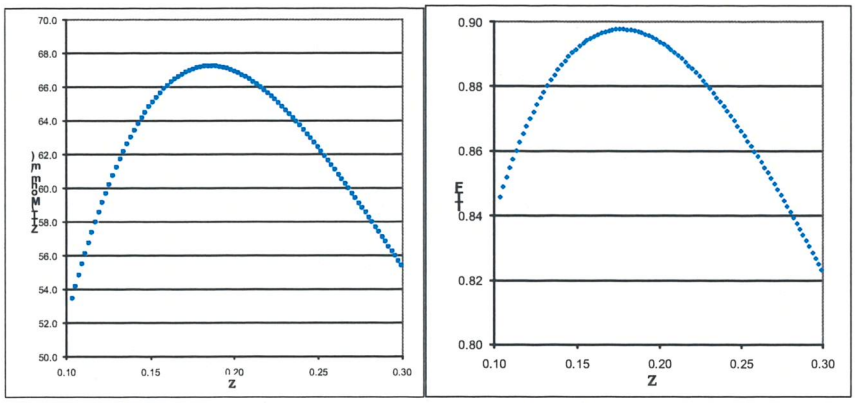

Fig. 4.20: *ZT^2(MΩ/m) and TTF as function of β in the range 5-43 MeV.*

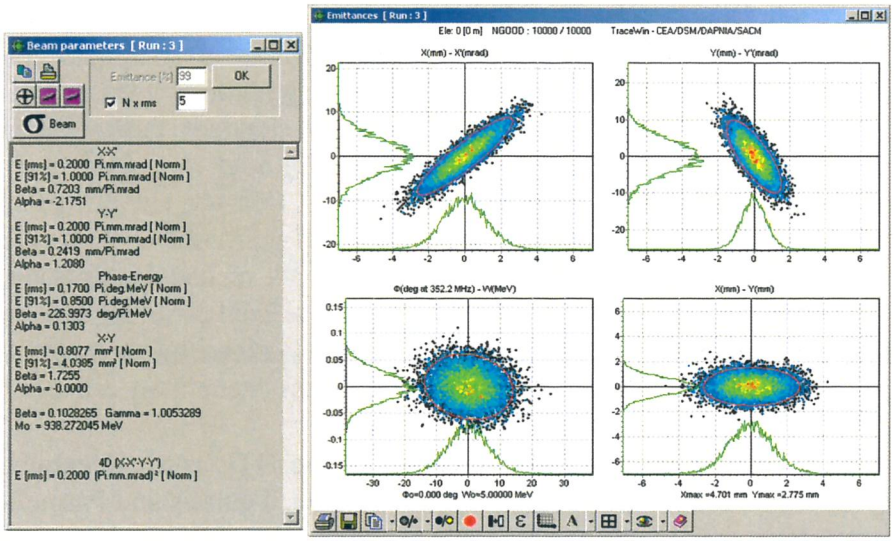

Fig. 4.21: *Matched input beam in the DTL (Gaussian distribution).*

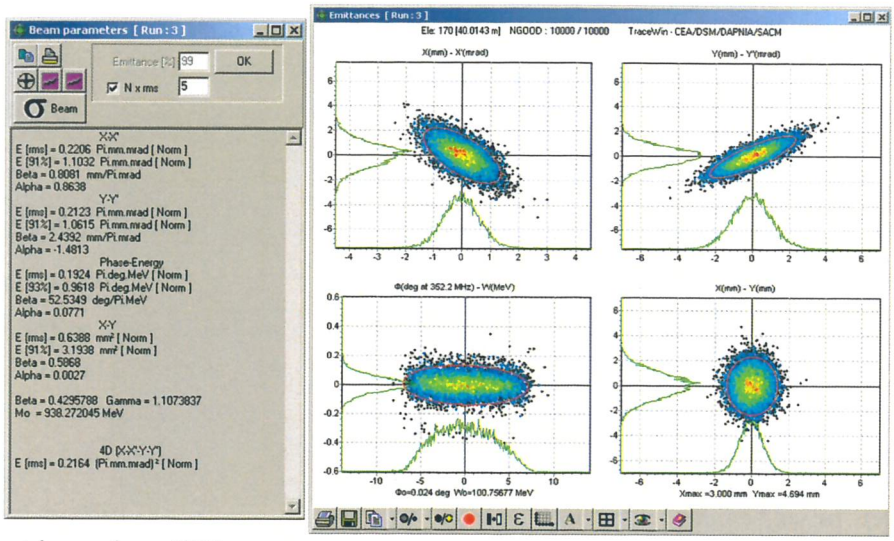

Fig. 4.22: Output beam from DTL.

The input and output rms normalized transverse emittances are 0.2/0.22 mm-mrad (riferimenti sbagliati) and the rms input/output longitudinal emittances are equal to 0.17/0.19 MeV-deg (Fig.4.23) by TRACEWIN, slightly higher the emittance results obtained by using PARMELA.

The beam Halo effect is described from the halo parameter hx: it evolves from 1 (gaussian beam) to 1.21 at the end of DTL for the transverse plane and 1.5 for the longitudinal plane.

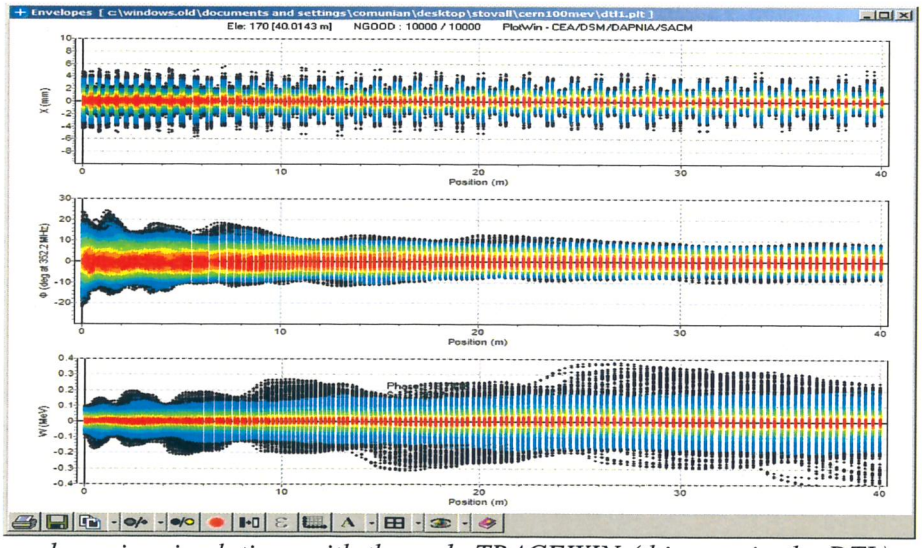

Fig. 4.23: Beam dynamics simulations with the code TRACEWIN (thin gap in the DTL) up to 100 MeV. The 10000 macro-particles transverse and longitudinal coordinates are plotted.

4.6 RF Systems

As described in the previous paragraphs, the driver linac has two working regimes: 35mA CW up to 5 MeV for the BNCT application and 50mA peak (with duty cycle up to 3%) up to 43 MeV for the injection in the target. The two systems differ in the power converter used for the RFQ and in the RF power sources employed: in fact, if in cw operation, a "slow" (some tenth of ms rise/fall time) modulator is needed in order to feed the modulating anode of the klystron, this does not hold anymore for pulsed operation, where a pulse forming network (with about 100 μs rise/fall time) is required. Indeed, for pulsed operation for the DTL, pulsed klystron will be used.

All the remaining components (waveguide distribution system, loads etc.) remain the same and therefore they will be described only for the CW case.

In the following the power budget for the RF system components will be calculated by the following expression, that takes into account appropriate margins

$$P_{RF} = (P_{Cu} \cdot \alpha_1 + P_b) \cdot \alpha_2$$

where P_{Cu} is the theoretical power dissipated in the structure calculated by 2D codes (SUPERFISH), P_b is the beam power, α_1 is a coefficient that takes into account the 3D details of the structure and α_2 is a coefficient that takes into account the losses in the waveguide system, reflected power etc. In our case both coefficients are assumed to be equal to 1.2.

4.6.1 RF System for the CW case

The RF power budget for the CW RFQ is equal to about 900 kW. It will be generated by one klystron and supplied to the RFQ by a WR2300 waveguide system. Due to the fact that each RF coupler is rated for a maximum of 140 kW power [23] , the RF power will be split in eight ways, according to the scheme of Fig.4.24 [24].

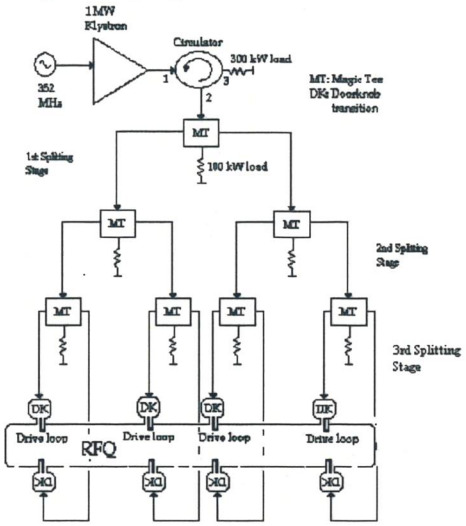

Fig. 4 24: *schematics of the RF distribution system.*

The klystron and its power supply (including crowbar, modulator, capacitors etc.) as well as the RF equipment will be housed in a separate hall with respect to the linac. In November 2006 the RF equipment (klystrons, circulators, 100 kW and 300 kW water loads, waveguides transitions and components) was delivered from CERN.

Fig. 4.25: The EEV klystrons stored at LNL.

The two klystrons (one as a spare) that will be used for feeding TRASCO-SPES RFQ were manufactured by the EEV Company (model K3513) and were used for LEP operations. The main klystron parameters are summarized in Table 4.7.

Tab. 4.7: Main klystron parameters

Maximum Output Power	1.3 MW
Operating Frequency	352.21 MHz
-1 dB Bandwidth (minimum)	1 MHz
Efficiency	65% (@ 352.21 MHz)
Drive power at rated output power	130 W
Beam Perveance	0.63 $\mu A/V^{3/2}$
Gain	40 dB
Load VSWR	<1.2:1
Typical e^- Beam Voltage	100 kV
Typical Mod Anode to cathode voltage	90 kV
Typical e^- Beam Current	20 A
Heater voltage range	22-28 V r.m.s.
Heater current range	22-26 A r.m.s.
Focus current range	5-10 A(main coils)
Focus current range	8-10 A(output coils)
Ion getter pump voltage range	3-5 kV
Ion getter pump operating current	0.1-2 μA

Each klystron is equipped with a modulating anode by means of which the cathode current can be controlled up to 20A, thus permitting the output power regulation in cw. The water cooling requires the usage of pure demineralized water and the body cooling inlet temperature must lie in the interval 25±2 °C, in order to get the correct tuning pattern of the klystron during operation, while mineral oil is requested to protect the electron gun.

The DC to RF conversion efficiency of the klystron determines the power requirements for the power supply and its related high voltage interface. If the klystron is run at maximum power the power supply should be capable to furnish about 2MW of DC power.

The high-voltage interface for the klystron in cw mode is inspired to the layout used for the LEP2 (Fig.4.26) with the tetrode operated as a triode and over-current protection system based on a thyratron crowbar. The achievement of the ±1% ripple on the voltage, as requested by beam dynamics can be obtained by means of a 2μF smoothing capacitor [25][26].

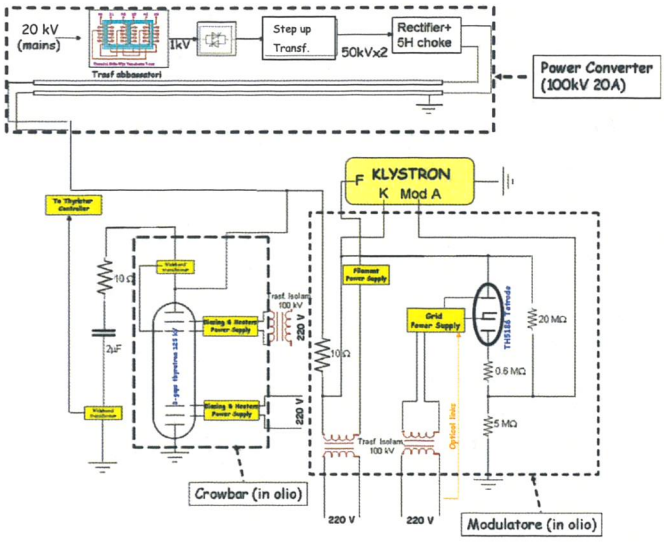

Fig. 4.26: Principle scheme of the cw power converted for the klystron.

The main parameters of the power supply are listed in Table 4.8

Table 4.8: Main input and output Power Converter parameters

Output characteristics	
Voltage amplitude [kV]	100
Current amplitude [A]	20
Flat-top voltage ripple [%]	0.1
Flat-top voltage droop [%]	1
Input characteristics	
Mains	3-phase, 20 kV, 50 Hz
Power consumption [kW]	2000
N. of converters	1

In order to protect the klystron from excessive reflected power than can propagate backwards, a Y-junction waveguide circulator (used as an isolator) will be employed (Fig.4.27). One arm of such circulator is connected to a 300 kW, 6 meters long coaxial water load, which permits the absorption of the reflected power.

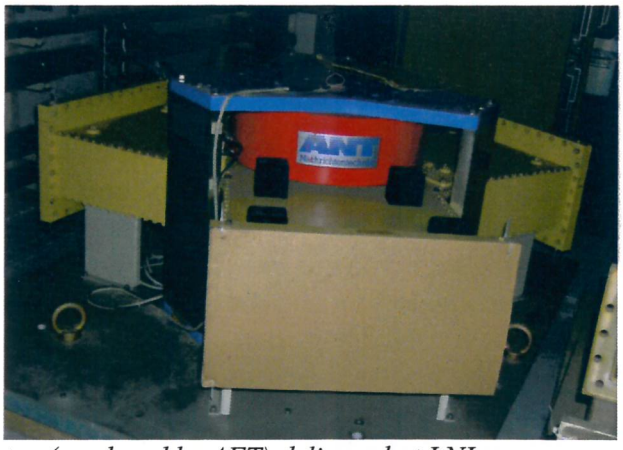

Fig. 4.27: The LEP circulator (produced by AFT) delivered at LNL.

In order to correctly split the RF power, magic-Tee hybrid junctions will be used. The dummy arm of each splitter will be terminated via a waveguide to coax transition by a 50 Ω, 100 kW water load. Reflected RF power is absorbed in the demineralized water which circulates in these coaxial loads. Indeed, in order to ensure that all the input for the couplers are in phase, the electric length of each path has been adjusted with capacitive matching posts located at the input port of each magic-Tee divider, whose dimensions have been optimized with HFSS simulations. Moreover, as the RFQ acts as a power combiner, high power three-stub motorized phase shifters at each waveguide arm are foreseen to be installed to make adjustments when needed in an interval of ±22.5° around the nominal value.

4.6.2 RF System for the pulsed case

The power budget of the RF system for the pulsed case has to take into account the peak power requirements for the RFQ and the DTL as well as the pulse duration. As for the RFQ, it has to be considered that the beam current for injection in the DTL is equal to 50 mA. Therefore peak RF power requirement for the RFQ becomes equal to 1.015 MW and to 4.836 MW for the DTL. In the following the parameters of the system will be rated for maximum flat-top pulse duration of 600 μs, corresponding to an average beam current of 1.5 mA. A good approximation of the average RF power rating that takes into account also the rise and fall time of the RF pulse can be obtained as it follows:

$$P_{RF} = \left(P_{Cu} \frac{2\tau_p + \tau_{on} + \tau_{off}}{2} f_p \alpha_1 + P_b \tau_p f_p \right) \cdot \alpha_2$$

where τ_p, τ_{on}, τ_{off} are respectively the flat-top duration and the rise and fall time of the pulse, while f_p is the pulse repetition rate. Therefore, upon assuming a rise time of 100 μs and a fall time of 150 μs, the average RF power required is equal to 35 kW for the RFQ and 161 kW for the DTL.

The availability of 2.5 MW pulsed klystrons permits to simplify the RF distribution scheme to the DTL, by making use of a couple of such klystrons for feeding the entire structure. Such klystrons, are an adaptation of the one developed by TOSHIBA being used for the 324 MHZ J-PARC linac (type E3740A OP 352), where 23 klystron were tested and put into operation, reaching the specifications [27] .

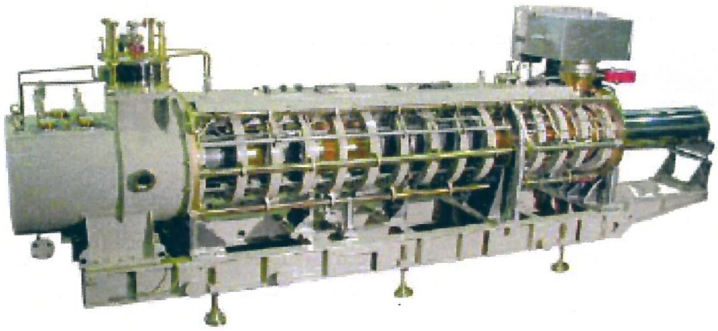

Fig. 4.28: *The TOSHIBA type E3740A pulsed klystron.*

The main parameters of such klystron are listed in the following table

Table 4.9: Main parameters of the 2.5 MW pulsed klystron

Output Power	2.5 MW
Operating Frequency	352 MHz
Pulse duration (rf)	620 μs
Efficiency	55% (@2.5 MW)
Drive power at rated output power	30 W
Beam Perveance	1.37 $\mu A/V^{3/2}$
Gain	50 dB
Load VSWR	<1.2:1
Typical e^- Beam Voltage	102 kV
Peak Mod Anode to cathode voltage	87.2 kV
Peak e^- Beam Current	44 A
Heater voltage range	9-15 V
Heater current	26 A
Focus current	20 A
Focus voltage range	20-375 V
Ion pump voltage	3.8 kV

In order to feed each klystron of the DTL, an unique High Voltage Power Supply (HVPS) can be used, with separated modulating anode pulsed modulators. It consists of a step-down transformer (20 kV-1 kV), the thyristor unit, the step up trnasformer (1 kV-110 kV), the rectifier, the ripple filter and a crowbar circuit against overcurrents. The power supply feeds the same voltage to each klystron cathode and the pulsed modulators, derived from the cathode DC line, generate the voltage pulse. This approach corresponds to the one employed at the J-PARC facility [28] , where this kind of HVPS underwent a long-run test [29], but in the case of the SPES linac, due to the lower power ratings required, some parameters can be relaxed. In fact, in our case, the overall peak power needed to feed the DTL klystrons is equal to 8.793 MW, corresponding to 293 kW average power, while for the RFQ the corresponding values are 1.846 MW and 64 kW respectively. Another scenario foresees the usage of a 50 Hz adapted version of the power converters for LINAC 4 [30] (presently used with 2 Hz rep. rate), with an increased number of switches and an improved pulse transformer. This development is also necessary at CERN for the use of LINAC4 as injector of SPL.

The main requirements of the pulsed power supply are the following

Voltage amplitude [kV]	110
Current amplitude [A]	90 (180 for J-PARC)
Rise-time [ms]	0.10
Fall-time [ms]	0.15
Flat-top duration [ms]	0.60
Repetition rate [Hz]	50
Flat-top voltage ripple [%]	0.1
Flat-top voltage droop [%]	1
N. of converters (including the RFQ)	2
Total n. of converters (including the RFQ)	3
Total power consumption, nom. operation (including the RFQ) [kW]	356

From all these considerations, the principle scheme of the RF system for the pulsed case is in shown in fig. 4.29. The proposed lay-out of the lines, with the maximum use of the wave guides elements already available, is shown in the next section.

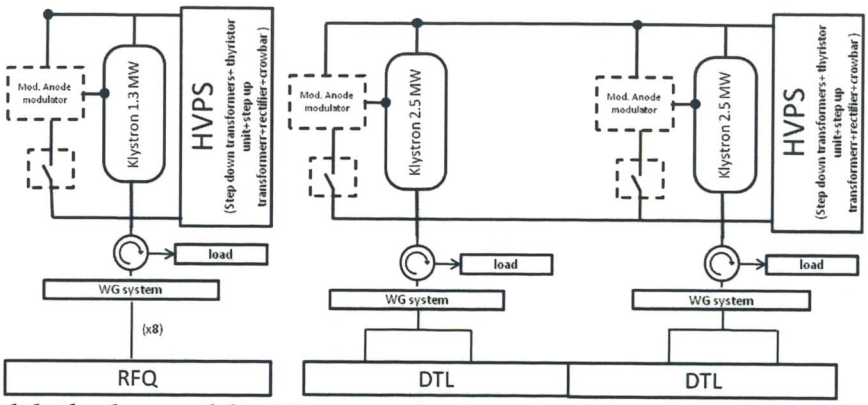

Fig. 4.29: *Simplified scheme of the RF system for the pulsed case.*

4.7 The building and the infrastructures

The installation of a high current linac requires a building composed by two parts with quite different characteristics: the accelerator tunnel hosts the ion source, the accelerating structure, the beam lines and very few equipments, and the service hall for the RF system (klystrons, modulators, and associated electronics, power distribution, the primary cooling loop for the frequency control, the magnets power supplies, the diagnostics racks and all the necessary electronics for the control system.

While the linac tunnel is characterized by a heavy biological shielding (with thickness increasing with beam energy), the service hall can be a light construction where the operators can reach the equipments during machine operation. The two parts are connected by wave guides, cooling tubes and cables passages, realized with suitable labyrinths to minimize the radiation leakage in the service hall.

Moreover in the building there is a downloading part, to prepare the accelerating structure ready to slide into the tunnel, the halls for the BNCT facility and an experimental hall for other neutron application (Lenos).

Outside the building space should be left for the large transformers and for the primary cooling circuit (about 4 MW).

In fig. 4.30 a possible layout of the linac building up to 43 MeV is shown. The linac tunnel can be 4m wide and 3 m high, the service hall 14 m wide and 6 m high. The DTL part is modular, so that one more module is needed for 61 MeV and two more for 96 MeV.

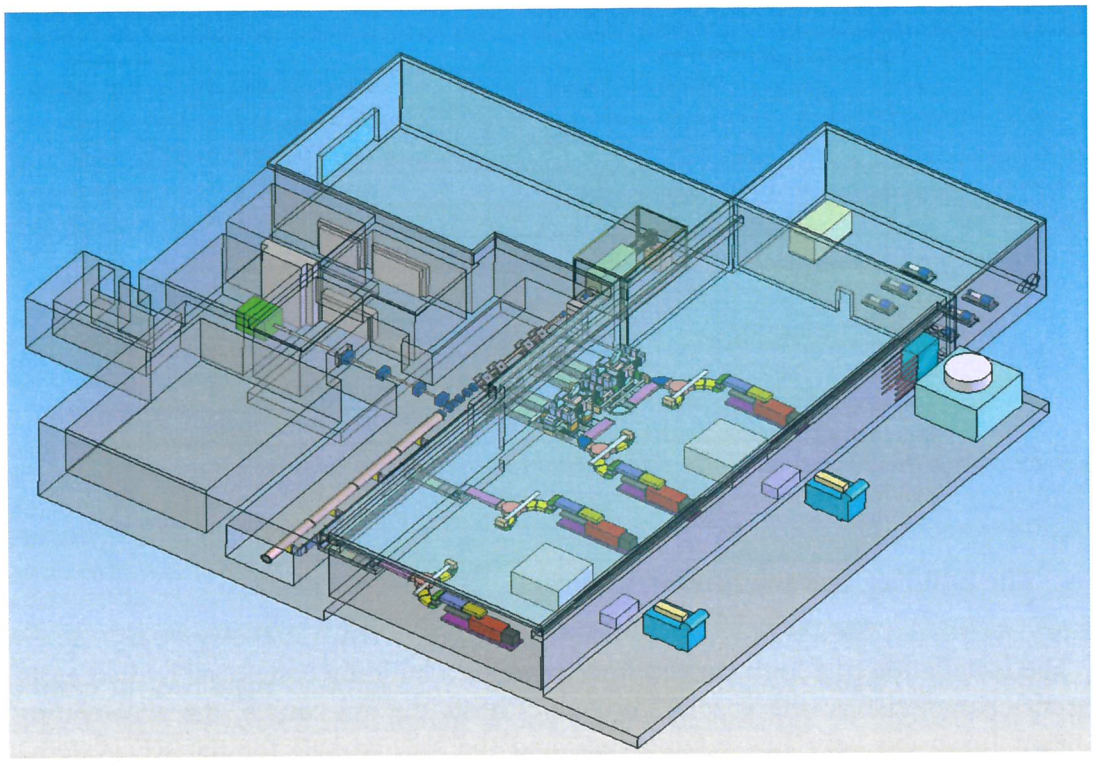

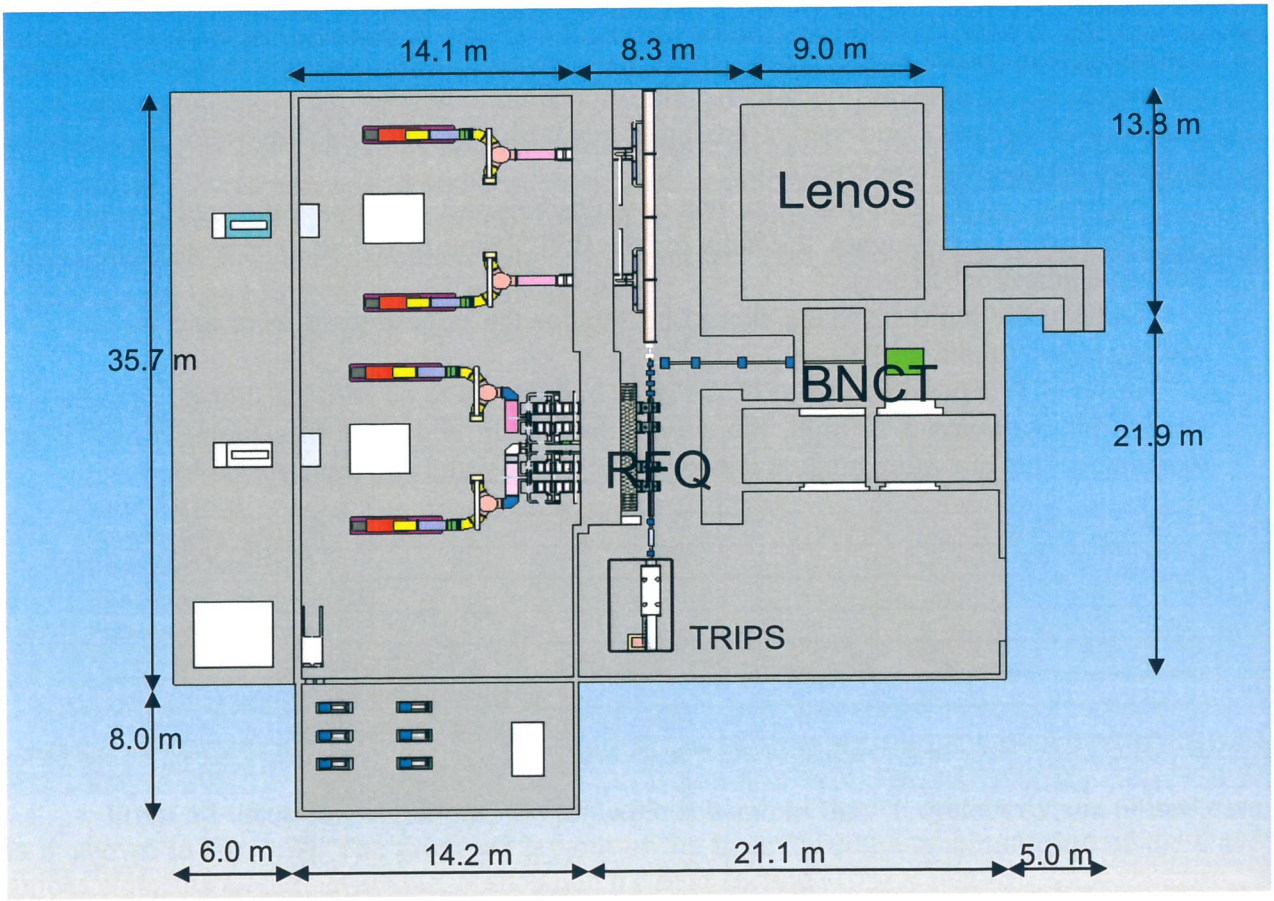

Fig. 4.30: *preliminary layout of the building for the 43MeV Linac: on the left, the klystron hall, at the centre the linac tunnel, on the right the BNCT facility and the LENOS experimental hall.*

4.8 Conclusions

The primary accelerator described in this chapter fulfills the requirements of RIB production, that have substantially changed respect to the previous TDR, integrates the well advanced work on the high intensity injector (source and RFQ), allows the future expansion towards a high power linac.

While many parts of the driver linac, like the proton ion source, the RFQ structure or the RF klystrons, are already designed and built, other components like the DTL structure and the high power RF system and power supplies have to be developed in more details. This work is for many aspects strictly related to the freezing of the lay-out for the construction of the buildings.

For what concerns the operation the linac is a high intensity machine, so that very clear operation procedures (developed during the commissioning) have to be followed. These procedures have to be implemented in a very robust control system. On the other hand it is a single energy single intensity machine, and therefore in operation it should be controlled in the main SPES control room as part of the facility without requiring dedicated operators in shift.

---

[1] INFN-LNL Rep. 181/02.
[2] S. Cevolani et al. LNL annual Report 2006 p. 161.
[3] L. Celona, G. Ciavola, S. Gammino, R. Gobin, R. Ferdinand, Rev. Sci. Instrum., 71 2, 771 (2000).
[4] G. Ciavola, L. Celona, S. Gammino, F. Chines, C. Campisano, Rev. Sci. Instrum., 73 2, 1030 (2002).
[5] P. Spädtke, AXCEL Version 3.43, INP, Wiesbaden, October 1998.
[6] R. Becker and W. B. Herrmannsfeldt, Rev. Sci. Instrum., 63, 2756 (1992).
[7] E. Fagotti, M. Comunian, A. Pisent, "Design of the SPES-1 LEBT", Proc. LINAC04 Conf., Lübeck (Germany), August 2004.
[8] L. M. Young, J. H. Billen, "PARMELA Version 3" Los Alamos National Laboratory report LA-UR-96-1835 (revised June 16, 2005).
[9] G. Ciavola, L. Celona, S. Gammino, E. Fagotti, M. Comunian, A. Pisent, Proc. LINA02 Conf., Gyeongju (Rep. Korea), 18-22 August 2002.
[10] E. Fagotti et al., Annual Report 2005, INFN-LNL 210(2006), 150.
[11] E. Fagotti, A. Palmieri et al., Annual Report 2006, INFN-LNL 217(2007), 189.
[12] E. Fagotti, A. Palmieri, S. Marigo, X. Ren, Annual Report 2006, INFN-LNL 217(2007), 191.
[13] E. Fagotti, A. Palmieri, X. Ren, "Enhancement of SPES Source Performances", Rev. Sci. Instrum., 79 2, (2008).
[14] A. Pisent et al " The TRASCO-SPES RFQ" Proc. LINAC04 Conf., Lübeck (Germany), August 2004.
[15] A. Palmieri et al LNL Annual Report 2006 p. 193.
[16] G.V. Lamanna, A. Palmieri, A. Pisent, S. Fu, O. Huafu " Field Tuning of TRASCO RFQ" Proc. EPAC02 Conf., Paris (France), April 2002.
[17] F. Grespan, A. Palmieri, A. Pisent "" Proc. EPAC06 Conf., Edimburgh (UK), June 2006.
[18] A. Palmieri et al. Proc. LINAC 02, Gyeongju (Rep. of Korea), August 2002.
[19] A. Makhankov et al, "An Accelerator-based Thermal Neutron Source for BNCT Application", 593-THPLT111 , EPAC 2004.
[20] LINAC4 Technical Design Report (F. Gerigk and M.Vretenar edt.) CERN-AB-2006-084 ABF/RF
[21] T. Ilg, R. Martineau, J. Sims, W. Fox, S. Ellis, R. Gentzlinger, L. Rowton, G. Johnson, Proc. PAC03 Conf., Portland, Oregon (USA) May 12-16, 2003.
[22] J. Stovall, Tecsource, unpublished.
[23] A. Palmieri et al " Study and design of The TRASCO RFQ High Power Coupler" Proc. LINAC02 Conf., Gyeongju (Rep. of Korea), August 2002.
[24] A. Palmieri LNL Annual Report 2006 p. 195.
[25] H. Frischholz "The LEP II RF Power Generation System" .Proc PAC 93 Conf., Washington (USA), May 1993.
[26] H. Frischholz et al. "The High-voltage Interface for the LEP 2 RF Power Generation System" Proc. EPAC94 Conf., London (UK), June 1994.
[27] T. Kobayashi et al, Proc. PAC 07 Conference, Albuquerque (USA), p. 2128
[28] hadron.kek.jp/~accelerator/TDA/tdr2003/chap3/3.1.3.4.pdf
[29] hadron.kek.jp/~accelerator/ATAC07/pdf/1a05.pdf
[30] project-spl.web.cern.ch/project-spl/documentation/l4tdr.pdf

CHAPTER V

DIRECT TARGET

4.1 The target concept

Three important parameters are required to optimize a fission ISOL target: first of all a high number of fission reactions (to provide high RIB intensities), then a low power deposition in the target materials (to avoid melting temperatures) and finally a fast isotope release time (to improve extraction efficiency). The main problem for the 1-step configuration concerns the power deposited by the incident beam in the production target, mainly due to the electromagnetic interactions. In order to solve this issue, only the protons with higher ^{238}U fission cross-section are exploited. As a matter of fact, the ^{238}U fission cross-section and the stopping power have opposite dependency on the proton energy, as shown in fig. 1 [2-4]. The low energy protons are less efficient for a production target because they have lower fission cross-section and higher values of stopping power.

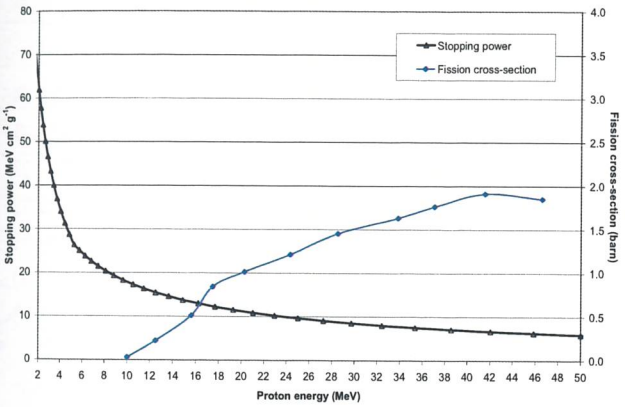

Fig. 5.1: *Stopping power and fission cross-sect for protons on UC_x*

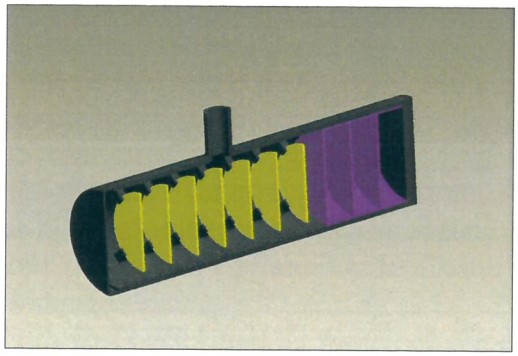

Fig. 5.2: *Reference target configuration (the UC_x disks are shown in yellow)*

If the low energy protons (for example with energy lower than about 20 MeV) are driven towards a passive dump, then the power deposited in the target is lowered considerably and at the same time the number of fission reactions is maintained high.

Even if high energy protons involve less dissipated energy per length and a longer range, they increase sensitively the cost of the apparatus. Moreover, the ^{238}U fission cross-section does not increase considerably for energies higher than 40 MeV. That is the reason why we chose this value for the primary proton beam.

In order to optimize the heat dissipation and the release time of the fission products [4a], a good solution is the use of a target made of multiple disks [5]: the target is splitted into several thin disks in order to allow the cooling of the system (by thermal radiation) by increasing the total exchange surface. The advantage of this configuration is the simplicity of the cooling system and the consequent relatively low cost.

The reference diameter of the target disks is 6 cm, but recent thermal simulations indicate the possibility to decrease the diameter down to 4 cm.

The detailed parameters used for the system are (see fig. 2) [6]:

- the incident 40 MeV proton beam has a current of 0.2 mA. The beam profile spans uniformly over a circle distribution, which matches the disk radii;
- the window, necessary to separate the beam line from the target void regions, is made of one (or two) thin carbon foil of 400 μm total thickness;
- the UC_x target (ρ=2.5 g/cm^3) is made of seven disks about 1.3 mm thick each;
- the beam dump is made of three carbon disks about 0.9 mm thick each;
- the box containing the disks is made of graphite.

4.2 The in-target yields

The following results are obtained through several MonteCarlo calculations (MCNPX code [7, 8] with the ORNL model) performed for the target configuration described in the previous section. It turns out that a power of 0.19 kW is deposited in the window, 4.1 kW in the seven UC_x disks, 1.7 kW into the three dump disks and 2.2 kW is lost outside the disks (due to proton scattering). Thus, the average power deposition for the UC_x target disks is about 4.1 kW / 7 disks = 0.58 kW. The power deposition with its radial profile in the disks is reported in fig. 3.

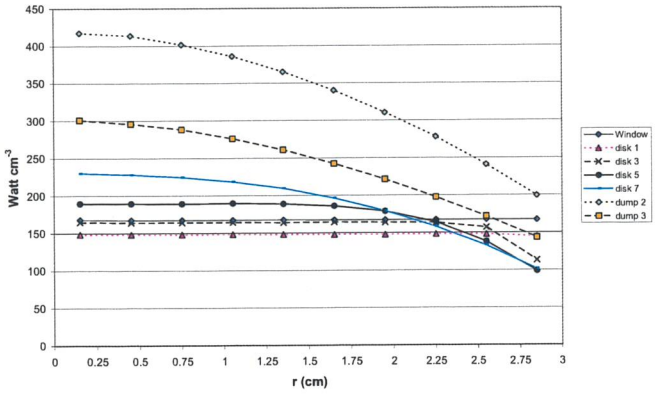

Fig. 5.3: *Radial distribution of the power deposition in the disks (without considering build up and decays*

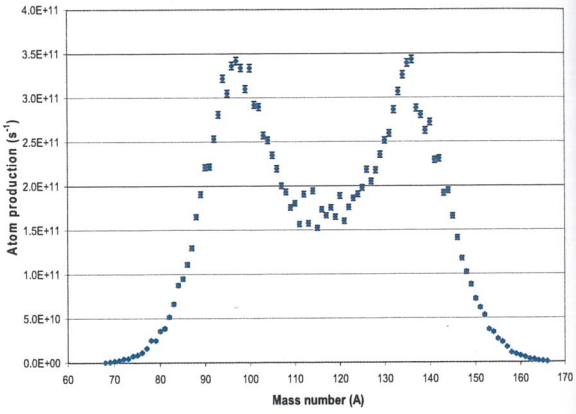

Fig. 5.4: *Fission mass spectra yields*

As expected, the radial profile is uniform in the window (following the entering uniform beam profile) and it becomes less and less flattened in the last disks, because of the proton scattering.

The total calculated fission rate in all the seven disks is about $1 \cdot 10^{13}$ fissions s^{-1}. The peak-to-valley ratio in the mass number distribution of the fission products, that is very pronounced in thermal neutron induced fissions at about A=115-120, is here only about a factor of 2 (see fig. 4).

The isotope in target production reaches values up to ~10^{11} atoms/s. The ^{132}Sn isotope, being a double-magic nucleus, is one of the radioactive nuclei of interest. Its production is here estimated to be ~$1 \cdot 10^9$ s^{-1}. A more general view of the in-target yields is given in fig. 5.

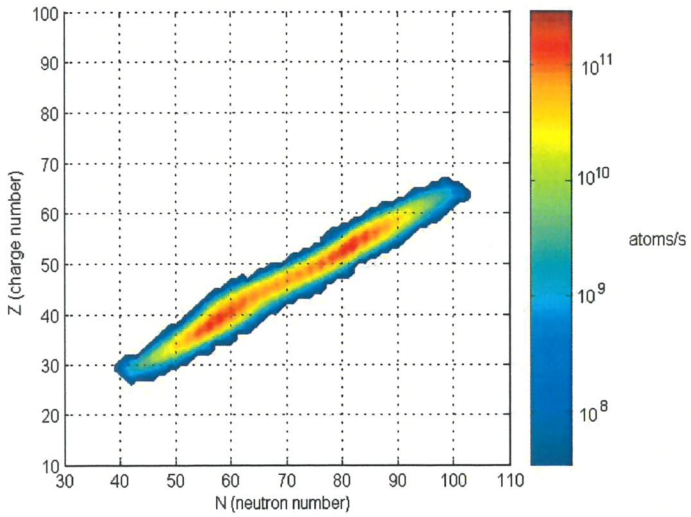

Fig. 5.5: Representation of the in-target isotope production.

4.3 The target thermal analysis

The power distribution shown in the previous section has been used for a target thermal analysis. The power is deposited in the target components (*i.e.* target disks, dump disks and box) mainly due to the beam-materials interaction. Due to the low pressure environment, this heat has to be removed by thermal radiation to the heat sink constituted by the chamber (see fig. 6). This process can be divided into two steps: the disks (of the target and of the dump) are radiating toward the box, which, in turn, will transfer the heat to the chamber wall, also by radiation. It has to be pointed out that the box has to be held at about 2000°C for optimizing the fission product extraction; the chamber wall will be at about room temperature.

The reference target steady state thermal analysis was performed by means of some *ad hoc* models and by using the ANSYS code; the results were mainly presented in [5, 6].

With respect to the disks, the analysis was mainly devoted to evaluate the maximum temperature, in order to warrant that no melting will occur. This analysis was performed by taking into account the actual power distribution both in the disk radial and axial (beam) directions. The results obtained for the UC_x disks show, even in the most heated disk, a safe margin with respect to melting. In the dump disks the temperatures are sensibly lower.

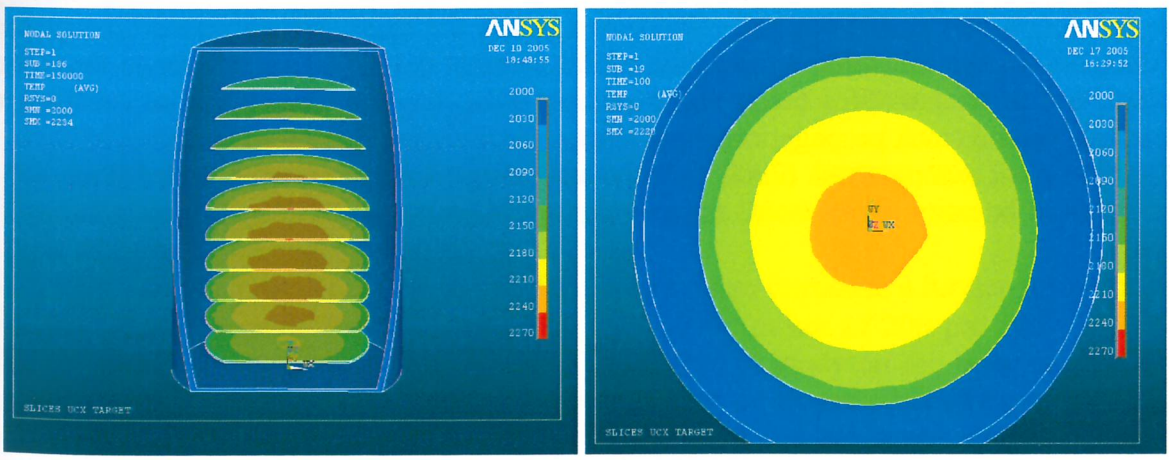

Fig. 5.6: Longitudinal and radial temperature distributions from ANSYS calculations.

With respect to the box, the heat deposited in the target is not enough to keep it at 2000 °C. This situation can be faced either by introducing thermal shields between the box and the chamber walls, or by adopting an independent power supply system for the box. The present proposal is to exploit both of these solutions: to introduce the power supply in order to face better the transient situation, and to insert the thermal shields in order to drive to some optimal amount the power to be supplied.

In the first calculations the chamber wall was assumed to be at room temperature; this situation can be easily achieved by adopting a simple water cooling system. Further investigations show the possibility to cool the chamber even by natural air convection: in this way the chamber temperature is increased but the effect on the target is negligible, particularly when thermal shields are present.

4.4 The target thermo-mechanical analysis

The disk thermo-mechanical state of stress was analysed referring to the previously calculated temperature distribution. A particular disk (the sixth) was chosen as representative of a adequately conservative operating condition. The calculation, however, was drastically simplified by the assumptions of elastic material and steady-state regime. Moreover, the UC_x physical properties are not sufficiently known and further measurements are to be carried out.

Differential thermal expansions are generated in each UC_x disk by the non-uniform temperature distribution originated from the distribution of the proton beam. The state of stress arising from such differential expansions was examined.

Different approaches were attempted and lead to similar results:

- an order-of-magnitude analysis [9];
- a numerical treatment of the equations of linear elasticity both in one- and two-dimensions [10,11];
- a commercially available code (ANSYS).

In this third approach, the disk has been generated by rotation of a rectangular area corresponding to ½ cross section view. The element used is a PLANE42 type, *i.e.* a basic 2D solid element supporting axis symmetry. Material properties and temperature distributions have been chosen to be comparable with those of the previous calculations. The state of stress at 2000 °C is represented by the isochromic of equivalent stress σ_{eq} reported in fig.7. The maximum tensile stress is σ_θ = 122 MPa, to be compared with the values 116 MPa (one-dimensional model) and 100 MPa (two-dimensional model). The maximum equivalent stress is σ_{eq} = 130 MPa at 2000 °C, to be compared with 138 MPa (two-dimensional model).

The conclusion is that the equivalent stress, when the operating temperature keeps below the ductile-to-brittle transition temperature of the material (1300 °C), is inferior to the value of fracture. But at temperatures below the transition point, the disk may be more susceptible to thermal shock and crack propagation; these modes of failure have not been analyzed hitherto.

At nominal temperature (2000 °C) the equivalent stress is low (~140 MPa), but the assumption of linearity is haphazard and the rheological properties of UC_x are poorly known.

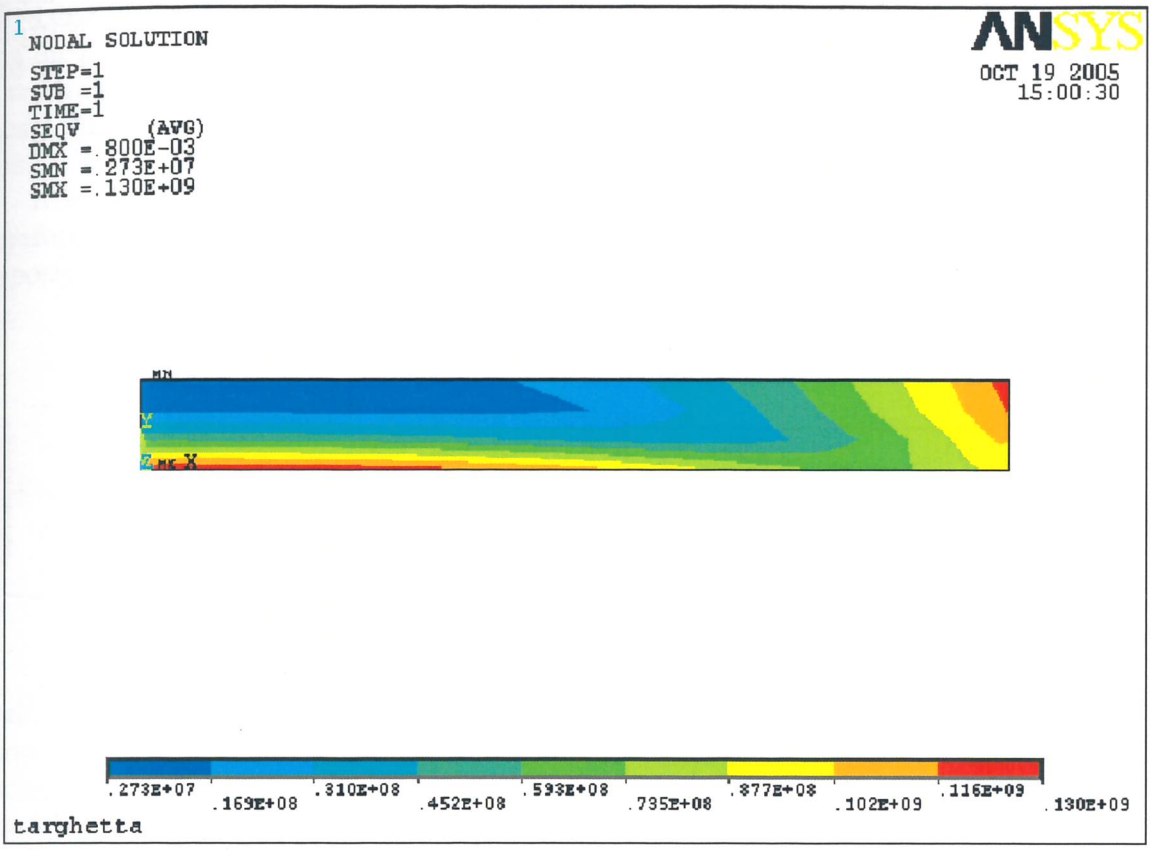

Fig. 5.7: *Equivalent Stress (Pa).*

The physical parameters adopted for thermo-mechanical analyses have been found in literature [12]. The elastic modulus E = 215 GPa is suggested for UC_x at room temperature, and it is put forward together with a matching value for the Poisson's ratio $\mu = 0.269$. A curve for the decrease in E for UC_x between room temperature and 1500 °C has been adopted from [12] and gives E = 176 GPa at 2000°C.

The mean thermal linear expansion coefficient of UC_x at 2000 °C was kept $\alpha_m = 12.4 \cdot 10^{-6}$ $°C^{-1}$.

As to fracture behaviour, UC is a brittle ceramic material which may be susceptible to catastrophic fracture at low temperature, but a brittle-ductile transition is expected to occur at some temperature in the range of 1100-1300 °C. It is assumed that, above this temperature, plasticity assures some relaxation of thermal stresses.

Fracture stress is given up to ~1300 °C only, where it is $\sigma \approx 200$ MPa.

The assumption of linearity seems rather adequate up to ~1300 °C, more questionable beyond. Therefore the study has been iterated at 1300 °C and 2000 °C. The first result (1300 °C) represents the brittle behaviour, while the second result (2000 °C) is a sort of 'best indicator' of what happens in nominal operation.

The use of a proton beam with a 50 Hz time structure introduce a further stress on the target as the mean current of 200 μA is obtained with 50 Hz pulses of 200 μs, 50 mA, 40 MeV. It means that each pulse has a peak power of 2000 KW. A study on the behaviour of the target system to this condition was performed by an "order of magnitude" approach and by Ansys simulation. The transient regime was evaluated both for the thermal and the mechanical properties of the disks. The result is that the time structure of the beam introduces a temperature oscillation with frequency-dependent amplitude [23]. The temperature variations are reported in

Tab.1. As the temperature inhomogeneity was evaluated in the order of 100°C due to the thermal behaviour of the system operated with a DC beam, a 10% themperature variation is expected if the beam repetition frequency is higher than 40 Hz. A quite safe value respect to the total thermal system evaluation.

Table 5.1

f [Hz]	ΔT [°C]
5	77
10	39
20	19
40	10
80	5

From the point of view of the equivalent stress, the pulsed beam introduce an oscillation of ≈10MPa, that is in the order of 10% of the total equivalent stress induced by the DC operating conditions. This result open new question on the fatigue of the the target disks, as experimental data are non sufficient to describe the criticity of the system, a research work is in progress to define the technique for high temperature characterization of materials.

4.5 Release time calculations

The final intensity of a radioactive ion beam depends on the efficiency of different processes: the target production yield, the target efficiency, the ionization efficiency, the transportation efficiency along the accelerator. In order to optimize the target efficiency it is very important to minimize the time needed by the radioactive species to join the ion source.

Several simulations have been performed using the GEANT4 toolkit [13], as well as the RIBO (Radioactive Ion Beam Optimization) code [14], in order to estimate the release time for some neutron-rich nuclei. The target temperature was 2000°C in all the simulations.

The main release mechanisms in an ISOL target is discussed in Chapter 3. The diffusion from the grains of the target materials, the effusion in the inter-grain space and the free-effusion are taken into account.

Additionally, each collision may involve an average adsorption-desorption time, t_s (sticking time).

Release time calculations were performed considering the release of the neutron rich atoms ^{132}Sn and ^{90}Kr.

In the calculations we assumed our UCx disks being made with standard ISOLDE UCx so the ISOLDE parameters have been used:

- average flight path in the powder FP = 15 μm,
- sticking time for Sn isotopes $t_s = 10^{-6}$ s,
- diffusion time constant for Sn isotopes $\tau_D = 1$ s
- diffusion time constant for Kr isotopes $\tau_D = 10$ s [15].

The average total effusion times t_{eff} = (0.41 ± 0.02) s and t_{eff} = (0.22 ± 0.02) s were calculated, for Sn and Kr isotopes respectively. Considering the average diffusion and effusion time the total release fraction was calculated for Sn and Kr isotopes as a function of the half-life, as reported in fig.8. The final total release fraction for ^{132}Sn is about 90% whereas the total release fraction for the short-lived ^{133}Sn is about 40%. The total release fraction for ^{90}Kr was found to be 80%.

It is clear that the diffusion time gives an important contribution to the total release time therefore it is very important to optimize the material structure of the target disks. To this purpose, an extensive study of the target materials is in progress at LNL.

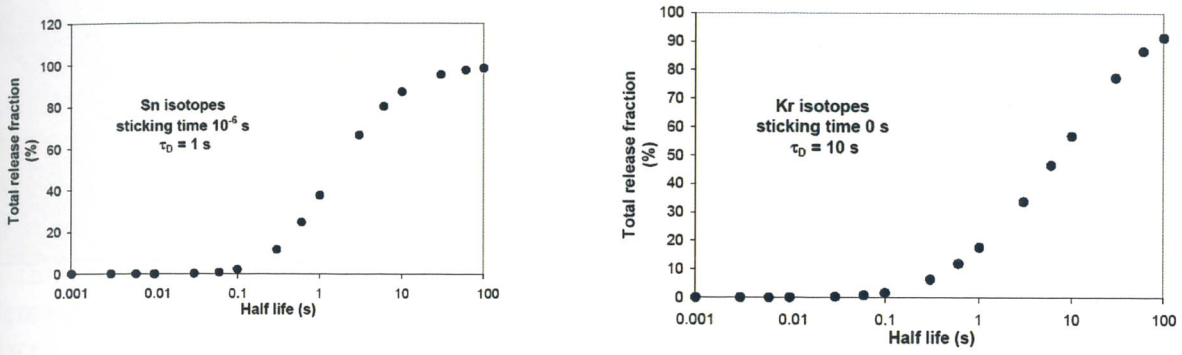

Fig. 5.8: Calculated total release fraction for Sn and Kr isotopes produced in UCx material

Experimental tests to be performed at ORNL and LNL are also planned in order to validate the simulations.

4.6 The target pellets development

Radioactive Ion Beam (RIB) production is deeply affected by the characteristics of the target impinged by the proton beam. The composition and the degree of purity of the constituent materials, the microstructure and morphology (i.e. crystalline phase, grain size, porosity) of the target are of particular importance to this purpose. The kind of isotopes produced, in turn, depends both on the energy of the incident beam and on the fissile material, whereas the efficiency release is mainly related to the isotopes diffusion inside the target and to their gas-phase effusion (molecular flow plus multiple ad-desorption) [16].

Both the diffusion and effusion of the radioactive species in/from the target strongly increase with the increase of the temperature. For this reason the target working temperature must be kept as high as possible, in order to grant atoms release faster than their decay. On the other hand, the working temperature of the target is limited by the vapour pressure of the target constituents, by the stability of the target at high temperatures and by possible reactions which may occur between the target and the target holder at high temperature.

For these reasons, refractory compounds like carbides and oxides have to be used as target materials in order to sustain these conditions. For the production of some of the RIB's planned in the SPES project, uranium and thorium fissile isotopes were already suggested and uranium and thorium oxides and carbides were accordingly employed. Mixtures of uranium oxide and graphite at high temperature showed particularly favourable release characteristics for many isotopes [17-19]. In particular, UC_x can be produced by reaction of a precursor (metal oxide) with a carbon based matrix (graphite powder or low density carbon foam generators) according to equation 2.

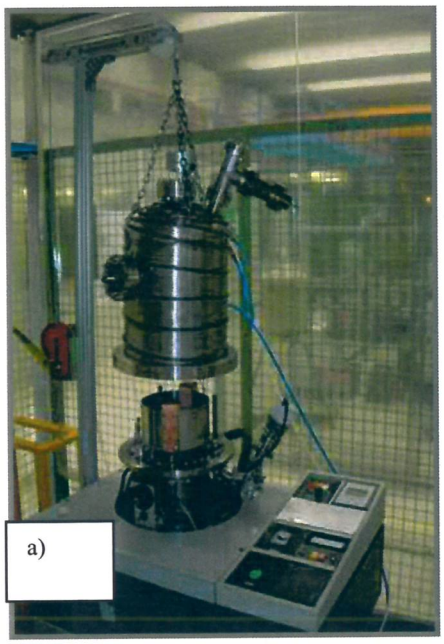

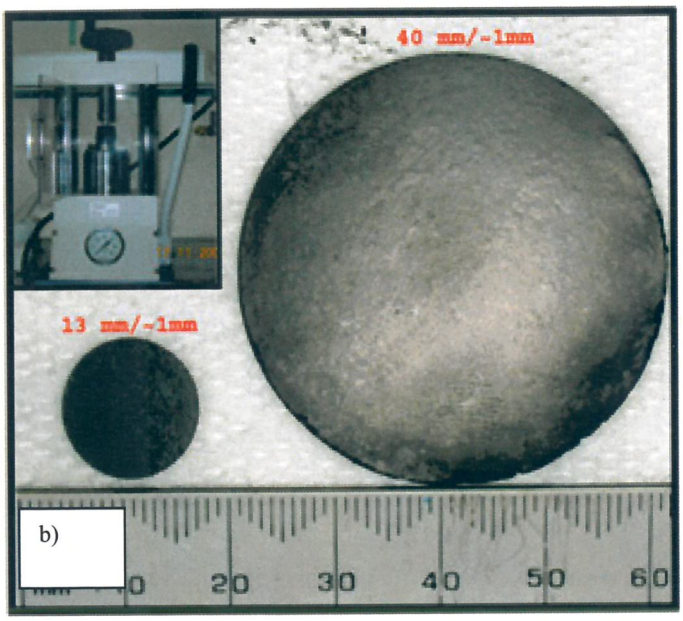

$$UO_2 + 4C + nC \rightarrow UC_2 + 2CO_{(g)} + nC \qquad (2)$$

Fig. 5.9: *Left, The evaporator assembled at LNL; right, picture of the 13-mm and 40-mm diameter pellets of LaC_2 dispersed in graphite before thermal treatment. In the insert the hydraulic press is shown.*

The formation of uranium carbide occurs under high vacuum at temperatures ranging from 1400 to 1700 °C. The gas released during carbothermal reduction (CO in eq. 2) is responsible for pores formation. Open porosity (interconnected structure) was demonstrated to improve isotope release [20]. Moreover, in order to obtain materials withstanding the extreme working conditions, sintering of the composite powder is a successive, necessary, step achieved at temperatures even higher than 1700 °C. The main goal here is to design a standard procedure aimed to the production of uranium carbide-based pellets with the best *online* performances. This can be achieved, by a careful characterization of pellets prepared by an optimized thermal treatment of several oxide and graphite mixtures, in different ratio and with dimensions ranging from nano- to micro-meters. In addition, similar procedures and characterizations will be extended to new promising porous, low-density ceramic materials (UC_x or LaC_x foams).

Handling radioactive material (even if of low activity like depleted uranium) requires special precautions, authorizations, and dedicated radiological controlled area to avoid workers and instrumentation contamination. All this often contrasts with the need to obtain results in a short time and indicated the usage of lanthanum dicarbide (LaC_2) as a valuable substitute of uranium compounds for preliminary bench tests on pellet production and characterization. Beside radiological aspect, preparation of pellets of lanthanum carbide and/or uranium carbide dispersed in graphite, present similar challenges in both synthesis and characterization. According to the schedule and priorities planned in the SPES direct target project, two production lines for 13-mm and 40-mm diameter pellets have been developed. In fig. 9 a) the evaporator assembly and b) a picture of the two kinds of pellets are reported. The insert shows the hydraulic press used for the pellet production.

At present, the production of disks of diameter 13 mm and thickness 1 mm made of LaC_2 dispersed in graphite is the most advanced. The disks are produced by mixing an appropriate amount of lanthanum oxide, graphite and polyphenol resin as binder, the green pellets are pressed and heat treated under vacuum. The heat treatment schedule has been designed as

consequence of Differential Scanning Calorimetry (DSC) analysis performed on the starting mixture, X-Ray Diffractometer (XRD) and SEM-EDAX investigations of samples carburized and sintered at different temperatures (see fig. 10).
At present, pellet carburization and sintering has been achieved.

Fig. 5.10: *(A) Scanning Electronic Microscope (SEM); (B) X-ray diffractometer (XRD); (C) TG/DSC thermal instrument.*

In fig. 11 the SEM micrograph obtained from the surface of a La-C sample after treatment at 1800°C, under Ar flow is reported. The images on the right in the figure show that EDAX elemental analysis performed with a narrow spot on different areas of the specimen is able to discriminate the different chemical compositions.

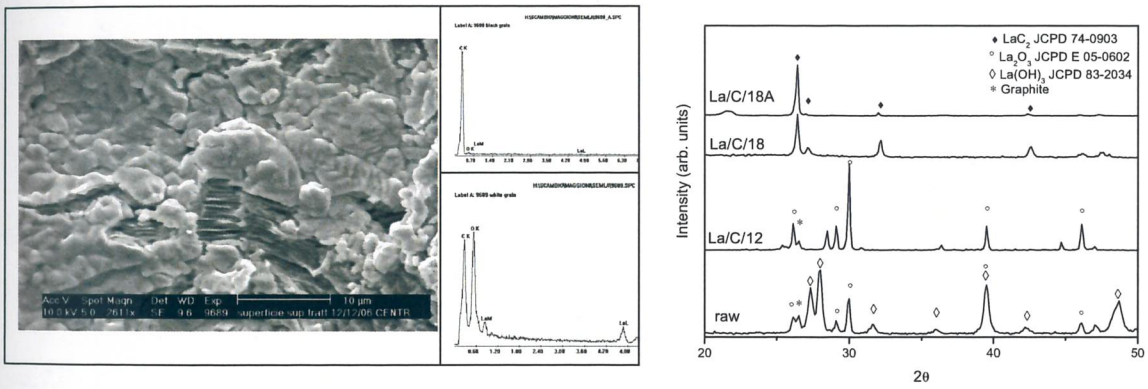

Fig. 5.11: *Left, SEM-EDAX analysis on LaCx samples after heat tretaemnt and;right, the process evolution by XRD measurements*

In order to improve and control the pellets porosity some raw samples were prepared by adding resin microspheres to the original powders mixture as sacrificial filler.

Three main routes are nowadays available for the production of porous materials: *a*) the replica technique: a polymeric sponge is impregnated by a slurry of appropriate composition, the system is then dried and the polymeric sponge burnt-off; *b*) the direct foaming technique: a foaming agent is introduced into a suspension of appropriate composition; *c*) the sacrificial templates technique: a sacrificial component with selectable shape and size is introduced in the system and then burnt-off, leaving empty spaces.

In the future production of LaC_x and UC_x pellets the different techniques will be employed to vary the sample porosity (from <10 %, dense target, to 70-80%, typical value of foams) and the pore dimensions and shape (spheroidal, acicular). In particular, the porosity will be realized either by means of sacrificial fillers (PMMA based micro-spheres that decompose completely

during the thermal treatment) or by direct foaming methods (mixing the raw materials with a low-temperature evaporation solvent) or with the replica technique (polymeric foams covered by ceramic powder and treated at high temperatures). In this way, it will be possible to acquire the necessary know-how to control not only the shape and dimensions of the pores but also their morphological characteristics: passage from a closed to an open structure would significantly improve the target permeability. All the correlations between the observed effusion properties of the *on line* targets and their structural properties will be exploited in order to improve technology of the pellet production.

4.7 The target chamber design

4.7.1 The target-ion source unit

We have adapted the engineering principles embodied in the target source modules used at CERN-ISOLDE for remote and safe handling [21]. The attractive feature of this approach is that loose contamination is enclosed in a relatively compact system. The target unit is made of a graphite box containing the UCx, windows and dumps (both in graphite) disks, and is contained in a tantalum cylinder which is resistively heated by passing a high current through it in addition to the heat supplied by the irradiating beam. A Tantalum tube (trasfert tube) connects the target unit to the ion source according to the ISOLDE concept (possibility to plug in many kind of ion sources).

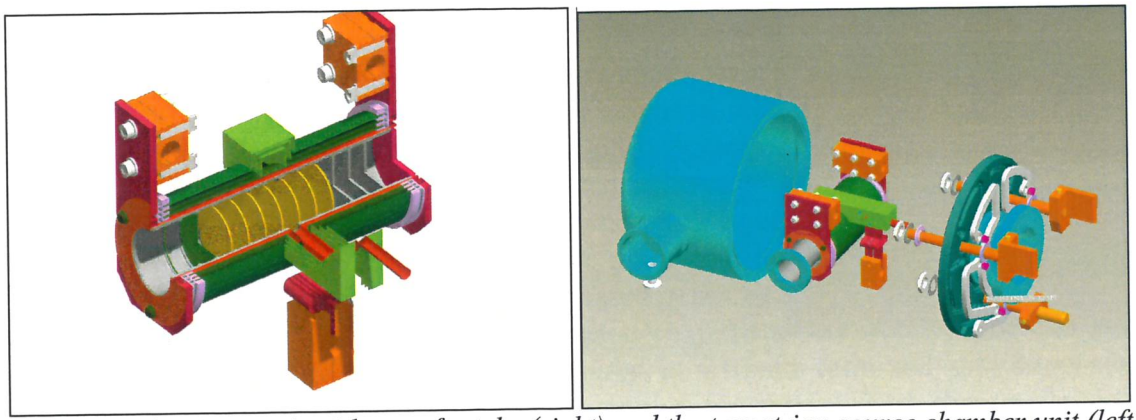

Fig 5.12: *The target unit with transfer tube (right) and the target-ion source chamber unit (left).*

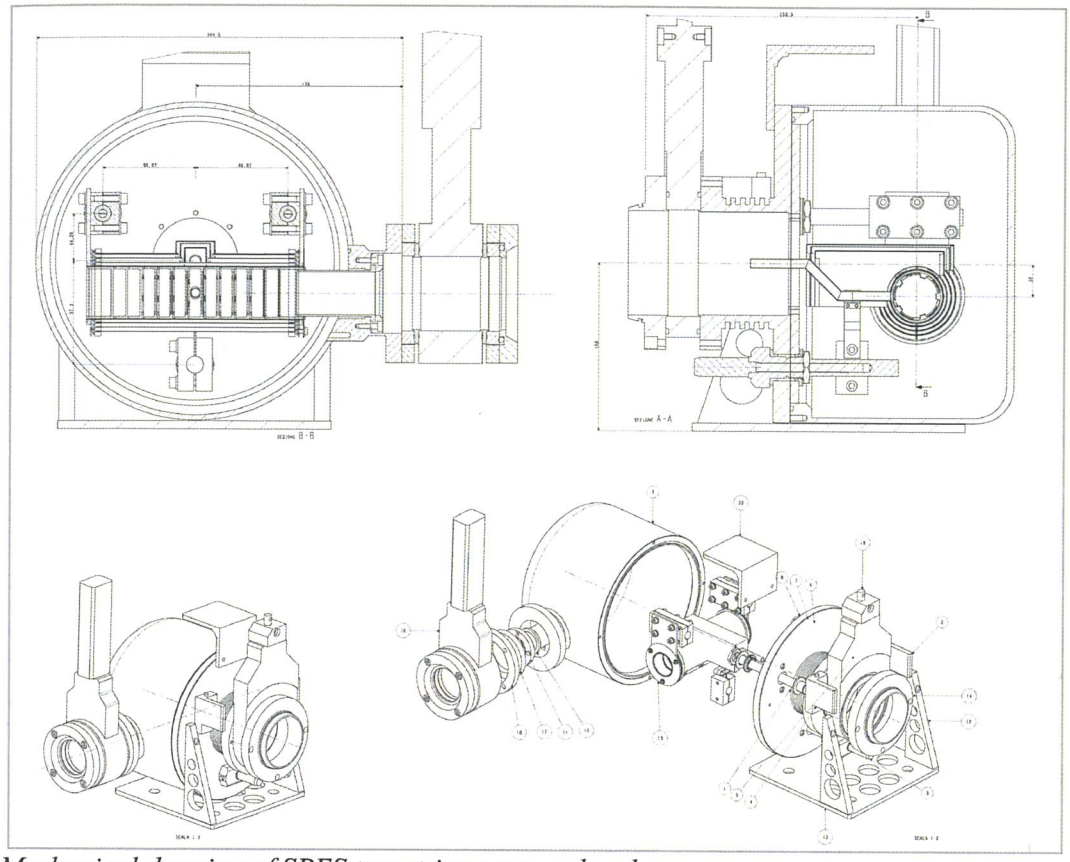

Fig. 5.13: *Mechanical drawing of SPES target-ion source chamber.*

The SPES target and ion source are mounted on vacuum feed-through situated in a water-cooled base plate and enclosed by an aluminium bell jar. Two valves isolate the system. A drawing of the target unit and the target-ion source chamber are shown in fig. 12 and 13.

4.7.2 The target chamber handling

The SPES target ion sources chamber can be removed for servicing or storage by disconnection from, or reconnection to the beam transport system. The unit is coupled to the injector and to the separator by means of two quick connectors and two pumping ports which can be sealed off with a valve. Since the target can be used several times, it will be stored into a container with thick (2 cm) lead walls while not used. The handling system, then, must be designed in order to transport such heavy container into the area where the target will be used, open the container and connect the source chamber to injector. After the experiment, the source chamber must be at first removed from the injector, then stored in the container and finally sent out of the "hot" area for further handling and long term storage.

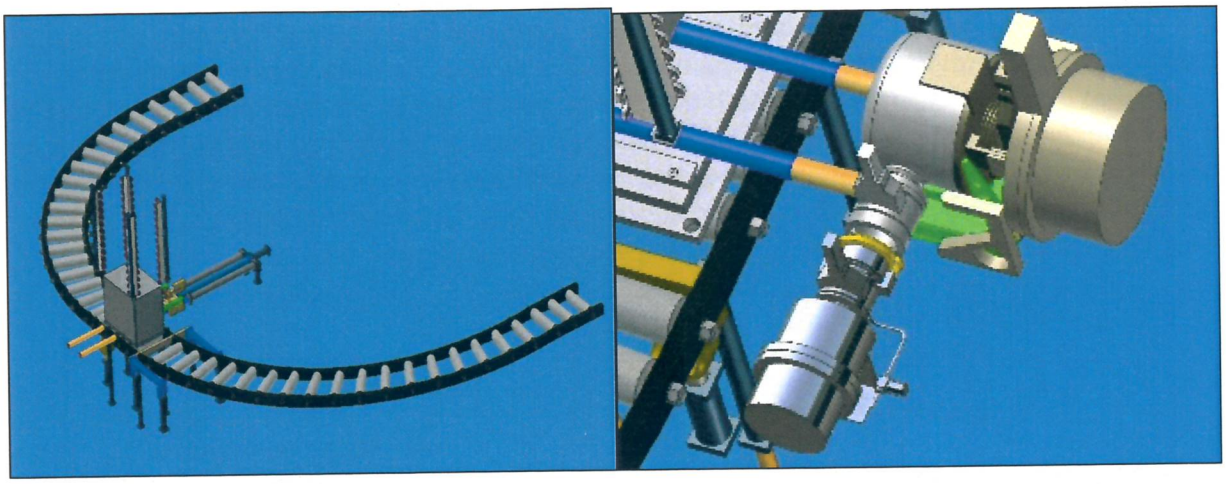

Fig. 5.14: *The conveyor for the target container and (left) and SPES target-ion source chamber coupled to the primary and RIB beam lines (right)*

Fig.14 shows the proposed handling system, composed of a semi-circular conveyor, on which the container slides. The container stops in front of the irradiation area and here it is opened and the target moved toward the injector, by using a self-aligning, high precision insertion system. After the experiment, the target is re-stored in the container, which is closed before being pushed out of the radiation area.

4.8 The target prototype

In order to develop the final SPES multifoil direct target a research program has been activated to test the target configuration with proton beams of suitable energy. The elective facility to perform these tests is HRIBF (Holified Radioactive Ion Beam Facility) at ORNL [22]. HRIBF is indeed based on a primary beam of protons at 40 MeV with current up to 20 μA. The first step in this program is to develop a target prototype with dimensions scaled to 1:5 with SiC disks (see fig. 15).

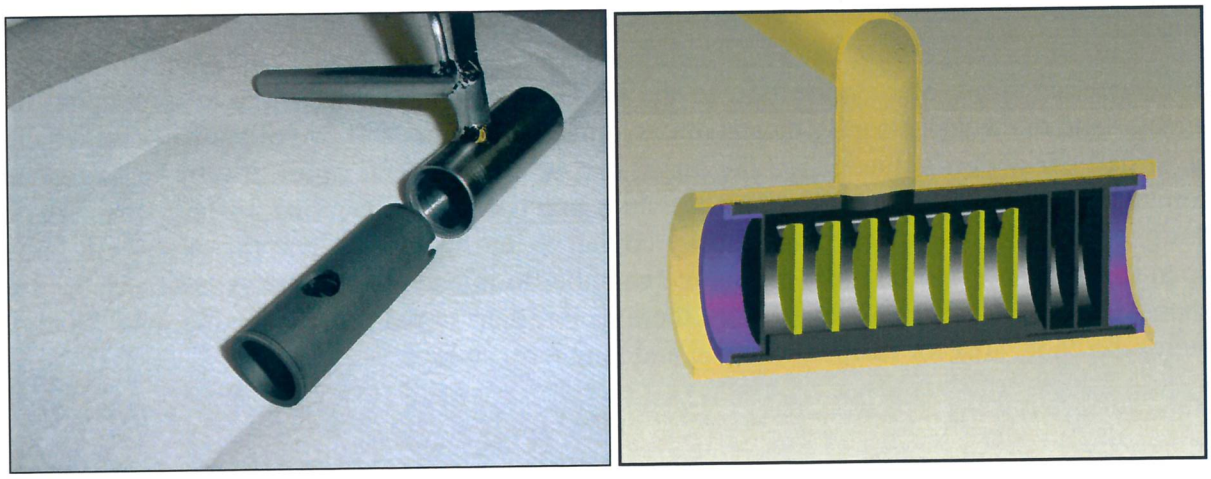

Fig. 5.15: *SiC SPES target prototype tested at HRIBF.*

This prototype fits inside the HRIBF target holder, allows testing the main ion release characteristics and gives the first experimental thermal behavior of the multi slide configuration in a condition of nominal power density up to about 600 W/g. The use of SiC target is devoted to the production of exotic aluminum beams, ^{25}Al and ^{26}Al , which are isotopes of astrophysical interest both at HRIBF and EXCYT.

The preliminary data of the first test performed in december 2006 with a SiC disks confirm the good prediction of the thermal simulations.

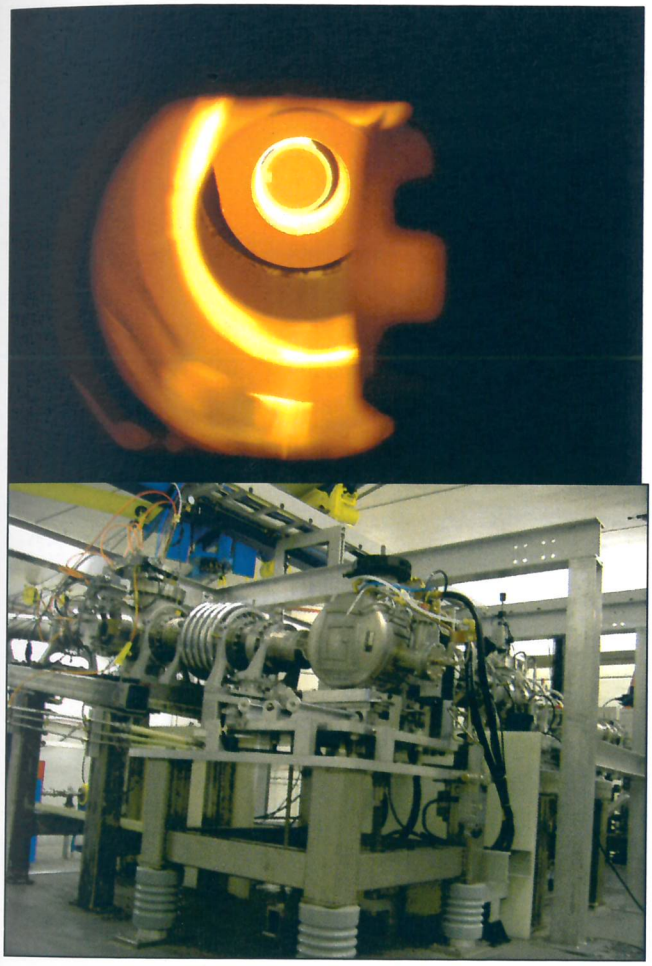

Fig. 5.16: *SiC SPES target inside the target heater (left) and the target area at HRIBF (right).*

A comparison between different target configurations and materials will be done. The first one is the standard HRIBF target, made of pressed powder or pills; the second one the multi-slide configuration proposed here.

[1] A. Andrighetto, Proceeding of Exon 2004 Internatioal Conference (2004).
[2] P.C. Stevenson et al., Phys. Rev. **111** (3), 886 (1958).
[3] S. Baba et al., Nucl. Phys. A **175,** 177 (1971).
[4] B.L. Tracy et al., Phys. Rev. C **5** (1), 222 (1972).
[4a] M.Re et al. RNB7 conference proceedings, Cortina, Italy, July 2006, in publication
[5] A. Andrighetto, S. Cevolani, C. Petrovich, Eur. Phys. J. A **25**, 41 (2005).
[6] A. Andrighetto, C. Antonucci, S. Cevolani, C. Petrovich, M. Santana Leitner, Eur. Phys. J. A **30**, 591 (2006).
[7] Denise B. Pelowitz (Editor), MCNPX™ User's manual, Version 2.5.0, LA-CP-05-0369 (2005).
[8] H.W. Bertini, Phys. Rev. 131 **4**, 1801 (1963).

[9] A. Andrighetto, C.M. Antonucci, S. Cevolani, C. Petrovich, ENEA contribution to the design of the thin target for the SPES project, FIS-P815-020 (ENEA, 2006), http://www.bologna.enea.it/pubblicazioni.html .
[10] Timoshenko, Goodier, Theory of Elasticity (McGraw Hill, 1970).
[11] Z. Zudans, T.C. Yen, W.H. Steigelmann, Thermal Stress Techniques in the Nuclear Industry (Elsevier, 1965).
[12] Hj. Matzke, Science of advanced LMFBR fuels (North Holland, 1980).
[13] S. Agostinelli et al., Nucl. Instr. Meth. A 506, 250 (2003).
[14] M. Santana Leitner, A Monte Carlo Code to Optimize the Production of Radioactive Ion Beams by the ISOL Technique, PhD. Thesis, UPC-ETSEIB / CERN (2005).
[15] J. Crank, The Mathematics of Diffusion, Clarendon Press (1956).
[16] R. Kirchner, Nucl. Instr. Meth. B 126, 135–140 (1997).
[17] Y. Zhang et al., Nucl. Instr. and Meth. in Phys. Res. A, 521, 72–107 (2004).
[18] G. D. Alton, Applied Radiation and Isotopes, 64, 1574–1603 (2006)
[19] C. Lau et al., Nucl. Instr. Meth. in Phys. Res. B, 204, 246-250 (2003)
[20] D.W. Stracener et al., Nucl. Instr. Meth. in Phys. Res. A, 521, 126–135 (2004)
[21] S. Sundell and H. Ravn, NIM B 70 160 (1992).
[22] G.D. Alton, NIM A 382 207 (1996).
[23] S.Cevolani FIS-P815-022

CHAPTER VI

RIB SOURCES

6.1 General criteria for target and ion-sources

The ion-sources dedicated to the production of Radioactive Ion Beams (RIB) have to be highly efficient, selective (to reduce the isobar contamination) and fast (to limit the decay losses of short-lived isotopes). For radioactive beam generation, the source must operate stably for extended periods of time at elevated temperatures (up to 2000°C). The selection of the most appropriate choice for the target/ion source is of paramount importance since its performance determines the intensity, the beam quality, and the number of radioactive beams that can be provided for experimental use.

The world wide spread RIB facilities came up with a large variety of solutions to meet part or all of these requirements such as: surface, plasma, electron cyclotron resonance and laser ion-sources [1]. A figure of merit of the 1+-ion sources for RIB is presented in fig. 6.1 as a function of the ionization potentials.

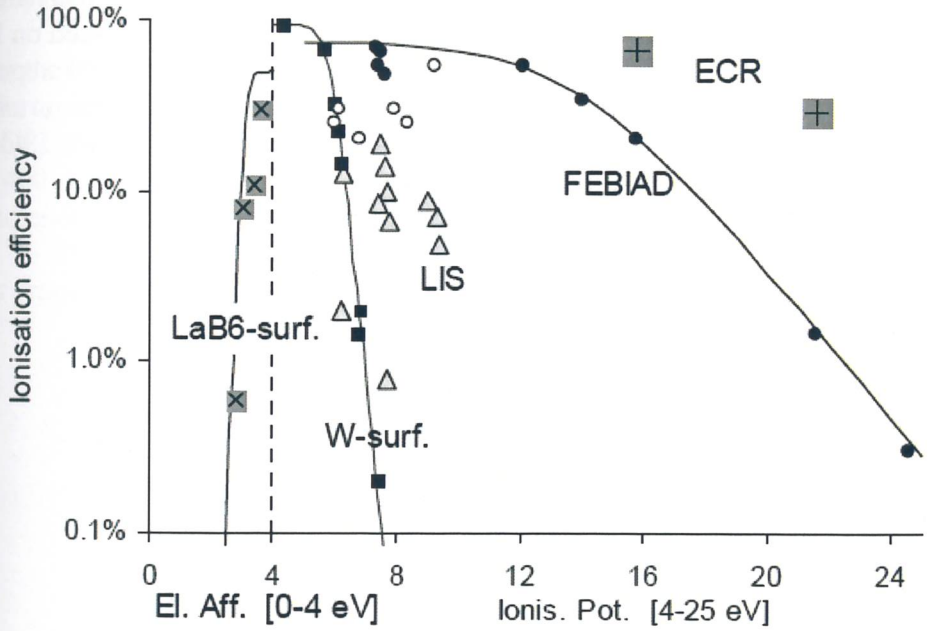

Fig. 6.1: *1+ Ionization efficiencies measured withsurface (black squares), plasma-FEBIAD (circles), laser (triangles) and ECR ion sources from Ref 1.*

The choice for SPES project to develop a Target-Ion Source Chamber unit based on the ISOLDE one, implies the possibility of using a great part of sources developed at CERN, with the ability to choose and then to plug one of those through the transfert tube of the multifoil SPES target. In a ISOL facility, the volatile nuclear reaction products are released from the target material and diffuse via a transfer line into the ion source, so the target and ion source system form a self-contained unit specifically optimized for each element or group of elements. The choice of ion source to be used has primarily been dictated by efficiency and secondarily by its

capability of selective ionization. All ions produced are accelerated towards the ion extraction electrode by a potential of 60 kV.

We consider here three kind of ion souces for SPES: the Surface Ion Source, the Forced Electron Beam Induced Arc Discharge (FEBIAD) and the Resonant Ionization Laser Ion Source (RILIS). All of these three sources are used at ISOLDE and they constitute a good reference point for further SPES goals in the ion-source development.

6.2 The Surface Ion Source

The concept of surface ionisation has proven to be particularly successful for production of singly charged positive and negative radioactive ion-beams due to its simplicity, high efficiency and selectivity [2]. As shown by the Langmuir equation ionisation efficiencies for positive ions of 50-100% may be obtained for elements with ionisation potential <5 eV and of negative ions for elements with electron affinity > 2 eV. Saha and Langmuir described the ionizing properties of a hot surface. Positive ions are produced when the minimal energy needed to remove an electron from a surface (its work function) is larger than the ionization potential, and negative ions are produced when the work function is smaller than the electron affinity of the atom impacting on the surface at thermal energies.

Surface ionization remains the most efficient ionization scheme for low ionization potential radioisotopes (alkalis and some lanthanides) that are currently produced with W, WO_3 and Re surfaces. Negative chlorine, bromine, iodine and astatine have been efficiently produced on LaB_6 Surfaces. In fig. 6.2 a picture of the EXCYT Positive surface Ion Source (PIS) is reported, successfully used to produce the first 8,9Li RIBs, it consists of a tungsten ionization tubular cavity connected to the target container transfer tube. This is a development of a MK1 ISOLDE ion source.

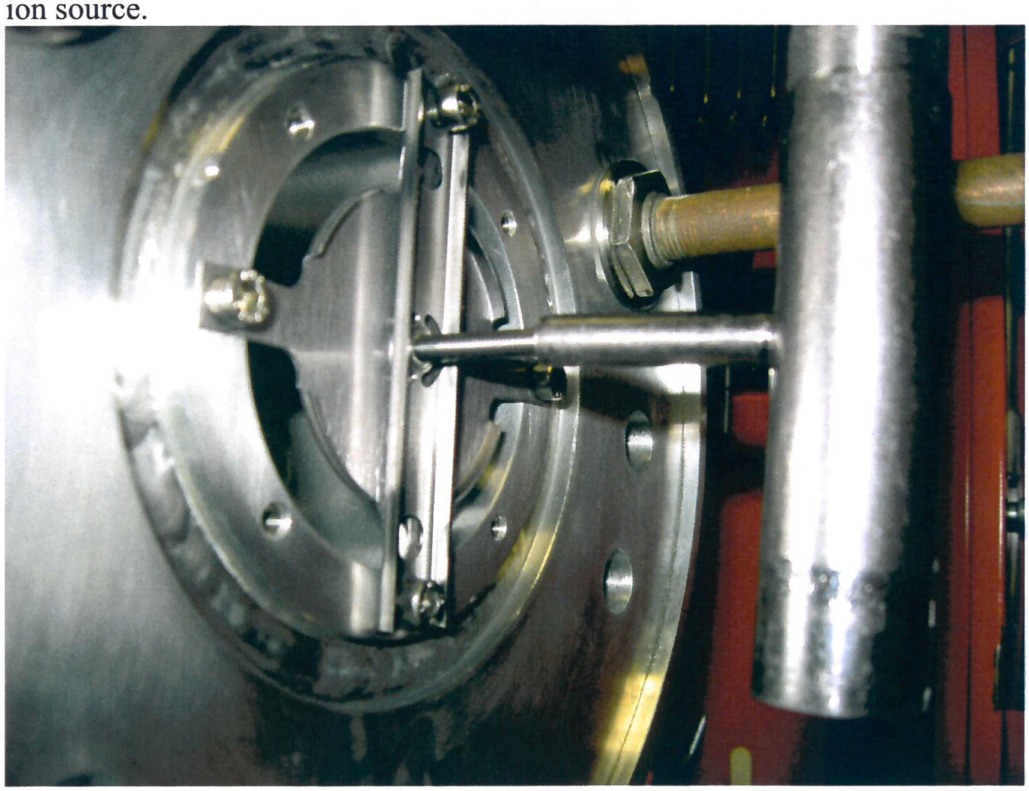

Fig. 6.2: *EXCYT Positive ion source set-up (evolution of ISOLDE MK1).*

6.3 The Plasma Ion Source: FEBIAD

The plasma ion-source currently used in several RIB facilities is based on the Forced Electron Beam Induced Arc Discharge (FEBIAD) concept originally developed by Kirchner [3] at GSI. The principle is based on the capability of electrons, coming from an indirectly heated disc-shaped cathode and accelerated into the anode chamber by means of a grid, to ionize any atoms, floating in the anode chamber, with ionization potential smaller than the energy of incident electrons. The source is well suited for ISOL applications it operates stably and efficiently in conjunction with high temperature thick target materials over a pressure range of 10^{-5} to 10^{-4} Torr.

The FEBIAD is particularly useful for the ionization of highly reactive or condensable elements for which wall sticking would limit their release from a surface ion source cavity. With electron impact energies of between 100 and 200 eV, also elements with very high ionization potentials (e.g. Xe and Kr) can be efficiently ionized. In fact the efficiency of the FEBIAD ion source is quite high for slow moving heavy ions; for low mass, fast moving atoms with high ionization potentials, the source is not as impressive. For example, the measured ionization efficiencies for the noble gas elements are, respectively: Ne: 1.5%; Ar: 18%; Kr: 36%; and Xe: 54%.

The FEBIAD ion source is also capable to produce multi-charged ions, but the limited selectivity offered by this kind of ion source can be improved by exploiting the chemical or physical properties of the atoms as they are released from the target.

The FEBIAD ion source developed at ISOLDE is named MK5 [4], and it could be used also in the SPES target-ion source assembly. The cathode is made of tantalum, and it consists of three parts welded together by means of electron beam welding and press fitted into the transfer tube; the cathode temperature, and thus thermionic electron emission, is controlled by a DC current (400 A max). The collimation of the electron beam is effected by adjusting the coaxially directed solenoidal magnetic field so as to optimize the ionization efficiency of the species of interest.

The discharge chamber and the anode assembly are made of molybdenum and screwed into a graphite cylinder rigidly fixed to the main target base as shown in fig. 6.3.

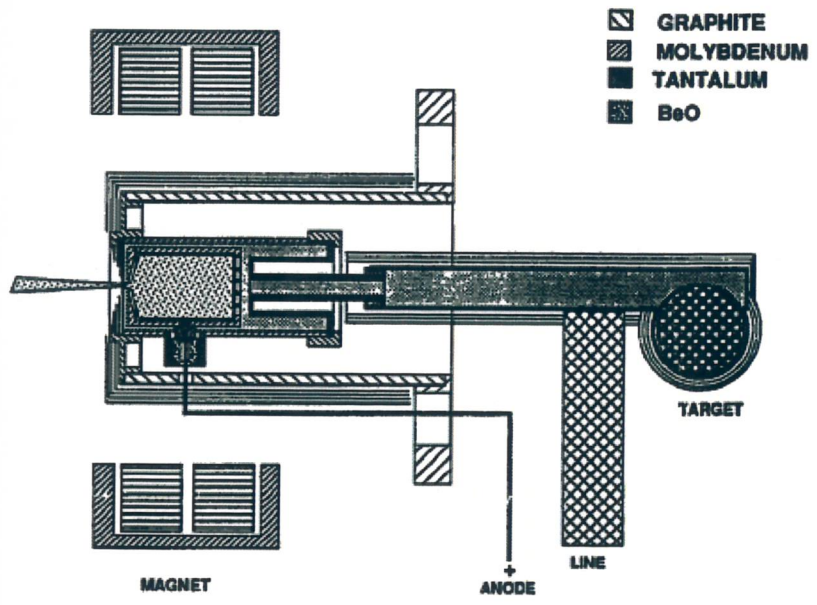

Fig. 6.3: *The ISOLDE MK5 high temperature plasma ion source with target container.*

The anode is insulated by means of three BeO insulators. The anode grid consists of a graphite disc with holes drilled through it to let electrons being accelerated into the discharge chamber. The source is surrounded by three heat screens made of molybdenum. A current flows through the transfer line via the cathode, the anode cylinder, the external graphite tube and back through the main target flange. The advantage of this design is that only one power supply is needed for heating the line, cathode and ion source. The same power supply can also be used for heating the tubular surface ionizers.

6.4 The Resonance Ionisation Laser Ion Source

The Resonance Ionization Laser Ion Source (RILIS) method is nowadays the most powerful tool for radioactive ion beam production at on-line facilities, because it provides a selective ionization process with inherent suppression of unwanted isobaric contaminations at the ion source. A photoionization scheme usually involves a few resonant photon absorption steps in which the valence electron is excited to a high lying Rydberg state close to the continuum before a final, often non-resonant ionization step. Using tuneable lasers (solid state or dye or a combination of the two) it is possible to match the photon energy of the laser light to the electronic transitions of a desired atomic species. For many elements, ionization by stepwise resonance photon absorption can provide an unmatched level of selectivity and rapidity. It is the unique electronic structure of different atomic species that gives this process its selectivity.

The ionization efficiency is heavily reliant on the saturation of the resonant photon absorption steps, therefore the spectral radiance requested to the laser system depends also from the physical parameters of the atomic sample released from the target. This task can be accomplished using pulsed laser that must also operate at high repetition rate in order to process all the fragments coming from the target.

Typical Laser sources are the RILIS (ISOLDE, Fig. 6.4) or, more recently, the FURIOUS (IGISOL) Resonance Ionization Laser Ion Sources [5,6] Fig. 6.5, which both provide beams for more than 20 elements. The laser beams are directed through a window in the ion beam line at the mass separator and focussed into the cavity of a standard surface ion source, shown in figure 6.4.

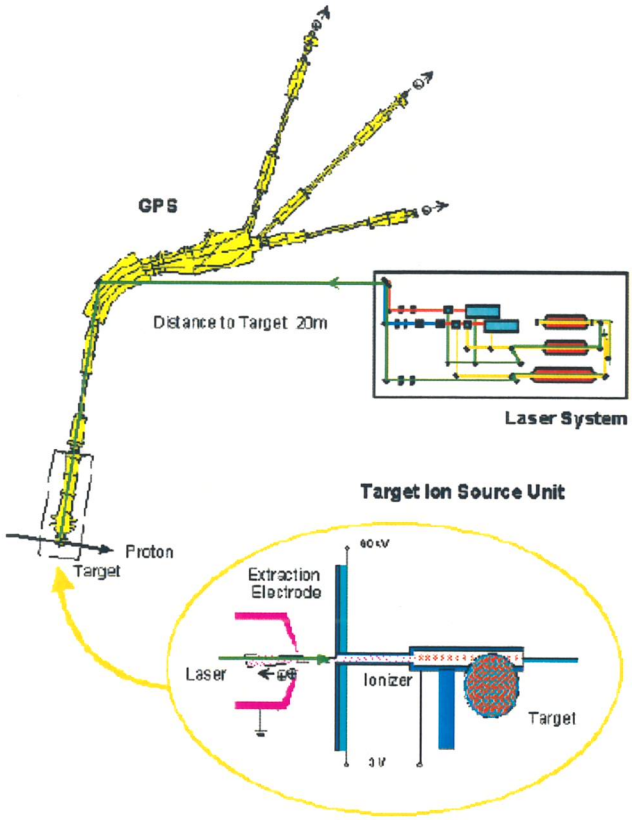

Fig . 6.4: *The ISOLDE Laser Ion Source*

In this hot cavity the reaction products exist as a thermal atomic vapour at a temperature of around 2300 K. Under these conditions Doppler broadening adds to the natural width of the resonant transitions (typically 10MHz) raising the linewidth to the order of a few GHz. In addition, atomic physics effects such as the isotope shift and hyperfine structure, when present, can effectively broaden the width of the transition, by splitting the resonance position into different hyperfine or isotopic components spread over a range of possibly tens of GHz. In these cases optimal efficiency is therefore achieved by the use of plain broadband lasers. For instance, the dye lasers used at ISOLDE have a typical bandwidth of 20 GHz. Vice versa isotopes or hyperfine components (even isomers) of some elements can be isolated by operating the lasers in a narrower band mode, typically inserting an etalon into the laser cavity.

The technique is still in progress. Few years ago it has been proposed to add an ion repeller and to surround the photoionization region by a linear RFQ, improving by orders of magnitude the suppression of surface ions contamination while ensuring a high collection efficiency of photoions. This technique was named LIST, Laser Ion Source Trap [7], Fig. 6.5.
Access to more than 80% of all known elements seems feasible with existing laser systems [7,8].

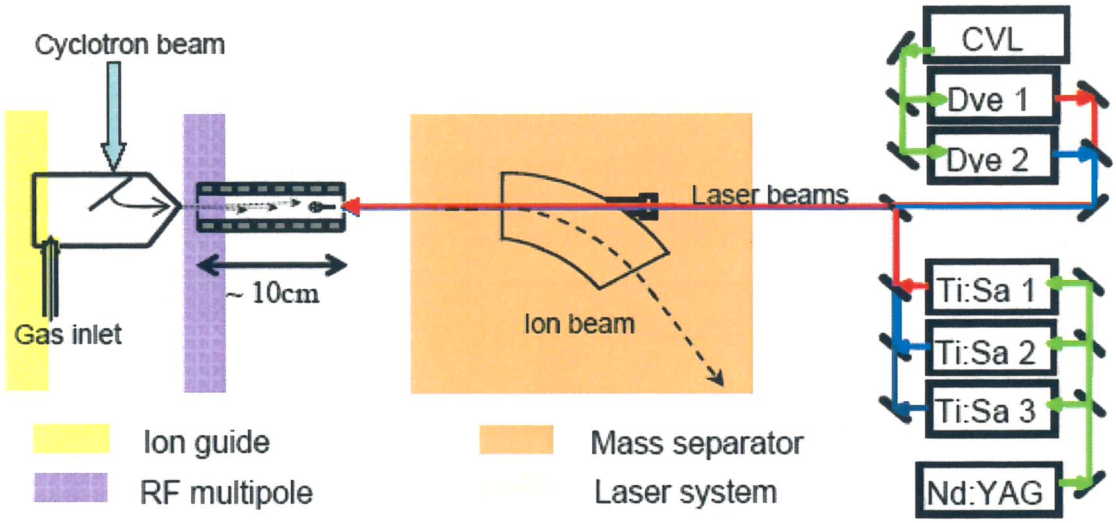

Fig. 6.5: *The LIS system at Jyväskylä*

[1] J. Lettry, Proceedings of the 1999 Particle Accelerator Conference, New York, 1999
[2] R. Kirchner, NIM **186** (1981) 275
[3] R. Kirchner and E. Roeckl, NIM **133** (1976) 187.
[4] S. Sundell, H. Ravn NIM **B70** (1992) 160
[5] J. Lettry et al, NIM **B404** (2003) 363
[6] I.D. Moore et al, J. Phys. G : Nucl. And Part. Phys. **31** (2005) S1499-S1502
[7] K. Wendt et al, Nucl. Phys. **A 746** (2004) 47c-53c
[8] U. Koester et al, Spectrochim. Acta **58B** (2003) 1047

CHAPTER VII

SECONDARY BEAM TRANSPORT

7.1 Beam lines

The secondary beam line transport system will manage the radioactive beam from the output of the ionization source to the low-energy experimental area and to the re-accelerator complex. At the source exit the beam has charge state +1 and energy 40 due to the source extraction voltage. One of the main problems to operate an ISOL facility is the beam purification as the extracted species are transported according to their M/q value. To improve the isotope selection two mass separators with different resolutions will be implemented along the transport line. Due to the low rigidity of the beam, electrostatic quadrupoles and deflectors will be used; this also guaranty the use of stable guide beams, very useful in the setting of the beam transport.

The fist selection element is the mass separator with an M/ΔM resolution of 300 followed by a 1/15000 isobar mass separator. At this stage the radioactive beam can be used in the low energy experimental area.

To allow an efficient acceleration it is necessary to improve the charge state of the selected isotope by a Charge Breeder. Several kinds of charge breeders are under discussion. We present in this report an EBIS for which a prototype was developed by INFN Bari. From the point of view of the beam transport the charge breeder is a trap with plasma in which the ions are stopped; the entrance velocity of the ions should be as low as possible. For this reason the charge breeder is mounted on a +HV platform which decelerates the incoming ions (+1) and gives the right velocity to the charge bred ions (+N) to be injected in the bunching RFQ.
The last pre-acceleration element is the Superconductive RFQ which gives the right velocity for the Linac ALPI injection.

7.2 High resolution separator

7.2.1 Isobar mass separator

The present plan has the goal to achieve a clean mass separation corresponding to a resolution M/ΔM ≈ 15000, before the injection into the ALPI LINAC of the selected RIB specie.

This allows, for example, the selection of the nucleus ^{100}Nb (Q_{β^-} = 6.245 MeV) in the A=100 isobaric chain.

As discussed in several proposals and originally proposed also in ref. [1], a clean mass separation can be achieved in an elegant way with a "two-stage separator". Both separators consist of magnets acting on the magnetic rigidities of the accelerated ions.

Ions leaving the first stage will be accelerated to a higher energy thus they will gain, in most cases, different magnetic rigidities. Therefore contaminants passing through the first separator with the same magnetic rigidity of the selected RIB will not be transmitted through the second stage. In general the potential elevation on the second stage can be as low as 10kV and does not need to be higher than 60kV.

The first stage of the separation has to operate necessarily with ions at the same energy of the extraction voltage from the ion source. These voltages range from 20 kV to 40 kV. Consequently the second separation stage has at least to handle with ions whose energies range from 50 to 100 .

The following boundary conditions have to be considered:

1. RIB ion source.
   The RIB source should be located at low voltage and the extraction electrode at ground. This would make the operation of the system, where a high level of radioactivity is involved, in much more friendly and easy way.
   However we have to notice that the RIB facilities at LNS (EXCYT) and ORNL have proved that it is possible to operate such ion sources at high voltages, up to around 300 kV.
2. The charge breeder.
   The charge breeder, necessary to have ions with the proper A/q ratio for the accelerating system, needs input ions with nearly zero energy. This has to match to the requirements of the accelerating voltages needed by the two-stage separation system prior to injection into the charge breeder.
3. LINAC acceleration.
   In order to use the present ALPI LINAC complex, without any additional accelerating systems, an injection voltage variable up to around 250 kV is necessary. The injection at very low energies needs the development of a new RFQ.
4. Beam transport from the RIB primary source to the LINAC.
   The primary RIB ion source will be located at ground level, also for safety reasons. The beam has subsequently to be transported to the LINAC underground level, by magnets (i.e. via two 90°-bending magnets) which can be well exploited also for mass selectivity.

Based onto these boundary conditions two alternative scenarios have been considered.

Solution A (presently selected).
The sequence is the following:

1. Platform1 at voltage ranging from +20 to +40 kV
2. RIB source mounted on platform1, extraction electrode at ground potential (which produces 1^+ charge state ions at energy 20-40).
3. First stage magnetic mass separation with resolving power M/ΔM around 300 at ground potential.
4. Platform2 at -60 kV to accelerate the ions to 80-100 energy (according to extraction voltage).
5. Second stage of high mass separation, and purification, with resolving power M/ΔM around 15000 with two 90°-bending magnets, operating on platform2.
6. Platform3 at the same voltage of the RIB source to decelerate the ions to 0 .
7. Charge breeder (ECR or EBIS) located on platform3 produce ions with A/q up to 7
8. Injection of accelerated ions (= KV_platform3 * q) into the first stage of new bunching RFQ and subsequent injection in the SRFQ (PIAVE) and ALPI LINAC complex.

Solution B.

1. High voltage platform1 at +210 KV
2. Source platform2 at +40 KV located over platform1
3. RIB primary source, which produces 1^+ charge state ions, located platform2, extraction electrode at platform1 voltage..
4. First stage magnetic mass separation with resolving power M/ΔM around 300 working at platform1 potential.
5. Second stage of high mass separation, and purification, with resolving power M/ΔM around 15000 with two 90°-bending magnets operating at ground potential. The analyzed ions have energy of 250 .

6. High voltage platform3 at +250 KV This allows to have ions at nearly 0 energy, well suited for the breeding process.
7. Charge breeding via ECR or EBIS source located on platform3
8. Injection into the existing SRFQ (PIAVE) and ALPI LINAC accelerator complex without any further energy manipulations.

Warning: the voltage of platform3 ought not to be fixed due to LINAC injection requirements but needs to be slightly varied. This requires some extra compensation between the voltages of the two high voltage platforms.

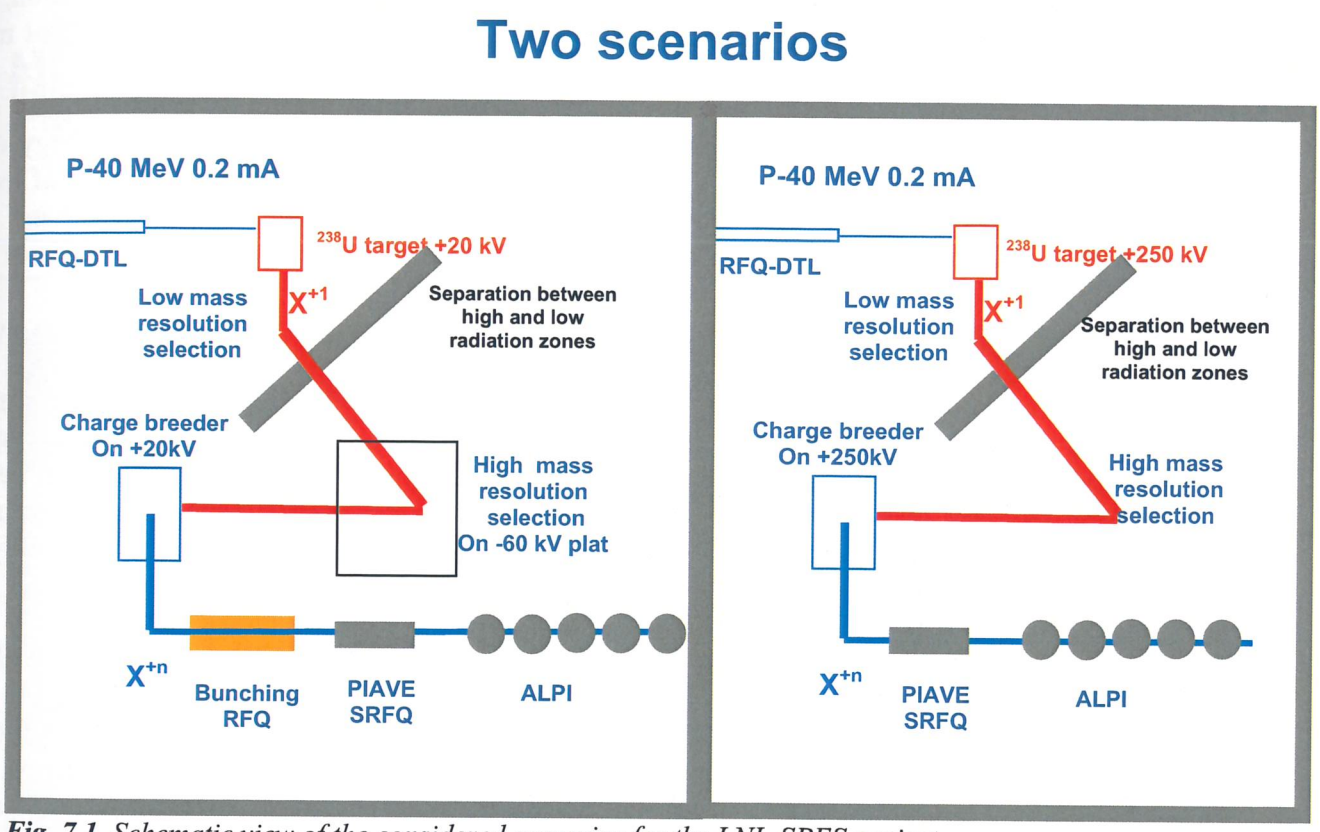

Fig. 7.1. *Schematic view of the considered scenarios for the LNL-SPES project.*

Presently the solution A seems to be more suitable for the SPES project. In such a way the most crucial and challenging parts of the whole project, namely the primary RIB production system (with high radioactivity environment) and the Charge Breeder (new type PHENIX under development at Grenoble+GANIL or EBIS developed at INFN-Ba), are working at relatively low voltage. This is at the cost of two 90° bending magnets operating at NEGATIVE but moderate voltage (around 60 kV) and of a new bunching RFQ, for the injection into the existing LINAC, to be newly developed by the LNL accelerator division.

7.3 The Charge Breeder

7.3.1 Introduction

The charge breeder is a device that accept RIB ions coming from the Target-Ion source complex with charge state *+1* and it transforms their charge states to *+n*.

The development of an efficient charge breeding scheme for Radioactive Ion Beams (RIB) production has a strong impact on the lay-out of the post accelerator needed to bring the unstable nuclei to the energies required to study nuclear reactions.

Since the cost of an accelerator is roughly related to the inverse of the charge state of the beam to be accelerated, a higher ion charge state beam can allow a sensitive lowering of the accelerator cost. This problem can be solved by using, before the post-acceleration, an appropriate device capable of increase the charge ion state of the radioactive element that must be accelerated

Just to give an example, let us consider the acceleration of an ion of mass 50 Amu and charge +1 with a typical accelerating mean field of 5 MV/m we could obtain an energy of 5 MeV/u with a LINAC length of 50 m giving a cost of 25 MUSD [2]. The possibility of using ions with high charge state, would reduce strongly the accelerator cost. On the other hand this advantage is paid by the introduction of a new device that will increase the complexity of the Facility lay-out.

Two types of ion sources are able of reaching the required charge states: the Electron Beam Ion Source (EBIS) and the Electron Cyclotron Resonance Ion Source (ECRIS). The first one develop a pulsed beam and the second a continuous wave beam. The REX-ISOLDE experiment has proved that charge breeding of radioactive beams is possible with efficiency, typically, up to 10% in one charge state and breeding times of ~50 ms for light beams and ~150 ms for heavy beams [3]. In order to become comparable in the overall efficiency with the more expensive stripper scheme [4], all the steps of the breeding process have to be optimized. The possibility of optimizing the charge breeding process trough several techniques has been explored in the European project EURON [5]. The main techniques considered in the project are:

(1) the narrowing of the charge state distribution by manipulation methods to obtain the highest efficiency in a single charge state
(2) the optimization of the purification for very weak beams (e.g. 100 fA of radioactive ions) and rather intense beams (e.g. 10 μA) from rest gas contamination in the same separator.
(3) the optimization of the transverse and longitudinal emittance for the extracted beams, using cooling techniques in the beam preparation and in the ion sources.

A common feature of a Charge Breeder is that the incoming particles must have a low velocity to be caught by the electron or ECR plasma. One can use a solid state catcher to decelerate the 1+ beam but the particles stick on the catcher before being released and this sticking time can be very long for some elements.

For radioactive ion beams, it is essential to have a short release time (<1 s), and this condition is not easy to realize when a solid catcher is used to decelerate the 1+ beam.

Other methods consist in adding an ion trap before the Charge Breeder, in case of pulsed beam, or in a careful electro-static deceleration of the 1+ beam before the injection into the Charge Breeder active volume.

Expertise in both EBIS and ECR are present inside INFN. The final decision on the Charge Breeder for SPES will be taken according to the final evaluation of the facility lay-out; taking into account budget, performances and construction schedule.

7.3.2 *The BRIC Charge Breeder*

A study to improve the charge breeding efficiency has been developed at INFN-Ba in the framework of the SPES project. It consisted in design, build and test a new type of "charge state breeder" device based on an EBIS source and named BRIC. The BRIC features have been presented in a detailed way in ref. [6,7]. The main new feature of BRIC is the use of a RF quadrupolar field to obtain, in the EBIS, a selective containment of the wanted ions and reach, in this way, a more efficient high charge state ion production.

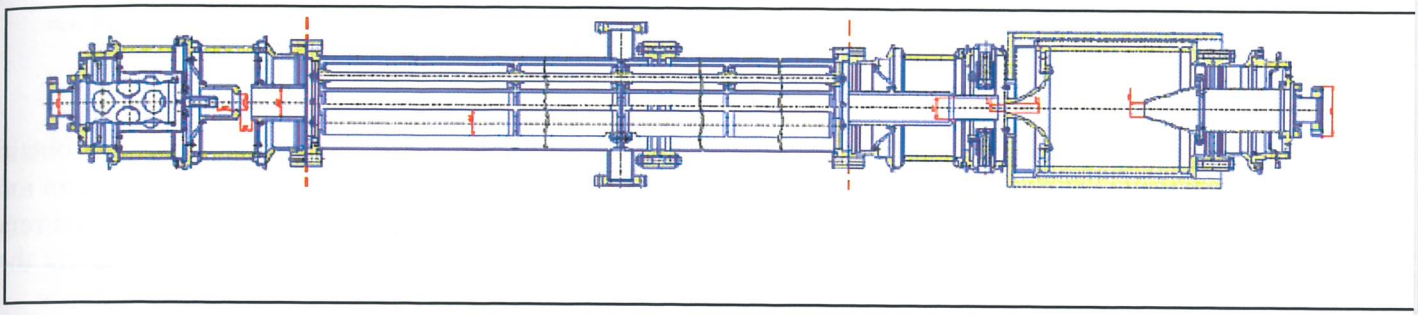

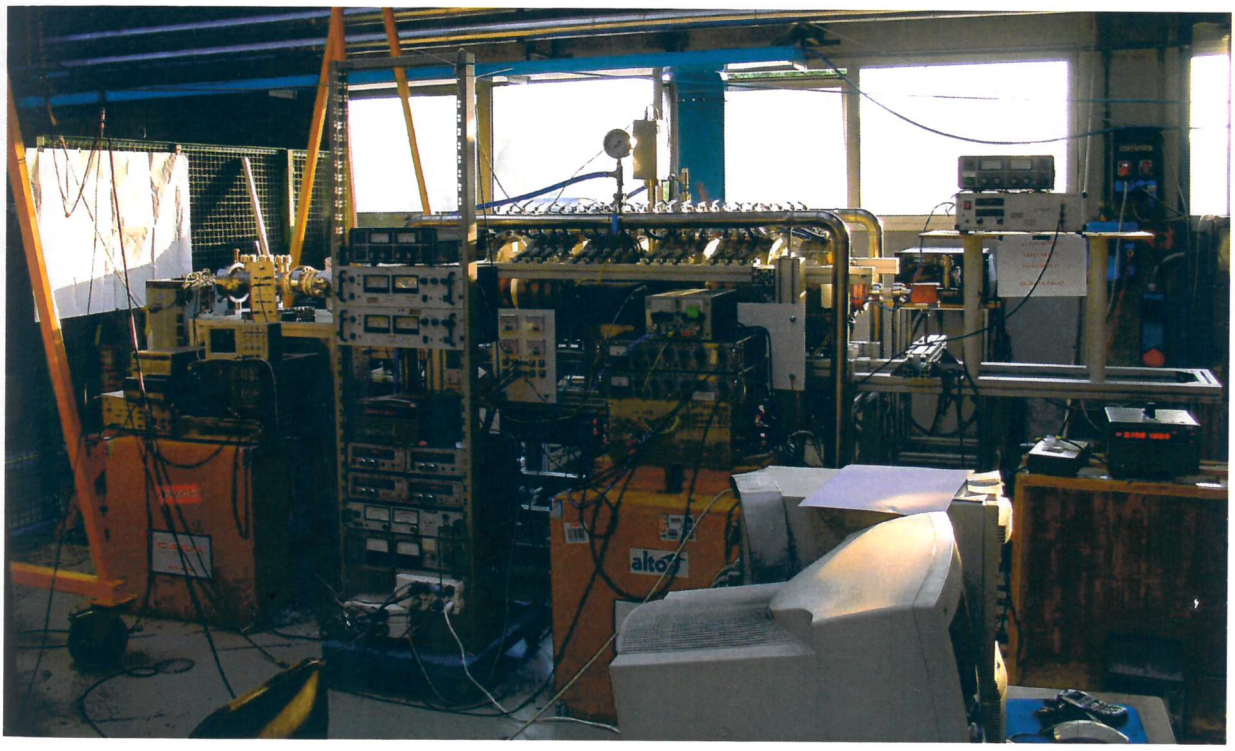

Fig. 7.2: *shows a drawing and a picture of the BRIC assembly installed at LNL.*

In order to study the ion motion stability and the ion charge state evolution inside the BRIC trap region in the presence of the rf field, a code has been developed in Bari INFN [8].

The high charge state ions are mainly produced by collisions with energetic electrons by a stepwise ionization process. For the ionization cross-section the empirical Lotz formula can be used:

$$\sigma_{ion,i\to i+1}(E_e) = 4.5 \cdot 10^{-14} \sum_{l}^{N} q_l \frac{\ln\{E_e / E_i\}}{E_e \cdot E_i}$$

Where q_l is the number of electrons on the atomic subshell l, E_i is the ionization energy of the ion with +i charge state. Notice that it decreases for the production of higher charge states ions and it can be seen that the time needed to reach a charge state +n ion is practically given by the time needed to get the last ionization [9].

Then, considering as SPES requirements for the re-acceleration of the radioactive ions a value of A/e of about 10 and an EBIS as charge state breeder, the confinement time in the source needed to get a certain ion charge state can be given by [9]:

$$\tau = \frac{e}{\sigma j_e}$$

where j_e indicate the electron beam current density of the EBIS. This means we can obtain shorter confinement times by increasing properly j_e. Just to give some number: if we want an ion of A about 100 and a charge state +10 the confinement time required with an electron current density of about 200 A/cm^2 should be 80 ms. This high current density can be reached by the magnetic compression techniques [9].

The results obtained in our test experiment for Ar are shown in fig.7.3a and 7.3b below. The Ar gas was injected inside the ion chamber up to a total pressure of about 1 x 10-7 Torr. In both those figures are shown the ion counting number N vs ion TOF for the case without the addition of the RF quadrupolar field in a), and the case with a quadrupolar rf field of □rf=0.8 MHz and Vpp=10 V in b). From the comparison of a) and b) it can be seen how the adding of the RF field to the ion chamber produced an amplitude reduction of some ion charge state peaks and the increase of others. Furthermore, on the case b), it can be seen the appearance of 2 further small peaks that refer to ions Ar5+ and O4+. Further measurements have been carried out for different RF frequencies and they all have shown that the frequency which gave major effect on selective containment, for the used parameters, was about 1.2 MHz.

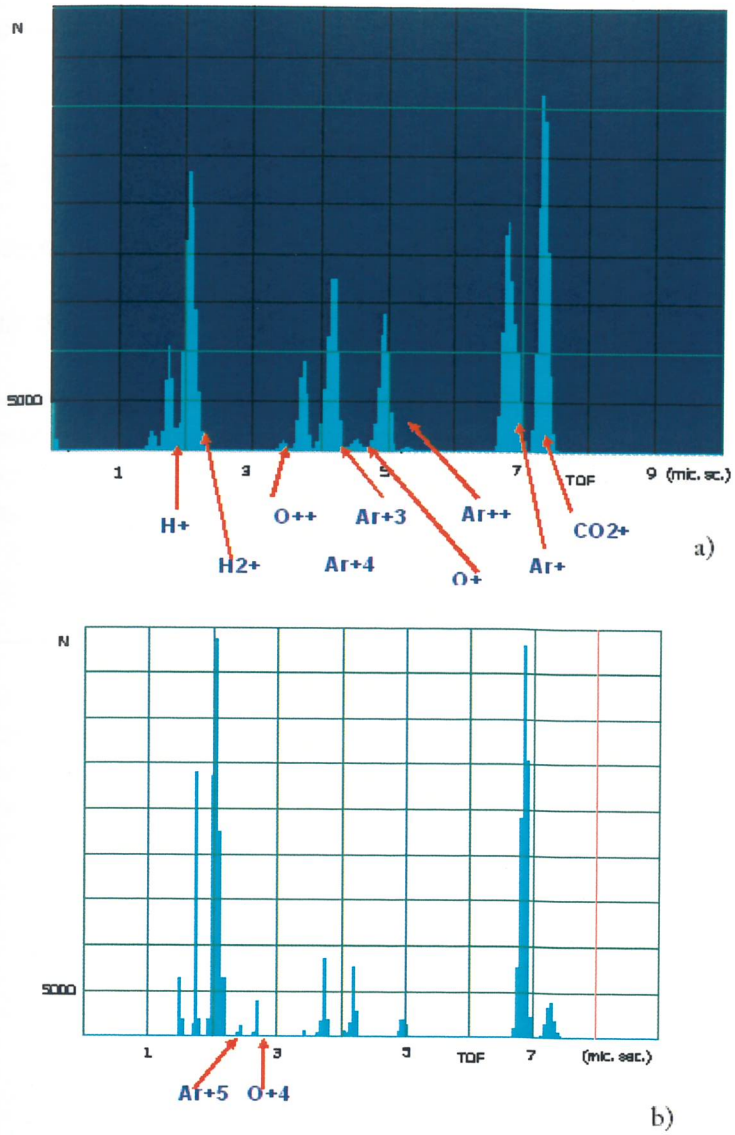

Fig. 7.3: *Ion charge states measurements. N (ion counting) vs ion TOF (□s): a) case without the application of RF field, b) case with RF field.*

The EBIS charge breeder is intrinsically a trap and a pulsed source, to be used for continuum beam production a possible solution is the use of two EBIS operated alternatively as proposed by the Michigan up-grade project [10]. In this case during the trapping time of EBIS1 the beam is supplied by EBIS2 and vice versa.

7.3.3. ECR Charge Breeders

The EBIS technique produces an intrinsically pulsed beam. For continuous RIB no charge breeders were known before 1995 except for inert gas ions which do not stick on the walls. Until that time the ordinary ECRIS only worked with neutral atom feeding, which in most cases is conducive to many atom/wall sticking with long release times before the 1+n+ process occurs. Since that time many efforts have been done in this field from different laboratories to develop compact and efficient charge breeders which are able to trap the 1+ RIB inside the ECR plasma built up with a support gas. Thus the injected radioactive ions are added to the pre-existing support gas plasma and then they are charge bred and extracted as all the other ions.

Although very simple at first glance, the process applies very involved plasma theories proposed by Chandrasekhar and developed later by different theorists.
There are three main goals for this transformation:

1. The efficiency of the 1+ to n+ conversion must be as high as possible.
2. This operation should have a short release time compared to the half-life time of the radioactive ions.
3. The method has to be applicable to various sorts of ions issuing from the fission source (gas and condensable elements)

An efficient way to capture the 1+ beam inside the ECR plasma is the electrostatic deceleration. The principle of the plasma capture is quite simple.

The 1+ ion source is biased at a potential $V+\Delta V$, when the ECR plasma chamber is biased at V. The 1+ ions have then enough energy ($e\Delta V$) to overcome the plasma potential (potential difference between the plasma and the plasma chamber), and the ECR plasma can transform the incident ions into a thermal population through plasma collisions (ion-ion collisions). Thus the incident particles are confined together with the ECR plasma, and the energetic electrons can strip the 1+ ions through step by step ionizing collisions and transform them into n+ ions. The n+ ions can then be extracted and delivered for further acceleration

This plasma capture was studied with two different experimental configurations:

1. In the first one, the 1+ ion beam is injected through the extraction hole of the ECR source (Fig. 7.4). This configuration is called ''retro-injection'' mode or backward injection mode. In this case the 1+ beam passes through a retro-injection magnet; it is injected along the axis of the ECR source and then caught by the ECR plasma and multi- ionized. The extracted n+ beam is focused, bent by the retro-injection magnet and then analyzed in mass and post-accelerated.

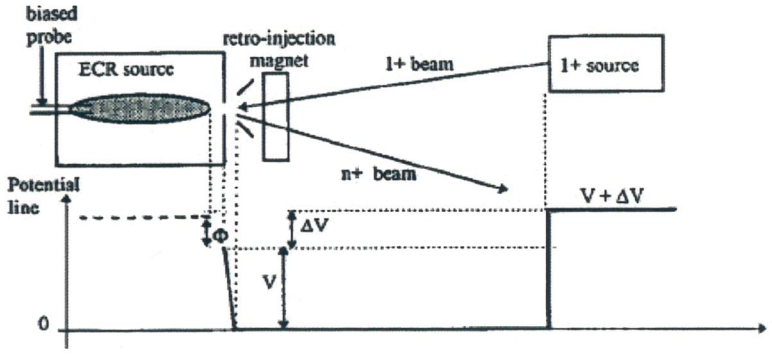

Fig. 7.4: *Schematic of the backward injection mode*

2. In the second one, the 1+ beam is injected on the gas injection side of the source (Fig. 7.5). This configuration is called forward injection mode and the experimental setup is simplified with respect to the previous case. In fact the 1+ injection is separated from the n+ extraction and the retro-injection magnet can be removed.

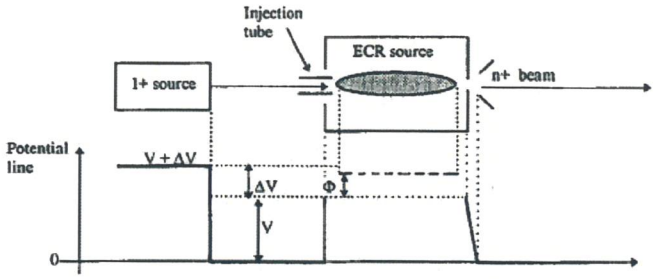

Fig.7.5: *Schematic of the forward injection mode*

Experimentally it was demonstrated that the forward or backward injection of 1+ RIB can be done with similar efficiencies. Moreover, it was shown that the time necessary for most of the $1+\rightarrow n+$ transformations was shorter than 0.2 s and in general did not exceed 30 ms. Thus the most tedious problem related to the extraction time was solved: the $1+\rightarrow n+$ process can become a very prompt phenomena inside an ECR plasma working in continuous regime with very short life isotope ions.

The efficiency η of the 1+ to n+ transformation is calculated by the formula:

$$\eta = \frac{1}{n} \cdot \frac{I_{n+}}{I_{1+}}$$

where I_{1+} and I_{n+} are the electrical currents of the 1+ and n+ beams respectively.

The total breeding efficiency is given by:

$$\eta_T = \sum_{i=1}^{N} \eta_i$$

where η_i is the efficiency for each charge state i extracted and N the highest charge state produced.

The use of an ECR ion source as charge breeder have been proposed and developed by the Grenoble group several years ago and this solution has been tested in several ISOL facility until now [11] (e.g.: the 14 GHz PHOENIX booster [12] is installed on the heavy mass parasitic beam line of the General Purpose Separator at CERN and it is going to be installed on-line even on ISAAC). The available efficiency data with RIBs such as Ar, Kr, Xe, Zn, Cr, Rb, Pb, U, etc. and support gases like O_2, N_2, etc… show that in a continuous regime we found $\eta \leq 10\%$ for Ar^{8+}, Kr^{12+}, Xe^{14+} (i.e., for non sticking ions). Taking into account all the charge spectrum one finds $\eta_T > 50\%$, which is an excellent overall efficiency. Thus the relatively low value of η is a consequence of the broad CSD of ECRIS.

However for some sticking metal ions like Pb, Rb, etc., η_T also reaches 30% which proves that even these ions are efficiently trapped in the ECR plasma.

Finally, it is of prime importance to recall that in all cw ECR ion sources one looks for a compromise between optimum plasma confinement and maximum extracted ion beam intensity.

If the confinement is too good, ions do not leak through the magnetic mirrors toward the extractor. So no extracted ion beams are available. Therefore in all cw ECRISs the magnetic mirrors are asymmetrical: on the extractor side the mirror field is weaker allowing a part of the plasma ions to leak permanently toward the extraction hole and thus to supply ions for the extracted cw beam (Fig. 7.6).

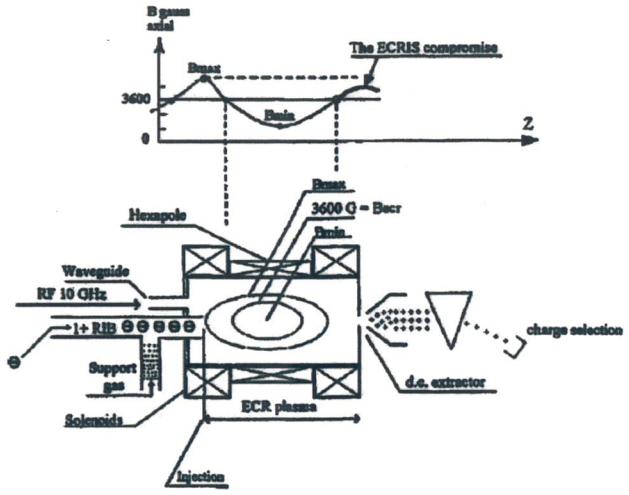

Fig.7.6: *Schematic of a charge breeder for CW RIB operations*

[1] H. Wollnik and K. Becker, Nucl. Instrum. and Meth. **A238** (1985) 206.
[2] F. Wenander, "Charge breeding techniques", NIM in phys.res. A 746 (2004) 40-46.
[3] U. Koster, O. Kester,and d. Habs, Rev. Sci. Instr. 69 (1998) 1316.
[4] J.A. Nolen et al. Rev. Sci. Instr. 69 (1998) 742.
[5] EURON project
[6] V. Variale, G. Brautti, T. Clauser, A. Rainò, V. Stagno, G. Lamanna, V. Valentino, A. Boggia, Y. Boilmelshtein, P. Logatchov, B. Skarbo and M. Tiunov, " An EBIS for charge state breeding in the SPES project", PRAMANA- journal of physics, Vol. 59 (2002) 765.
[7] V. Variale, A. Boggia, T. Clauser, A. Raino', V. Valentino, G. Verrone, P. Bak, G. Kusnetsov, B. Skarbo, M. Tiunov, "Test Measurements On The RF Charge Breeder Device BRIC", Journal of Physics: Conference Series 2 (2004) 117-126.
[8] V. Variale and M. Claudione, "BRICTEST: a code for charge breeding simulations in RF quadrupolar field", NIM in Phys. res. A 543 (2005) 403-414.
[9] B. Wolf, Handbook of Ion Sources, CRC press (1995) 157.
[10] Isotope Science Facility at MSU, MSUCL-1345 (2006) 289
[11] T. Lamy et al., Rev. Sci. Instrum. 69,3 (1998), 1322.
[12] T. Lamy et al., Charge breeding method results with the PHOENIX booster ECR ion source, Proceedings of EPAC 2002, Paris, France.

CHAPTER VIII

THE ALPI LINAC AS RIB ACCELERATOR

8.1 Introduction

The linear accelerator ALPI [1], with a β range between about 0.04 and 0.2 and CW operation, represents an ideal re-accelerator for the radioactive beams. Radioactive ions can be accelerated above the Coulomb Barrier with high efficiency. The quasi-continuous time structure and the possibility to adjust finely the output energy make it very well suited for nuclear physics experiments. A time structure suitable for TOF measurements can be implemented by a low energy bunching system.

ALPI underwent a number of significant upgrades, in recent years, which made it a world-class facility in heavy ion stable beam accelerators and which will represent an important added value for its use as a RIB accelerator as well. These upgrades (described in more detail in chapter 8.2) were the following.

- In 2000-2003 the performances of ALPI were improved by means of a new coating of the copper cavities, from the original Pb (by electroplating) to Nb (by sputtering).
- Another crucial development is the refurbishing of the lower beta resonators and their control system, aimed at increasing the average accelerating field from 3 to 5 MV/m or more and the number of such resonators from 12 to 16.
- In spring 2006, the commissioning of the higher current injector (named PIAVE [2] and made of superconductive RFQ[3]) of the linac booster ALPI was completed. PIAVE, an injector of higher mass and higher current than the tandem, based on an ECR Ion Source (placed on a 350 kV platform), and on superconducting RFQs, is designed to accelerate ions with A/q=<8.5 up to 1.2 MeV/u. Since fall 2006, regular operation of the new heavy ion complex started, using O, Ar, Ne, Kr and Xe beams, with scheduled experiments approved by the international Programme Advisory Committee.
- A consolidation program of PIAVE and ALPI is planned, so as to deliver a larger variety of beams with a current range 10÷100 pnA and with an energy exceeding the Coulomb barrier in relevant nuclear reaction cases. To this purpose, a new ECR ion source (Supernanogan) was purchased and will be installed in 2008.
- First tests with an external stripper station, located at 1/3 of ALPI, were successful; it is expected that the final ALPI energy can significantly increase, for those cases in which one can accept the ~70% transmission drop due to the stripper itself.

Further developments of ALPI will make it best suitable for the re-acceleration of radioactive nuclear species, after charge breeding and isotope selection: PIAVE shall have to be moved from its actual position to intercept the beam line coming from the RIB target; a normal conducting bunching RFQ will be built and placed just downstream the charge breeder, after which the ion velocity will match the initial velocity of SRFQ1; beam diagnostics stations, ideally suited for both high current stable and low current unstable beams, shall have to be developed and constructed. The changes, which are needed on ALPI, so as to make it an excellent stable-unstable beam accelerator, are described in chapter 8.3.

In addition to performance upgrades and relocation or construction of some components, it will be necessary to launch an extraordinary maintenance work on a number of ALPI

components, so as to allow ALPI (a machine which started operation ~13 years ago) to work efficiently for more than another decade (chapter 8.4).

Chapter 8.5 shows the very relevant energy increase, which one would obtain from a further upgrade of ALPI resonators and the construction of seven additional cryostats, and the related impact in cost and human resources.

Management issues such as time schedule and required personnel are treated in chapter 8.6.

8.2 Present status and further upgrade of the PIAVE-ALPI complex.

INFN-Laboratori Nazionali di Legnaro pursue a continue upgrade of their accelerator facilities, so as to keep them at pace with the new requirements of the nuclear physics community. Twelve years after the first operation of ALPI, the major upgrades have been: construction of the lower beta section of the linac (aimed at efficient acceleration of medium-heavy nuclei) and recent upgrade of the cryogenic system in order to refrigerate these resonators effectively; upgrade of the linac equivalent voltage from 20 to 48 MV (by replacing the superconducting layer on medium-high beta resonators[4]); construction and commissioning of the new higher current injector named PIAVE, based on an ECR (Electron Cyclotron Resonance) Ion Source[5] and on superconducting RFQs (Radiofrequency Quadrupoles).

Further upgrades on the existing facilities have been conceived and part of them was already funded, such as a better performing ECRIS for PIAVE and the refurbishing of the low beta linac section.

8.2.1 ECR Ion source developments

Concerning the ECR source, two important developments were conducted in 2006, which will improve the potentiality of the present ion source Alice: the construction of a new oven for metal species; the refrigeration of the source plasma chamber, so as to increase the microwave power level (by a factor ~3) and hence the average charge state and ion current. Nevertheless, a larger breakthrough in both charge state (and consequently final PIAVE-ALPI energy) and ion current is expected by the installation of a new, more modern, ion source (Supernanogan[6], purchased from Pantechnik), with which even the heaviest ion species (e.g. Pb or Bi) will be delivered to Nuclear Physics apparatuses. Supernanogan is a compact source, equipped with permanent magnets for both the confinement solenoids and the hexapole, well compatible with the present setup of the high voltage platform. Table 8.1 shows, for a few ion species, the extracted currents expected from the Supernanogan source. Multiplying them by the overall PIAVE-ALPI transmission (~50%), the current at the experimental station can be obtained. Source replacement is presently planned for year 2008. It must be pointed out, however, that the maximum beam current accepted by the superconducting RFQs is 5 eμA.

Table 8.1: Extracted currents in eμA expected, from the Supernanogan source, for some ion species of reference. Multiplying them by the overall PIAVE-ALPI transmission (~50%), the current at the experimental station can be obtained.

Ions/q	6+	8+	14+	25+	30+	24+
O	200					
Ar		250				
Kr			15			
Xe				5		
Ta						1
Au					1	
Pb				2		

8.2.2 Progress in the performance of ALPI SC resonators

This section deals with the upgrades of ALPI accelerating cavities which, both the recent past and the present or possible future ones are clearly of advantage for both stable primary heavy ions and unstable nuclear species.

In 2000-2003 ALPI medium-beta resonators were fully refurbished: the Pb layer previously deposited on the inner surface of Cu-based Quarter Wave Resonators (QWR) was stripped and replaced with a Nb layer, obtained by the sputtering technique [4]. The average operational accelerating field increased from 2.6 to more than 4 MV/m. The original ALPI goal in terms of final energies was then reached without using all the available cryostat positions and seven remain available for further energy upgrades. Moreover, the low beta resonators, the construction of which was completed a few years ago, could be efficiently refrigerated in 2004 by means of a significant reshaping of the liquid helium distribution line circuit. At the conclusion of these activities, the final energy of nuclei, after acceleration by the Tandem-ALPI complex, ranged between 20 and 5 MeV/A (considering ^{12}C to ^{104}Ru as the two reasonable mass extremes), with currents from 10÷20 to 1 pnA.

ALPI comprises, at present, 12 lower beta resonators – built in full Nb – which operate at the rather modest accelerating field (E_a) of 3 MV/m: this was in the early nineties the original ALPI design value. However, the off-line performance of the cavities was – since their first tests – significantly better (~ 6 MV/m or higher[7]). The maximum on line field attainable by low-beta QWRs is mostly limited, at present, by the micro phonic noise in the linac vault. Moreover, slow pressure-driven frequency drifts must be compensated for by slow mechanical tuners. One of the most straightforward ways to keep micro phonics under control is to increase the RF power available to the cavity control system (frequency bandwidth increases) so that, at need, part of this power can be fed in quadrature to the resonator and keep the phase difference between each resonator and the master clock to a minimum. This upgrade requires, besides purchasing new amplifier equipment, to redesign the RF lines feeding the resonators so that they can withstand a higher dissipated power (e.g. by cooling them with either liquid nitrogen or cold gaseous helium). This programme started in fall 2006: it began with the development of a prototype cryostat, which will be equipped with brand new QWRs (the construction of which started in 2007) and new RF lines. The prototype cryostat will be added in front of the low beta branch of ALPI. One can eventually expect, by 2008-2009, to have 16 QWRs available at an accelerating field of at least 5 MV/m. As anticipated in the introduction, the lower beta resonator refurbishment is essential for both stable and unstable ion acceleration and is hence considered as part of the SPES project and is funded therein.

Albeit being not part of the present SPES design, it is worth recalling that 7 cryostats with higher beta resonators can still be added at the end of ALPI. Given the expected accelerating field of these cavities (Ea between 6 and 7 MV/m), which were originally designed for the Nb-sputtering technique, this means that the equivalent accelerating field of ALPI can still be increased, from the present 48 to around 80 MV. This particular upgrade, of not negligible cost, is quoted separately and is not included in the core part of the present project design (see chapter 8.5). The completion of ALPI would also require the reallocation of the present debuncher, downstream along the beam line.

Fig. 8.1 shows the increase of ALPI equivalent voltage since its completion in 1995. The medium beta resonator refurbishment programme (from Pb/Cu to Nb/Cu) can be mostly appreciated, as well as the recent contribution of the lower beta cavities.

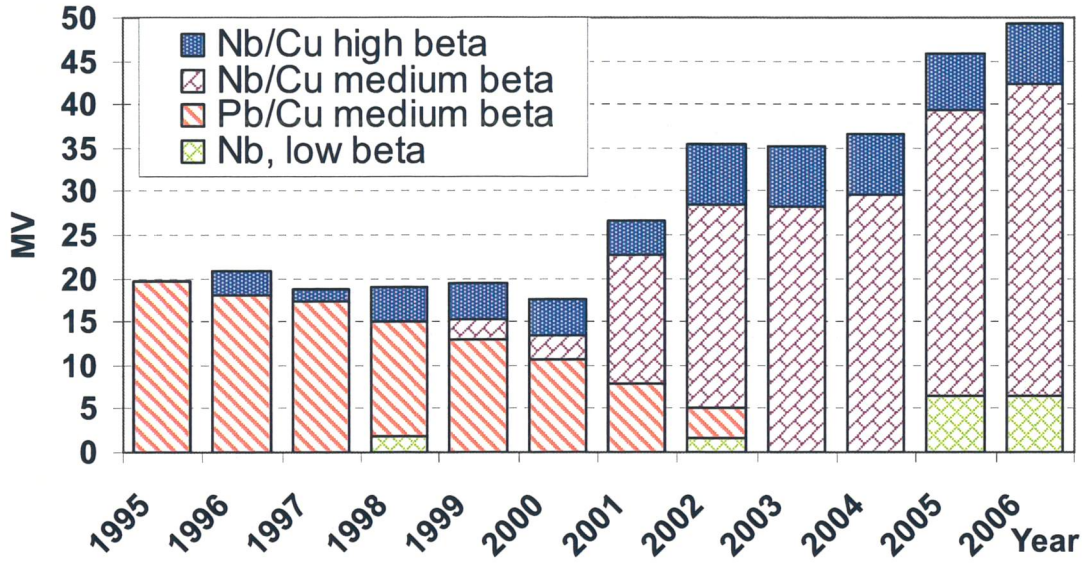

Fig. 8.1: *the figure shows the increase of the equivalent voltage V_{eq} of ALPI along the years. In the histogram, the contribution to V_{eq} by the medium beta Pb/Cu resonators, which were progressively replaced by Nb/Cu ones, can be noted; the contributions of the Nb/Cu high beta and of the full Nb low beta resonators are also shown.*

8.3 PIAVE-ALPI as a RIB accelerator

All the developments of lower, medium and higher beta resonators, presented in the previous chapter, contribute in making PIAVE-ALPI an extremely powerful and efficient accelerator of RIB species. But they are clearly not sufficient.

8.3.1 New location of the PIAVE injector

First of all, the actual location of PIAVE (parallel to the beam lines between Tandem and ALPI and between ALPI and experimental halls II and III) is not best suited to receive beams from the target – separator – charge breeder area.

What is here proposed (shown in fig. 8.2) is to move the whole PIAVE injector just upstream the ALPI tunnel. The beam coming from the charge breeder is immediately injected into the bunching RFQ which, increasing its energy from 2.5 to 37 keV/A, makes transport – in

the long transfer line between the breeder and PIAVE - easier (the required transverse focusing elements are not shown in the picture). New bunching elements, after the bunching RFQ and then the superconducting RFQs, are required. It is finally proposed to move the present ECR source and its platform south of the transfer line and to continue using it as the main injector for stable beam operation.

The present location of the cryogenic cold box, on the roof of the PIAVE tunnel, does not need to be modified. However, proper modifications of the cryogenic lines are clearly required and the location of the valve box needs to be defined.

As far as the radiation shielding is concerned, the proposed layout of the injector calls only for an additional radiation shielding around the RFQ section.

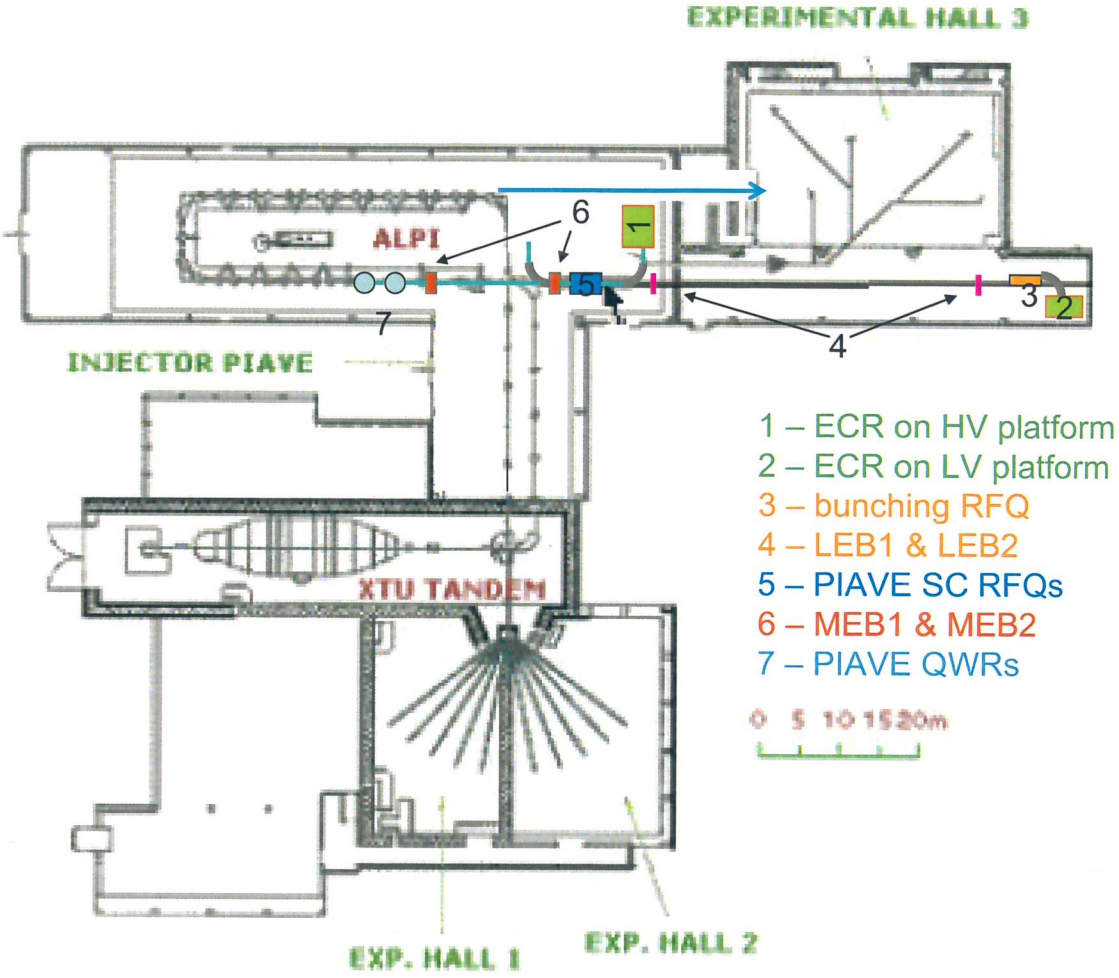

Fig. 8.2: *Block diagram of sources and cavities in the new layout of PIAVE-ALPI, as a RIB accelerator. One notes, in particular, the new location of the present ECRIS and platform (1), the ECR to be used as pilot beam injector (2), the bunching RFQ (3), low and medium energy bunching elements (4 and 6), PIAVE superconducting resonators (5 and 7)*

The next paragraphs will cover, besides the necessary changes in PIAVE-ALPI layout, those topics representing the most relevant developments of the modified linac configuration, i.e. the new bunching RFQ and the diagnostics concepts for rare isotopes beams.

8.3.2 The bunching RFQ

As shown in fig.8.2, the superconducting RFQs in their new location will receive the RIB beam coming from the long transfer line located aside the present 3rd experimental hall. Being

the charge breeding source located on a 60 kV platform (same voltage as the target platform), the ion velocity after the charge breeder is lower than required by the SRFQ1 input velocity. The appropriate accelerating element between the charge breeder and PIAVE is a so called "bunching RFQ" which, besides providing the mentioned velocity matching, will provide adiabatic focusing and bunching of the particles ejected by the breeder, providing nearly full beam transmission. The bunching RFQ is best located just downstream the charge breeder, since it is easier for higher than for lower velocity particles to cover the large transfer line (~ 70 m) between the charge breeder and PIAVE.

Table 8.2 shows the main features of the bunching RFQ, together with those of SRFQ1 and SRFQ2 of PIAVE. The bunching RFQ can either be superconducting or normal conducting. The latter option, being technically feasible because of the fairly low inter-electrode voltage, is easier to build and less expensive, and it is also dictated by the huge distance between the cold box and the structure.

Table 8.2: main parameters of the bunching RFQ, compared with those of SRFQ1 and SRFQ2 of PIAVE.

	SRFQ buncher		SRFQ1		SRFQ2		
	in	*out*	*in*	*out*	*in*	*out*	
Energy	2,35	37,1		423,4		672	keV/A
	0,56	40,18		100,77		159,93	MeV
Beta	0,0022	0,019		0,0302		0,038	
Voltage	43,3	43,3	200	200	290	290	kV
Length		2000		1281		833	mm
Ncell		360		29		13	
m_{max}		1,6		2,8		2,8	
a_{min}		2,5	80		80		mm
R0		3,4	10	10	16	16	mm
Synchr. phase	-90	-25	-40	-18	-8	-8	deg
Max.Sur. Field		18		25,4		23,7	MV/m
Stored Energy		0,51		3,1		4,2	J
Frequency		80		80		80	MHz

The bunching RFQ parameters are calculated for an A/q=8.5 ratio. Given the expected performances[8] of the charge breeder on the RIB species coming from the target-mass separator, however, a more conservative value of A/q=7 could also be assumed for A values between 40 and 140, thus further relaxing the design parameters of the bunching RFQ and allowing the superconducting RFQs to operate at a lower voltage.

The design of the bunching RFQ was outlined. Since the inter-vane voltage is limited to 43.3 kV (with a power dissipation of ~ 10 kW), a four-vane geometry is proposed, where the vanes are simply bolted to the tank, without any brazing nor electron-beam-welding seams (similarly to the Spiral II RFQ option for the primary accelerator). The 2D section was optimized, with the aim of keeping the current density on the joints below a level consistent with the above mentioned technical solution (i.e. $J_{limit} < 40$ A/cm). This result was achieved with a factor 4 safety margin. However, the 3D simulation (performed with the HFSS code) showed that the highest current density is located, as expected, in the end cell regions ($J_{max} \sim 20$ A/cm, i.e. retaining a factor 2 safety margin).

A detailed error study was performed in order to check the sensitivity of the structure to vane misalignment and mechanical machining errors. The next steps will be to design the tuning system (with both slug tuners and water flow), the cooling system and the input power coupler.

8.3.3 Performances of the RIB accelerator: the example Acceleration of ^{132}Sn

8.3.3.1 Evolution of ALPI final energy: the cases of 132Xe (stable) and 132Sn (unstable) beams.

The increasing performance of PIAVE-ALPI resonators, during the years, both as a stable or as a rare isotope beam accelerator, is shown in table 8.3 as it reflects on the final energy of selected ion species.

Table 8.3: Final ALPI energy, following subsequent upgrades of the accelerator facilities.

Year		2006	2007	2008	2009	2010	2011
E_{acc} [MV/m]	CR03	0	0	6	6		6
	CR04-CR06	3	3,5	3,5	6		6
	CR07-CR20	3,6	4,2	4,2	4,2		4,2
Energy [MeV/A]	$^{132}Xe^{20+}$	*6,1*	*7,1*	*7,9*			
	$^{132}Xe^{26+}$				*11*		11
	$^{132}Sn^{20+}$						9,1

In the table, the expected evolution of the accelerator performance, described in the previous paragraphs and last updated in summer 2007, is shown. In the upper part of the table, one notes the increase in the accelerating field of lower beta (CR03-CR06) and medium-higher beta resonators (CR07-CR20) along the past and coming years. Progressively one expects: the recovery of the full acceleration potential of mid-higher beta cavities from 3.5 to 4.2 MV/m (the latter being the value expected at the nominal dissipated power value of 7 W), due to a better setting of the cryo-plant parameters (result already achieved in Spring 2007, while writing this report); the increase in the accelerating field of lower beta cavities from the present 3 to 3.5 MV/m (operation with more powerful amplifiers, but old RF lines), to 6 MV/m (modified RF lines on all such cavities). Related to this scenario, the final energy of a ^{132}Xe beam (case of stable beams) and of a ^{132}Sn rare isotope beam is shown.

In 2009 it is planned to have the new Supernanogan ion source available, with the estimated usable charge state q=26+. The charge state for ^{132}Sn, i.e. 20+, represents then the updated performance of charge breeding ECR ion sources. After modifying the linac layout, possibly during 2010, both stable and unstable beams will be available.

Eventually, one can expect a final energy 9,1 MeV/A for the unstable ^{132}Sn and 11 MeV/A for the stable ^{132}Xe. Due to beam dynamics issues (treated in the next paragraph), the CR03 cavities must work at reduced field (2÷3 MV/m) in the present PIAVE configuration (till 2009). Only with the new design of the beam line after the SRFQs (modified linac layout), it is possible to operate those cavities at full field.

8.3.3.2 Beam dynamics for ^{132}Sn in the modified linac.

The beam line from the bunching RFQ, through the modified PIAVE, to the beginning of ALPI was designed and a few changes on the linac optics of ALPI itself were introduced.

The initial conditions for the overall simulation, comprising PIAVE (in its new place) and ALPI, are the following:

- a $^{132}Sn^{20+}$ beam was chosen, a species of top interest for nuclear physics applications and a charge state which is consistent with the capability of updated charge breeding ECR ion sources;
- the beam simulation starts at the exit of the second superconducting RFQ (SRFQ2), in its new location, assuming those transverse and longitudinal emittance values which are consistent with those experimentally observed at present in PIAVE.

Concerning the cavity accelerating field, the low beta section has an average value of 6 MV/m (expected at the end of the being carried out upgrade), whereas the medium beta one has an average value of 4.2 MV/m (available at present).

Optimization of ion transport was performed through several iterations with both TRACE3D and the multiparticle code PARMELA.

The layout of the line between the output of SRFQ2 and the entrance of ALPI is sketched in fig. 8.3.

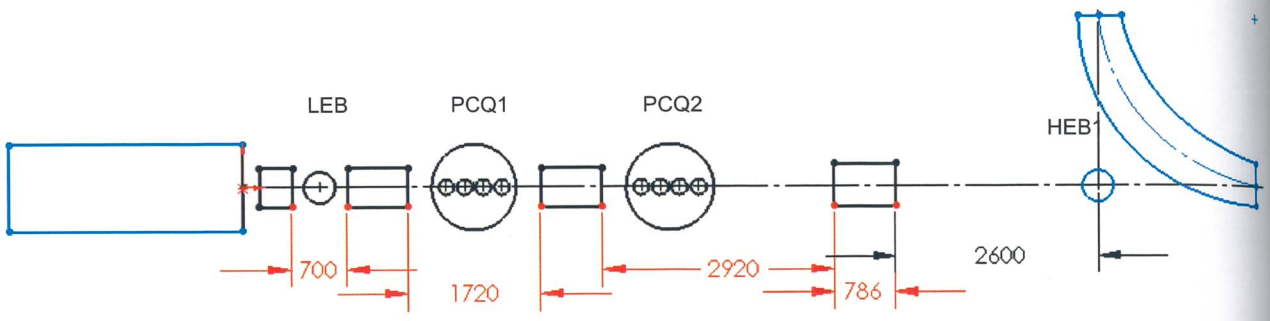

Fig. 8.3: *Layout of the new beam line following the superconducting RFQs: the position of two of the three bunchers and the QWR cryostats*

The magnetic elements are distributed along the beam line in a pattern which differs from that of present PIAVE: however, all over the line between the RFQs and ALPI, it makes use of already existing magnetic lenses, only located in a different place.

A piece of news is the addition of a new bunching element between the SRFQs and the first QWR cryostat (which we shall call Low Energy Buncher, LEB); then both presently installed higher energy bunchers (HEB1 and HEB2[9]), the first located before ID2 (90° dipole of the line coming from the tandem) and the second inside the ALPI vault, nicely match the longitudinal phase space into the first resonator of CR03.

Due to the increased ion beam rigidity, most magnetic lenses along ALPI shall have to be replaced with new ones, featuring a maximum field of 25 instead of 20 T/m. Nonetheless, it is possible to keep the physical length of the magnetic lenses unchanged, so that the modification of ALPI layout is kept minimum. For instance, the position of all cryostats (and consequently of the cryogenic distribution lines) remains the same. Therefore, one obtains an upgrade of ALPI with limited impact of time, cost, workload and human resources.

Fig. 8.4 and fig. 8.5 show the beam envelope in the two transverse and longitudinal phase spaces along the first and the second straight sections of ALPI, respectively. The simulation was obviously carried out for the entire linac.

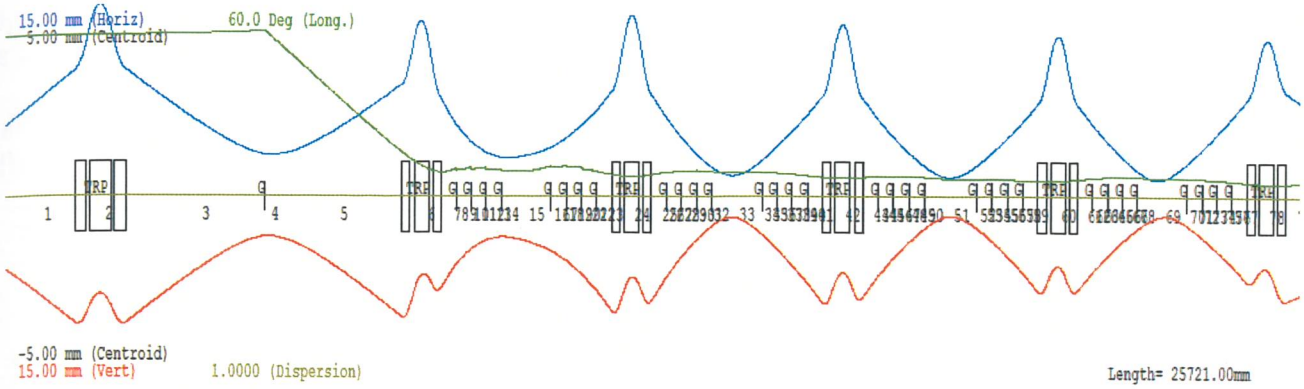

Fig. 8.4: *TRACE3D simulation of ALPI lower energy straight line*

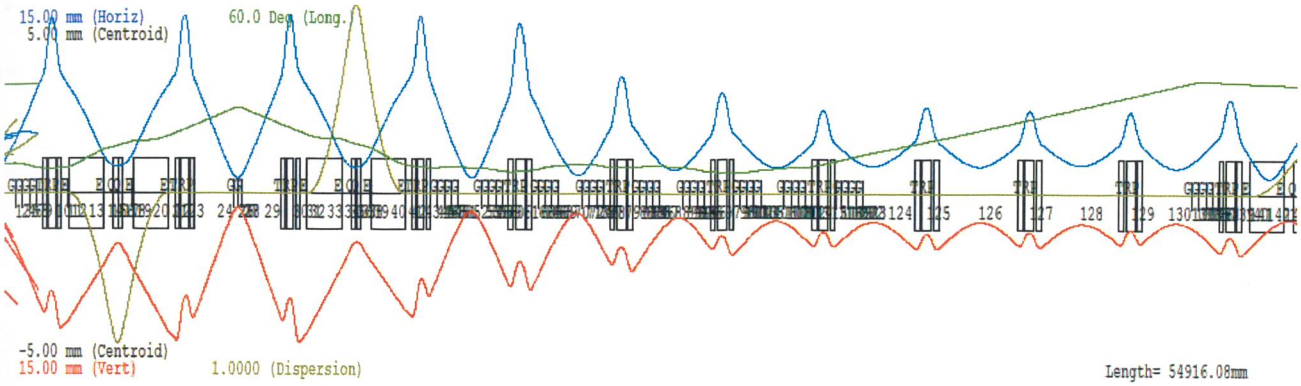

Fig. 8.5: *TRACE3D simulation of ALPI higher energy straight line*

8.3.4 Other beam lines

The present ECR platform, equipped with the new Supernanogan ECR ion source, will continue to be utilized for stable beam acceleration in PIAVE-ALPI. It is hence planned to locate the stable beam ECR ion source, on its platform, south of the new location of PIAVE. A new location of the HV transformer must be looked for, a possible option being the nearest possible location south of, and adjacent to, the linac building. In addition, the stable beam ECR ion source will be used for tuning purposes in case of very low intensity RIB beams: to tune the machine one has to use an intense phantom beam with the same charge over mass ratio.

The new locations of the platform and of the beam line insertion into the transfer line from the charge breeder to PIAVE will probably impose to move the transport line between ALPI and the 3rd experimental hall: the beam would rather continue on the same straight line of the higher energy branch of ALPI and will enter the hall in a different place, from which transfer lines to each experimental apparatus shall have to be designed.

Another change regards the beam line which connects directly the Tandem accelerator to the 3rd experimental hall. This line will be eliminated and possible beam requests of this type, which were always marginal so far, would imply to transport the beam through ALPI, used as a transfer line, with a slight decrease of the overall transmission.

8.4 Special Maintenance on ALPI

The ALPI linac was commissioned in 1994. The majority of its components was acquired earlier on and is ~15 years old. Clearly, the proposal of using ALPI as the rare isotope accelerator of SPES implies considering all special maintenance work, on the various

components of the accelerator, which is required for another ~ 10÷15 years of reliable operation (including the SPES construction period, during most of which operation of the linac with stable beams will continue).

It is proposed to concentrate the large part of the execution of the special maintenance during the period (probably the 4th year of execution of the SPES project) in which it will be anyhow necessary to stop stable beam operation, so as to adapt the linac to become an accelerator of both stable and unstable ion species.
This chapter lists the most important topics of this special maintenance.

8.4.1 Cryogenic system, cryogenic lines and cryostats

A third turbine needs to be added to the plant, in order to ensure some redundancy in the supply of cryogenic fluids to all cryostats.

At least 75% of the linac valve boxes need to be redesigned and built, in order to limit the intervention time in case of valve fault (this time is at present intolerably high).
If the layout of the lower energy branch will be modified, a new distribution line system must be planned and executed.

8.4.2 Vacuum system

Most of linac pumping systems is very old and a rather expensive replacement plan, regarded as ordinary maintenance, is in progress. The acceleration of RIBs will probably imply redesigning the vacuum system, and its control, to make it compatible with the evacuation of radioactive matter. On that occasion, it is recommendable to change at least the 50% older pumps with new ones.

8.4.3 RF components

Besides the resonators themselves, the performance of which is not expected to degrade appreciably during the next years, all their ancillary components need to be modernized: RF controllers, RF control system, RF power amplifiers, and all actuators of couplers, pickup and tuners. It is recommendable that a prototype work may start soon, and new components may be ordered, so that the replacement might also take place during the to-be-scheduled shutdown of the stable beam operation.

8.4.4 Resonator and cryostat assembly room

It is not too late to equip LNL with a clean room for superconducting resonator assembly. One needs to reserve a proper space for this activity, possibly in the buildings of the new accelerators, enough wide in space to accept all cryostat types (160 MHz QWRs, 80 MHz QWRs and S-RFQs). Cryostat ordinary maintenance is, as we learnt during 13 years of ALPI operation, a crucial activity and it reasonable to assume that 2-3 cryostat per year will continue to be maintained also in the future 10-15 years. It is necessary to ensure the best possible resonator performance, by providing clean rooms of least two classes (e.g. 1000 and 100) for resonator and cryostat assembly respectively.

8.5 An additional option: further energy upgrade of ALPI

Although not included in the SPES project work programme, it is noteworthy to remember that the present ALPI layout leaves ample margin for a further energy increase of the machine, whether used for stable or for unstable beam acceleration.

This further upgrade can be divided into two parts, independent from each other: replacement of part of the existing resonators with newly prepared (and more performing) ones; addition of up to seven more cryostats in the available space within the ALPI vault.

8.5.1 Further upgrade of existing resonators.

Looking at the present performance of existing resonators, it can be easily deduced that by re-sputtering with a new superconducting Nb layer 50% of the existing resonators and by producing completely new substrates and cavities for another 25%, the average accelerating field would increase from the present 4.2 MV/m to 5.5 MV/m. Consequently, the equivalent accelerating voltage (V_T) of this part of the linac would increase from 40 to 50 MV.

This would imply, for the project, an additional cost of 0,5 M€ and the work load of 5 people (among professionals and technicians) for about three years. During this period, a relevant fraction of the work load would go into removing installed cryostats from the beam line, maintaining them by mounted new or improved resonators, and setting them back in operation. It is assumed that this will be done starting from those cryostats hosting the worse performing cavities, and allowing a substantially unmodified machine calendar for the machine users.

8.5.2 Construction of seven additional cryostats.

The ALPI linac tunnel, beam lines and cryogenic lines are capable of hosting 7 additional cryostats. Should they be built, obviously assuming the more recent average performances (~ 6 MV/m), V_T would increase from 50 to the exceptional value of 80 MV.

The cost for seven fully equipped cryostats would be around 4,4 M€, to which the cost of an additional cryogenic plant should be added (~2,5 M€). The latter could be sized in such a way as to release the present tight refrigerating capability of the ALPI cryogenic plant, providing a safe redundancy in the refrigerating power.

8.6 Management issues

8.6.1 RIB accelerator schedule

Table 4: Gantt diagram of the SPES RIB-accelerator project.

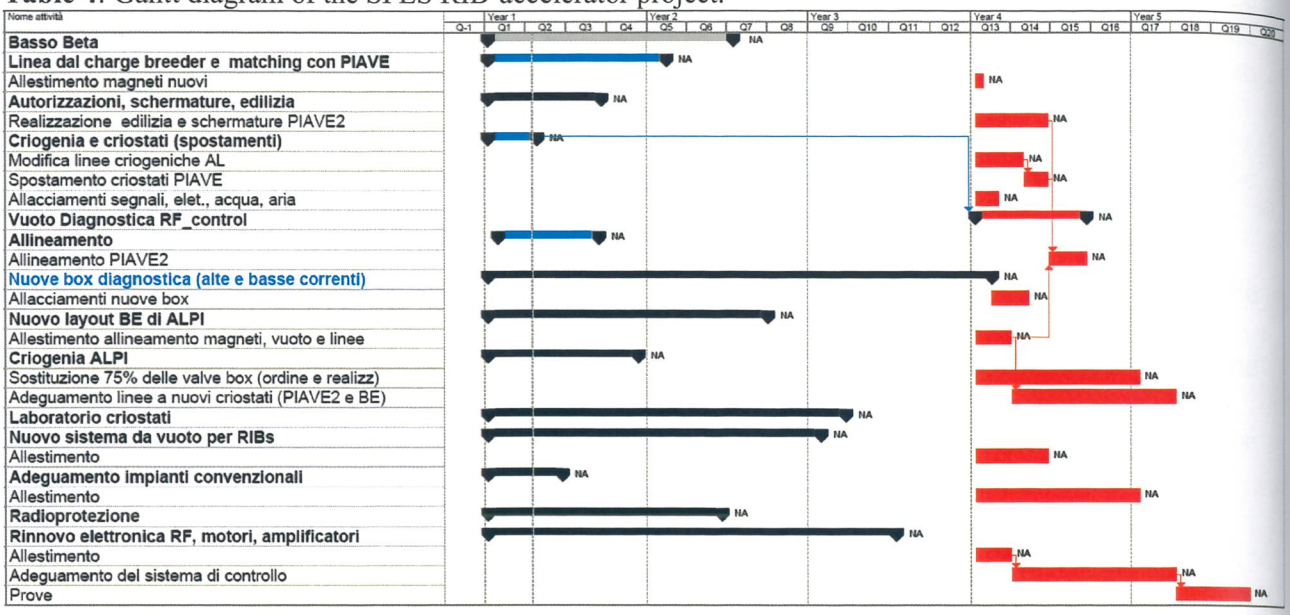

As shown in table 8.4, the time evolution of the activities described in this chapter is estimated to last around 4 to 5 years.

This estimation deserves a few comments.

- All activities concerning both PIAVE-ALPI upgrades, its special maintenance and the actions which are specific to the RIB accelerator are planned together;
- it is assumed that operation of PIAVE-ALPI for regular users must continue during most of this period: consequently, in this exercise, only during the last 1,5 years operation will be stopped and all actions requiring access to the accelerator halls will be concentrated;
- within the first 3 years, the mentioned activities are all assumed to start a t=0 time, contemporarily; more sensibly, mostly due to overlap of personnel duties, this will not happen; however, with the exception of a few branches (diagnostics, RF electronics, cryostat laboratory, RIB vacuum system), activities last less than three years and their execution can be diluted over the available time span;
- commissioning of the RIB accelerator, first with stable and pilot beams and then with RIBs, is not included in the chart; it might take at least one year, but it is more reasonable to discuss it in the framework of the overall machine commissioning.

8.6.2 Personnel

As can be easily argued from paragraph 8.5.1, most of the planned work will be executed during normal accelerator operation and will be carried out by many of the people presently involved in the operation and upgrades of the two linacs.

The estimation of the needed personnel resources were carried out, starting from the professional profile of the accelerator experts (both physicists, engineers and technicians) and adding new resources whenever required by the particular task. This assignment was made task by task.

It was clearly taken into account that most of the people involved have the charge of regular accelerator operation during years 1, 2 and 3. This has been considered by attributing a uniform

80% of work load to anyone involved, for this regular activity. This work load goes to 0 during the installation period, when all machines are stopped except possibly the tandem accelerator.

The resource estimation has not, unless marginally, affected those people mostly involved in the developments of the driver linac and its related topics. It has instead involved some resources from the Technical Division, in particular on the topics of infrastructures, shielding walls, utilities and small building construction work.

The main result is that, over all the 4÷5 years of project execution, at least 3 additional technicians are required for the group which should take care of managing the cryogenic systems, assembly of cryostats and other accelerator components, alignment procedure and activity.

Moreover, one additional technical unit is required for each of the following activities: one for the vacuum systems (management of current apparatuses and design and assembly and tests of the new ones), one for RF hardware electronics (this figure is currently missing in the accelerators structure and is clearly indispensable), one RF technician for resonator assembly, preparation and characterization. Further additional technical support (albeit amounting to probably less than 1 additional stable unit) is needed also in the field of: beam diagnostics, radioprotection evaluations and preparations (a physicist in this case) and beam dynamics studies (also a physicist and particularly in the first 1,5 years of the project).

In total, 11 equivalent professionals (1 of which new) and 15 technicians (5 of which new) are required for the 4,5 years for the execution of the works described in this chapter. Marginal optimization can be expected by joint personnel optimization with other branches of the SPES project.

---

[1] G. Fortuna et al, Proceedings of LINAC 1996, Geneva (CH), 170
[2] G. Bisoffi et al., Proceedings of EPAC 2006, Edinburgh (UK), 1597
[3] G. Bisoffi et al., Proceedings ofEPAC 2002, Paris (F), 266
[4] A.M. Porcellato et al., Proceedings ofEPAC 2002, Paris (F), 608
[5] M. Cavenago et al., Proceedings ofEPAC 2002, Paris (F), 1694
[6] http://www.pantechnik.com/eng/products/super.html
[7] A. Facco et al., Proceedings of EPAC 1998, Stockholm (S), 1846
[8] T. Lamy et al., Proceedings ofEPAC 2002, Paris (F), 1724
[9] A. Facco et al., Proceedings of EPAC 2000, Vienna (A), 2037

CHAPTER IX

CONTROL SYSTEM AND BEAM DIAGNOSTIC

9.1 Control system

9.1.1 Introduction

The Control System is a key component for the operation of the facility. It has to integrate in a homogeneous architecture many subsystems that have different levels of complexity and safety requirements and, because of this, will be based on different hardware technologies.

An Ethernet network is the most effective way to connect together a variety of heterogeneous devices: optical fibers will be used to implement long distance backbones at 1 GB/s (i.e. from the control room to the accelerator plant), while 100Mb/s switches can be used to link the components belonging to the same subsystem. The control system layout is presented in fig. 9.1. At the upper level, graphic workstations provide the interface to the operator while one

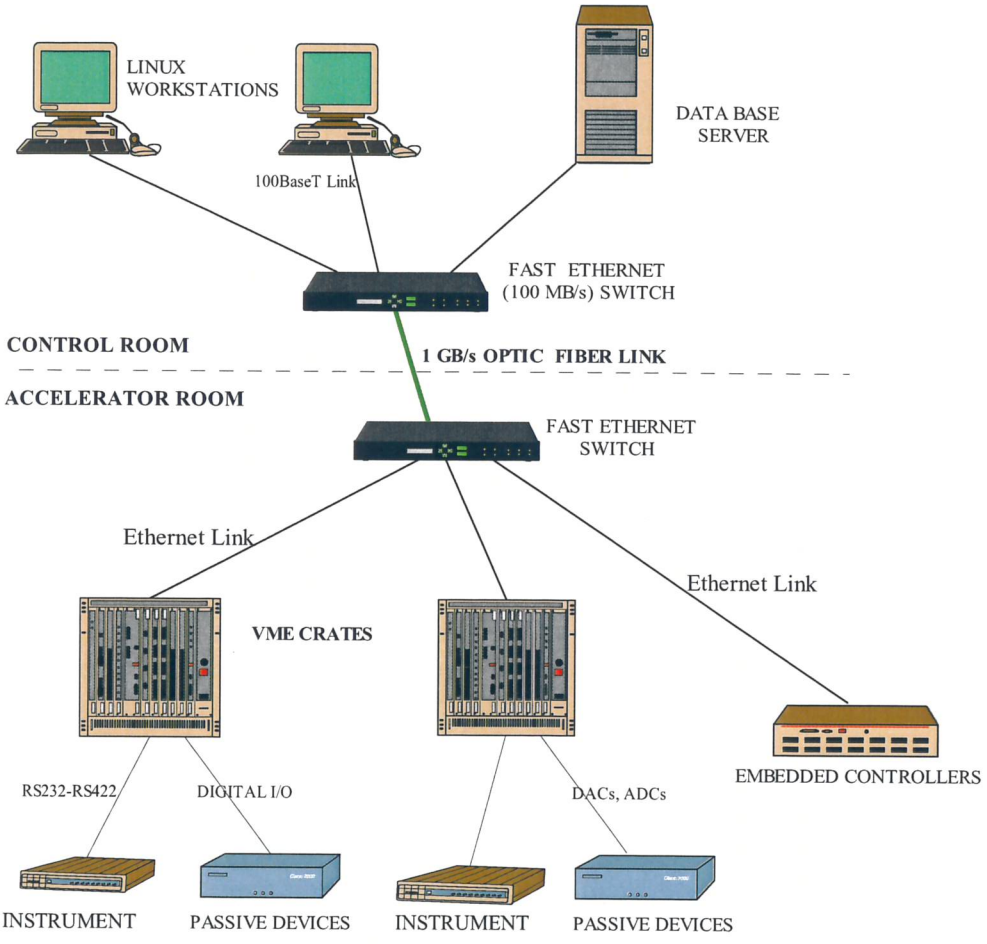

Fig.9.1: *Hardware architecture.*

(or more) servers are dedicated to the data base management. The lower level includes the computers that interface to the accelerator hardware and instrumentation and realize the local

feedback on specific components. Depending on their application, these devices can range from a simple embedded controller to a VME crate with a large number of I/O functions.

9.1.2 Hardware for low level controls

The control of each subsystem will be based on dedicated devices. PLCs will be used for the control of the vacuum and the radioprotection system, where the reliability is of critical relevance for the safety.

Most of the modern PLCs have, as network option, an Ethernet port that, from the hardware point of view, makes the system integration very simple; in turn, these devices may use proprietary field busses to communicate with I/O modules distributed over long distances. However, unless the PLCs are used only in conjunction with the supervising software provided by their manufacturers, a gateway software is required to interface them to the control network since the high level communication protocols still lack standardization. An OPC server is a good example of such gateway, although it has some limitations inherited from the DCOM protocol. Redundancy is a key feature where the continuity of service is of critical importance: many of high end PLCs (i.e. the Allen Bradley Control Logix /1756 family) full support the implementation of fault tolerant systems.

Where the control application requires the realization of complex functions or there are severe constraints in term of response time, the VME standard represents the best solution, thanks to the availability of powerful processor modules (i.e. PowerPC) and a large number of I/O cards from independent manufactures. The choice of the operating system strongly affects the overall performance; a real time OS like Vxworks provides an excellent basis to implement time-critical tasks because of its deterministic behavior and high speed: its response to asynchronous events can be as fast as a very few microseconds. For some specific applications, i.e. for the control of RF cavities, we plan to develop dedicated controller boards based on DSP and FPGA technology.

9.1.3 Graphics and Data Base management.

The computers on the highest layer realize two main functions: the Operator Interface and the Data Base Management. The Operator Interface will be provided by a number of Linux PCs, mainly located in the control room but also displaced in the accelerator vane for local tests and diagnostic purposes.

The supervisory PCs should be equivalent and interchangeable, in the sense that all information related to any facility subsystem will have to be accessible from any node of the control network; on the other hand, the capability of changing the operation parameters on a given subsystem must be granted to a restricted personnel only, and this will be done on a password verification basis. Selected categories of informations can be made available, in read-only mode, outside of local network, through a web server.

An essential function for the control system operation is the Database Management, that will be provided by a redundant server to guarantee a fault tolerant operation. The Data Base has to store the parameters for the setup of all facility subsystems, to collect and archive the data useful for the analysis of the operation, including alarms and all kind of events that can be significant for problems correlation and diagnosis. ORACLE will be used to implement the SPES data base.

9.1.4 *Control software*

Although different hardware technologies can be used in the control of SPES subsystems, it is mandatory that a common model be adopted to exchange data among them. According to the positive experience reported by more than one hundred research Institutions worldwide, the control system software will be based on EPICS. This software is used in the Labs where RIB facilities are in operation or under construction, in particular Oak Ridge (USA), TRIUMF (Canada) and Ganil (France) for the Spiral2 project.

The basic concept underlying EPICS architecture is a memory resident distributed data base; process variables (PV), which are part of a record structure, are collected from (or transferred to) the field according to a mechanism (periodic scan, interrupt, etc.) that is configurable by the user by means of graphic tools. Once the process variable has been stored in the data base, it is accessible by name from any node of the control network; the software infrastructure that locates the variable and makes it available to the requesting client is named Channel Access (CA). A computer that hosts a portion of the data base, updates the value of local PVs and processes them according to the scheme defined by the record links is named IOC. Creating the support for new devices is by far the most time consuming task when realizing a control system based on EPICS; however a large number of drivers either for I/O cards and general purpose instrumentation is available from the community of users. On the client side, many utilities exist to create a fully functional control system with no need of writing application code; some examples are: the Alarm Handler (AHL), the Backup and Restore Tool (BURT), the Extensible Display Manager (EDM) and the Histogram Tool. The system designer can easily develop its own client application: the only rule he has to observe is the compliance to the Channel Access protocol. A graphical IDE, based on ECLIPSE, is available to support the creation of user applications based on Java CA interface. Fig. 9.2 shows the software architecture of a control system based on EPICS.

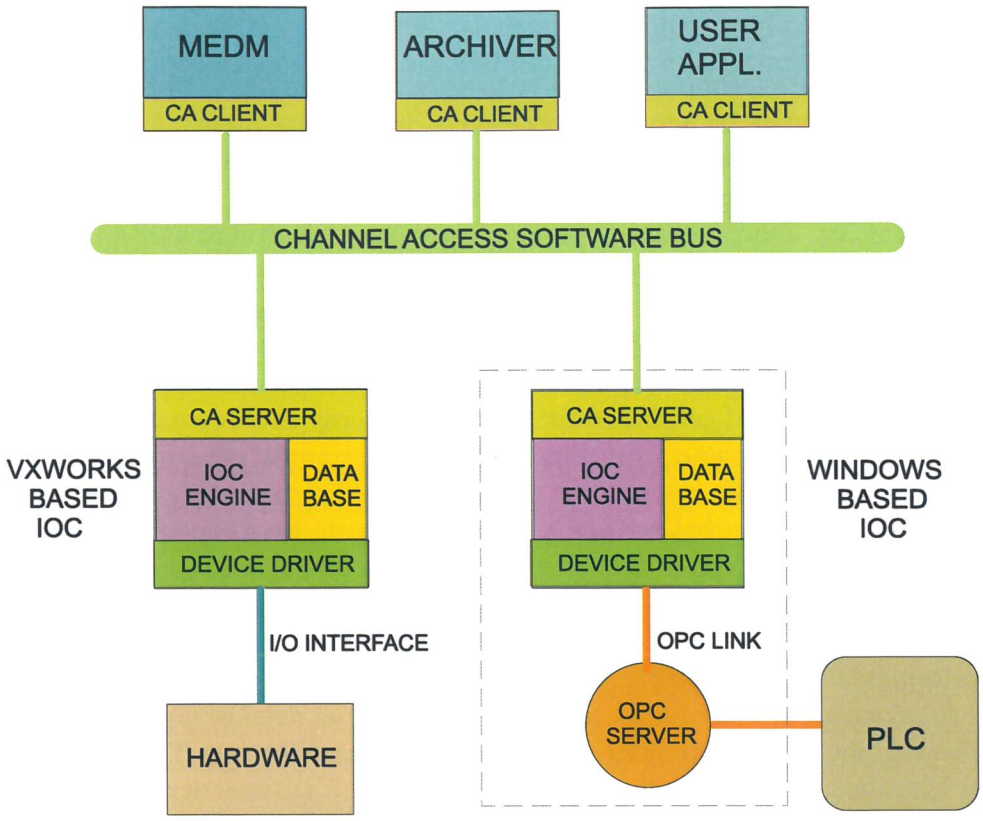

Fig.9.2: *Software Architecture*

9.1.5 Man power requirements

Most of PLC code will be developed in outsourcing. However, a professional profile with a sound experience in PLC programming is necessary either to supervise the work of external companies and to take care of the integration in the control network. An ORACLE expert is also necessary to design the layout of SPES Data Base, to deploy and maintain it till the completion of commissioning phase. A valid support on this task can be obtained from external consultants.

At least two EPICS developers must be part of the permanent staff either in the design stage and to maintain and update the installed software, once the facility will enter its regular operation.

The learning time to get acquainted with EPICS tools is usually estimated around 6 months. Adequate financial support must be foreseen to organize training courses, stages and visits of external consultants.

An estimate of human resources required to develop the control system can be summarized as follow:

1 Project Manager
2 EPICS experts (device driver and client application developers)
1 ORACLE expert (will work in collaboration with external consultants)
1 PLC expert (will work in collaboration with external companies)
1 Electronic technician to support the hardware installation, test and maintenance.

9.1.6 Cost

According with the experience reported from other laboratories where similar facilities have been built, it is reasonable to estimate that the cost of the control system will be around 5% of the cost for the construction of the overall facility.

9.2 High beam power diagnostic

The presence in the Spes project of a proton driver with beam power about 200 kW and the use of the PIAVE –ALPI as radioactive ion beam (RIB) accelerator, suggests the use of beam diagnostic systems with a wide range of capability: from some halves a score of mA, produced by TRIPS source, down to 10^4 ion/second of the produced RIB.

Expertise on standard techniques for beam monitor is present at LNL and LNS where Tandem, Linac and Cyclotron accelerators are running for stable beams.

At LNS a specific expertise was developed on radioactive beam management to operate EXCYT.

Both high power and low current diagnostic systems will be discussed.

The high power beam diagnostic systems are related to the operation of the proton driver in the SPES project. Different types of specific beam diagnostics must be installed and used to bring the accelerator and the beam transport lines into an operational condition. A first type of measurements is needed during the commissioning period:

- to help to reach the nominal performances of the accelerator;
- to confirm the results of beam dynamics calculations;
- to help in the understanding of the beam behaviour under both normal and abnormal conditions of operation.

A second type of measurement concerns the establishment of full beam power and the normal daily operation. The beam instrumentation must thus provide sufficient and necessary beam information for the accelerator operators in order to run the machine. In case of beam breakdown, beam diagnostic instrumentation must minimize the time needed to identify a problem, to restore the beam and to revalidate the beam characteristics. Moreover, it is also necessary to control and monitor beam losses along the accelerating structure.

The accelerator proposed for SPES leads to some difficulties for obtaining a complete characterization of the beam: mainly because of space-charge forces and the energy dispersion of the beam, beam dynamics studies lead to beam line designs with little room for diagnostic devices.

Even if some beam-destructive sensors could be used for specific measurements, the large quantity of beam energy deposited in any material forces us to use non-interceptive sensors. In addition to destroying the sensor, the interception of some fraction of the beam will lead to high activation of the accelerator structure and its surroundings.

Diagnostics must be designed to carry out beam measurements under the two different operation conditions of the accelerator: continuous wave (CW) and pulsed mode.
In CW operation the proton beam intensity may reach 40 mA. It is related to the RFQ part of the proton driver with energy up to 5 MeV and it allows the production of the neutron beam.

The pulsed-mode operation, with low-duty-factor (0.2 ms, 50 Hz), is the operation mode of the DTL which push the proton energy up to 40 MeV and allows the operation of the target for the rear ion beams production.

The basic parameters to be measured to characterize the beam are:

- the intensity of the beam
- the position of the transverse centroid of the beam
- the transverse beam profiles.

Secondly, more sophisticated characteristics of the beam may have to be measured or may be drawn from these measurements: bunch shape, phase measurement of the bunch with respect to the accelerating RF voltage, transverse emittance and energy of the beam.

9.2.1 Intensity measurements

Two categories of measurements are possible to evaluate the beam intensity: non destructive and destructive measurements.

Non destructive techniques allow the on-line beam operation. According to the time structure of the beam DC or AC measurements can be performed. The measurement of the intensity of the DC component of the beam can be achieved along the accelerator structure by using a current transformer (DCCT), the working principle of which is based on the magnetic amplifier. 100 μA accuracy can easily be reached by present commercial devices. This performance allows the measurement of the DC component of the 40-mA proton beam current. Better resolution, in order to measure the intensity of the ions beams, will be obtained by selecting high quality sensors, decreasing the bandwidth of the associated electronics or increasing the integration duration. In this case, best obtainable resolution may be as low as 1 μA for a 1- second integration time. Thus the DC component of the intensity of the ions beams can be correctly monitored. In the low-energy beam transport (LEBT) system, the use of DCCTs is the only way to monitor the DC beams delivered by ECR sources. DCCTs will therefore have to be located at the exit of the ECR sources.

After the RFQ, the beam is bunched and an AC beam current transformer (ACCT) has to be used to monitor the accelerated particle bunches under CW operation. Once again, commercial devices are available. Their upper cutoff frequency may be as high as 1.5 GHz. However, careful attention has to be paid to the response droop of ACCT under low-duty factor, pulsed-mode operation. The ACCT may be also considered as a powerful tool for evaluating the fluctuations of the beam current under CW as well as low-duty-factor pulsed-mode operation. In addition, an ACCT is very useful in the LEBT system, to help the ECR sources tuning in order to deliver a high quality beam to the RFQ.

Destructive measurements are the simplest way to measure the beam current under both CW and pulsed-mode operation.. This technique requires stopping the beam in a Faraday cup. A classical water-cooled Faraday cup can withstand a 10 kW beam and allows intensity measurements The current is measured over a large dynamic range and the resolution may be as low as 1 nA.

Up to the exit of the linac, the use of water cooled Faraday cups (WCFCs) has to be considered according to the power of the beam under the different modes of operation and the range of protons in copper, which remains below 2 mm up to 40 MeV.

Several Faraday cups will be installed along the accelerator. We plan to install a movable WCFC as close as possible to the RFQ. This installation will be possible (the available room ranges roughly from 20 cm to 25 cm) after an optimization of the beam dynamics and the mechanical design of the WCFC.

This WCFC will act as a beam stop during the tuning of the sources and it will monitor the beam current at the entrance of the RFQ allowing a crosscheck with the DCCT (on operation during normal running of the accelerators).

Downstream of the RFQ accelerating section, the WCFC cannot withstand the power of the beam under CW operation. Only low-duty-factor pulsed-beam operation can be considered.

During the commissioning period, tests and tuning, the WCFC will act as a beam stop and will monitor the current beam.

The transmission efficiency of the RFQ can be measured.

A crosscheck can be made with ACCT measurements (in operation during normal running of the accelerators).

Downstream the second DTL accelerating section, the use of a WCFC will need thermo-mechanical simulations in order to estimate the possible duty factor under full-power operation.

Sputtering effect will be considered: since the WCFC will intercept the beam, atoms and ions of copper may be ejected from the WCFC by sputtering and may travel along the beam pipe to the inside of the DTL cavities. This effect can seriously disturb the running of the cavities. Further investigations on this subject have to be made to achieve a better understanding and find possible cures.

9.2.2 Position measurements

Position measurements of the beam centroid in the beam pipe are of prime importance for the accelerator operation. This information may be drawn from the beam profile measurements. On-line and non-interceptive measurements are required wherever possible.

In the LEBT, the beam is in DC mode, therefore electromagnetic sensors, which sense the electromagnetic field accompanying the beam, cannot give any response. A quantitative measurement of the position of the beam will be deduced from the transverse profile measurements achieved by beam-profile grids [1]. Other possibilities may be investigated, as light detection by CCD camera. Owing to the energy loss by the incoming particle, the atoms of the residual gas are excited and they emit light as soon as they return to the ground state. A CCD camera can sense this light and the position of the beam can be deduced from this measurement.

After the RFQ the beam is pulsed and a response to the electromagnetic field accompanying the beam is available from electromagnetic pickups. We contemplate the use of capacitive or electromagnetic sensors such as strip-line or button pickups. These well-known sensors have four electrodes exposed to the electromagnetic field of the beam, each connected to a signal amplifier.

Strip-line are very popular for proton accelerators and provide higher amplitude signals, but 'button' electrodes have to be considered first, due to the reduced space available (<10 cm length) for any diagnostic box between DTL tanks.

The position measurement of the beam depends on the ratio of the signal amplitudes delivered by the electrodes. Several analogue or digital processing techniques allow the evaluation of the beam centroid position from the signal delivered by opposite electrodes.

9.2.3 Beam profile measurements

The measurements of the transverse horizontal and vertical profiles are extremely important along the linac structure and especially in the DTL section.

Three kinds of detector can be selected for SPES.

SPES accelerator beams are too intense under CW operation for traditional interceptive techniques such as harps, secondary-electron monitors, and wire scanners. The temperature

attained by the wires would be too high and would lead to their destruction. Therefore, only under low-duty-factor, pulsed-mode operation one can expect slow wire scanner or harp profile measurements operate reliably: these beam profile diagnostic methods are all of the same family. We have to focus now on their capability to withstand higher average power beam than the beams presently produced at LNL.

Another minimally interceptive technique is worthwhile noting: the residual-gas ionization profile measurement. The interaction between the beam and the background-residual gas creates electron-ion pairs which can be collected by a micro-channel plate (MCP) followed by a one plane position sensitive device [2,3]. The profile of the primary beam is deduced from the measurements of these collected and amplified charges.

Monitors based on the fluorescence of the residual gas interacting with the primary proton beam may also be considered here. The light in the visible range can be sensed by a CCD camera and it allows getting useful information, at least on the size of the beam. For this purpose, glass windows have to be installed on the LEBT beam pipe. Obviously the efficiency of this kind of monitor decreases as the beam energy increases.

9.2.4 Beam energy and bunch phase measurements

The bunch length of the beam can be measured by Start-Stop technique using the time difference between a MCP (Start), which amplifies the electrons from residual gas, and the RF master oscillation (Stop). The THREE-GRADIENT method, coupled to this information, gives a measurement of the beam longitudinal emittance. One of these detectors could be used to phase cavities and with two of them (or some other non destructive pick-up monitor) in a time-of-flight configuration it is possible to measure the proton beam energy.

9.3 Low intensity beam diagnostic

9.3.1 Introduction

An R&D work on beam diagnostic started in 2006 at LNL [4], aimed at developing new diagnostics stations for higher current beams in ALPI, using wires thicker than the actual (20 microns) and maintaining the same spatial resolution (250 microns). Also the possibility to use carbon fibre wires with melting point about 100°C higher than tungsten was investigated. The goal is to withstand 100 watts of beam power foreseen from Piave. Collaboration with ITEP in Moscow was signed for this subject. Moreover, always for high beam power, non-intercepting diagnostics devices are under study in collaboration with iThemba lab of Capetown. Beam profile and position measurements using a residual gas-ionization beam profile monitor system was tested to verify this technique in several configurations.

During the last years at LNS an increasing interest has come out concerning the production of radioactive ion beams (RIB), together with the renewed efforts around the cancer therapy by means of protons and ions. These two subjects share a common feature, namely the low intensity of the produced ion beams.

In some cases one can also need to handle very low intensity beams - e.g. when accelerating some rare radioactive isotope, or during the phase of beam tuning - and this task can be greatly simplified if suitable devices are available. Sometimes the need arises for single particle counting, so the ideal device should be able to operate in two, partially overlapped, intensity regimes.

Based on the experience gained during the EXCYT project development at INFN-LNS Catania, we propose now a set of viable solutions as for the RIB diagnostics at the forthcoming SPES facility.

9.3.2 *Main requirements*

The main features a beam monitoring device should have is the robustness, since it has to withstand beam tuning, implying long operating periods, human errors leading to over exposition to the beam, and all of the normal run operations. For the same reasons another important requirement is the cost: a low-cost device can be operated easily if one thinks to develop several interchangeable samples. Last but not least, the simplicity of the operating principle can help to get friendly and reliable devices.

On the other hand we start from the assumption that, in order to be sensitive to low and very low beam intensities, we need to borrow some technique from nuclear particle detectors. In order to increase the sensitivity of a beam sensor device there are two possible strategies: reducing the noise or increasing the signal. The former should be attained by improving the electronic design and the shielding of the usual devices, while the latter can be pursued by employing a particle detector that is generally sensitive to the energy released by the particle rather than to the carried charge.

In light of all these points we propose to employ as main beam sensors the scintillation detectors. A scintillation detector usually consists of a piece of scintillating material, optically coupled to an active photo sensor. This implies that the active element can be, at least in principle, protected from the direct exposition to the beam. On the other hand we observe that the price of scintillators is generally bound to their volume, and in any case it is not so high. In the framework of the EXCYT project several different beam sensors have been developed, tested and produced, based on this technique, and are currently in operation. Moreover, in some cases Silicon detectors have been employed, in particular where the identification of the accelerated beam species is required.

The use of Germanium detectors, in order to fully characterize the beam composition by means of a precision γ-ray fingerprints spectroscopy, is purposefully left to the experimentalists because we think it is not a standardized technique to be left in the hands of the beam operators.

9.3.3 *Scintillator-based beam sensors*

Scintillators are well known to the physicists since a long time. Their basic property is to emit as light part of the energy deposited by an impinging particle. The most used material for a long time was NaI, which has a good light yield: the average energy to produce a scintillation photon is $\approx$10 eV. Unfortunately it is strongly hygroscopic and needs to be used with special precautions.

A large family of fast polymeric plastic scintillators is today available on the market, and they are usually rather cheap and easy to be produced in any shape. Plastics can be practically chosen within a large spectrum of characteristics like decay time, emission wavelength, attenuation length, etc. Their main drawbacks are the poor radiation hardness and power dissipation; so special care should be taken when using a plastic scintillator in a high counting rate environment. The usage of a plastic on the beam is practically limited to a low intensity regime and for short time intervals.

Inorganic scintillator crystals have then come up to the attention of physicists, showing to have rather good mechanical properties, radiation hardness, scintillation efficiency, and some of them have a surprisingly short decay time, even shorter than plastics. Most of the currently used scintillators require an average energy of the order of $\approx$10-100 eV to produce a scintillation photon. The cost has large variations due to type, shape, quantity, doping, but we can still say

that it is cheap. Among the inorganic scintillators we can also put some amorphous materials, like glasses, usually doped with rare earths elements like terbium, gadolinium, cerium, etc.

Concerning the light readout devices, many types of photo sensors exist on the market, some of them better suited for current readout (photodiodes), some others for pulse counting (photomultipliers, avalanche photodiodes). Special devices also exist that are suitable for single photon counting (photomultipliers, hybrid photodiodes SPADs).

9.3.4 The proposed beam diagnostics devices

What we propose for the RIB diagnostics is the following set of basic sensors, while keeping open the possibility of developing additional configurations and/or devices should the need arise in some particular beam environment.

- LEBI (Low Energy Beam Imager)
- SBBS (Scintillator-Based Beam Sensor) bulk sensor
- HYSS (High Yield Scintillating Screen)
- P-FIBBS (Plastic Fibre-Based Beam Sensor)
- G-FIBBS (Glass Fibre-Based Beam Sensor)
- HEBI (High Energy Beam Identifier)
- PSHEBS (Position Sensitive High Energy Beam Sensors)
- gas detectors

9.3.5 LEBI (Low Energy Beam Imager)

The beam diagnostics in the pre-acceleration stage is a crucial point, since the requirement of a quick beam tuning is to have an efficient real-time check of the beam properties. The low energy diagnostic devices should be able to locate the beam position, to measure its transversal size and to identify its nuclear composition. The proposed LEBI sensor provides beam imaging (and possibly identification) by exploiting the radiation emitted by the radioactive ions (fig. 9.3). The core of this system is a scintillator plate of CsI(Tl) and a thin Mylar tape arranged in front of the plate. When the film and the scintillator are placed along the beam line in order to intercept the beam, the ions get implanted onto a small film area, which thus becomes a radioactive source. The emitted radiation (mainly β and γ rays) crosses the plate and produces scintillation light inside it. Since a large part of the solid angle covered by the plate is near the source, the sum of the contributions due to each particle crossing the plate brings to the formation of a light spot on the exit surface of the plate. Its intensity depends on the radial distance from the source centre, being higher at the centre and decreasing going away from it.

Observing the light spot by means of a CCD camera, it is possible to determine the presence of the beam, its location and to roughly measure its size.

The brightness of the light spot is related to the beam intensity, to the activity of the implanted nuclei and to the type and energy of the radiation produced by the decay. LEBI also features a bulk plastic scintillator, read-out by means of a suitable photomultiplier, capable of counting the radioactive decays. The well known exponential decay law, giving the number of particles per second emitted by each kind of isotope implanted on the tape, allows to extract the half-life.

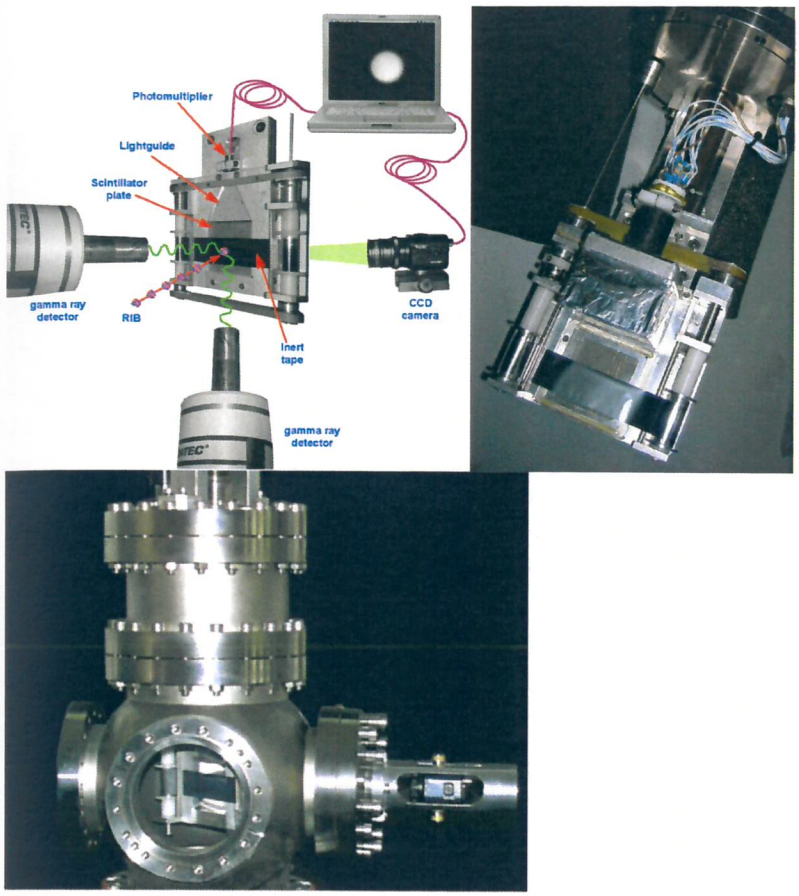

Fig. 9.3: *The LEBI sensor*

As an example in fig. 9.4 we show the image of a spot acquired with a ^{8}Li beam, $\approx 10^{4}$ particles per second (pps), and the corresponding reconstruction of the time-decay profile which allowed to identify the beam itself. We stress that the beam spot is rather wide in the vertical direction because of the needs of the mass separator acceptance, in front of which the LEBI was placed [5-7].

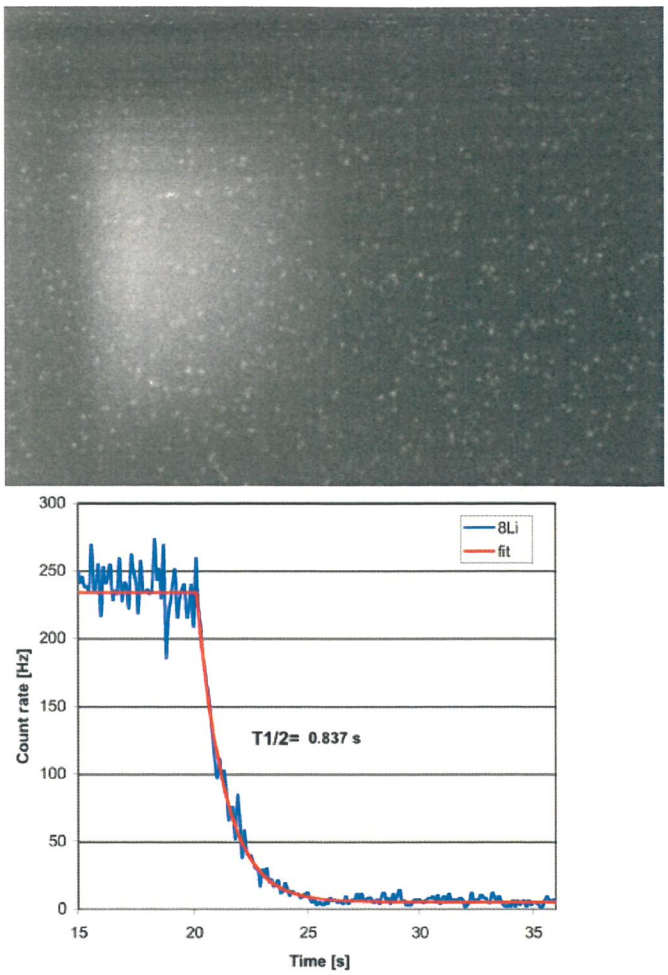

Fig. 9.4: *Lefthand side: spot acquired with a ^{8}Li beam, ≈10^{4} particles per second (pps). Righthand side: the corresponding reconstruction of the time-decay profile which allowed to identify the beam itself.*

9.3.6 SBBS (Scintillator-Based Beam Sensor) bulk sensor

For unstable beams with short half-life it is also possible to employ bulk scintillators, as they are not contaminated by long-lived species. What we propose is a scanning-slit sensor, with a bulk CsI scintillator placed behind a thin pair of mutually perpendicular slits, and read-out by means of a photomultiplier. Such a device, useful to measure the X and Y beam profiles, has proven to be able to operate both in the single particle regime and in the continuous, thus being self-calibrating [8,9]. Such a device is feasible for low and high energy.

9.3.7 HYSS (High Yield Scintillating Screen)

CsI scintillating screens can also be exploited to reconstruct the beam spot by means of a CCD camera, as well as special scintillating screens, made from doped glass fibres, featuring a space resolution around 20μm [10-15]. Other interesting scintillating materials are of course available, but they are generally rather expensive. Their use can be decided as a trade-off between cost and radiation hardness. An example of a beam spot, taken with the LEBI built-in CsI screen at very low energy and very low intensity (10keV, 10^{4} pps) with a radioactive beam, is shown in fig. 9.5. Another example, of 0.2mm diameter spot taken with a $^{1+}$Ag beam at 170keV and 0.6pA ($4{\cdot}10^{6}$ pps) intensity using a CsI(Tl) screen, is shown in fig. 9.5 left. In figure 9.5 centre is shown a 0.15mm diameter spot, taken with a proton beam at 10MeV and 30pA ($2{\cdot}10^{8}$ pps) intensity, using a SFOP made from scintillating glass fibres. In figure 9.5 right is

reported a 0.05mm diameter spot, taken with a proton beam at 10MeV and $\approx 10^5$ pps intensity, using a SFOP.

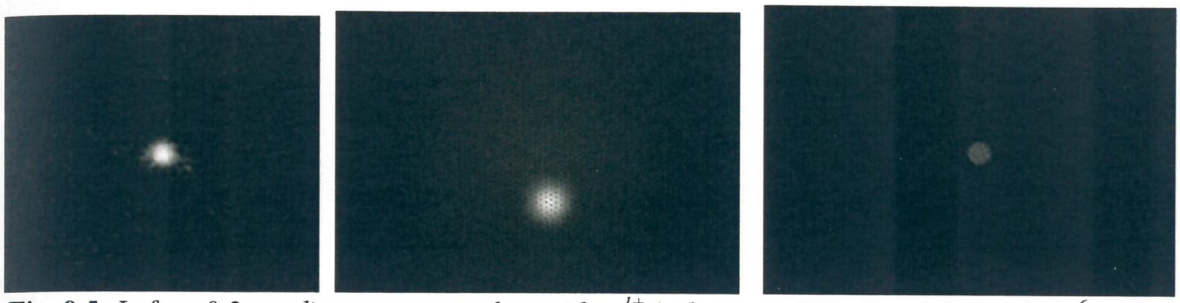

Fig. 9.5: *Left: a 0.2mm diameter spot, taken with a $^{1+}$Ag beam at 170keV and 0.6pA ($4 \cdot 10^6$ pps) intensity, using a 1mm thick CsI(Tl) screen. Center: a 0.15mm diameter spot, taken with a proton beam at 10MeV and 30pA ($2 \cdot 10^8$ pps) intensity, using a SFOP. Right: a 0.05mm diameter spot, taken with a proton beam at 10MeV and $\approx 10^5$ pps intensity, using a SFOP. The magnification factor throughout the three pictures is different.*

9.3.8 P-FIBBS (Plastic Fibre-Based Beam Sensor)

A pair of mutually perpendicular plastic scintillating fibres, read-out by means of a photomultiplier, motorized in order to scan the beam. Such a device, useful to measure the X and Y beam profiles, is feasible for high energy beams i.e. after the acceleration. This device is shown in fig. 9.6 and it has to be employed in order to reconstruct the beam profile by single particle counting [16].

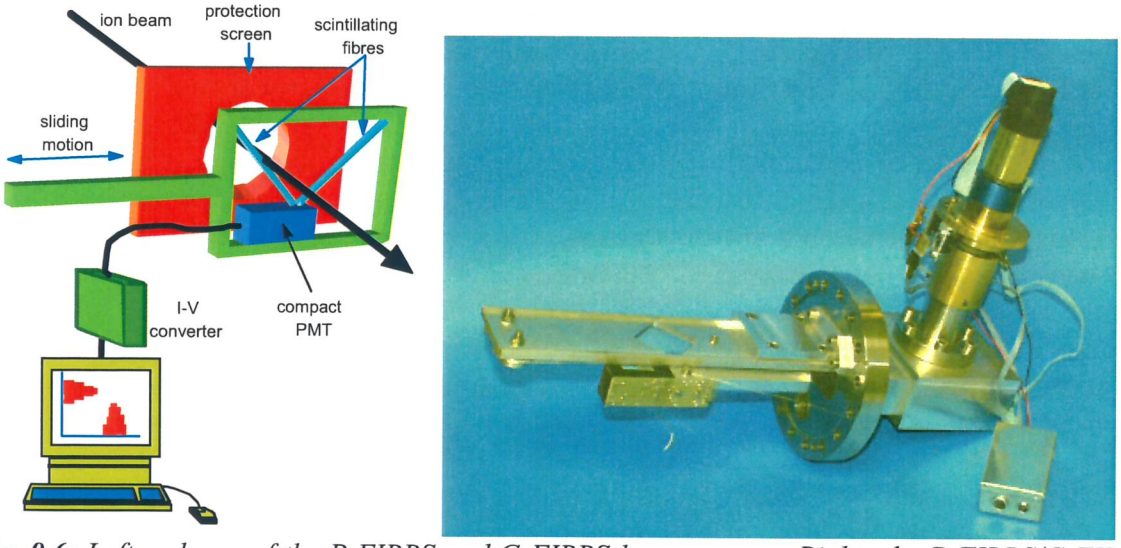

Fig. 9.6: *Left: scheme of the P-FIBBS and G-FIBBS beam sensors. Right: the P-FIBBS/G-FIBBS beam sensor.*

9.3.9 G-FIBBS (Glass Fibre-Based Beam Sensor)

Same as the previous one, but employing glass scintillating fibres. This device has to be employed in order to reconstruct the beam profile in current mode, as the glass fibres have a millisecond-scale light decay time but are more radiation tolerant than the plastic ones [17]. A sketch and a picture of P-FIBBS/G-FIBBS are shown in fig. 9.7.

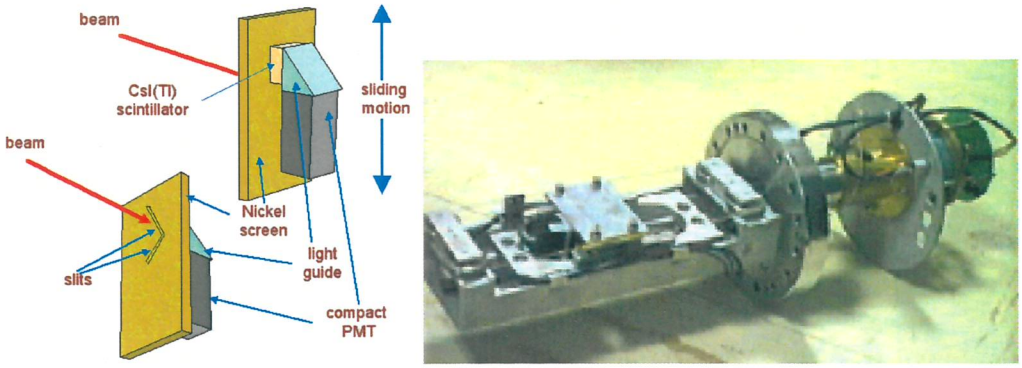

Fig. 9.7: *The SBBS beam sensor, based on slits and a bulk scintillator. Left: the scheme. Right: a prototype*

9.3.10 HEBI (High Energy Beam Identifier)

In order to perform a suitable beam identification after the acceleration, a possible device is a silicon telescope. An ordinary one, featuring a 20μm ΔE layer, followed by a 300μm E layer, can do a very nice job. As an example we consider the case of ^{130}Sn/^{130}In. In such a case the mass difference Δm is about 10MeV, while the ratio Δm/m is $8 \cdot 10^{-5}$. The expected separation on a ΔE versus E scatter plot comes from the difference in the deposited energy on the ΔE layer, in this case around 223 MeV for ^{130}Sn and 217 MeV for ^{130}In, i.e. 6 MeV. This results in a separation of the order of 0.6%, that given the expected performance of this kind of detector results at least of 3σ. Calculations and beam tests performed in the framework of the EXCYT facility, even though with lighter ions, confirm this expectation [5].

As for the beam intensity, that in order to operate such a detector should be below 10^4 pps, there are two possible schemes: (i) attenuation of the beam at the source whenever this measurement has to be performed; (ii) elastic scattering onto a thin heavy target (e.g. Au) and detection at a suitably chosen forward angle.

A possible problem could arise with longer-lived species, as they would get implanted into the E layer and spoil the following measurements because of detector contamination. In such a case the solution is to reduce the thickness of the E layer in order to have the impinging ion punching through it; this, by the way, would further improve the resolution and then the separation.

9.3.11 PSHEBS (Position-Sensitive High Energy Beam Sensor)

A larger area silicon detector, featuring multi-electrode perimetral readout, can be suitably used as position sensitive detector. A typical example is a square detector read-out from the 4 corners, employing a position reconstruction algorithm. Such a system, with the same constraints on beam intensity as the previous one, is capable of reconstructing the beam profile on a particle by particle basis.

9.3.12 Gas detectors

Several configurations of gas detectors can in principle be used for beam profile reconstruction and/or beam identification via energy loss. Their possible use has to be thought of as a trade off between effective advantages and their counterpart in terms of overall system reliability, robustness, ease-of-use by the operators, need of a gas flow system. Some indications can be found in [18-20] and references therein.

9.3.13 *Conclusions*

Particle detectors have been fruitfully exploited for developing high sensitivity beam diagnostics devices. The performance we have estimated for the EXCYT case, confirm that these systems will allow performing beam imaging and identification of low intensity radioactive ion beams also for the SPES case, satisfying the quick beam tuning requirements. These devices will be equipped with software tools in order to take into account the peculiarities of the different beams in terms of intensity and decay chain.

[1] M. Poggi et al, "Activity of the diagnostics laboratory", to be published in Annual Report 2006

[2] M. Bellato, A. Dainelli, S. Marigo, M. Poggi, "Residual gas based beam profile monitor", LNL-INFN (REP) 72/93 pag. 207

[3] J. C. Muller, H. H. Kiewiet, J. M. Schippers, "Beam profile measurements using residual gas in the beam line", http://www.kvi.nl/~annrep/ar1997/node61.html

[4] M. Poggi, et al, "A beam 'spot' monitor for beam current down to fA range", LNL-INFN (REP) 198/2003 pag. 259.

[5] S.Cappello, L.Cosentino, P.Finocchiaro, Off-line testing of beam diagnostics devices for characterization of low-intensity radioactive beams, Nuclear Instruments and Methods in Physics Research sect.A, 479 (2002) 243

[6] L.Cosentino, P.Finocchiaro, Recent developments of the excyt radioactive beam diagnostics, DIPAC 2003 Proceedings, Mainz, Germany

[7] L.Cosentino, P.Finocchiaro, Beam diagnostics for low-intensity radioactive beams, DIPAC 2001 Proceedings, ESRF, Grenoble, France

[8] P.Finocchiaro, G.Ciavola, L.Cosentino, M.Gu, G.Raia, A.Rovelli, A self-calibrating ion beam profiler based on a CsI scintillator, Nuclear Instruments and Methods in Physics Research sect.A 437(1999)552

[9] L.Cosentino, P.Finocchiaro, A.Pappalardo, A.Hermanne, H.Thienpont, M.Vervaeke, B.Volckaerts, P.Vynck, Ion micro-beam diagnostics with photodetectors, Nuclear Instruments and Methods in Physics Research B 209 (2003)340-344

[10] L.Cosentino, P.Finocchiaro, Ion beam imaging at very low energy and intensity, Nuclear Instruments and Methods in Physics Research B 211 (2003)443-446

[11] L.Cosentino, P.Finocchiaro, A.Pappalardo, A.Hermanne, H.Thienpont, M.Vervaeke, B.Volckaerts, P.Vynck, Ion micro-beam diagnostics with scintillators for application of Deep Lithography with Particles, IEEE Transactions on Nuclear Science, August 2003 Issue (vol.50, no.4) 774-777

[12] L.Cosentino, P.Finocchiaro, A.Pappalardo, A.Hermanne, H.Thienpont, M.Vervaeke, B.Volckaerts, P.Vynck, Ion micro-beam diagnostics with photodetectors, Nuclear Instruments and Methods in Physics Research B 209 (2003)340-344

[13] G.Ciavola et al., Status of the EXCYT facility at INFN-LNS, Nuclear Physics A 701 (1-4) (2002) pp.54-57

[14] L.Cosentino, P.Finocchiaro, Particle beam and X-ray imaging with thin CsI scintillating plates, IEEE Transactions on Nuclear Science, Vol.48, No.4, (2001)1132

[15] P.Finocchiaro, A.Amato, G.Ciavola, G.Cuttone, M.Gu, G.Raia, A.Rovelli, Scintillating detectors for low intensity ion beam monitoring, IEEE Transactions on Nuclear Science Vol.45, No.3, (1998)508

[16] P.Finocchiaro, A.Amato, G.Ciavola, G.Cuttone, M.Gu, G.Raia, A.Rovelli, A scintillating fiber based profiler for low intensity ion beams, Nuclear Instruments and Methods A385(1997)31

[17] P.Finocchiaro, A.Amato, G.Ciavola, L.Cosentino, G.Cuttone, M.Gu , G.Raia, A.Rovelli, Low intensity ion beam profiling with glass scintillating fibres, Nuclear Instruments and Methods A419(1998)83

[18] S.Aiello, P.Finocchiaro, S.Pirrone, G.Bellia, G.Cuttone, G.Politi, A.Rovelli, MINIT: a new gas detector for very low threshold particle identification, Nuclear Instruments and Methods in Physics Research sect.A 400(1997)469

[19] P.Finocchiaro, Particle Detectors for Low Intensity Ion Beam Diagnostics, Invited talk at the 15th International Conference on the Application of Accelerators in Research and Industry, 4-7 November 1998, Denton, Texas, USA, Conference Proceedings

[20] P.Finocchiaro, A.Amato, G.Ciavola, G.Cuttone, M.Gu, G.Raia, A.Rovelli, Low intensity ion-beam diagnostics with particle detectors, Invited talk at the DIPAC97, 12-14 October 1997, Frascati (Rome), Italy, Conference Proceedings page 53

CHAPTER X

RADIOPROTECTION

10.1 Introduction

A radiation protection programme identifies elements necessary to operate and maintain the SPES accelerator and the source region safely from a radiological point of view. Some radiation protection criteria to be met during the design stage are established.

Location and magnitude of radiation hazards related with have been identified and it is intended to provide the basis to control both the radiation hazards and the exposure of personnel. The main objectives are:

- Prevent occupational doses over legal limits
- Maintain personnel doses As Low As Reasonably Achievable (ALARA)
- Prevent unplanned exposures
- Minimize spread of contamination

The main topics covered are the following:

- Designation of radiation areas and access control
- Shielding calculations of the accelerator tunnel
- Induced radioactivity at the accelerator structures
- Preliminary radiation protection analyses of the SPES target

10.2 Designation of radiation areas and access control

One of the most important workplace safety issues is to ensure that both individual worker occupational exposure and environmental exposure are maintained below legal limits. Table I indicate the values of maximum effective dose admitted in a year exposure of a worker under normal conditions and the radiation area involved. For 2000 hours of operation of the accelerator, doses constrains, also named project guidelines, are assumed. The upper limit of effective dose for members of public outside of the Laboratory is placed a 10 μSv/y. In the case of a full beam loss the maximum dose received by an individual in the Laboratory is chosen at 10 μSv.

Table 10.1 - Limits and project guidelines.

Type of area	Effective dose (mSv/y)	Project guidelines (mSv/y)	Max. H*(10) rate (μSv/h)
Not classified	1	0.5	0.25
Supervised	6	3	1.5
Controlled	20	10	5

10.2.1 Worker classification

Radiation worker (RW)

These are workers required to be in the radiological areas for operation, maintenance, and field support. Workers performing special experiments, diagnoses, etc., that regularly access radiological areas may also be designated as RW

RW will be classified into two different categories: Radiation workers category A (RWA) and Radiation workers category B (RWB). RWA are workers that regularly access controlled radiological areas to perform their job and are likely to be exposed to an annual whole body effective dose higher than 6 mSv. RWB access occasionally to the controlled radiological areas and are likely to be exposed to an annual whole body effective dose higher than 1 mSv, but lower than 6 mSv.

Non-Radiation Workers (NRW)

These are administration, scientific, operations, and maintenance personnel whose responsibilities do not require, normally. access to areas with radiological hazards. The annual effective whole body dose limit for non-radiation workers is 1 mSv.

10.2.2 Access control

Access control is achieved by defining access zones as a function of expected hazards, and by applying procedures for movement between these zones. During beam acceleration very high hazards are anticipated in the accelerator tunnel and the target zone, and it is needed to assure the restriction of access to these areas. An Access Restriction System, consisting of physical as well as procedural barriers (locks, key card access, self-locking doors, monitoring tools), is therefore implemented to control entry.

10.3 Shielding calculations

Preliminary shielding calculations of the tunnel, where accelerator will be installed, were made with an analytical method [1-4] taking into account the following assumptions:

- maximum energy of the protons 40 MeV
- maximum current of the beam 500 μA
- maximum continuous beam losses 1 W/m
- constant losses of 10 W could occur in selected points (magnets, bending sections etc)
- constant losses above can be considered equivalent to a uniform loss of 1 W/m
- thick copper was chose as material target
- distance from the beam line equal a 4 m
- in the case of a full beam loss the maximum dose received by an individual in the Laboratory is fixed at 10 μSv.

Four representative loss points along the accelerator were considered, at energies ranging from 10 to 40 MeV. The lost protons were assumed to strike a thick copper target simulating a magnet coil o yoke. Copper was chosen because of similar density with iron and stainless steel.

Considering the source at a selected point as a "point source" then the total ambient dose equivalent $H_{tot,\theta}$ (E_p, θ , d) due to the neutrons and induced gamma rays at a certain depth of shielding is given by:

$$H_{tot,\theta}(E_p,\theta,d) = H_0(E_p,\theta)/r^2 \exp[-d/\lambda_\theta]$$

where E_p is the energy of incident protons, θ is the neutron emission angle with respect to the proton beam, d is the shielding thickness, r is the distance between the source point and the point of interest (4 m), λ_θ is the attenuation length and H_0 is the source term (Sv m^2 per proton).

Given the distance between loss points, the dose at a given location outside the shield only depends on the facing loss point. For lateral shielding the conservative source term in the forward direction H_0 was used taking into account that for high-Z target materials (like copper o Ta) the source term remains more o less isotropic.

Table II shows the shielding parameters used in the calculations and the resulting minimum thickness required to keep dose rate in the representative points at 0.25 μSv/h (non designated area), 1.5 μSv/h (supervised area) and 5 μSv/h (controlled area) for a proton beam loss of 10 W; concrete of 2.4 g/cm^3 density was considered.

A rough estimation of the thickness of the tunnel's roof ceiling was also made according to the beam energy and the intensity of the beam losses. A dose rate of 1 μSv/h at the top of the roof shielding was considered and a distance of 8 meters between source point and the roof. The lack of any information at this stage of the building near the facility makes difficult any further consideration.

Table 10.2

Proton energy (MeV)	Source term (mSv/h)	Attenuaton length (cm)	Concrete thickness (cm) Non designated area	Supervised area	Controlled area	Roof
10	100	12.1	125	100	85	90
20	494	12.5	145	125	110	110
30	1430	12.7	165	140	125	125
40	2800	13.7	185	160	145	145

Fig. 10.1 shows a schematic layout of the SPES accelerator preliminary shielding which will reduce the prompt radiation along the accelerator to a level compatible with a supervised area. Roof thickness shielding at the different energy sections is also reported. They guarantee at the top a dose rate of 1 μSv/h.

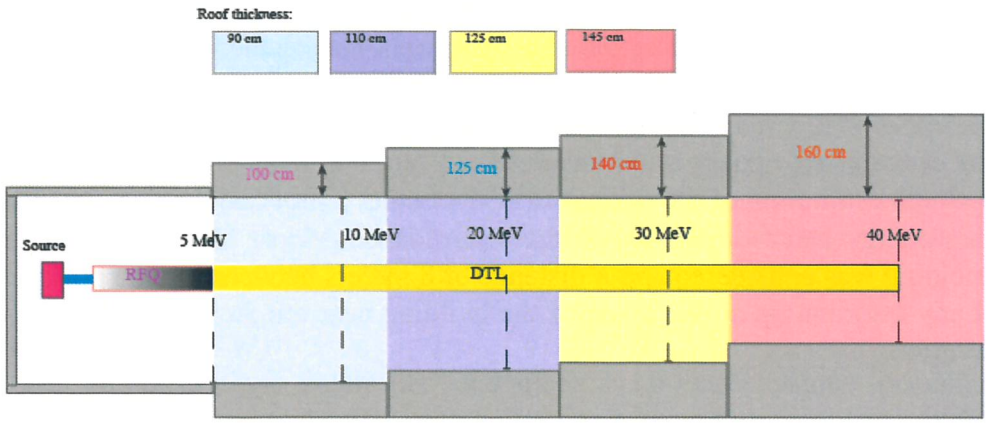

Fig.10.1: *Schematic layout of SPES accelerator shielding*

In the case of a full beam loss the total beam power will be deposited at the point of interest. Dose rates outside the proposed shielding (for having 1.5 μSv/h, continuous losses at selected energies) for a full beam loss is reported in table III.

Table 10.3

E (MeV)	10	20	30	40
Beam Power (kW)	5	10	15	20
Dose rate (mSv/h)	0.85	1.40	2.14	2.96

The maximum instantaneous dose rate with the proposed shielding is 2.96 mSv/h. For 10 μSv accumulated dose by one full beam loss implies that beam must be switched off within 12 seconds in the case of the worst loss scenario, condition easily met with an interlock system.

The shielding thickness of the floor of the accelerator tunnel, for a dose rate of 0.1 μSv/h, 2.2 m distance and 10 W constant losses in selected points, changes from 150 cm of concrete, at 10 MeV proton energy, up to 210 cm at the final stage energy of the accelerator.

10.4 Induced radioactivity in the accelerator structures

The estimation of the induced radioactivity in the accelerator components is important for maintenance interventions and final disposal of radioactive waste. The produced radioactive nuclides depend on the exact chemical composition of the irradiated materials which at the present state are not known. The radioactivity that may be induced by the neutrons generated from the beam interactions, assume that the "target" material surrounds the source point is given by:

$$A = N_0/W\ \sigma\ \varphi_0\ \rho\lambda$$

where

- N_0 is Avogadro's number, W is the atomic weight of the target material in g/mole, σ is the production cross section in cm^2, ρ is the material density in g/cm^3, λ is the attenuation length, and φ_0 is the neutron source strength in n/sec.

For proton energy of 40 MeV and a point loss of 10 W on a copper target, the neutron source strength is approximately 3.6E+10 n/sec. For concrete as target material with average atomic weight W = 30, a $\rho\lambda$ value in the region of interest of 33 g/cm^2, the induced saturation radioactivity is approximately 25 MBq per mb cross section. The total activity estimated in such a way is independent of the detailed geometric distribution of the material surrounding the source point as long as there are no strongly neutron absorbing materials in the path of the neutrons.

For cross sections of the order of a few times 10 mb the expected total saturation activity will be approximately 1 GBq. With a workload of 2000 hours per year of SPES operation, for long lived species the saturation activity will be much closed to 230 MBq. Most of this radioactivity will be fixed in place in the material surrounding the source point and only a very serious accident can have as effect the spread or loose of radioactive material.

The above estimate assumes that the expected beam loss in the accelerator system is concentrated in a given point. In the case of a realistic scenario the losses will occur along the entire length of the accelerator (number of discrete points) so the induced radioactivity at each point will be only a fraction of the 230 MBq total saturation activity.

10.5 Preliminary radiation protection analyses of the SPES target

The objective here is a preliminary assessment of some radiation protection quantities. The proton beam interacts with the target disks (28.6 g of UCx) and the structures around the disks (the target configuration is shown in fig. 10.2 and described in detail in [5, 6]). The inelastic collisions produce neutrons and gammas (which can escape the target system) and radioactive residual nuclei (which can emit gamma, beta and alpha particles). The produced neutrons, in turn, can activate other structural components in the surroundings of the target. Here some quantities are estimated [7] by means of computer codes:

- the dose due to the produced neutrons and prompt gammas;
- the gamma dose coming from the activated UC_x disks;
- the gamma dose coming from the activated anticorodal containment.

In the target configuration analyzed, the disks are surrounded by a graphite box (2 mm thick) and a layer of tantalum (1.5 mm thick). Then the target is placed inside an anticorodal sphere of radius r=15 cm and thickness 0.5 cm (see fig.10.2). Even if the MCNP model of the target system is simplified (no model of foreseen blocks of tantalum, copper and other structural materials has been made), this description is considered good enough for assessing the mentioned radiation protection quantities.

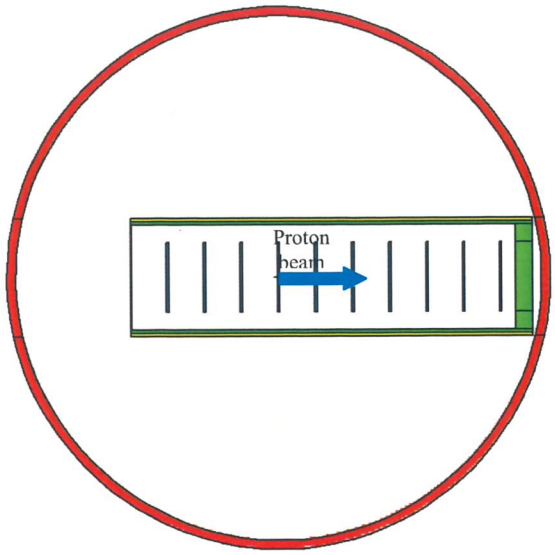

Fig. 10.2: *Reference target configuration for the calculations.*

Two computer codes have been used for the calculations:

1. MCNPX version 2.5.0 [8], a Monte Carlo particle transport code used with the Bertini-Dresner model [9] for the description of the proton nuclear interactions and with the ORNL model [10] for the description of the fission fragment distribution.
2. SP-FISPACT [11], that is an extension of the activation code FISPACT [12] for neutron energies higher than 20 MeV and for protons. This allows to calculate the activity (Bq), the evolution and the accumulation with time of the residual nuclei provided by MCNPX (about 15% of the atoms provided by MCNPX are expunged because not included in the FISPACT decay library).

The calculations here refer mainly to the ambient dose equivalent H*(10) (the dose equivalent at a depth of 10 mm in the ICRU sphere), which represents a "reasonable estimate" of the effective dose [13] (at least for the energy ranges considered here). The flux-to-dose conversion factors are taken from [13] for neutrons and from [14] for gammas.

10.5.1 The neutron dose

The 40 MeV proton beam impinges on the disks and on the structures surrounding them, producing neutrons which can escape the target system. According to MCNPX, the neutrons created in the target for 0.2 mA are $4.9 \cdot 10^{13}$ neutrons/s. The neutron dose at a distance of 1 m (averaged over the sphere surface) from the centre of the target turns out to be 535 Sv/h. Table 10.4 summarizes these results for r=15.5 cm and r=100 cm.

Table 10.4: Neutron doses.

Radius of the sphere (cm)	**Average neutron flux (cm^{-2} s^{-1})**	**Average neutron ambient dose equivalent H*(10) (Sv/h)**
15.5	**$1.9 \cdot 10^{10}$**	**$2.5 \cdot 10^{4}$**
100	**$3.9 \cdot 10^{8}$**	**$5.4 \cdot 10^{2}$**

Even if there is not spherical symmetry for the neutron dose (because of the angular distribution and the different energy spectra of the neutron flux), the difference taking into account the angular direction is limited: in the forward direction (with respect to the proton beam) the dose reaches values up to 650 Sv/h, laterally up to 490 Sv/h and in the backward direction up to 500 Sv/h.

The dose due to the prompt gammas has been evaluated to be negligible (<2%) with respect to the neutron dose.

The obtained results can be utilized to assess preliminary shielding thicknesses to lower the doses to acceptable limits.

10.5.2 The gamma dose from the UC_x disks

The gamma dose from the activated UC_x disks is evaluated here. The proton inelastic collisions in the UC_x disks are $8.9 \cdot 10^{12}$ collisions s^{-1}. These include fission reactions as well as other nuclear reactions (such as (p,n), (p,pn), etc.). Table 10.5 shows the reaction rates and the corresponding number of produced residual nuclei.

Table 10.5 Inelastic collisions in the UC_x disks.

	Number of reactions (s^{-1})	Number of produced atoms (s^{-1})
Fissions	$7.0 \cdot 10^{12}$	$1.4 \cdot 10^{13}$
Other inelastic collisions	$1.9 \cdot 10^{12}$	$1.9 \cdot 10^{12}$
Total	**$8.9 \cdot 10^{12}$**	**$1.6 \cdot 10^{13}$**

About 88% of the atoms produced in the disks are fission fragments. If we include also the production of ^{1}H ($5.7 \cdot 10^{12}$ s^{-1}), ^{2}H ($6.5 \cdot 10^{11}$ s^{-1}), ^{3}H ($4.5 \cdot 10^{8}$ s^{-1}) and ^{4}He ($3 \cdot 10^{12}$ s^{-1}), then the total number of produced atoms becomes $2.5 \cdot 10^{13}$ s^{-1}.

The irradiation time is assumed to be seven continuous days (at 40 MeV, 0.2 mA). The activity of the UC_x disks, during irradiation and during the cooling period, is reported in table 6 and shown in fig. 3 and fig. 4. The activity at shutdown is about $2 \cdot 10^{13}$ Bq and becomes, after one year of cooling, about 10^{10} Bq. The last column of table 3 shows the gamma dose for only 1 g of UC_x at 1 m distance without any shielding.

The tritium production in the UC_x is estimated to be $\sim 10^{9}$ atoms/second. This becomes, after 7 days of irradiation, about $6 \cdot 10^{14}$ atoms of ^{3}H, with an activity of about $\sim 10^{6}$ Bq.

As far as the alpha activity is concerned, while the ^{238}U has an activity of $3 \cdot 10^{5}$ Bq, the maximum alpha activity of the disks is $6 \cdot 10^{8}$ Bq. This is mainly (but not only) due to the formation of ^{236}Pu.

The behaviour of the gamma source is very similar to that of the activity: the ratio between the activity (disintegrations per second) and the gamma source (gammas emitted per second), turns out to vary between 1.3 and 0.3 in the cooling period considered. For the dose calculations also the spectra of the emitted gammas have been taken into account (most of the gammas lie in the energy range between 0.01 MeV and 2 MeV).

Table 10.6 Activation of the UC_x disks (28.6 g).

	Activation			Gamma source		Gamma dose* for 1 gram at 1 metre without shielding
IRRADIATION STEPS	**Bq**	**Bq/kg**	**cm^{-3} s^{-1}**	**s^{-1}**	**Average energy (MeV)**	**Sv/h**
0 Secs	3.0E+05	1.0E+07	2.3E+03	2.6E+04	0.01	6.0E-11
1 Secs	4.3E+11	1.5E+13	7.7E+10	8.8E+11	0.6	2.4E-03
1 Mins	4.1E+12	1.4E+14	5.9E+11	6.7E+12	0.6	1.8E-02
1 Hours	1.1E+13	3.7E+14	1.4E+12	1.6E+13	0.6	4.8E-02
1 Days	1.5E+13	5.2E+14	1.9E+12	2.1E+13	0.6	6.2E-02
4 Days	1.7E+13	6.0E+14	2.0E+12	2.3E+13	0.6	6.7E-02
7 Days	1.8E+13	6.3E+14	2.1E+12	2.4E+13	0.6	6.8E-02
COOLING STEPS						
1 Secs	1.8E+13	6.1E+14	2.0E+12	2.3E+13	0.6	6.6E-02
1 Hours	7.4E+12	2.6E+14	6.7E+11	7.7E+12	0.6	2.1E-02
1 Days	3.0E+12	1.1E+14	2.5E+11	2.9E+12	0.4	6.2E-03
3 Days	1.6E+12	5.6E+13	1.4E+11	1.6E+12	0.4	3.5E-03
30 Days	1.6E+11	5.5E+12	1.2E+10	1.3E+11	0.6	3.5E-04
90 Days	4.5E+10	1.6E+12	2.4E+09	2.8E+10	0.6	7.6E-05
365 Days	9.0E+09	3.1E+11	3.2E+08	3.7E+09	0.4	8.6E-06
10 Years	5.6E+08	1.9E+10	2.2E+07	2.5E+08	0.4	5.4E-07
100 Years	1.1E+08	3.7E+09	2.8E+06	3.2E+07	0.6	9.2E-08

** The method for this gamma dose calculation is reported in [12].*

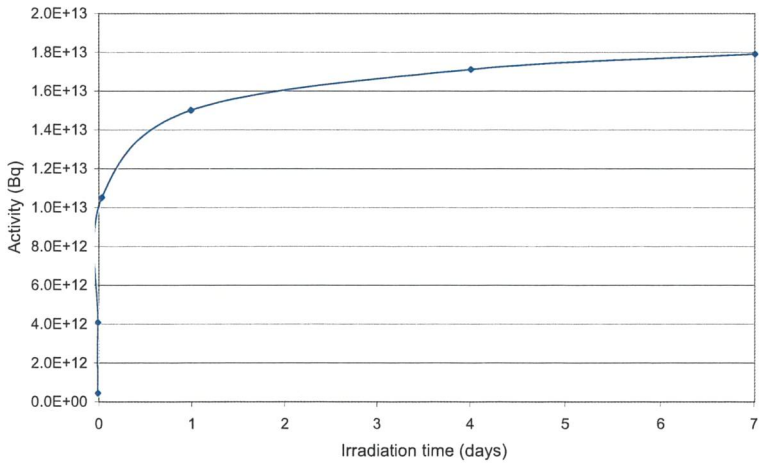

Fig. 10.3: *Activity of the UC_x disks during irradiation.*

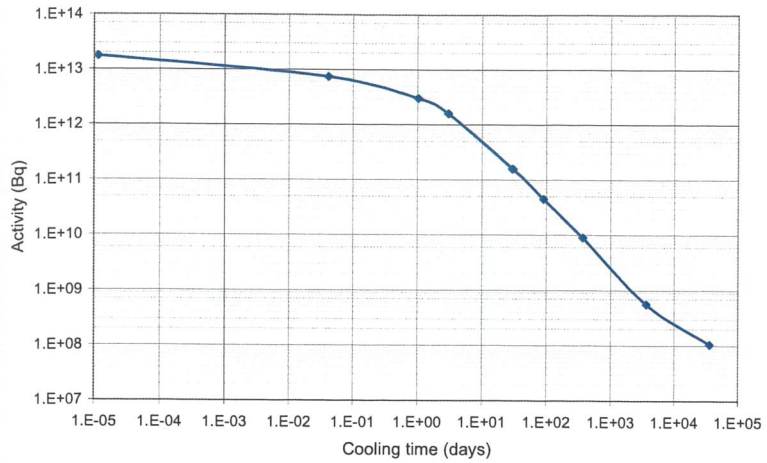

Fig. 10.4: *Activity of the UC_x disks after seven irradiation days.*

Since the gamma dose is approximately proportional to the gamma flux (if the spectra do not change too much) and the gamma flux is proportional to the gamma source, we can expect that the gamma dose is approximately proportional to the gamma source of table 10.6. The gamma doses over the anticorodal sphere after 3 cooling days and after 365 cooling days are reported in table 10.7.

Table 10.7. Calculated γ dose. The radius of the anticorodal sphere is r=15.5cm.

	γ source	**Average γ dose on the anticorodal sphere surface**	**Max γ dose on the anticorodal sphere surface**
3 cooling days	**$1.6 \cdot 10^{12}$ s^{-1}**	**~4 Sv/h**	**~6 Sv/h**
365 cooling days	**$3.7 \cdot 10^{9}$ s^{-1}**	**~8 mSv/h**	**~13 mSv/h**

The doses are still high even after 365 cooling days. Monoenergetic gamma rays of 0.6 MeV (that is the average energy of the gammas) can be attenuated by a factor of 10 by a lead shielding thickness of about 1.6 cm [15].

10.5.3 The gamma dose from the anticorodal

The activation of the anticorodal sphere around the target is evaluated here. The neutron flux averaged over the anticorodal turns out to be $2.8 \cdot 10^{10}$ cm^{-2} s^{-1} with a flux-averaged energy of 1.8 MeV. The activation results, obtained from this neutron flux, are shown in table 5: after one irradiation week, the activation turns out to be $2.3 \cdot 10^{10}$ Bq. The gamma source (s^{-1}) of the anticorodal (due to neutron activation) is negligible (<0.2%) with respect to the gamma source of the UC_x disks (due to proton activation).

Table 10.8. Activation of the anticorodal sphere (inner radius=15 cm, outer radius=15.5 cm, ρ=2.7 g/cm^3, mass=3.9 kg).

	Activation		**Gamma source**			**Gamma dose* for 1 gram at 1 metre without shielding**
IRRADIATION STEPS	**Bq**	**Bq/kg**	**cm^{-3} s^{-1}**	**s^{-1}**	**Average energy (MeV)**	**Sv/h**
1 Secs	2.1E+09	5.2E+08	1.4E+06	2.0E+09	0.5	3.4E-08
1 Mins	3.6E+09	9.2E+08	2.5E+06	3.7E+09	0.8	9.3E-08
1 Hours	1.6E+10	4.1E+09	1.1E+07	1.6E+10	1.0	5.1E-07
1 Days	2.0E+10	5.1E+09	1.7E+07	2.4E+10	1.4	9.6E-07
4 Days	2.2E+10	5.7E+09	1.9E+07	2.8E+10	1.5	1.2E-06
7 Days	2.3E+10	5.7E+09	2.0E+07	2.9E+10	1.5	1.2E-06
COOLING STEPS						
1 Secs	2.0E+10	5.2E+09	1.8E+07	2.7E+10	1.5	1.2E-06
1 Hours	6.5E+09	1.6E+09	8.8E+06	1.3E+10	2.0	6.9E-07
1 Days	2.1E+09	5.2E+08	2.8E+06	4.2E+09	2.0	2.2E-07
3 Days	2.3E+08	5.8E+07	3.1E+05	4.5E+08	2.0	2.4E-08
30 Days	4.9E+06	1.2E+06	2.8E+03	4.1E+06	0.6	8.3E-11
90 Days	3.3E+06	8.4E+05	2.3E+03	3.3E+06	0.6	7.1E-11
365 Days	1.7E+06	4.3E+05	1.2E+03	1.7E+06	0.7	3.8E-11
10 Years	9.5E+04	2.4E+04	5.7E+00	8.3E+03	0.3	8.1E-14
100 Years	1.3E+03	3.3E+02	8.6E-02	1.3E+02	1.0	3.8E-15

* *The method for this gamma dose calculation is reported in [12].*

Table 10.9. Target radioactivity and cooling

Steps	Activity (Bq)	Dose* gram (Sv/h)	Total Dose (Sv/h) at 1 m	Total Dose (Sv/h) at 2 m	Total Dose (Sv/h) at 2 m with 2cm of lead
IRRADIATION					
1 Days	1.50E+13	6.20E-02	1.77E+00	4.43E-01	
4 Days	1.70E+13	6.70E-02	1.92E+00	4.79E-01	
7 Days	1.80E+13	6.80E-02	1.94E+00	4.86E-01	
14 Days	2.00E+13	7.30E-02	2.09E+00	5.22E-01	
COOLING					
1 Secs	2.00E+13	7.26E-02	2.08E+00	5.19E-01	5.19E-02
1 Days	3.33E+12	6.82E-03	1.95E-01	4.88E-02	4.88E-03
3 Days	1.78E+12	3.85E-03	1.10E-01	2.75E-02	2.75E-03
14 Days	6.67E+11	1.44E-03	4.12E-02	1.03E-02	**1.03E-03**
30 Days	1.78E+11	3.85E-04	1.10E-02	2.75E-03	2.75E-04
90 Days	5.00E+10	8.36E-05	2.39E-03	5.98E-04	5.98E-05
10 Years	6.22E+08	5.94E-07	1.70E-05	4.25E-06	4.25E-07
100 Years	1.22E+08	1.01E-07	2.89E-06	7.24E-07	7.24E-08

The dose rate due to beta emission has not been evaluated here. Since the anticorodal is thin (5 mm) this contribution will not be negligible compared with its gamma emission.

The activation of the "front-end" (that is of the part of the remaining materials after the removal of the sphere containing the target) from the beam losses and from the neutron flux has not been considered here. Nevertheless, if there are some anticorodal materials at a distance of r=30 cm from the centre of the target, the neutron activation (of the anticorodal) can be estimated. Since the neutron flux varies approximately with the square of the distance, at r=30 cm the neutron flux can be estimated using that at r=15.5 cm by multiplying by the factor $(15.5^2/30^2)=0.267$. Then the activations (in Bq/kg) and the gamma doses (in Sv/h of 1 g at 1 m) can be obtained by multiplying the values of table 10.8 by the same factor 0.267.

Table 10.9 report the total radioactivity of the target with shielding as can be used to evaluate the total dose during the operation of target handling.

10.6 The target bunker

The target building will host two targets which can be operated simultaneously or alternatively.

To better confine the radioactive areas each target will be hosted in a separate bunker. The lay out is presented in fig. 10.5.

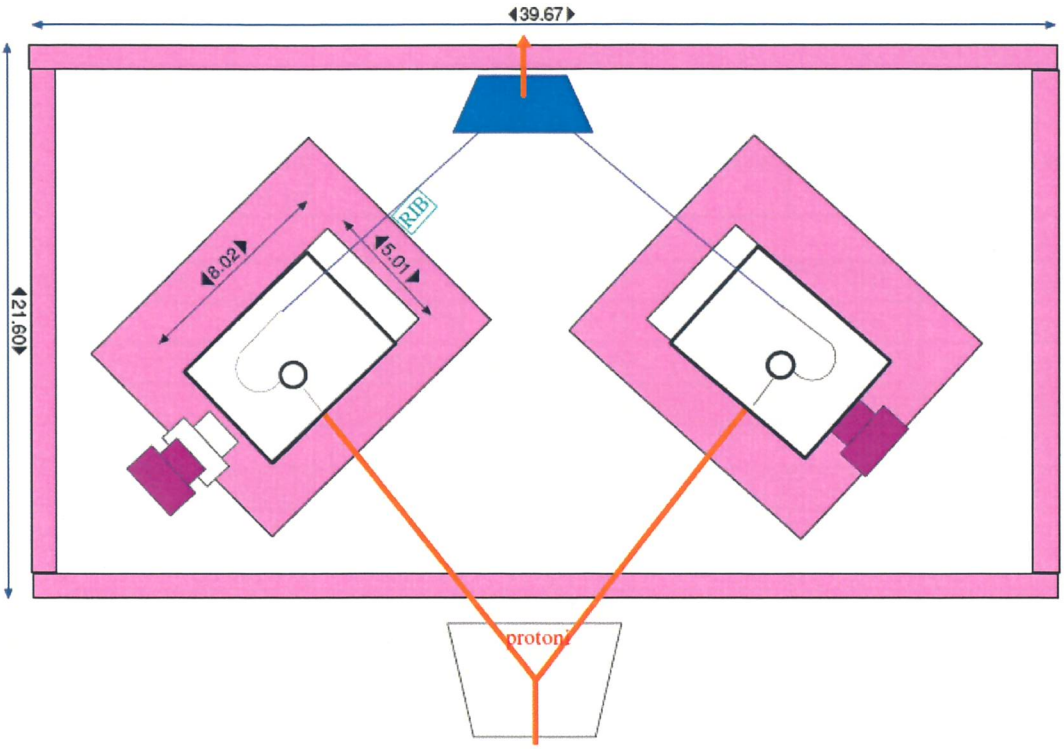

Fig. 10.5: *Lay out of target bunker*

The shielding of each target requires a bunker with a wall of 3 m in the forward direction and 2 m on the other sides to reduce the dose to 1.5 μS/h outside the bunker during the irradiation time. The dose is related to the neutron flux reported in Tab.10.4.

References

1. Linac4 Technical Design Report, Chapter 5, CERN-AB-2006-084-ABP/RF
2. C.C. Chen et al. "Calculations of neutron shielding data for 10-100 MeV proton accelerators", Radiation Protection Dosimetry (2005), Vol. 116, n. 1-4, pp. 245-251
3. L. Moritz, TRIUMF-ISAC II Safety Report June 2006
4. K. Tesch " A simple estimation of the lateral shielding for proton accelerators in the energy range 50 to1000 MeV", Radiation Protection Dosimetry (1985), Vol. 11, n. 3, pp. 165-172.
5. A. Andrighetto, C.M. Antonucci, S. Cevolani, C. Petrovich, *ENEA contribution to the design of the thin target for the SPES project*, FIS-P815-020 (ENEA, 2006).
6. A. Andrighetto, C.M. Antonucci, S. Cevolani, C. Petrovich, M. Santana Leitner, *Multifoil UC_x target for the SPES project - An update*, Eur. Phys. J. A 30, 591 (2006).
7. C. Petrovich, *The SPES target – Power deposition and preliminary radiation protection analyses*, FPN-P815-007 (ENEA, 2006).
8. Denise B. Pelowitz (Editor), *MCNPX™ User's manual,* Version 2.5.0, LA-CP-05-0369 (2005).
9. H.W. Bertini, Phys. Rev. 131 **4**, 1801 (1963).
10. J. Barish, T.A. Gabriel, F.S. Alsmiller, R.G. Alsmiller jr., *HETFIS High-Energy Nucleon-Meson Transport Code with Fission*, ORNL-TM-7882 report (Oak Ridge National Laboratory, 1981).
11. C. Petrovich, *SP-FISPACT2001. A Computer Code for Activation and Decay Calculations For Intermediate Energies. A Connection Of FISPACT With MCNPX*, RT/ERG/2001/10 (ENEA, 2001).
12. R.A. Forrest, *FISPACT-2001: User manual*, UKAEA FUS 450 (December 2001) http://www.fusion.org.uk/easy2001/

13. International Commission on Radiological Protection, *Conversion Coefficients for Use in Radiological Protection Against External Radiation*. ICRP Publication 74, Ann. ICRP 26(3/4) (Oxford: Elsevier Science) (1996).
14. International Commission on Radiation Units and Measurements, *Conversion Coefficients for use in Radiological Protection Against External Radiation*, ICRU Report 57 (Bethesda, MD: ICRU Publications) (1998).
15. A.H. Sullivan, *A guide to radiation and radioactivity levels near high energy particle accelerators* (Nuclear Technology Publishing, Ashford, Kent: England. NTP) (1992).

CHAPTER XI

SAFETY AND RADIATION PROTECTION

11.1 Facility description

The SPES project will produce secondary beams of unstable ions to perform basic research studies in the nuclear physics field with the aim to produce and characterize isotopes far from stability and to study the properties of the nuclear reactions at variation of isospin.

The production method is based on the ISOL technique with direct target: a primary proton beam impinges directly on a UCx target inducing the U fission with a maximum rate of 1E13 f/s, the fission products are extracted, ionized, selected and reaccelerated to produce the secondary radioactive beam.

This chapter presents the preliminary safety and radiation protection analysis of the SPES project.

11.2 Site and buildings

The facility will be located at LNL and represent an extension of the present accelerator complex.

The buildings of the new facility will be constructed in the expansion area of the Laboratory in contiguity with the actual "third experimental area".

The species produced by SPES will be reaccelerated by the present ALPI complex.

LNL is located at 2 Km from Legnaro (east) and 1 Km from Ponte San Nicolò (west).

Padova is located 10 Km in the west direction. The highway Bologna-Padova is just on the border of the LNL site area which has a surface of 10000 m^2.

The whole SPES facility will consist of several buildings with design criteria adequate to perform an effective safety environment.

The main buildings are:

Proton driver building

It will host the accelerator for the production of the primary proton beam.

The safety in this area is related to the normal operation of a proton accelerator with a proton current of 500-700 microA and a final energy of 40 MeV.

The main radioactive source is due to the beam losses which produce neutrons and activate the beam line.

Production Target building

The UCx target is the critical point of the facility from the point of view of the safety due to the large level of radioactivity induced by the fission reactions.

The target follows the design already developed in several laboratories where radioactive beams are operated recently or since long time as EXCYTE (LNS) or ISOLDE (CERN) and HRIBF (ORNL).

The total amount of UCx is in the order of 30g and the power released in the target is 8 KW to produce 7E12 f/s with 200 microA of protons at 40 MeV.

Mass selector

The mass selector is the first beam selection element just after the target and +1 source. It is mounted on the same platform of the target itself and will perform the mass selection with a resolution of 1/250 (??).

The expected radiation level is evaluated to be of the same order as the production target in the hypotheses that all produced elements are extracted.

Low Energy building

The Low Energy building is an already existing building and it will host the High Resolution Isotope Separator (HRIS) and Low Energy experimental hall.

At the entrance of the HRIS only a selected mass will be injected and the radiation level will be one or two orders of magnitude less than in the Mass Separator.

The HRIS is expected to have a resolution of $\Delta M/M = 1/20000$, at its output only a beam of selected isotope should be present and the radiation level will be further reduced for the transmitted beam.

At this level the radioactivity is induced by the radioactive beam itself that is expected to be of the order of 1E12 pps in the optimum case and 1E3 pps for the very rear beams.

After the beam selection a further stage is required before reacceleration, namely the charge breeding to allow an efficient acceleration of the exotic beam.

This stage is performed by an EBIS mounted near to the pre-accelerator PIAVE.

The charge breeder has an efficiency of 10% and a large part of the produced beam is expected to be lost inside this element. From the point of view of the radioprotection we consider that the radioactive beam completely lost inside. A local shielding will be used for this element

Post accelerator building

Already existing accelerators: the PIAVE RFQ pre-accelerator and the ALPI Linac Accelerator, will accept the beam from the Charge Breeder.

Both machines are installed in an existing building. At this level the radioactivity is induced by the beam that is expected to have an intensity of 1E11 pps in the optimum case.

If necessary additional shielding will be installed to maintain the radiation level at the actual limit.

11.3 Radiation levels

The higher radiation level is around the UCx target where the fission process is induced by the proton beam.

A total activity of 2E13 Bq is present inside the target with a dose of 4-10 Sv/h at the surface of the target container. The operation temperature of the target is 2000 °C and all elements with melting point lower than this temperature are extracted ionized in the 1+ source and transmitted to the Separator. We consider for this process a 100% efficiency.

After the separator the mass-selected beam is guided to the Low Energy lines and to the Charge Breeder where the species are further ionized (+n) and reaccelerated by the RFQ and the Linac ALPI. An efficiency of 5% for the Charge Breeder and 40% for the reacceleration is considered.

A schematic radiation activity for the different stage is reported in table 11.1.

Table 11.1 Radioactivity at different stage of the facility

	Activity (Bq) Saturated	after 1 y	Gamma dose Sv/h Saturated	after 1 y	
target	2 E13	1 E10	10	2 E-3	Surface of target container
Mass Separator	1 E13	5 E9	1	1.6 E-4	1m no shielding
Isotope Separator	1 E11	5 E7			
Before Charge Breeder	1 E10	5 E6	1 E-2	2 E-6	1m no shielding
After Charge Breeder	2 E9	5 E5	1 E-7	2 E-11	1m no shielding

11.4 Design criteria

The sensitive parameters for the safety and radioprotection are:

- Beam intensity
- Beam energy
- Beam losses
- High voltages
- RFQ Radio frequency

The most relevant issues are:

- Fission fragment production target (7 E12 f/s)
- High current low energy proton beam (30mA, 5MeV)
- Medium current high energy proton beam (500microA, 40MeV)

11.5 Proton Driver

The proton driver is a normal conductive accelerator with a current on the order of 500 microA and 40 MeV energy.

The proton source and the first stage of the accelerator are designed to supply up to 30 mA 5 MeV protons to be used for BNCT and Neutron Facility. Only a small part of this high current is further accelerated up to the final energy of 40MeV to induce the fission on the UCx target.

The following parameters are used to design the shielding for radioprotection.

Table 11.2 Design parameter for shielding design

	Energy (MeV)	Intensity (microA)	Losses (microA)	HV	
Proton source	0.02	30000		+20 KV	
LEBT	0.02	30000			
Trasco-RFQ	0.02 → 5	30000			
BNCT Neutron facility	5	30000	30000		
DTL	5 → 40	500 (design)			
Beam dump	40	1000 (design)	1000 (design)		
Radioactive target	40	200	200	+60 KV	
Mass separator	0.060	10^{13} pps	99%	-60 KV	
HRIS	0.150	10^{11} pps	90%		
Charge Breeder	0	10^{10}	90%	+60 KV	
PIAVE	0.150→ 5	10^{9} pps			

11.6 Production Target

The production target is designed to sustain a power of 8KW of proton beam and to produce a fission rate of 7E12 f/s. The active material is 30 gr of UCx in the shape of 7 disks of 4 cm diameter and 1mm thickness each.

The radiation levels in the target area are reported in table 11.1.

Targets similar to the SPES one are in operation from long time at ISOLDE-CERN and HRIBF-ORNL. The main differences are the total beam power supplied to the target and some details on the disks dimensions and displacement. The SPES target has a diameter 2.7 times the usual one and is designed to cool down by irradiation. The fission rate is 30 times higher than HRIBF but with the same power density released in the target.

The design follows the ISOLDE project and all the mechanical parts, as well as the feed-through for cooling and power supply, are studied and tested at CERN to sustain the high dose rate expected. In the follow we refer to the whole target container as "plug"; a pictorial drawing of the plug is reported in fig.11.1.

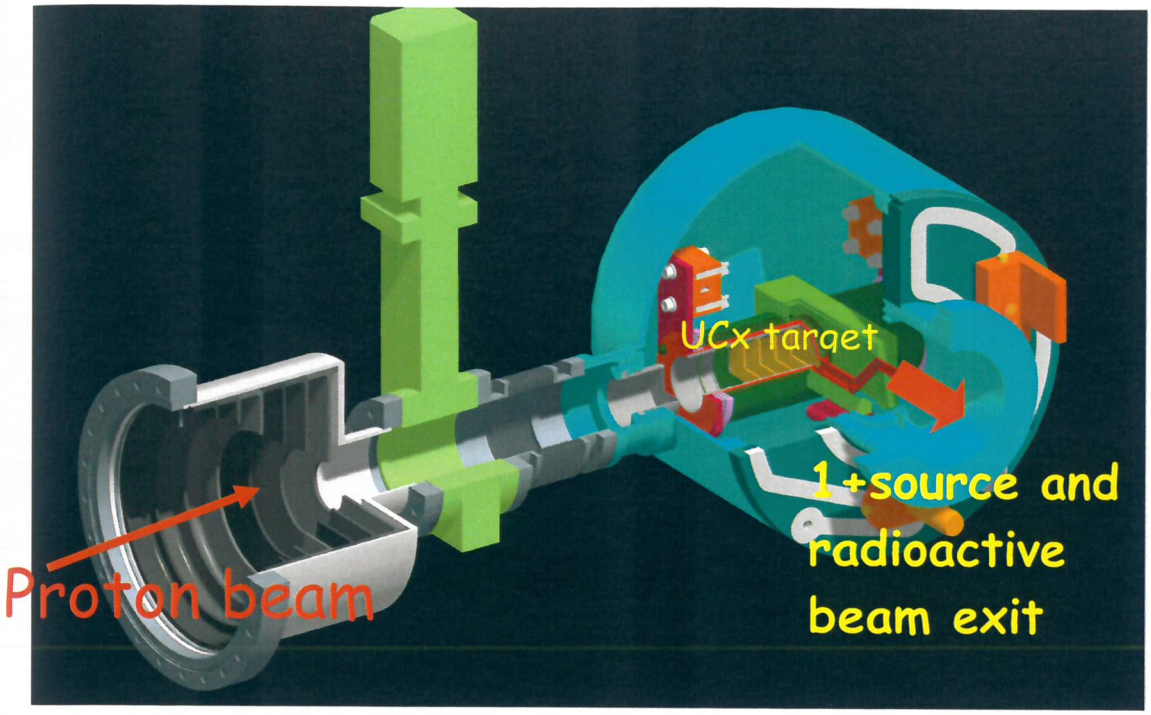

Fig.11.1: *Spes target assembly*

From the safety point of view the production target is certainly the most dangerous item of the SPES project and special care must be taken to all its details and to all the operations in which it is involved.

In addition to the fission rate during irradiation the target has two more critical points: the operation temperature is around 2000 °C and after irradiation it must be removed and substituted with new one.

The inner container of the target disks is a cylinder with a double entrance window and a beam dump for low energy protons. All these elements are made of graphite. The window is made by two layers of graphite with a thickness of 0.5 mm each. It is the physical separation between the reaction chamber and the proton driver beam pipe. The choice to use a two layers window is suggested by thermal calculation and to improve the safety of the system. The melting point of the graphite is 3500 °C well above the temperature of operation of the target. Special care will be taken to avoid an over heating induced by the proton beam. Even if the target structure can sustain the expected power it is of paramount importance that the proton beam is not concentrated on a small target surface to avoid local over heating and pin holes. The beam shape is monitored by the beam diagnostic system and automatic interlocks on the proton beam will be activated if beam parameters as shape and intensity do not fit the safety limits.

The removal of used plugs and the insertion of new one will be performed without any manual operation by a servomechanism.

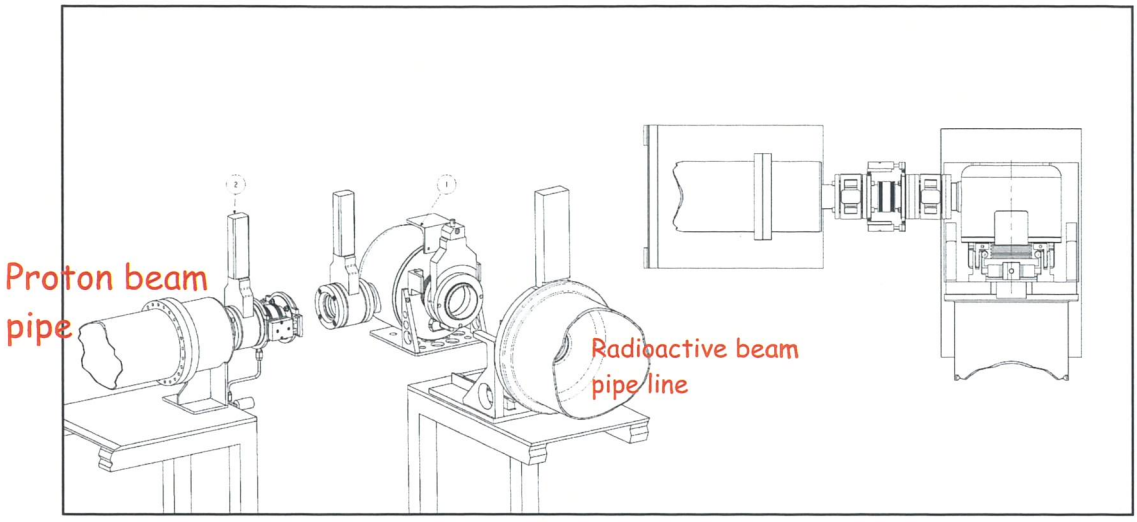

Fig. 11.2: *Mechanical drawing of SPES target interconnection to pipes.*

11.7 Radioactivity inventory and handling

11.7.1 Target

A correct estimate of radiation and radioactivity levels is essential at the design stage of the facility to incorporate the radiation safety into the infrastructure layout, for predicting the risks of radiation damage and/or material activation as well as for an estimate of the environmental impact of the facility (air, water activation). Remote control handling methods have to be developed especially for the target area. Since the production target consists of fissionable material (mainly ~30 g of depleted ^{238}U), some trans-uranic elements are produced and have to be controlled at any time throughout the facility. High activation levels have detrimental effects such as large inventories of radiotoxic nuclides, large decay power (gamma heating), as well as radiation damage of components.

The inventory of radionuclides produced in-target was done by ENEA as well as the estimation of the radioactivity produced in the target area.

The actinides and fission fragments production are calculated, as well as the energy spectra of photons emitted by the fission products. In addition, the code gives information on the energy spectra of neutrons emitted in (α,n) reactions and from spontaneous fission. After 30 days of irradiation, inside the ~30g UCx target are collected about 60 mg of fission fragments and a relevant quantity of actinides elements like: U236 (0.34 mg), Np 237 (0.52 mg), and Pu236 (0.10 mg). The corresponding activity is about 10^{13} Bq. After 3 months from irradiation the target still shows an activity of 4x 10^{10} Bq and after 1 year 9x10^{9} Bq. Detailed calculations can be found in Ref. [1].

Because of the high radiation level, the production targets and all the materials surrounding the target itself have to be removed only by a remote handling system. A trail and pneumatic system allows the insertion and disconnection of the target box which has a weight of ~80 Kg (input and output valves included). The activated target is safely sealed in a shielded container made of lead, iron and cupper. This container has dimensions less than 1 cubic meter and a total weight of 400 Kg. A remote operated crane allows the deposition of the container inside a special concrete sarcophagus for long term storage.

A site will be dedicated to the storage of the sarcophagi for long term cooling down before the decommissioning.

Table 11.3: Target radioactivity and cooling

Steps	Activity (Bq)	Dose * gram (Sv/h)	Total Dose (Sv/h) at 1 m	Total Dose (Sv/h) at 2 m	Total Dose (Sv/h) at 2 m with 2cm of lead
IRRADIATION					
1 Days	1.50E+13	6.20E-02	1.77E+00	4.43E-01	
4 Days	1.70E+13	6.70E-02	1.92E+00	4.79E-01	
7 Days	1.80E+13	6.80E-02	1.94E+00	4.86E-01	
14 Days	2.00E+13	7.30E-02	2.09E+00	5.22E-01	
COOLING					
1 Secs	2.00E+13	7.26E-02	2.08E+00	5.19E-01	5.19E-02
1 Days	3.33E+12	6.82E-03	1.95E-01	4.88E-02	4.88E-03
3 Days	1.78E+12	3.85E-03	1.10E-01	2.75E-02	2.75E-03
14 Days	6.67E+11	1.44E-03	4.12E-02	1.03E-02	**1.03E-03**
30 Days	1.78E+11	3.85E-04	1.10E-02	2.75E-03	2.75E-04
90 Days	5.00E+10	8.36E-05	2.39E-03	5.98E-04	5.98E-05
10 Years	6.22E+08	5.94E-07	1.70E-05	4.25E-06	4.25E-07
100 Years	1.22E+08	1.01E-07	2.89E-06	7.24E-07	7.24E-08

The target radioactivity will reach a saturation level at 2E13 Bq after 14 days of continuum operation. The radioactive dose during the cooling time was evaluated and is reported in Tab.11.3.

After 14 days of cooling down, the target can be removed with some care but in quite safe conditions. A minimum shield of 2 cm of lead and an operation distance of 2 m, allows an eventual manual operation with a total dose of 1mSv/h. An operation of 5min gives a dose of 83 µSv, quite low respect to the 20 mSv max dose/year of classified personnel.

11.7.2 Radioactive gases

Several elements produced in the target have melting point less than 50°C and are considered as gases. Although the objective is to ionize as large a fraction of radioisotopes in the 1+ source, a significant fraction is expected to leak as natural atoms and is handled as residual gas in the pumping system. To mitigate the risk to activate the vacuum system and to avoid the release of radioactive gasses in the environment, two actions are actuated:

1) a cryogenic trap will be used after the HRIS to decrease the eventual contamination of the beam line and the vacuum system of the post accelerator. A design of such a trap is currently performed at SPIRAL2, it is based on cryogenic layers at different temperatures and active carbon, to stop with high efficiency the different radioisotope gasses according to their properties.
2) the exhaust gas of the vacuum system will be filtered and stored in silos for a given time and the release will be submitted to the measure of radioactivity and further filtering.
   The evaluated activity due to the gas is 4E12 Bq after 3 months of operation and it reduces to 2.7E9 Bq and 7E8 Bq after 3 months and 1 year of storage respectively.

11.7.3 Induced radioactivity in air and refrigerating fluids

The presence of a neutron flux may be responsible for the activation of air and refrigerating fluids in the target area. An evaluation will be performed for SPES, but as an indication one can consider the study performed for ISAC at TRIUMF [2] which quote the following annual release rates produced by a proton beam of 500MeV, 100μA on a UCx target of ~100 gr.

Table 11.4

Isotope	Annual release rate (Bq)	Bq gr^{-1}
3H (12y)	1.5E5	1.7E-5
7Be (53d)	1.2E6	1.4E-4
11C (20m)	8.6E9	9.5E-1
13N (10m)	6.9E10	7.7
15O (2m)	1.0E11	11
41Ar (109m)	4.1E9	4.6E-1
	1 year=3.1E7 s, air flux=0.23 m3/s, Air density=1250 gr/m3	

To overcome the risk of dispersion of radioactivity a careful design of the ventilation system will be performed.

The refrigerating fluids of the target station will have a separate circuit and will be monitored for radiation activity as well as the refrigeration fluid of the mass separator.

No problems are expected for the other systems as the activation is induced by neutron reaction and the larger neutron field is confined around the production Target.

11.7.4 Ventilation system

The ventilation system will be designed to maintain the target area at lower pressure to avoid the escape of airborne radioactivity. Three separate systems with controlled differential pressures will be used in the Target Building: a small one for the target cave, a larger one for the surrounding area (mass separator) and finally the main ventilation system of the Target Building. The zoning is such that air flows from areas of lower to areas of higher potential contamination. The Target cave is the most critical area respect to the presence of contaminated air and the ventilation system will be designed to maintain as low as possible the air change in this zone. Special care will be devoted to seal it at the best.

The system will be designed according to the request of a nuclear ventilation system with HEPA and charcoal filters monitored for pressure loss and radiation activation.

11.7.5 Concrete study for radioprotection applications

The radiation tolerance of concrete is an important item for the safety of high radiation structures. Special care is devoted to the study of cemet based materials to be used for bunker construction and for the sarcofagous of long term target containement.

The radiation damage induced on concrete affects the fire resistance and the long term stability. For the SPES project special materials will be used in the critical points.

A specific study on this subject is undergoing at Padova University, Dipartimento Costruzioni e trasporti. In the following the basic appoch is outlined.

The study of the long-term behaviour of cement-based materials in relationship with nuclear management requires the assessment of a long-term stability of concrete vessels with emphasis on material-mechanical properties. Different environmental conditions - atmospheric and water saturated environments - could affect the material and structural response. Corrosion and air

carbonation of reinforced concrete can be identified as the two main phenomena which could jeopardize the long-term performances of cemented containers.

Additionally, concrete vessels can undergo radiation-induced degradation by alkali-silica reaction of aggregates: the effect of Ar ion irradiation on the reactivity of crystalline and amorphous quartz to alkali has been examined by Ichikawa and Koizumi [4] for clarifying whether radiation from nuclear reactors accelerates the degradation of concrete by inducing alkali-silica reaction of aggregates. Distorted amorphous quartz generated on the surface of quartz by irradiation of a 200 keV Ar ion beam is at least 700 times and 2.5 times more reactive to alkali than crystalline and regular amorphous quartz, respectively. The high reactivity of the distorted amorphous quartz indicates that the degradation of concrete by alkali-silica reaction is possible to be induced by nuclear radiation even if the aggregates are inert to alkali before the irradiation.

Rutherford back-scattering spectrometry, combined with ion channelling's data, suggest the possible formation of a radiation-induced metastable phase in the damaged region, which may be analogous to pressure- or temperature-induced phase transformations in other ilmenite-group oxides. In particular, these materials transform to either the lithium niobate or the orthorhombic perovskite structure at high pressures and temperatures. These results and similar investigations on the olivine system suggest that ionicity, composition and melting temperature may play important roles in the radiation response of ceramics, and particularly in predicting the relative radiation tolerance of materials within a solid-solution series.

On the basis of such first experimental evidences, a fully coupled chemo-thermo-hydro-mechanical model able to describe concrete behaviour under medium and high temperatures is proposed to asses the radiation damage induced by nuclear radiation within concrete vessels and radioactive leaching within waste storage concrete systems. The model incorporates coupled elastoplastic and damage behaviour plus creep effects. The stress–strain numerical model is derived according to thermodynamic consistency and is based on real experimental findings [5-10].

The objectives of the modelling are:

- characterization of the safety performances of ordinary, high performance and ultra-high performance concrete structures devoted to radiation protection and nuclear waste storage;
- definition of long-term scenarios for risk assessment and concrete durability to radiation phenomena and radioactive leaching;
- evaluation of minimum cemented thicknesses for environmental safety assessment in standard conditions;
- evaluation of the structural response under extreme accidents (fire, earthquake, blast) and proposal of remediation measures to possible spalling, fracturing, collapse.

11.8 Safety analysis

11.8.1 Normal situation

The radiation protection program reports on the zone classification of the facility and on the access controls.

The respect of the radiological zone will be monitored by specific barriers and real-time dose measurement. The access control system and the dose monitoring will be integrated in the operation control system of the facility to prevent dangerous situations, as loss of primary proton beam over the allowed limits and over-contamination of the facility components.

The radioactivity transported in the facility will be monitored and at least two barriers are installed between radioactive zone and the environment. Interlock valves ensure the containment

of the target and a second barrier is the vacuum system. The target area is inside a two layer bunker with controlled and separate ventilation.

Additional monitoring and bunkers will be added in the existing rooms if necessary, according to the radiation level of elements as High Resolution Isotope Spectrometer or Charge Breeder.

An adequate fire prevention system will be installed in the new buildings and integrated with the existing one. The water used for fire extinguish will be collected in separate sump to allows the radioactivity controlled before the intake in the exhaust system

11.8.2 Incidental situations

The incidental situations will be evaluated and managed in such a way that all significant impacts will be confined inside the site and no hazards to the environment will be introduced.

The major incidental situation is related to the sublimation of the target. This can be induced by a malfunctioning of the heating control system or by an error in the primary-beam handling.

The impact on the installation is the contamination of the beam lines downstream from the target and the over-contamination of the vacuum system.

The incident is mitigated by the valves along the beam line that will be closed by the control system.

The alarm for this incident can be deduced by several parameters: the heating of the target (controlled by a pyrometer and thermocouples), a sudden decrease of the vacuum in the target box (controlled by vacuum measurement).

The parameters (current, shape and energy) of the primary beam are controlled by the beam monitor system and fast valves are introduced on the beam line to interlock the beam in case of beam anomalies.

The activity injected into the facility is two times the expected one owing a target efficiency of 50%

No radiological impact on the environment is expected as the vacuum system exhaust is submitted to a storage tank.

In the scale of hazard the next serious incident is represented by the target window breaking. It has a similar impact on the installation but with fewer consequences from the contamination point of view.

The main alert comes from the vacuum monitor in the target and +1 source vessel.

The same safety systems as in target sublimation will be activated.

11.8.3 Accidental situations

The accidental situation may cause a release of radioactive material to outside of the site.

The worst situation is fire in the target bunker.

The fire prevention system will act to extinguish the fire without the use of water and the bunker will be permanently closed. All ventilation ducts and the pipelines of the refrigerating fluids will be interlocked.

The bunker will be constructed as small as possible and will be closed inside a second bunker.

The injured target station will be put off line and the access will be allowed only after a careful evaluation of the contamination eventually present inside the bunker.

The main risk of radioactivity dispersion is related to the ventilation system. The very worst case is that the whole target material is put into suspension and is processed by the ventilation system.

In this case the larger part of the particulate is trapped in the HEPA filters, if the all gaseous elements are released outside the facility the radiological impact is evaluated to be of 2 mSv without the charcoal filtering and 0.4 mSv if charcoal filters are effective [2,3].

No dispersion of radioactivity is expected if the target vessel does not brake.

11.9 Risk evaluation

A detailed analysis of the risk will be performed by a specialized company with special regard to the radiation aspects. Generic and specific hazards will be analyzed. Among them earthquake, fire, overflow, explosion will be considered.

[1] ENEA fpn-p815-007

[2] ISAC TRI-DN-17-5-1, 2000

[3] SPIRAL2 ADP, 2005

[4] Ichikawa, T., Koizumi, H., "Possibility of radiation-induced degradation of concrete by alkali-silica reaction of aggregates", *J. Nuclear Sc. Tech.*, **39**(8), 880-884, 2002.

[5] Majorana, C.E., Salomoni, V., Schrefler, B.A., "Hygrothermal and mechanical model of concrete at high temperature", *Mat. Struct.*, **31**(210), 378-386, 1998.

[6] Gawin, D., Majorana, C.E., Schrefler, B.A., "Numerical analysis of hygro-thermal behaviour and damage of concrete at high temperature", *Mech. Coh. Frict. Materials*, **4**, 37-74, 1999.

[7] Khoury, G.A., Majorana, C.E., Pesavento, F., Schrefler, B.A., "Modeling of heated concrete", *Mag. Concrete Res.*, **54**(2), 77-101, 2002.

[8] Schrefler, B.A., Gawin, D., Khoury, G.A., Majorana, C.E., "Thermo-hydro-mechanical modeling of high performance concrete at high temperatures", *Eng. Comp.*, **19**(7), 87-81, 2002.

[9] Majorana, C.E., Salomoni, V.A., "Parametric analyses of diffusion of activated sources in disposal forms", *J. of Haz. Mat.*, A113, 45-56, 2004.

[10] Salomoni, V.A., Mazzucco, G., Majorana, C.E., "Mechanical and Durability Behaviour of Growing Concrete Structures", *Eng. Comp.*, 2007 (in press)

CHAPTER XII

SPES NEUTRON BEAM

12.1 The SPES BNCT project: a thermal neutron beam facility for skin melanoma experimental treatment

12.1.1 Introduction

BNCT is a binary radiation therapy. First, a boronated substance is injected in the patient body, secondly the patient is irradiated with thermal or epithermal neutrons. The boranated substance is harmless and designed to be preferably absorbed by tumour cells. Because of the high ^{10}B thermal neutron capture cross section (3837 barn), the nuclear reaction $^{10}B(n,\alpha)^{7}Li$ is likely to occur. The nuclear reaction products (^{4}He of 1.47 MeV and ^{7}Li of 0.84 MeV) are densely ionizing charged particles, the ranges of which in soft tissues (~8 μm for the α particle, 5 μm for the lithium ion) are as short as a cell diameter (~10 μm). Therefore, only cells containing ^{10}B are damaged, remaining the aside cells intact. This peculiar behaviour of energy releasing allows of conceiving a cellular radiation therapy, which is very useful whenever tumour cells infiltrate the healthy tissue extensively. For exploiting this nuclear reaction in radiation therapy, a large research activity is going on in Europe, Japan and United States that aims to find optimal ^{10}B carriers able to maximise ^{10}B uptake in tumour cells with respect the healthy cell uptake, as well as the best radiation dosimetry to use.

Up to now two carriers have been used: the boronated phenylalanine (BPA) and the borocaptate (BSH). Both of them have only a limited selectivity for tumour cells. In spite of that, the first patient with malignant skin melanoma (MM) was treated by BNCT on 1987. The tumour was a subcutaneous metastatic lesion of the occipital region. The irradiation was delivered in a single fraction after perilesional administration of BPA, at the Kyoto University [1]. Thanks to the completely positive response and tolerability reported, about 20 patients with MM were treated in Japan with thermal neutrons applying the BNCT technique. In more recent clinical trials, because of the tumour deeper location, epithermal neutrons were used instead of thermal neutrons [2, 3]. Skin MM has been treated also by the Bariloche reactor in Argentina on 2004 with good therapeutic results [4].

However, available reports and retrospective studies show that the method is not standardized [5][6]. Moreover, published reports are not exhaustive. One of the actual limits for the therapeutic plan optimisation is the poor knowledge of the maximum sustainable healthy tissue damage; datum that determines the radiation-field maximum exposition. Such information depends in fact on the knowledge of radiation tissue sensitivity, which changes with radiation changes. Dosimetric measurements nowadays used in BNCT research centres are poorly significant for the biological effectiveness [7]. Intensively research is going on to improve the radiation quality assessment of BNCT and other hadronic beams [8].

The Legnaro BNCT project aims to use the intense proton beam provided in the framework of SPES facility to generate an intense thermal neutron source, which will be used for MM experimental treatments.

12.1.2 The Skin melanoma case

Once a rarity in oncological management, there has been an exponential increase in incidence of MM during the past 20 years. 9000 new MM cases were observed in the United States in 1975 with approximately 5000 expected deaths. The large MM increase is documented by the fact that in 1995 were estimated 34100 new cases with an expected 7200 cancer deaths [9]. In the Veneto region (Northeast of Italy) we have 15 new MM per 100,000 inhabitants a year (about 750 new cases per year). Veneto region has therefore the supremacy for this tumour in Italy [10], where the new cases per year are assessed to be about 5,000. The actual MM therapeutic treatment uses a multi-technique approach: surgery, hyperthermia, chemotherapy, radiation therapy. However, the actual radiation therapy, performed with low-LET radiations, is poorly effective. On the contrary, high-LET tumour-targeted radiations have shown to be highly effetive. The 5% of MM tumours develop surface metastases, which can bet treated with BNCT. The 40 % of patients with MM develop metastases in other parts of the body. Some of these metastases could be successfully treated with BNCT. However it is worthwhile taking into account that MM cannot always be controlled locally without mutilating surgery, there may be a role for high LET radiotherapy in association with conservative surgery as a primary treatment such as in limb sparing and in head and neck tumours.

12.1.3 The SPES-BNCT project

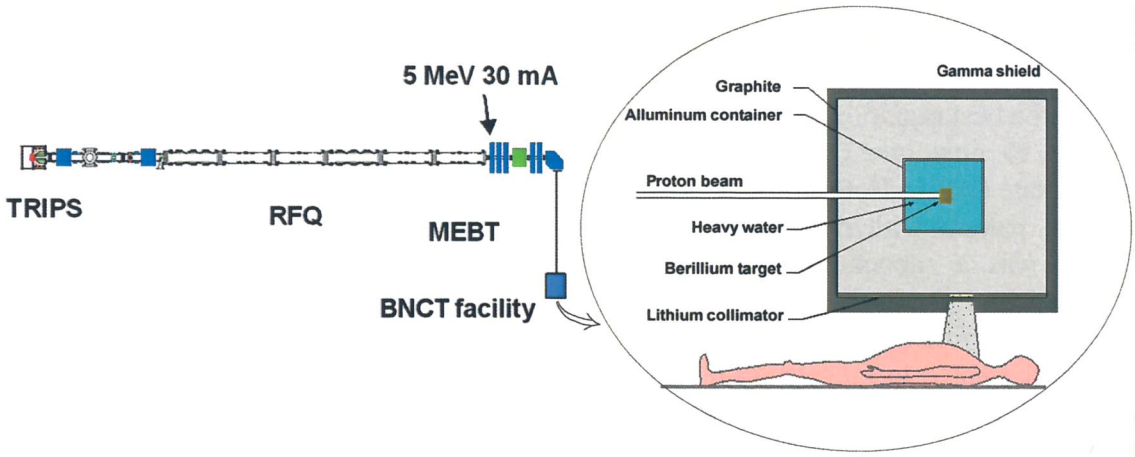

Fig. 12.1 *Schematic layout of the accelerator-driven SPES-BNCT irradiation facility*

In the framework of SPES project, a high fluence-rate thermal neutron facility will be constructed for treating patients with MM. The facility layout is shown in figure 12.1. The ion source (TRIPS) will supply 50 mA of protons at 80 keV of energy. Protons will be accelerated by a radio frequency cavity (RFQ) up to 5 MeV of energy, bent at 90° and driven by a dedicated high intensity proton beam line onto a high power (150 kW) neutron converter. The neutron converter exploits the reaction 9Be(p,n)9B (Q = -1.85 MeV), which gives rise to a fast neutron spectrum, the average energy of which is of about 1.5 MeV when the beryllium target is thick. In order to moderate the neutron energy down to thermal or epithermal energy, the beryllium target will be put inside a multilayer structure called neutron moderator or energy shifter. In figure 12.1, the moderator is sketched. It has a heavy water core. Nuclear graphite and a lithium layer are designed to obtain a collimated thermal neutron beam, which will be properly used to treat patients affected by MM.

Patients affected by MM have been already treated in Japan and Argentina by using borophenylalanine (BPA) as boron carrier. Although MM have been treated successfully,

dosimetric treatment protocols used will cannot be transferred to the future LNL facility, since its radiation quality, hence the its biological and therapeutic effectiveness, will be certainly different. The only known radiation quality measurement that can be processed to give the biological effectiveness of the radiation field is the microdosimetric spectrum of the field. Therefore, the SPES-BNCT project includes research and development of microdosimetric detectors. The research aims to construct miniaturized tissue-equivalent gas proportional counters (twin TEPC) able to perform fast and reliable microdosimetric measurements in therapeutic BNCT fields.

Since the beginning, the photobiology group of Padova University biological department joined the project to study and to develop new boron carriers for increasing the effectiveness of the BNCT technique. Together with the radiation field flexibility (due to the possibility of changing radiation field just changing neutron moderator) and the microdosimetry technology, the research of new MM-highly-selective boron carriers characterizes the SPES-BNCT project.

12.1.4 High intensity proton-beam transport line (HIPL)

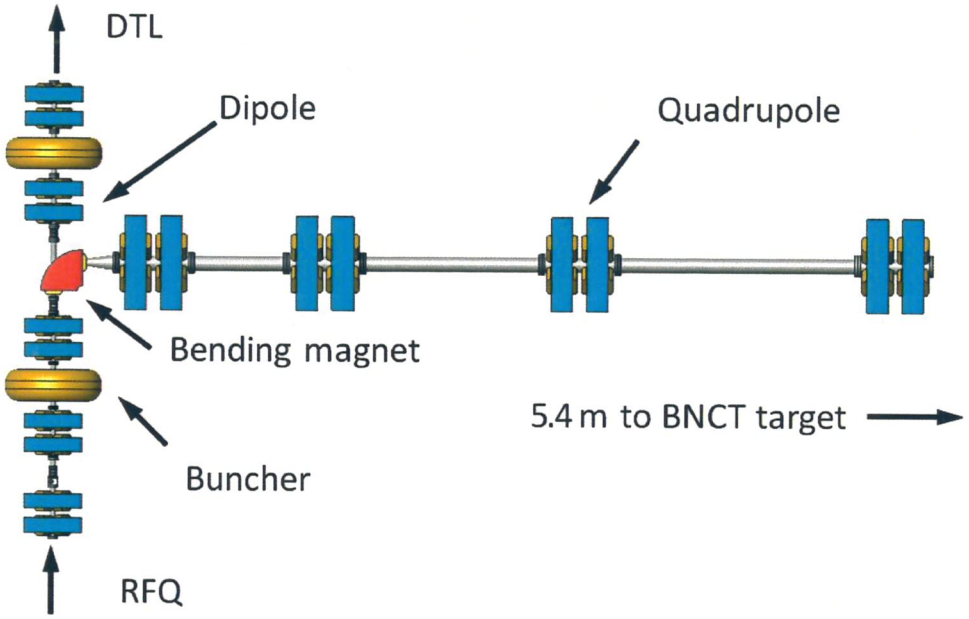

Fig. 12.2: *The BNCT beam line (HIPL) is connected with the Medium Energy Beam Transfer (MEBT) line with a 90° bending magnet.*

After the RFQ exit, the 5 MeV proton beam (165kW) has to be transported to the BNCT facility with a dedicated transport line, the so-called HIPL (see figure 12.2). Since the same RFQ will inject the proton beam into the high energy linac (DTL) trough a Mediun Energy Beam Transfer (MEBT) line, for eventually produce radioactive nuclei, a bending magnet inserted in MEBT centre will turn the beam toward the BNCT facility. The 90° dipole is inserted in between two focusing quadrupoles, which are 600 mm apart. Such a short distance has been chosen to maintain the quality of the beam going to the DTL.

In order to have the designed proton beam intensity of 30 mA on the neutron converter, 33 mA have to be extracted from the RFQ, because the HIPL has 6% of beam loss. The 40 mm proton beam will run inside a 100 mm pipe line. However, in order to arrive at the neutron converter with big enough geometrical cross section for reducing the power density, the last transport line quadrupole focalizes the proton beam at about 5 meter apart the neutron converter. After the focus, the proton beam will run therefore inside a 200 mm pipe line. At the end of the HIPL, proton beam is collimated to properly copy the neutron converter (see paragraph 12.3.2)

projection area. The squared collimator will be cooled in order to dissipate 8 kW (1.6 mA of stopped proton current) of power.

The neutron converter activation after 1600 hours of continuous beam time is very high (see paragraph 12.3.3). Even at two meters of distance from the converter, dose rates due to gamma

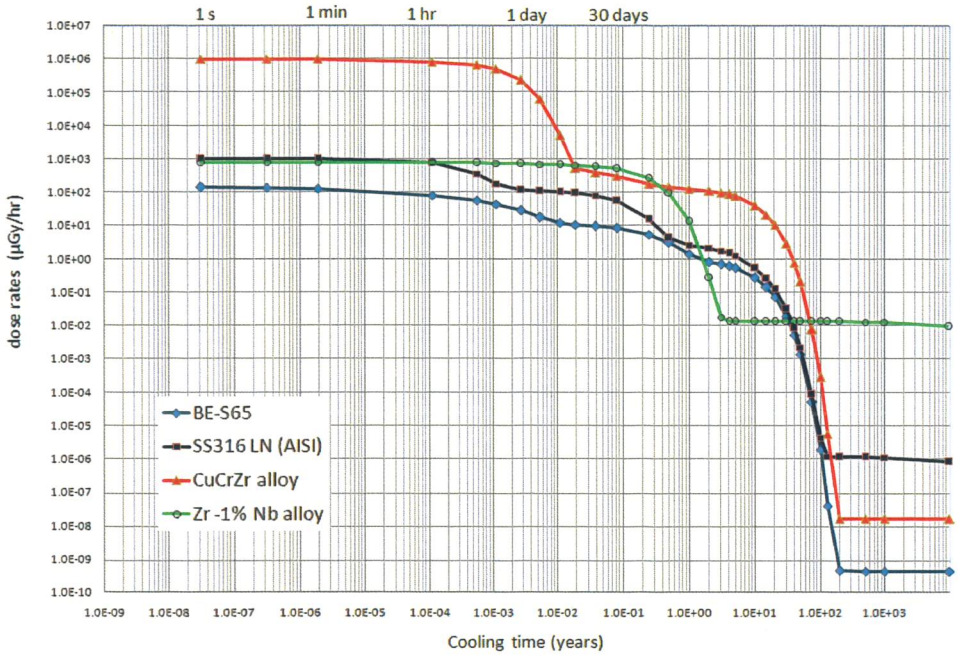

Fig. 12.3: *Maximum dose rates, after 1600 hours of 4 MeV 30 mA proton beam, at 2 m of distance from the Be-tile neutron converter due to different target components.*

emitters are very high. In figure 12.3 dose rates of different materials are plotted against the cooling time. Calculations have been performed with a 4 MeV proton beams, because neutron yield data at 5 MeV miss (see paragraph 12.3.4). Dose rate data of figure 12.3 are expected to be more than 3 times higher at 5 MeV of protons. However, data of figure 12.3 have to be considered as well an upper limit, because they are simple analytical calculations based on the point-source approximation and point out the activation dose after the maximum permissible proton fluence (1600 hours of 30 mA protons). Although more precise calculations will be done as soon as neutron yields of 5 MeV protons will be available (see paragraph 12.3.5), it is already rather clear that the last part of HIPL can not be easily serviced. Weeks after the last beam stop, the total dose rate at 2 m will be likely close to 1 mGy/hr. Conversely, it could be the need of quickly substituting the neutron converter for some unexpected failures. Therefore, the HIPL last piece will be equipped with a full-remote target extraction system, the sketch of which is in figure 12.4. The target extraction system will be housed in a 3x4x5 radiation shielded room (see figure 12.5).

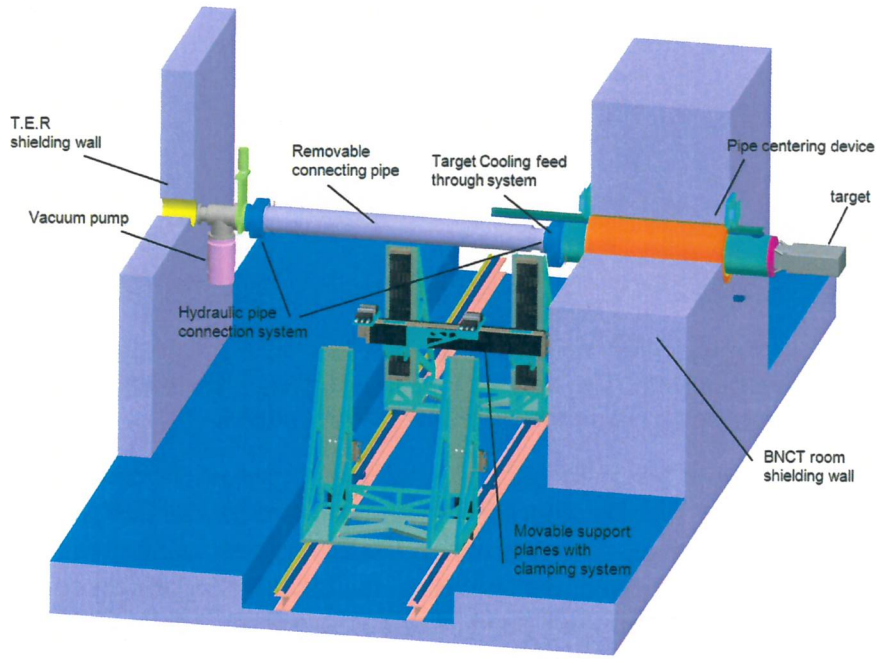

Fig. 12.4: *The target (neutron converter) extraction system. Main structural components are pointed out.*

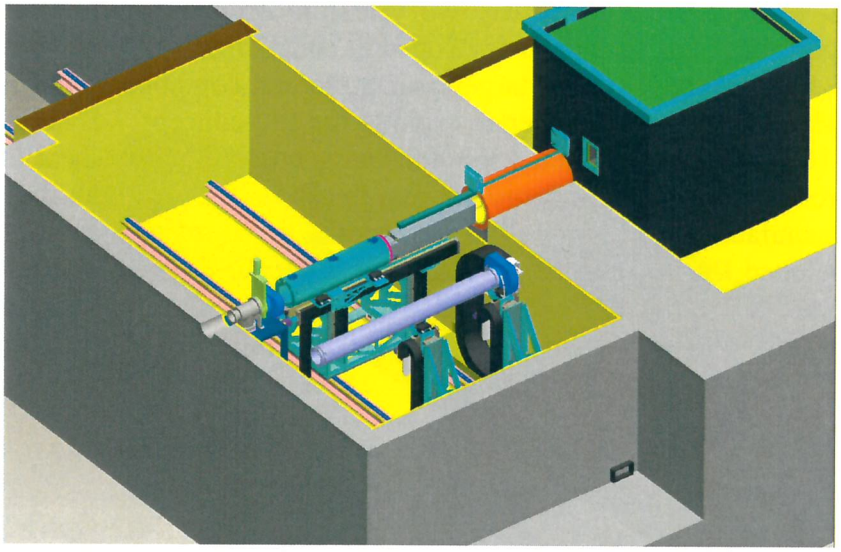

Fig. 12.5: *The room housing the target extraction system. In order to extract the target, the pipeline is first removed. The target is then slipped out the neutron moderator (the cube in right upper side of the figure) and transported to the storage room (not in the figure).*

12.1.5 The neutron converter

A R&D effort has been carried out in order to select the proper neutron converter type consistent with SPES design specifications. After extensive MCNPX simulation trials on the LNL-CN demonstration facility [11], beryllium has revealed as a whole the best solution, taking into account the neutron yielding performance as well as the related target engineering know-how. As a general rule the target design is closely linked with the design of the neutron beam shaping and filtering assembly (see next paragraph), which must take into account the geometry

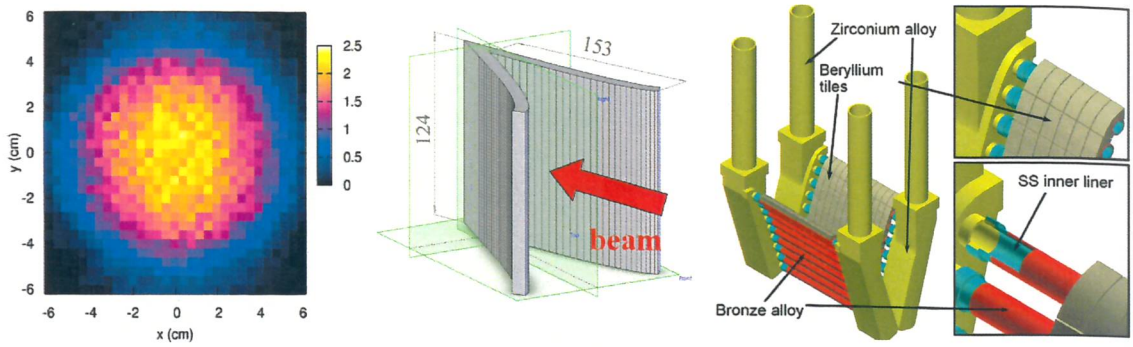

Fig. 12.6: *Proton beam power density distribution (kW/cm^2) at the target collimator on a plane normal to the beam line (left). The neutron converter profile with main sizes given in mm (center). Be-tile neutron converter and main structural components (right).*

of the neutron converter and the support structure effects on the neutron and gamma transport. Different engineering as well as operative and safety issues, concerning the neutron generator have thus to be carefully assessed, depending on the main SPES project constraints.

Because of the high impinging power (50 kW of thermal power load) the best solution for target cooling has been the most important item under investigation. In order to make use of reliable and already proven target cooling systems, the beam spot area has to be modelled to keep the surface heat load to a level ≤ ~0.7 kWcm^{-2}. After both neutronic as well as technological feasibility studies lasted two years, an original beryllium-based target concept, shown in Figure 12.6, has thus been developed in collaboration with the STC Sintez of Efremov Institute in S. Petersburg [12]. The target main structural component is of zirconium alloy (Zr + 2.5% Nb), while the neutron converter exploits the tile concept, i.e. beryllium tiles which are brazed on a 10 mm outer diameter, 1 mm thickness, cooling pipes. These latter are produced by casting of bronze (CuCrZr) alloy onto 0.3 mm thickness SS pipe with the following quenching and ageing manufacturing process. Such a composite pipe structure allows for the application of the well-developed Be-Cu joint technology, thus avoiding the corrosion of copper alloy by the coolant. In order to remove the 150 kW heat load with an almost constant power distribution on the beryllium target surface (along beam axis direction), a V-shaped target profile has been chosen.

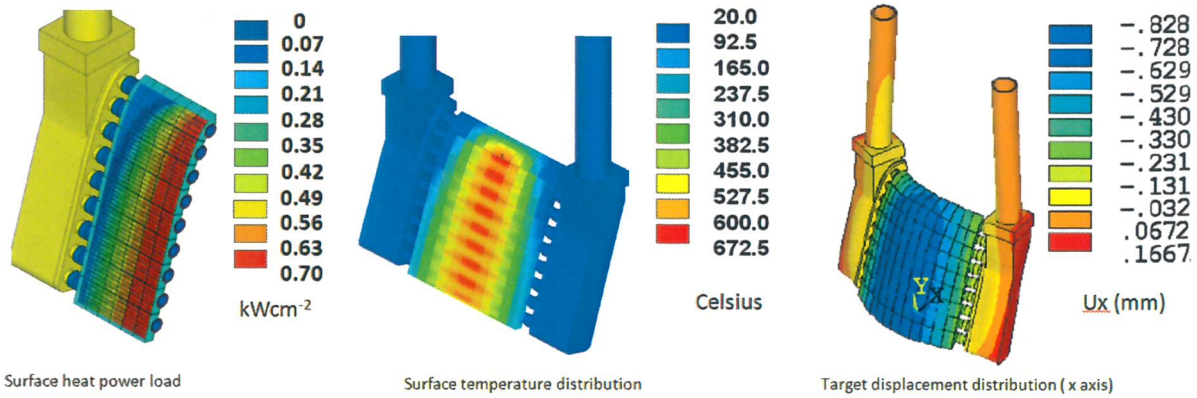

Fig. 12.7: *Target surface heat power load distribution from SPES RFQ parabolic beam shape (left). Corresponding surface temperature distribution in steady state operation (center). Target deformation (displacements along beam normal direction) under thermal stress condition (right). ANSYS® code.*

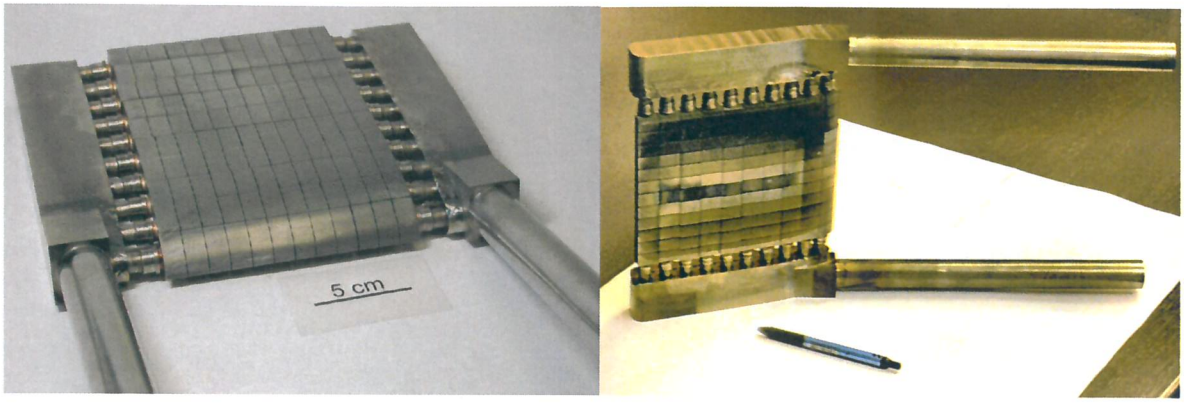

Fig. 12.8: *Neutron converter prototype with beryllium tiles (left) and surface visual inspection after the first electron beam power test performed at the HHF facility (right).*

The V-shaped profile allows also to satisfy the constrain of having peak-power densities ≤ 0.7 kWcm2. Such a target approaches as close as possible the ideal point-like source. Target has been designed to be removable from the BNCT facility, for easy inspection as well as maintenance purposes. Some concerns relating to cooling fluid capability, cooling system simplicity as well as its cost has led light water to be chosen as coolant, for both the target and the related collimator. A detailed thermal-mechanical coupled analysis has also been performed

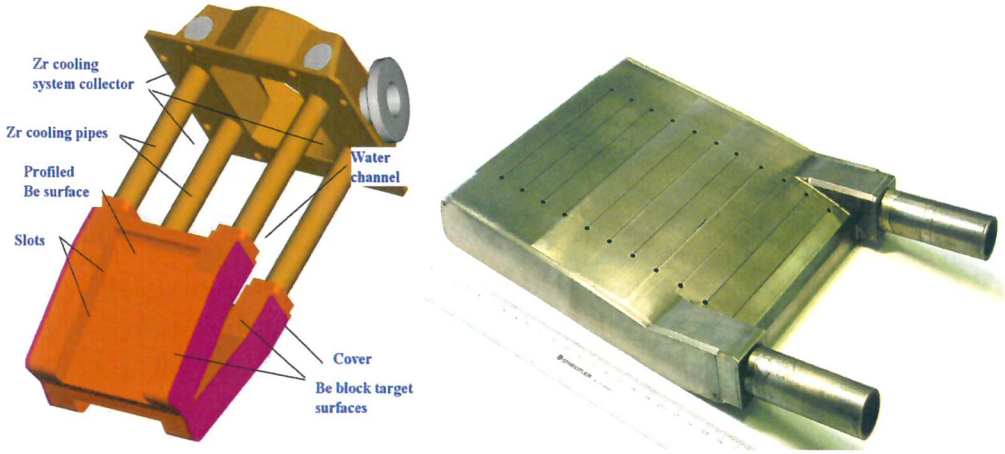

Fig. 12.9: *Be-bulk neuron converter design (left) and the half-converter constructed prototype (right)*

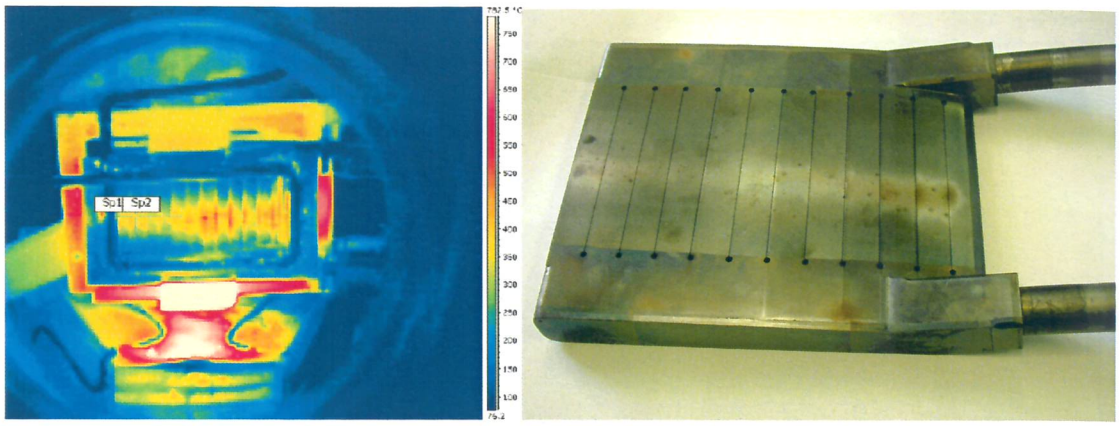

Fig. 12.10: *Target surface temperature measured with IR camera during each thermal cycle at 60 kW total power (left). Target surface visual inspection after the whole electron beam power tests performed at the HHF facility (right)*

to assess the maximum working temperatures, the related target mechanical stresses and deformations, both under static and cycling loading operating conditions. Target lifetime estimation was performed as well. The steady state thermal analysis results are reported Figure 12.7. The maximum temperature calculated in different components: beryllium (673 °C), bronze (362 °C), SS (344 °C) and Zirconium alloy (21 °C) are well below the correspondingly melting points. The stress intensities calculated at loading stage in all structural parts are well within the design limits.

Several mock-ups have been manufactured and tested at the High Heat Flux (HHF) Tsefey electron-beam facility at the Efremov Institute, with different power density levels, up to 1.1 $kWcm^{-2}$. All destructive analyses performed on inspected samples revealed good brazing quality, with an uniform brazing layer. The joint between tiles and cooling pipes was not damaged during the tests and no any visible cracks and erosions have eventually been observed inside Be thickness. The first, full-scale target prototype, shown in Figure 12.8, finally constructed at the end of 2004, successfully passed preliminary series of both operative and critical electron-beam power test conditions up to 0.75 $kWcm^{-2}$ in March-July 2005.

Technology to brazing beryllium layers on bulk CuCrZr supports, although well proven in the framework of ITER project, has the drawback to give rise to relatively high prompt gamma ray yield at the facility beam port. In order to reduce such unwanted gamma component, a technological research has started aiming to a reliable neutron converter made of bulk beryllium only. All target components like manifolds, cooling pipes, neutron converter layers have been designed starting from a full Be block. The main advantage obtained, in addition to a lower gamma yield, is less assembling parts and considerably less brazing joints. Moreover, the same neutron yield would be provided, with a better neutron moderating power than the Be-tile converter. In other words, since the Be bulk partially moderates by itself fast neutrons, neutron moderator dimensions can be smaller.

After a feasibility study by STC Sintez of Efremov Institute (S. Petersburg) lasted four years, a first full-scale prototype (see Figure 12.9) has been assembled on mid 2005. High pressure tests with He gas to find out cracks inside bulk material have passed on late summer 2005. The Be-bulk target works with a slightly larger beam spot area (120x210 mm^2) in order to lower the peak power density down to 0.5 $kWcm^{-2}$. That because the Be thermo-mechanical properties are less effective than those ones of copper alloy.

The half target prototype has then undergone a series of both operative and critical power test conditions on fall 2006 at the (HHF) Tsefey electron beam testing facility. The main goal was to assess the target reliability under heat loading condition as close as possible to the real ones. The electron scanning beam was tuned to heat the target surface with a power deposition parabolic profile (Figure 12.10), which is close to that one provided by the RFQ proton accelerator. The half target has undergone a series of tests ranging from 0.5 $kWcm^{-2}$ up to 0.7 $kWcm^{-2}$ peak power densities. The half target positively passed the test: no any visible damage (cracks) has been observed at the visual inspection on the heated surface. Therefore this second target version may be taken into account as a possible, alternative solution for the BNCT facility. Additional tests concerning radiation damage the target undergoes after 5MeV 30mA irradiation are scheduled on 2007. The radiation damage study will be done by using both proton and high neutron flux beams.

12.1.6 Neutron converter activation

Simple analytical calculations have been performed to assess the maximum neutron converter activation. Calculation have been performed taken into account the Be-tile converter. Activation has been calculated after a single run of 1600 hours, which is assessed to be the mean lifetime of the converter. This assumption is conservative, since the neutron converter unlikely

Table 12.1. Neutron converter irradiation parameters due to 30 mA, 4 MeV proton beam.

Neutron source	Thermal neutron fluence rate	Total neutron fluence rate	Continuous operation	Total neutron fluence
$3.15 \cdot 10^{13}\ s^{-1}$	$5.0 \cdot 10^{11}\ cm^{-2}\ s^{-1}$	$7.0 \cdot 10^{11}\ cm^{-2}\ s^{-1}$	1600 hours	$1.0 \cdot 10^{19}\ cm^{-2}$

will work for more than 8 hours a day. Therefore, 1600 hours correspond to 6-12 months of continuous daily work. The proton beam energy used for calculating the neutron yield has been of 4 MeV (see next paragraph). The assumed target irradiation conditions are listed in table 12.1.

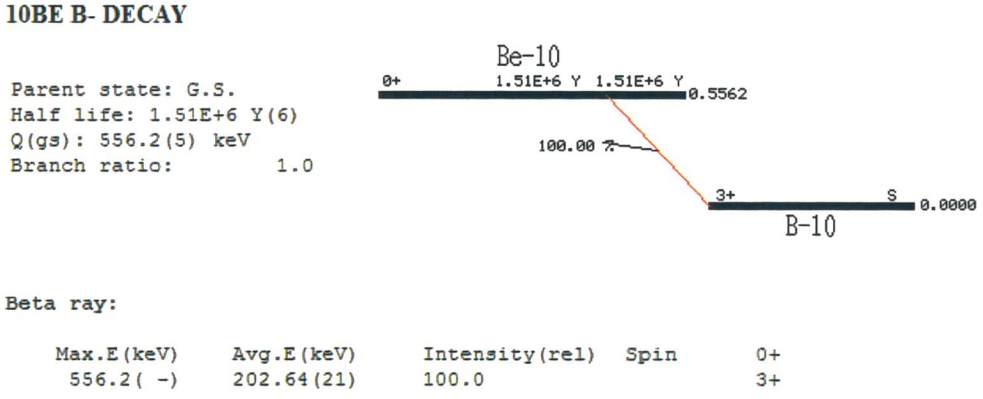

Fig. 12.11: *Decay schema of ^{10}Be.*

The exact components fraction and the elemental impurities of the 4 industrially-produced structural materials used for constructing the Be-tile neutron converter are listed in table 12.2.

Results of post irradiation residual activity and contact dose-rates estimations are reported in figures 12.12 and 12.13. Irradiation conditions are those ones of table 12.1. Copper alloy pipes are responsible for the highest activation and dose contribution. This is mainly due to the short

half lives of ^{64}Cu and ^{66}Cu, the decay of which dominates the first 3 weeks of target cooling. Impurities play the biggest role after 1 month, because of their intermediate (mainly ^{64}Zn ^{54}Fe, ^{60}Co) half lives. Impurities with very long lives like ^{93}Zr ($T_{1/2}$ = 1.53 10^6 years) and Nb ($T_{1/2}$ = 20300 years) prevent the converter total decay. The activity of beryllium that is due to nuclides created by the direct (p,xn) reaction channels opened at 4 MeV may be considered negligible. Therefore, beryllium activation depends only on ^{10}Be, which is created by ^{9}Be neutron capture. However, ^{10}Be is a pure beta emitter, as shown in figure 12.11. Therefore, activation of the Be alloy used entirely comes from the impurities included. This conclusions are valid also for a 5 MeV proton beam. However, it is worthwhile to remember that, because of the higher neutron yield at 5 MeV, activation will likely be higher of a factor 3-4.

Table 12.2. Elemental composition weight fraction of the Be-tile converter materials.

Be S65 (wt%)		SS316 LN (AISI) (wt%)		CuCrZr alloy (wt%)		Zr-1%Nb alloy (wt%)	
Be	98.5	**Fe**	64.94	**Cu**	99.01	**Zr**	99.0
O	0.64	**Cr**	17.5	**Cr**	0.75	**Nb**	1.0
C	0.1	**Ni**	12.25	**Zr**	0.11		
Fe	0.08	**Mo**	2.5	**Co**	0.06		
Si	0.06	**Mn**	1.8	**O**	0.03		
Mg	0.06	**Si**	0.5	**Si**	0.011		
Al	0.06	**Ti**	0.15	**Fe**	0.009		
N	0.0225	**Cu**	0.1	**P**	0.0069		
Ni	0.0145	**N**	0.07	**Zn**	0.0069		
Ti	0.0105	**Al**	0.05	**S**	0.0023		
W	0.01	**Co**	0.05	**Pb**	0.0017		
U	0.0085	**P**	0.025	**Al**	0.0016		
Zr	0.0075	**C**	0.0225				
Cu	0.007	**Nb**	0.01				
Cr	0.0065	**Ta**	0.01				
Pb	0.002	**S**	0.008				
Mo	0.002	**V**	0.004				
Mn	0.002	**O**	0.002				
Ca	0.002	**Zr**	0.002				
Na	0.0015	**Sn**	0.002				
Zn	0.001	**B**	0.001				
S	0.001	**W**	0.001				
Ta	0.00097	**Pb**	0.0008				
Co	0.0009	**Bi**	0.0008				
Sc	0.0005	**K**	0.0005				
F	0.0005	**As**	0.0005				
Cl	0.0005	**Sb**	0.0005				
Li	0.0003	**Ba**	0.0005				
Ag	0.0003	**Tb**	0.0005				
Cd	0.0002	**Ir**	0.0005				
B	0.0002	**Ag**	0.0002				
P	0.000046	**Cd**	0.0002				
Nb	0.000012						
Hf	0.000003						
Total mass estimated (gr)							
352.5		**20.9**		**1597.3**		**2393.5**	

When the neutron converter is hit by 30 mA 5 MeV proton beam becomes an intense fast neutron source with a maximum of energy of about 3 MeV and an average energy of 1.57 MeV in forward direction. In order to treat MM tumours, fast neutrons have to be moderated down to thermal energy, for superficial tumours, or to epithermal energy for deeper tumours. The

Table 12.3: BNCT in-air neutron beam port recommended limits

BNCT beam port parameters		**Required limits**
ϕ_{th}	[$cm^{-2}s^{-1}$]	$\geq 1 \cdot 10^{9}$
ϕ_{th} / ϕ_{total}		> 0.9
$(\dot{D}_{n,fast} + \dot{D}_{n,epi})/\phi_{th}$		$\leq \sim 2 \cdot 10^{-13}$
$\dot{D}_{\gamma}/\phi_{th}$		$\leq \sim 2 \cdot 10^{-13}$
Fast energy group	ϕ_{fast}	E > 10 keV
Epithermal energy group	ϕ_{epi}	10 keV ≥ E ≥ 0.5 eV
Thermal energy group	ϕ_{th}	E< ~ 0.5 eV

neutron-moderator design aims to optimise in-air radiation field parameters, called *figures of merit* (FOM), at the irradiation port of 10x10 cm^2 nominal area . The BNCT community, has a quick and useful method to assess the design's FOM for thermal neutron fields (see table 3) [13].

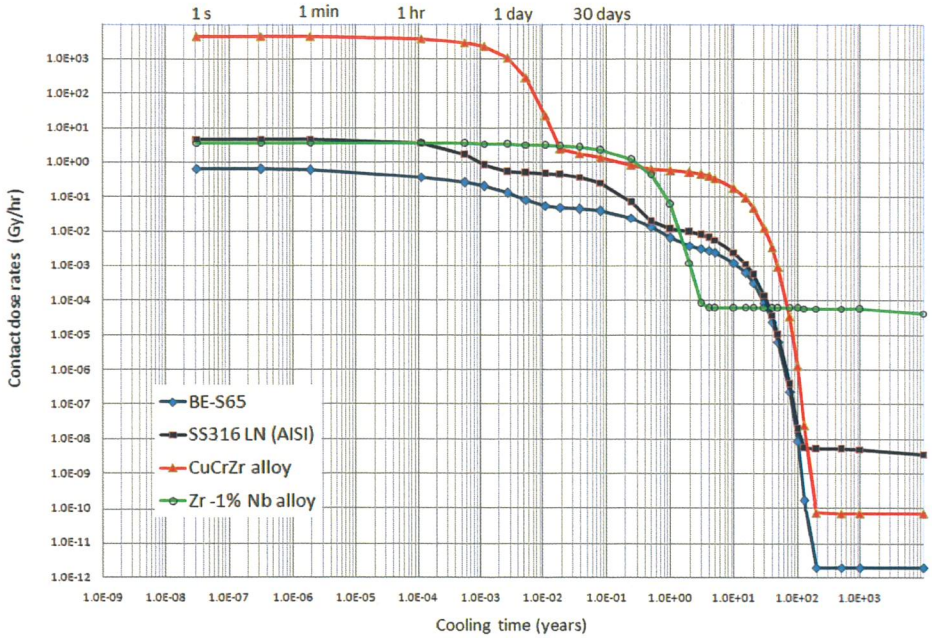

Fig. 12.13: *Contact doses against cooling time due to activated materials of figure 12.12*

Exploiting the know-how gained in designing the BNCT demonstration facility constructed at the CN 7 MV Van de Graaff laboratory [14, 15], a realistic neutron moderator for MM treatments has been designed. The neutron source is the real Be-tile neutron converter of figure 12.6. However, due to lack of an experimental set of complete double-differential neutron yield data at 5 MeV of proton energy, the experimental data set at 4 MeV [16] has been used in this preliminary design. Such a choice is expected to be conservative with respect the FOM, in spite of the higher mean neutron energy at 5 MeV than at 4 MeV of proton beam, 1.57 MeV and 1.06 MeV respectively [16]. In fact, because of the known resonances between 4.5 and 5.0 MeV, the total neutron-yield production is expected to be much higher at 5 MeV than at 4 MeV of proton [17, 18]. Recent experimental neutron yields at 0° confirm such an expectation. Neutron production at 5 MeV has been in fact measured to be 3.8 times higher than at 4 MeV [16].

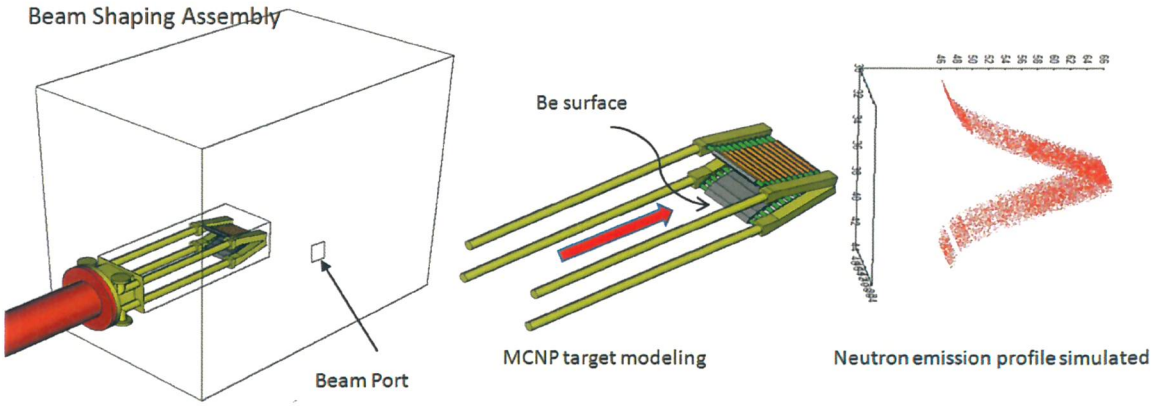

Fig. 12.14: *MCNPX real-like geometry modeling of the neutron converter inserted inside the neutron moderator (left). Close-up view of the Be neutron converter (centre). Neutrons emission points over the entire source emitting surfaces (right).*

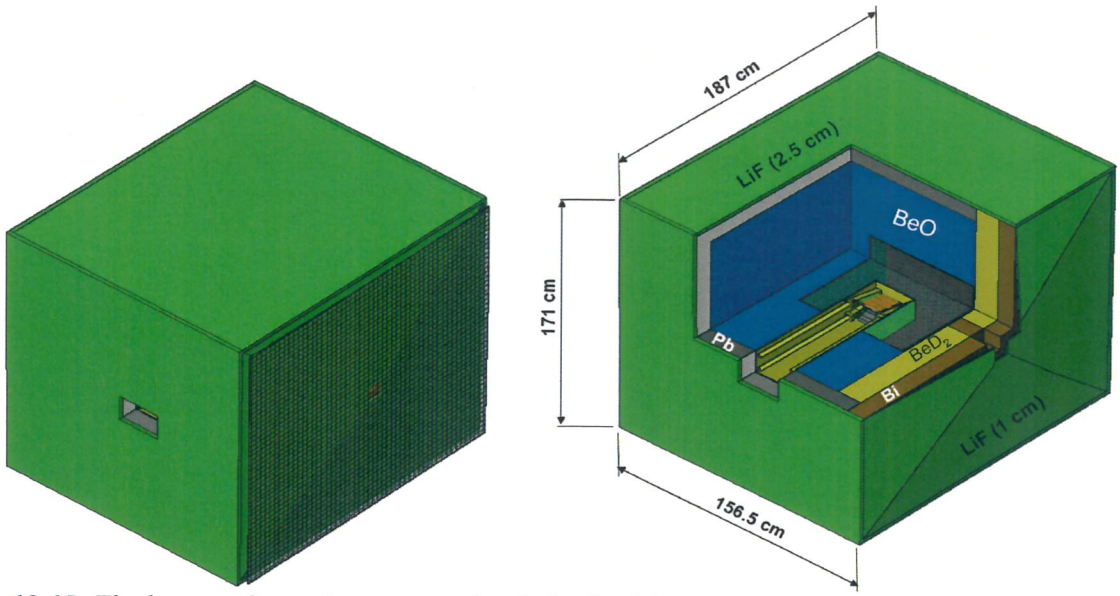

Fig. 12.15: *The best configuration proposed with the final Be neutron converter: MCNPX geometry*

In figure 12.14, the neutron converter is sketched, together with the 3D plot of the neutron emission points, all generated within a thin layer of about 300 μm, due to a 4 MeV proton beam and following the profile of the neutron converter surface. More detailed are published elsewhere [14].

After having calculated several moderator models best results have been obtained with the moderator shown in figure 12.15. The facility main features are the heavy-water tank, around the neutron converter and the beryllium oxide (BeO), which reflects neutrons towards the irradiation port with high efficiency thanks to its *albedo* properties. Another important feature is the 2.5 cm thickness of hydrogen-free lithium fluoride (LiF) panels around five out of six walls of the moderator for absorbing thermal neutrons that escape throughout walls. The sixth wall (where the irradiation port is) has a thicker panel of 1 cm.

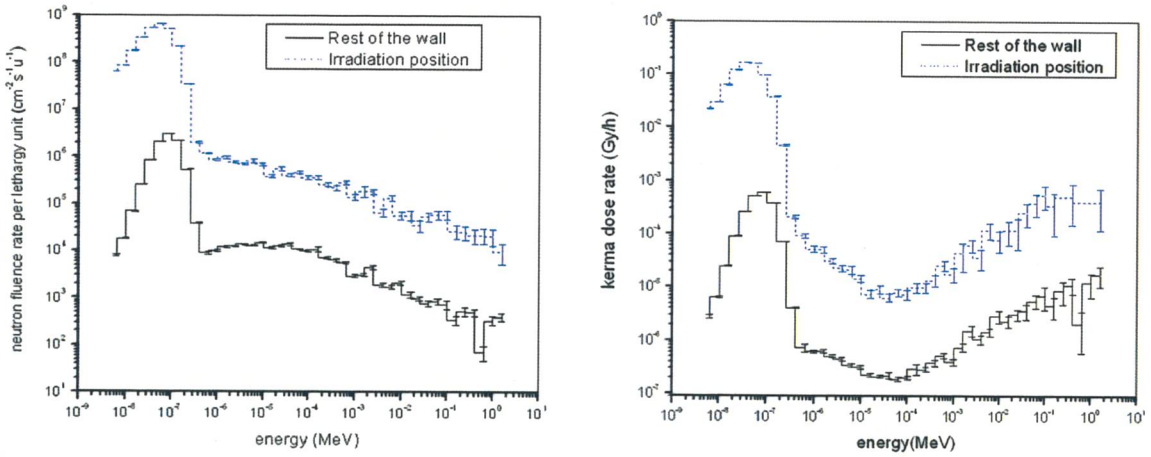

Fig. 12.16: *Neutron fluence rate per lethargy unit (left) and neutron kerma rate (right) spectra at beam port irradiation position (dotted line) and averaged all over the rest of the wall (full line) of moderator of figure 15.*

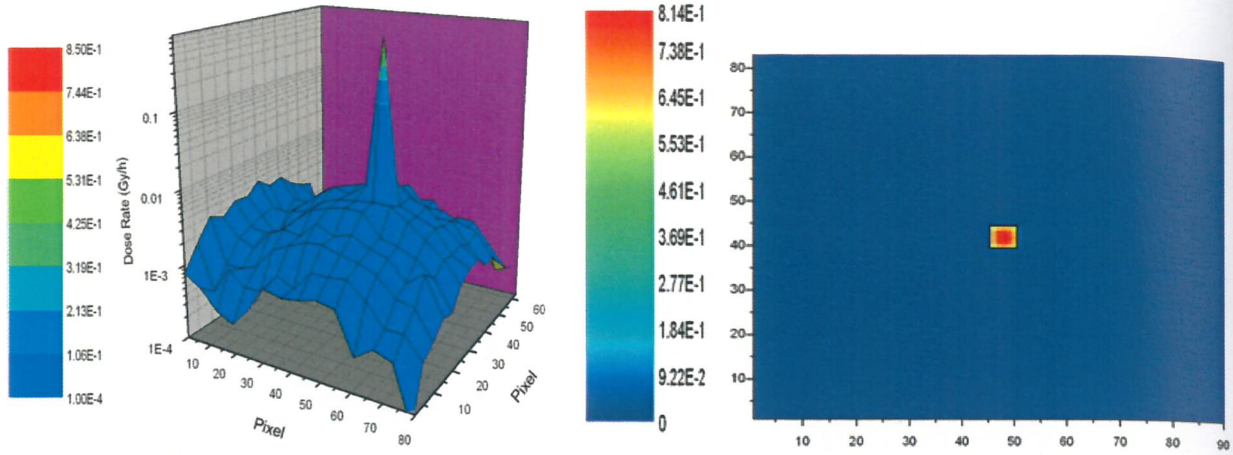

Fig. 12.17: *Thermal neutron dose rate (Gy/h) 3D profile over the patient-facing wall surface (left). The same plot in 2D view: the square is the irradiation beam port position (right).*

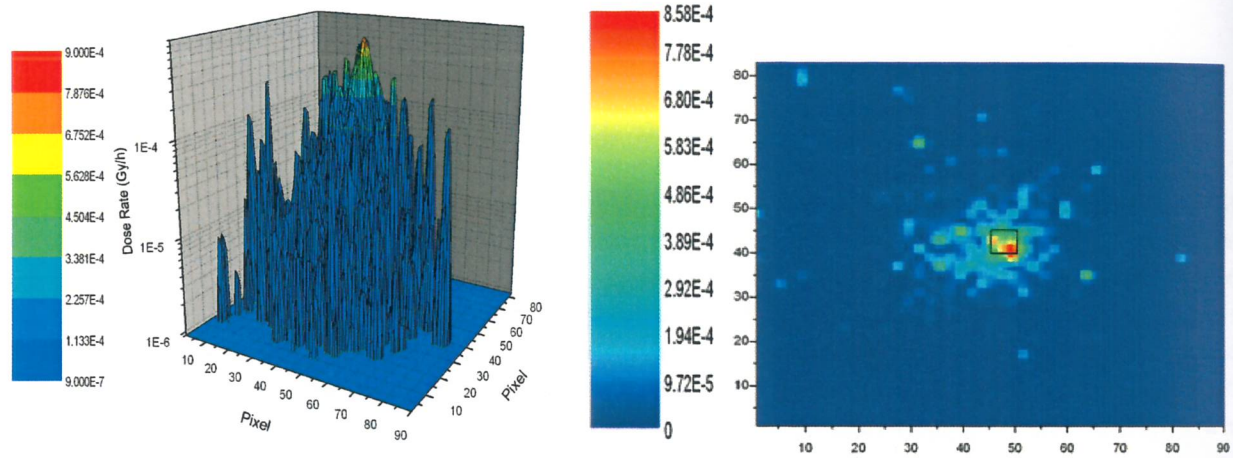

Fig. 12.18: *Epithermal neutron dose rate (Gy/h) 3D profile over the patient-facing wall surface (left). The same plot in 2D view: the square is the irradiation beam port position (right).*

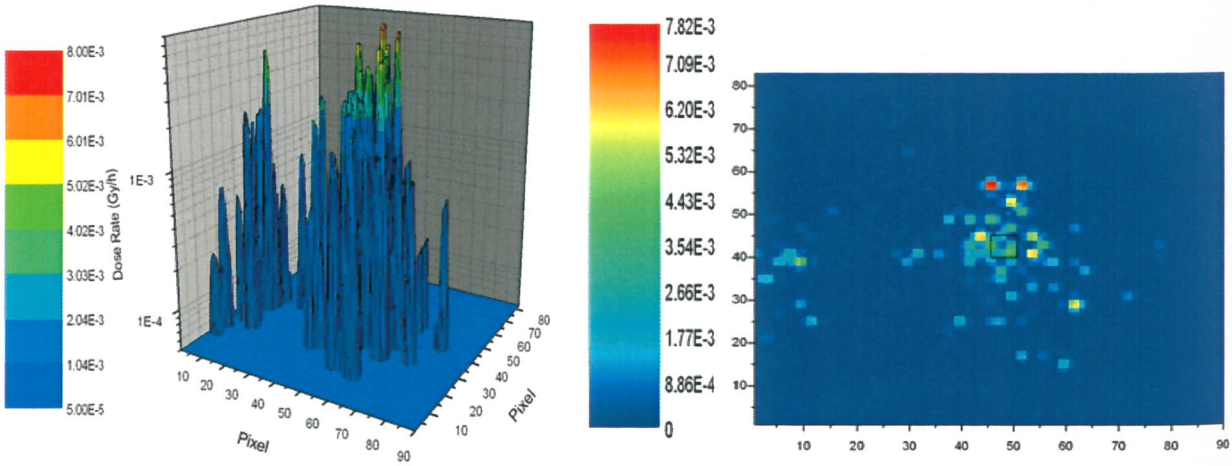

Fig. 12.19: *Fast neutron dose rate (Gy/h) 3D profile over the patient-facing wall surface (left). The same plot in 2D view: the square is the irradiation beam port position (right).*

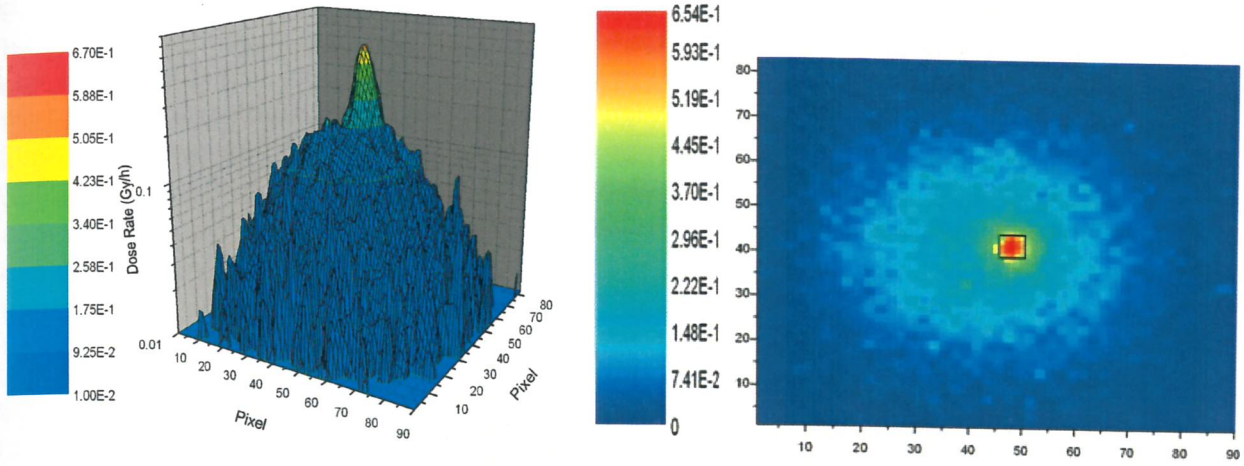

Fig. 12.20: *Gamma dose rate (Gy/h) 3D profile over the patient-facing wall surface (left). The same plot in 2D view: the square is the irradiation beam port position (right).*

Figure 12.16 shows the neutron fluence rate per lethargy unit ($cm^{-2}s^{-1}u^{-1}$) and the related neutron kerma rate (Gy/min) spectra at irradiation port and averaged all over the rest of the wall. As it can be seen, neutron collimation properties of the moderator are very good (a factor bigger than 10^2). The FOM values are listed in table 12.4. All the calculated parameters are better than the recommended values listed in table 12.3.

In order to study dosimetric properties in more detailed way, a grid of 2x2 cm^2 pixel size has been put in front of the irradiation wall of the moderator of figure 12.15. Figures 12.17-12.19 show kerma values in air at any pixel position for the thermal, epithermal and fast neutrons components of the beam, while figure 12.20 shows kerma values for gamma rays. As it can be seen the thermal neutron beam is confirmed to be very collimated. The ratio of the irradiation port value on the background value (the area were only patient healthy tissues are supposed to be) is of about 100. Fast and epithermal neutron doses are less collimated. However, their absolute values are well less the recommended values, pointing out a possible total body dose of about 3 mGy only. Gamma dose is poorly collimated, because prompt gamma rays are mainly produced by radiative capture of thermal neutrons throughout the moderator. The gamma ray source is widespread over all the neutron moderator volume, because thermal neutrons diffuse stochastically inside it. Nevertheless, the neutron moderator succeeds to concentrate 92 % of the gamma yield at the irradiation port. 1 hour treatment with moderator of figure 12.15 could give to a total body dose of about 100 mGy. However, gamma shields can be easily implemented by simply adding lead layers outside the moderator. More details about the moderator design are in reference [20].

For concluding, we remember that the present computational MCNPX design, based on 4 MeV 30 mA proton beam, provides a high collimated thermal neutron beam (99.7 %), fulfilling

Table 12.4. FOM of the neutron moderator of figure 15. MCNPX calculations for 4 a MeV 30 mA proton beam.

Beam port data	Φ_{th}	$\frac{\Phi_{th}}{\Phi_{tot}}$	$\dot{D}_{n,(epi+fast)}/\Phi_{th}$	$\dot{D}_{\gamma}/\Phi_{th}$
	($\times 10^9 \cdot cm^{-2}s^{-1}$)		**($\times 10^{-13}$ Gy·cm^2)**	**($\times 10^{-13}$ Gy·cm^2)**
	1.17	0.99	0.008	1.38

all the established design requirements for a BNCT irradiation facility. Next step will be to measure neutron yield spectra from 0° to 135° for 5 MeV protons by using the CN Van de Graaff accelerator of Legnaro Laboratories (see next paragraph). As soon as 5 MeV data will be available, the final neutron moderator design will start. New design will use both the Be-tile converter and the Be-bulk neutron converter (see figure 12.9), which has neutron moderating capability bigger than that one of the Be-tile neutron converter. Its use is therefore expected to reduce neutron moderator dimensions, as well as the residual activation.

12.1.7 Neutron yield measurements

In order to proper design neutron beams for BNCT purposes, source neutrons have to be transported first through the neutron converter and then through the neutron moderator by using Monte Carlo codes like MCNPX. Calculation result accuracy depends mainly on the neutron-source knowledge accuracy. The neutron source is defined by the neutron energy spectrum, which however changes with the neutron angle emission. For our purposes, a good enough neutron-source knowledge means knowing energy spectra down to less than 100 keV for emission angles from 0° to 135°.

Because of the lack of experimental data about neutron yields of the reaction 9Be(p,xn)9B at 5 MeV of protons [16], an experimental campaign has been open to measure neutron yields by using the LNL 7 MV CN accelerator and the superheated drop detectors (SDD). SDDs are superheated gels, which give rise to very small evaporation drops when hit by neutrons. A sonic detection system able to listen drop formation makes SDDs active detectors. The neutron energy detection threshold can be changed by changing SDD temperature. Energy detection thresholds as low as 25 keV are accessible. More details about are published elsewhere [21]. In figure 12.21 a SDD is mounted on a motorized trolley in the CN experimental hall by Legnaro Laboratories.

12.1.8 Microdosimetric detectors

BNCT radiation dosimetry is complex because of the co-presence of different radiation components with different biological effectiveness. Living cells experience in fact radiation

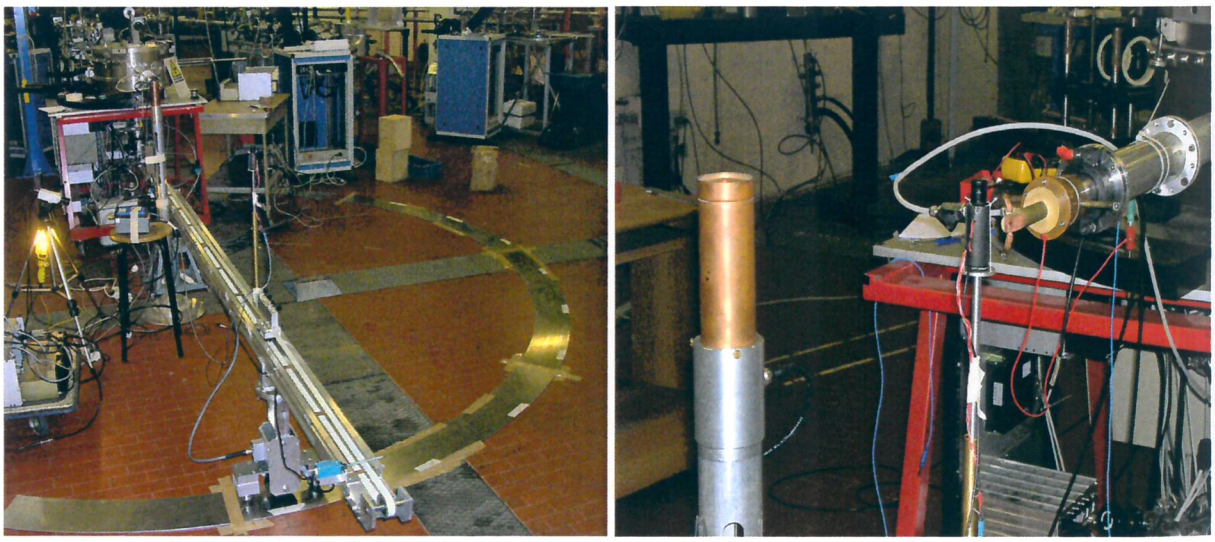

Fig. 12.21: *The superheated drop detector (the black vial in the right side picture) and the remote-controlled trolley (left side picture) for neutron yield measurements at different emission angles. The Be target is inserted in the air-cooled holder that is visible in the right side picture. The Be-target-holder end is inclined of 30° with respect the beam line.*

events with large LET spreading, ranging from less than one tenth of keV/μm (2.2 MeV gamma rays), to several hundreds of keV/μm (^{7}Li ions). Moreover, their relative contributes change with the depth and, if the proton beam fluctuates, also with the time possibly. In order to take properly into account radiation field variations for foreseeing resulting biological effect variations, the expression "radiation quality" has been introduced, which points out some radiation-field physical quantities that are somehow significant for the biological effect. In BNCT research centres the ratios of table 3 are supposed to be also good markers of radiation field quality in conjunction with the neutron-gamma dose ratio Dn/Dγ. Such a ratio, which is measurable with the standard twin ionisation chamber method, is in fact expected to be significant for healthy tissue damage. However, a recent radiobiological intercomparison between 7 different BNCT radiation field has pointed out that the biological effectiveness is poorly correlated with the ratio Dn/Dγ [7]. Although doesn't exist yet a widely accepted radiation action theory, microdosimetric measurements are instead considered significant in radiation therapy [22].

Tissue-equivalent proportional counters (TEPC) are the best detectors for measuring microdosimetric spectra. They have been proved to be able to measure absorbed dose and its quality with high accuracy both for high energy [23] and low energy [24] neutrons, as well as for fast neutron therapeutic beams [25] and BNCT applications [26], [27]. In order to study TEPC performances and precision in BNCT, a first TEPC with an easy tissue equivalent A-150 plastic cathode shell replacement was constructed. The TEPC could be assembled with different cathode walls, the ^{10}B concentration of which ranged from 0 to 100 ppm in order to measure both the radiation quality experienced by cells with and without ^{10}B. However, because of its large sensitive volume (2.3 cm^3) the counter was able to measure only in relatively weak radiation fields. Measurements were performed inside the irradiation cavity of TAPIRO ENEA fast reactor thermal column only at very low (20 W) power[28].

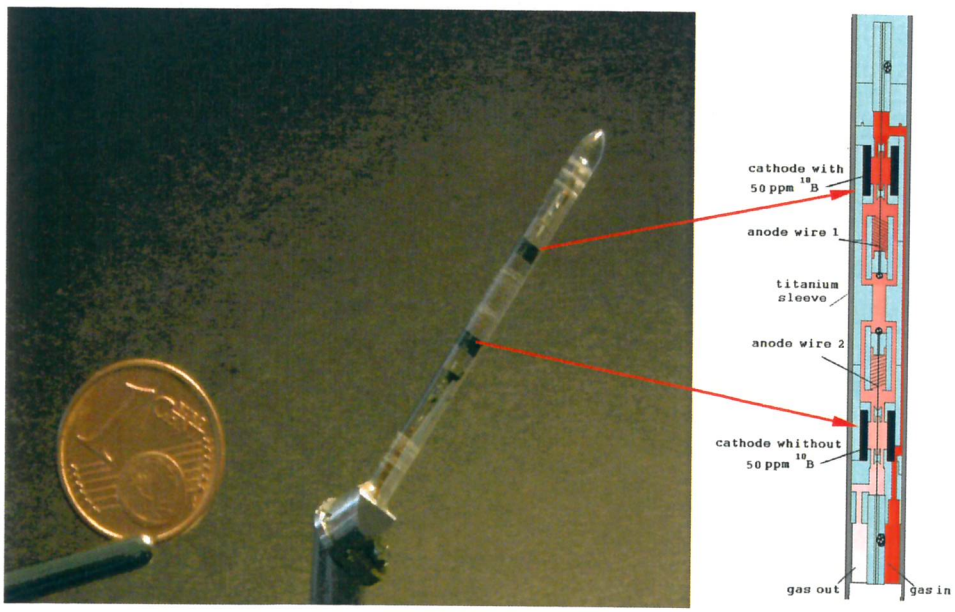

Fig. 12.22: *Cutaway view (right) of the twin TEPC prototype. The red pipeline points out the counting gas circuitry: full red is gas inlet, rose is gas outlet. Real size detector picture is on the left side of the figure. Proportional counter cathodes are the two 1 mm tissue-equivalent black plastic cylinders in the*

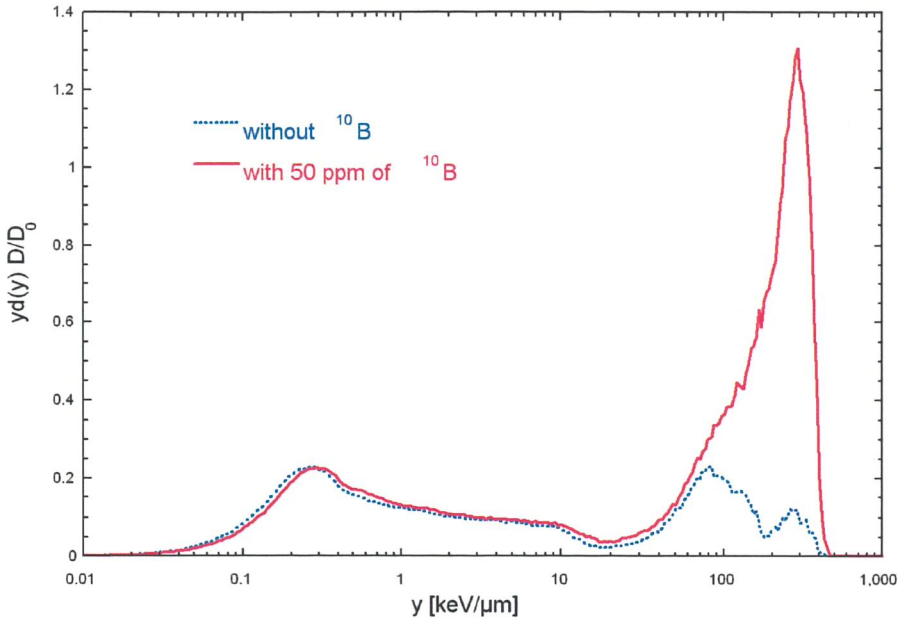

Fig. 12.23: *Microdosimetric spectra measured inside HYTHOR (see § 12.3.8) cavity by twin TEPC (see text).*

In order to prevent pile-up event distortions in microdosimetric spectra when radiation field intensity is high, much smaller counters with sensitive volume less than 1 mm3 are necessary [29]. The cathode wall of such a mini TEPC can not be changed. Therefore, a new counter has been designed that is made of two cylindrical TEPCs with two cathode walls, one of them with 50 ppm of 10B, the other one without 10B. Such a compact counter, called twin TEPC, could be the main instrument to measure the radiation quality both in air, in phantom and also in vivo, thanks to its millimetric dimensions. To test such a design feasibility, a twin TEPC prototype with two mini TEPCs encapsulated inside the same insulating cylinder (see figure 12.22), which is in turn inserted inside a thin titanium sleeve, has been constructed [30]. The 20 cm long 2.7 mm large titanium sleeve allows for inserting twin TEPC into the irradiation cavity (see figure 12.24) as well as in a phantom and inside the patient body possibly.

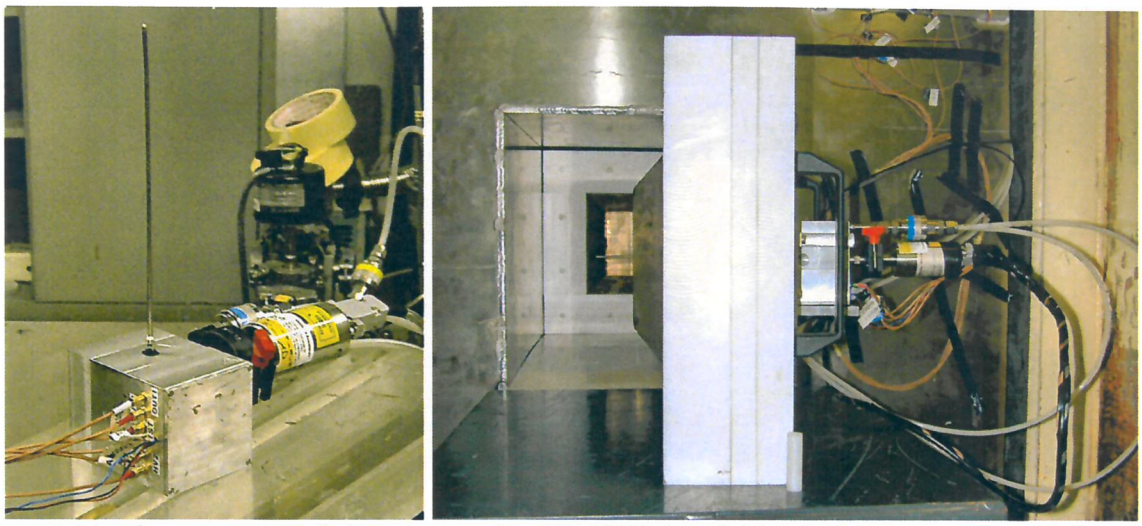

Fig. 12.24: *The twin TEPC (left) is inserted in HYTHOR (see § 12.3.8) irradiation cavity lid (right). The irradiation cavity is visible in background*

First measurements [31] with the twin TEPC prototype are shown in figure 12.23. The microdosimetric spectrum is the TEPC pulse height spectrum that is processed to give the fraction of absorbed dose given by pulses between y and y+Δy, where y (ratio of the imparted energy on the sensitive-volume mean chord length) is the lineal energy. Measurements of figure 12.23 have been performed with a sensitive volume thickness as big as a chromosome (1 μm). D is the total dose measured by the 50 ppm ^{10}B TEPC. D_0 is the total dose measured by the TEPC without ^{10}B. Spectra of figure 12.23 are scaled by the ratio D/D_0. Therefore, the area under the ^{10}B curve for a given Δy logarithmic interval minus the area under the without-^{10}B curve for the same Δy logarithmic interval is the percentage increasing of the absorbed dose in that given Δy interval, when 50 ppm of ^{10}B are added. As expected, absorbed dose due to gamma rays (event size < 20 keV/μm) doesn't increase significantly when ^{10}B is added in the TEPC wall. On the contrary, absorbed dose due to events of size > 50 keV/μm increases largely because of the events due to He and Li ions. Spectra of figure 12.23 can be processed to give the total field RBE (relative biological effectiveness) [32] or precise evaluation of the different absorbed dose components. More details about are published elsewhere [31, 33].

R&D continues for studying and improving twin TEPC accuracy. The new twin TEPC will use low-gamma and low-beta emitters constructing materials to minimize gamma dose due to counter activation caused by the intense thermal neutron field.

12.1.9 New boron carriers

BNCT optimisation research aims to maximise biological damage in tumour cells without inducing relevant healthy tissue damage. For a given radiation field, it does depend on the ratio of ^{10}B concentration in tumour tissue with respect the ^{10}B concentration in healthy tissue as well as on the location of ^{10}B carrier inside the tumour and healthy cells. In BNCT research centres, the ^{10}B carriers more used are Borophenylalanine (BPA) and Sodiumdodecaborate (BSH). Both of them can not be easily traced inside the cells. On the contrary, fluorescent ^{10}B carriers can.

First attempts of using fluorescents carriers have been made with phtalocyanine. A novel ^{10}B-enriched carboranyl-containing phthalocyanine (B-Pc) has been at the purpose synthesized. In figure 12.25, it can be seen how this molecule can be easy traced inside MM cells. By superimposing the first 3 pictures of figure 12.25, the forth picture is obtained. It shows that the boronated phtalocyanine (B_4Pc, red fluorescent stuff) enters inside MM cells passing through

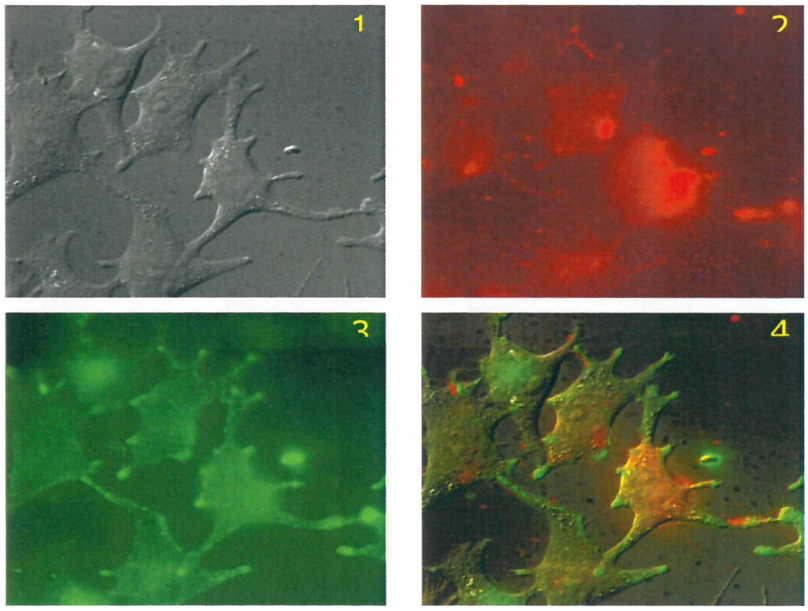

Fig. 12.25: *Fluorescence micrographs of cells after 24 h incubation with 7 μM DOPC liposome-incorporated B_4Pc. 1. bright field image 2 fluorescence of phthalocyanine. 3 fluorescence of endosomal probe Lucifer Yellow. 4 overlay of images 2 and 3 (see text).*

cell membranes, which are pointed out by the green fluorescent light. First irradiation trials were performed, at the Tapiro reactor thermal column in Casaccia, to observe the thermal neutron effect on mice MM tumours after B_4Pc supply. In spite of the small ^{10}B concentration in tumour tissue (less than 1ppm) a significant delay in tumour growth was observed [34]. Such an expected positive effect could be due to the high efficacy of high-LET He and Li events, as they occur just inside the MM cell. Boronated porphyrines, having similar behaviour, have been synthesised too. Radiobiological research to maximise boronated porphyrines effects is in progress with by the HYTHOR facility (see the following paragraph).

The use of phtalocyanines or porphyrines as ^{10}B carriers open the way to combined therapies, since such molecules are already used in photodynamic therapy (PDT). Such molecule can be in fact photoactiveted by visible or near infrared light with production of cytotoxic species, which lead the tumour to necrosis. Synergic effects between BNCT and PDT will studied.

12.1.10 HYTHOR

HYTHOR (acronym for HYbrid Thermal spectrum sHifter TapirO Reactor) is a neutron moderating column designed and constructed by LNL and installed by ENEA Casaccia research centre. HYTHOR can be easily inserted inside the 5 kW TAPIRO reactor (see figure 12.26) and it can as much easily pulled out. HYTHOR irradiation cavity (10X20X25 cm^3) can contain up to 6 mice. It is used for microdosimetry and radiobiological studies (see § 12.3.6 and 12.3.7). HYTHOR's radiation field calculated parameters are in table 5. Hythor's FOM satisfies the reference parameter condition of a BNCT facility Therefore, experimental studies performed with HYTHOR are significant for a future therapeutic facility. More details about HYTHOR are published in reference [35].

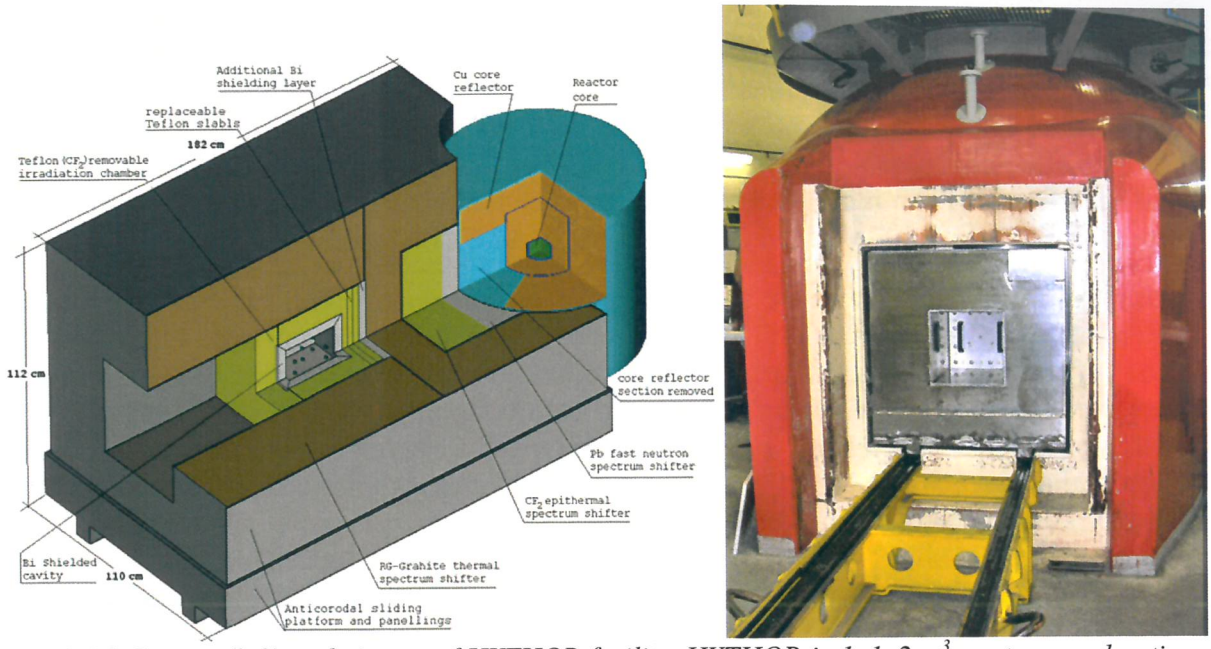

Fig. 12.26: *Layout (left) and picture of HYTHOR facility. HYTHOR is 1x1x2 m^3 neutron moderating structure. In the HYTHOR center, the irradiation cavity is visible.*

12.2 The LEgnaro NeutrOn Source (LENOS)

12.2.1 Introduction

In the last years a renewed interest in the low energy neutron physics has triggered the construction of new facilities as well as many experimental apparatus. This process has been mainly boosted by the needs of nuclear data in several fields like nuclear astrophysics, nuclear waste transmutation, generation IV reactors, fusion reactors, decommissioning of first generation fission reactors, radioprotection, dosimetry and by the material science community. For this reasons a great number of facilities have been built or are in preparation all over the world:

Table 12.5. HYTHOR Figure Of Merit. Φ_{th} range of values points out that the thermal-neutron fluence rate decreases inside the irradiation cavity with the distance from the reactor core.

Beam port data	Φ_{th} ($\times 10^9 \cdot cm^{-2} s^{-1}$)	$\frac{\Phi_{th}}{\Phi_{tot}}$	$\dot{D}_{n,(epi+fast)}/\Phi_{th}$ ($\times 10^{-13}$ Gy·cm^2)	$\dot{D}_{\gamma}/\Phi_{th}$ ($\times 10^{-13}$ Gy·cm^2)
	3.48	0.92	0.14	0.85

n_TOF (CERN), Frankfurt (Germany), Obninsk and INR-Troitsk (Russia), JPARC (Japan), SNS and LENS (USA) just to cite some of them.

One of the most interesting topic in nuclear astrophysics is related to nucleosynthesis of the elements beyond iron, which are mainly produced via neutron-capture reactions called s (slow) and r (rapid) processes [36]. The main goal of nuclear astrophysics models is to reproduce the observed abundance of the elements in the Universe. In particular, recent data made available by

silicon grains studies, has triggered new hypothesis and has underlined the need of more accurate neutron-capture cross section data.

The neutron-capture cross section data are the fundamental ingredient for the calculation of the stellar reaction rates and thus the possibility of reproducing the observed abundance of the elements in the universe. The s process follows the valley of beta stability and of particular relevance are the branching points, because also the thermodynamic condition of the stellar site can be estimated. The most important quantity needed for the calculation of the stellar reaction rate is the Maxwellian Averaged Cross Section (MACS), defined as

$$MACS = \left(\frac{\langle \sigma v \rangle}{v_T} \right)$$

$$\langle \sigma v \rangle = \int_0^\infty \int_0^\infty P(v_x) \cdot P(v_y) \cdot \sigma(v) \cdot v \cdot dv_x \cdot dv_y$$

Where P(v) is the Maxwellian velocity distribution and v_T the mean thermal velocity.

Since the relevant quantity is the MACS, measurements of the capture cross section as a function of the energy can be performed with a relative low resolution. The MACS can also be evaluated directly by measuring the total capture cross section having a neutron beam shaped with a Maxwellian spectra with a kT≈30 keV, as obtained by Kaeppeler et al. [50,51]

Despite their importance in the development of stellar nucleosynthesis models, the measurements of neutron-capture cross sections on unstable nuclei are difficult, often technically not feasible [40] due to the induced background, costs and safety related problems. A great effort has been performed by different groups to update and compile the experimental and theoretical nuclear data of interest in astrophysics [37] [38] [39], but have still to be measured some very important isotopes, most of them are unstable.

Beside the important topic of fundamental physics, there is a compelling need for nuclear data also for many field of applied nuclear physics and, in particular, those related to the applications to the new technologies for the production of nuclear energy and to the compilations of evaluated database (ENDF, JEFF, JENDL). The request of nuclear data covers a wide energy range and different processes, as reported in many official documents compiled by the most important agencies, like NEA [41] and IAEA [42].

The evaluated nuclear data libraries are used in many codes, from MCNP to GEANT and, consequently, the accuracy of such programs is strongly dependent from the accuracy of nuclear data collected in the databases.

Because the production of nuclear waste is one of the main problems for a sustainable nuclear energy production, the transmutation of long lived isotopes (mainly actinides and fission fragments) must be pursued. Actinide transmutation is proposed to take place by fission reactions in subcritical reactor like accelerator driven systems (ADS) and in fast spectrum critical reactors such as some proposed Generation IV reactors like the sodium fast cooler reactor (SFR) and gas cooled fast reactors (GFCR), strongly studied by many agencies all over the world. For many isotopes there are no cross section data or the accuracy needed is lower than existing data. Measurement of capture, fission and inelastic cross sections on transuranic elements, fission fragments and specific structural materials are needed. In Particular, the capture cross section on some FF, generated during the burn-up of the new proposed fuel can play a fundamental role as a neutron poison, in the same way of ^{135}Xe and ^{142}Sm take place in the safety operation of the actual reactors.

Because the spectrum is quite new, if well characterized, the facility can also be used as a benchmark to validate evaluated nuclear data [43].

12.2.2 Main characteristics of the facility

Thanks to the possibility of having in situ the presence of SPES, which produces Radioactive Ion Beams (RIB) by Uranium fission and a high current proton beam which can produce an intense neutron beam, we are investigating the possibility to perform neutron induced cross section measurements for isotopes never or poorely measured before. The name of the future neutron complex is LENOS and could be completed within the time framework of the SPES project.

In LENOS, special targets can be constructed by implanting a selected beam of SPES in a thin baking target, in order to obtain an exotic target to be measured at least, by using the irradiation activation methods. All new generation of RIB facilities have the possibility of performing exotic target, but often the neutron beam is far from the RIB facility, so if the sample is highly radioactive, the possibility to transport it can be limited for safety reasons. The main profit can be obtained having a beam line which transports the low energy exotic beam of SPES directly to the neutron experimental hall. In this way, two lines converges into the same measuring target, the low energy exotic beam and the neutron beam, so the target to be measured can be implanted and consequently irradiated by the neutron beam without moving it.

Beside such characteristic, which is the most important one, measurements with low energy resolution on stable targets can also be performed.

Our purpose is the construction of LENOS within the framework of the SPES project, by using the TRASCO RFQ the neutron production. The already tested BNCT technology will be used for the construction of the Beryllium target, which has an experimentally measured neutron yield at 0 degree of 443 n/pC [44-46] for the reaction ^{9}Be(p,xn) at 5 MeV. With a current of 50 mA in CW mode a total flux of about 10^{14} n/s on the full solid angle could be achieved. The energy spectra obtained from a thick target shows a peak around 2.6 MeV. Our goal is to have both an activation facility using the proton beam in CW mode and 30mA and a Time of Flight (TOF) facility (which can work at 50 mA CW equivalent), by pulsing the proton beam with a time resolution of about 6 nsec, with a repetion rate from 25 to 250 kHz and a duty cycle from 1% to 0.1% accordingly.

A schematic layout of SPES, with the lines of LENOS, is reported in figure 12.27.

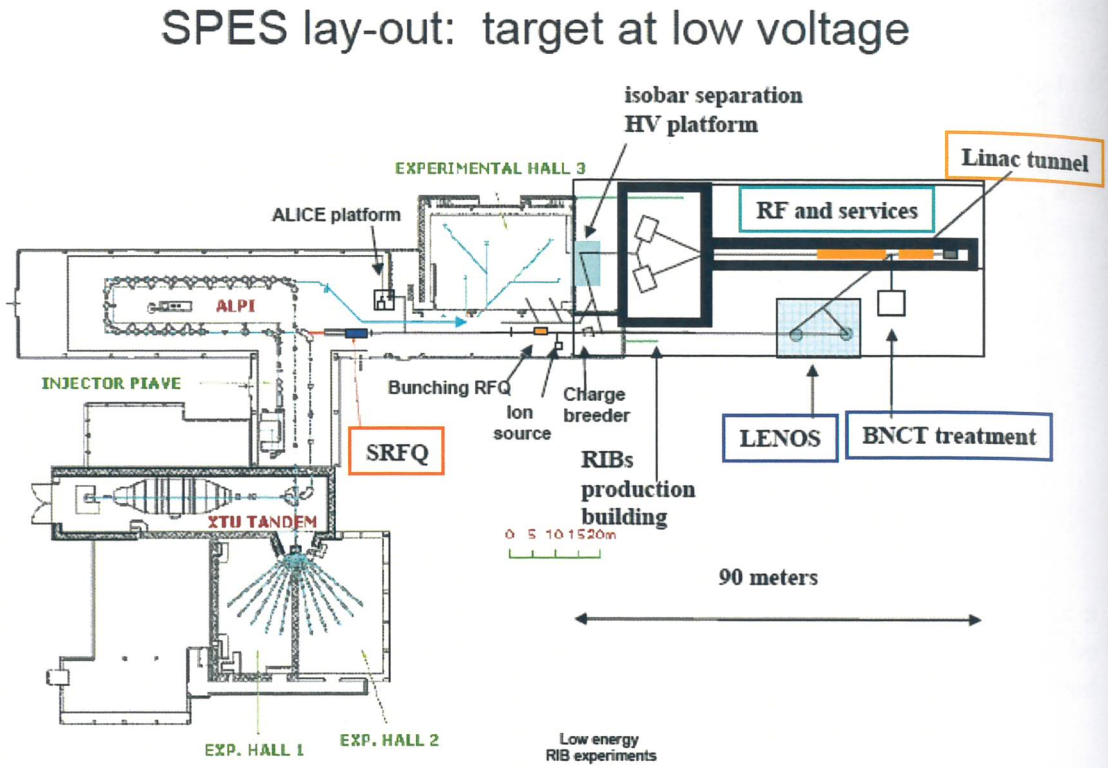

Fig. 12.27: *SPES lay-out*

The main characteristics of LENOS facility should be the low background due to the reaction used to generate neutrons and the high neutron flux in a small energy range, which can be especially tailored for the astrophysics measurements (1-300 keV) as well as for the low energy neutron induced reactions for applied nuclear physic (1keV-1MeV). The high flux is obtained using a short flight path, so the energy resolution is expected to be poor, but we consider a value lower than 20% acceptable for our kind of measurements. Preliminary results gives a value of about 10% energy resolution for neutron of 300 keV energy and a significant lower value for slower neutrons.

12.2.3 Primary proton driver

In order to use the synergy with the SPES project, the proton beam used will come out from the TRASCO RFQ (see chapter IV).

The RFQ will work in pulsed mode with an equivalent CW current of 50mA. Such value can be achieved because in pulsed mode operation the real average current will be of 0.5 mA considering a repletion rate of 250 kHz and a duty cycle of 1%. The duty cycle of 1% provide to maintain the power dissipated on target at 2.5 kW which is easy sustainable from the beryllium target.

12.3 The Time Of Flight line

12.3.1 The bunching system

Because of the high current, a bunching system of Mobey type [47] is probably the best choice, in order to have a compact system able to work with a so high spatial charge and low

beam momentum. The dipole magnet should have a size of about 1,5x1.5 m length and should be able to compress 8 pulses of the RFQ microstructure for a total macropulse of about 40 nsec into a single pulse of 6 nsec at the Be target position. The value of 6 nsec has been chosen in order to have a maximum energy resolution of 20% at 70 cm from the target. We have calculated that higher time resolution do not increase significantly the final energy resolution.

12.3.2 The moderator

The neutron spectra generated by the Be(p,n) reaction 5 MeV is peaked around 2.7 MeV, and our goal is to maximize the neutron flux between 1 to 500 keV using a suitable moderator. The best material for our purpose is water, which can work both as a moderator and as a coolant to dissipate the power impinging the target. Heavy water have a capture cross section lower than light water, reduce the thermal tail of the neutron energy distribution but need an higher thickness and give a lower concentration of neutrons in the energy range of interest (1-500keV). Thus, we decided to use light water and a thin layer of neutron absorber at the end. The most desirable energy cut-off should be at 1keV, in order to increase up to 250kHz the repetition rate and so to maximize the average proton current (which could be of 0.5mA).

In order to define the thickness of the moderator, we calculated the quantity N/N_0 as a function of the moderator thickness δx, where N is the number of neutrons which falls in the range of 1-500keV and N_0 is the number of neutron generated from the Be(p,n) reaction (443 n/pC as taken by EXFOR [48]). The calculation have been performed using MCNPx code, with neutrons emitted at zero degree on the surface of 0.5 cm thick beryllium target with the energy distribution from [45]. The target geometry used for the calculation was a tablet of beryllium surrounded by a sphere of water and an shell of Cd, Gd and Ir for a total of 6 mm thickness to have a low energy cut-off. The value of N/N_0 is calculated as a current outside the absorber shell and the results for different thicknesses of the water sphere is reported in figure 12.28. The thickness which maximizes the number of neutrons which falls in the 1-500keV energy range is from 5 to 7 cm.

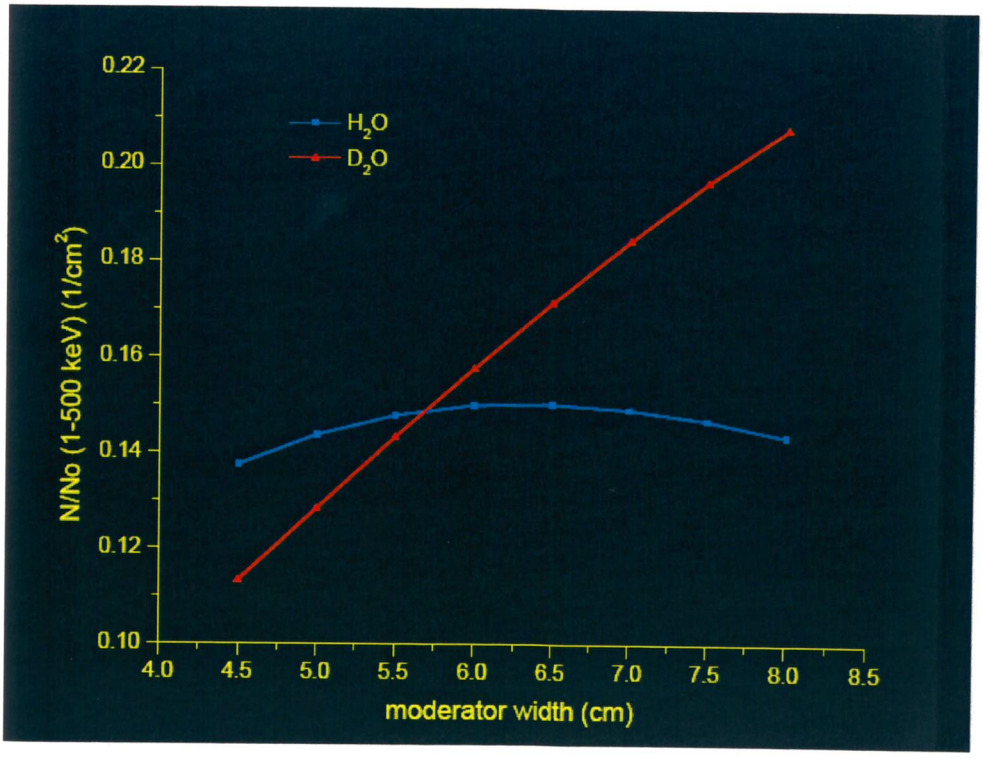

Fig. 12.28: *N/N_0 is calculated as a current outside the absorber shell and the results for different thicknesses of the water sphere.*

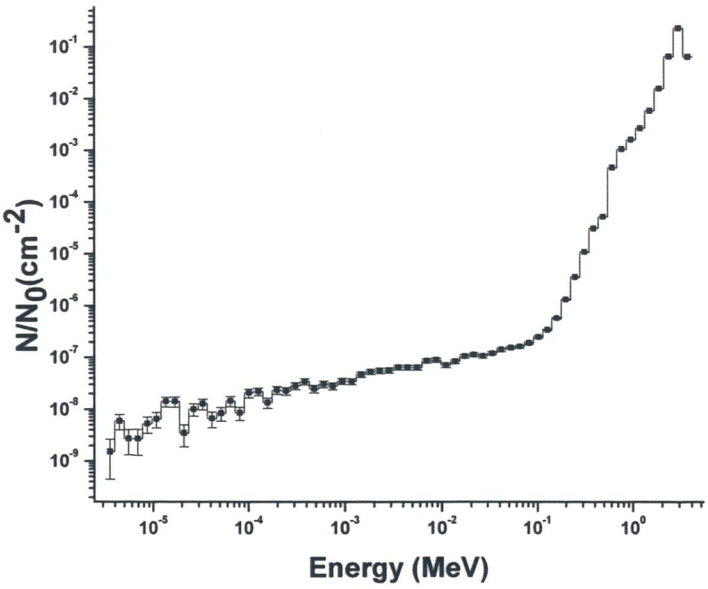

Fig. 12.29: *Neutron flux(in unit of N/N_0) obtained in the adopted configuration calculated with MCNPx code on a tally surface of 1 cm^2*

In figure 12.29 is reported the neutron flux (in unit of N/N_0) obtained in the adopted configuration calculated with MCNPx code on a tally surface of 1 cm^2. The figure 12.30 report the energy resolution for neutrons with energy of about 300 keV calculated with the ptrac card on MCNPx.

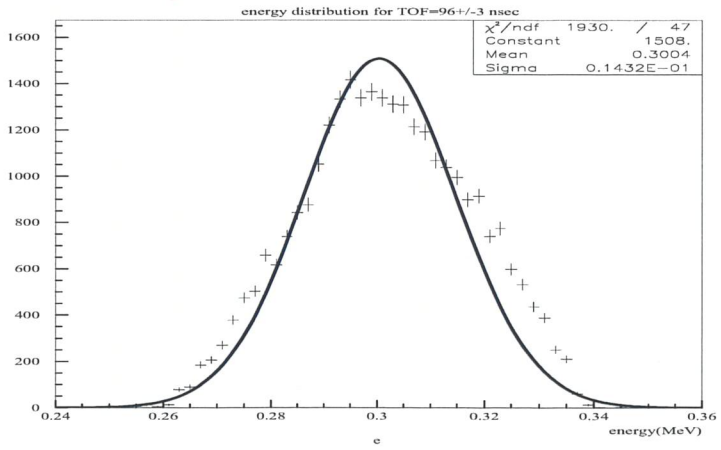

Fig. 12.30: *.energy distribution of neutrons arriving on tally surface atTOF=96+/-3 nsec. The tally surface is 1 cm2 area and is placed at 70 cm fromthe beryllium target. The energy resolution is about 10%*

In order to calculate the absolute neutron flux, N_0 must be transformed to the total number of neutrons generated in the beryllium target per second. Because the Yield of the 5MeV Be(p,n) reaction is 442 n/pC, to obtain the total number of neutron per second the yield must be multiplied by the average proton current, which essentially depends from the time of flight of the slowest neutron.

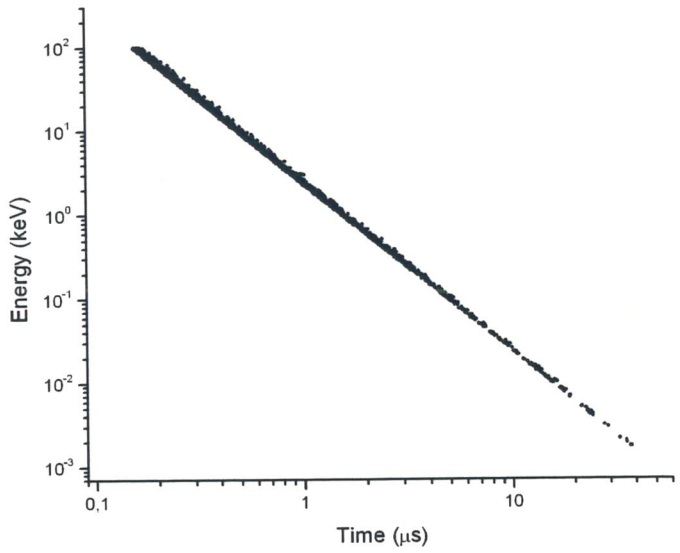

Fig. 12.31: *scatter plot of the energy as a function of the flight time.*

In figure 12.31 is reported the scatter plot of the energy as a function of the flight time. The cut of energy is at 2 eV and correspond to a time of flight of 40 μsec. So the repetition rate will be of 25 kHz, while with a value of T= 40 μsec the average current will be of 50 μA. Table 12.6 gives a comparison of LENOS neutron flux in the region 1-300keV with the flux of other important neutron facilities in the world.

Table 12.6. Comparison between the main neutron facilities. Data for LENOS are calculated with a repetition rate of 25 kHz , an average current of 0.05 mA , a flight parth of 70 cm, with 5 cm of light water which works as moderator and as a coolant, and considering the energy range between 1-300 keV . Data from [11]

Facility	**GELINA (@ 10 m)**	**N-TOF (@ 186 m)**	**SNS (@ 20m)**	**ORELA (@ 10m)**	**LANSCE (@ 20 m)**	**LENOS (@0.7 m)**
Total flux (1-300 KeV n/sec/cm2)	**$3\ 10^5$**	**$3\ 10^4$**	**$2.1\ 10^8$**	**$2.0\ 10^6$**	**$4.6\ 10^6$**	**$4.2\ 10^5$**
Time resolution	**1 nsec**	**6nsec**	**350 nsec**	**24 nsec**	**125 nsec**	**6 nsec**
Power dissipated (Kw)	**15**	**45**	**2000**	**8-50**	**64**	**25**

12.3.3 The Lead Slowind Down Spectrometer (LSDL)

In order to cover the energy range down to 1 eV, a construction of a LSDS is also under investigation. It is demonstrated [49] that using a LSDL a time of flight measurements can be achieved in the energy range from 1 eV to 10 keV with an energy resolution of about 30% with a neutron flux which can be 10^4 times higher than in an equivalent traditional time of flight facility. Using an LSDL, sample with very low mass can be measured, so this kind of instrument will be very useful to measure exotic sample obtained with SPES beam.

12.3.4 The activation/irradiation facility

In nuclear astrophysics measurements, where the most important quantity is the MACS, instead of measuring the cross section in the 1-500 keV energy range and calculate analytically the integral of eq 1, the MACS value can be obtained directly from an irradiation/activation measurements, providing to have a moderator able to shape the energy distribution of the outgoing neutron as much as possible similar to a Maxwellian spectrum with a mean value of kT≈30 KeV. A very good approximation of the stellar spectrum has been obtained by Kaeppler [50] and Popov [51], using the reaction 7Li(p,n) at proton energy close to the threshold. The sample to be irradiated is placed close to the target, in order to have a very intense neutron flux. The MACS can be calculated by thought the activated ions by measuring the emission lines with a high resolution gamma detector. This kind of measurements are very accurate, since they don't take care of isomeric states and thanks to the high flux and the peculiarity of the method, very low mass natural samples can be used. The next step forward in the neutron facility will be the calculations of a moderator able to shape the 5MeV Be(p,n) neutron spectra to a Maxwellian one. In this line, the proton beam will works at 30 mA in CW mode so the power dissipated in the target will be of 150 kW,. In order to sustain so high power, the beryllium target will be the one already developed and tested for BNCT. Our goal is to obtain a neutron flux higher than 10^{10} neutrons/s, in order to measure samples with 10^{16} atoms/cm^2, easy obtainable with 2 weeks of implantation with SPES beam at 10^{10} particle/s.

[1] Y.Mishima et al. Lancet, 388-399; 12.8.1989

[2] J.A.Coderre et al. J.Neurooncol. 33:141-152;1997

[3] H. Madoc-Jones A phase I dose escalation trial of boron neutron capture therapy for subjects with metastatic subcutaneous melanoma of the extremities. E-mail: gsolares@mit.edu.

[4] S.J.Gonzales et al. First BNCT treatment of a skin melanoma in Argentina: dosimetric analysis and clinical outcome. Appl. Rad. and Isot. 61, 1101-1105, 2004.

[5] Y.Mishima et al Allen, B.J. et al. eds. Progress in neutron capture therapy for cancer. New York, NY: Plenum Press; 1992:577-583

[6] H.Fukudaet al. Gan.To.Kagaku.Ryoho. 21:374-378;1994

[7] J.Gueulette et al., *Quality Assurance (QA) Program in BNCT: RBE of 7 NCT beams for intenstinal crypt regeneration in mice*, Prooceedings of the 12th International Congress on Neutron Capture Therapy, Takanatsu, Japan, October 9-13, 2006.

[8] Discussion seminar about radiation quality assessment in hadrontherapy. Workshop held in Legnaro on 30-31 October 2006. INFN report: INFN-LNL-215 (2007)

[9] Wingo PA, Tong T, Bolder S : Cancer Statistics, 1995. CA Cancer J Clin 44:8-30, 1995

[10] CR Rossi et al. Proceedings of the Workshop BNCT: Present and Future in Italy, held in Padua 24-25 February 1998. TERA 98/2 GEN 22 and INFN/TC-98/12

[11] S.Agosteo, G.Curzio, F.d'Errico, R.Nath, R.Tinti. Characterisation of an accelerator-based neutron source for BNCT versus beam energy. NIMA 476, 106-112 (2002).

[12] A. Makhankov et al. An accelerator based thermal neutron source for BNCT application Proceedings of EPAC 2004, Lucerne, Switzerland p. 2745
[13] Current Status of Neutron Capture Therapy, IAEA-TECDOC-1223, International Atomic Energy Agency, IAEA, 2001
[14] J. Esposito et al., LNL Annual Report 2001, 236-237
[15] J. Esposito et al., LNL Annual Report 2003, 65-67
[16] W.B. Howard, S.M. Grimes, S.I. Al Quarinshi, D. K. Jacobs, C.E. Brient J.C. Yanch, Measurements of thick target ^{9}Be(p,n) neutron energy spectra. Nuclear Science Engineering 138, 145-160, 2001
[17] J.H. Gibbons et al. Total neutron yields from light elements ubder proton and alpha bombardment. Phy.Rev. 114, 571-580, 1959.
[18] J.K.Bair et al. Neutrons from the proton bombardment of Li^{6}, Li^{7}, Be^{9}, B^{11} and O^{18}. Nuclear Physics 53, 209-218, 1964.
[19] J. Esposito et al., LNL Annual Report 2005, 152-153
[20] C. Ceballos, J. Esposito, The SPES-BNCT project : Current Status of the accelerator-driven thermal neutron facility Monte Carlo modeling, INFN-LNL-219(2007)
[21] F.d'Errico. Radiation dosimetry and spectrometry with superheated emulsions. NIM B 184, 229-254, 2001.
[22] A.Wambersie et al. Biological weighting of absorbed dose in radiationtherapy. Rad.Prot.Dos. 99, 445-452, 2002
[23] H.G. Menzel et al., Ionisation distributions and A-150 plastik kerma for neutrons between 13.9 and 19.0 MeV measured with a low pressure proportional counter. Phys.Med.Biol. 29, 1537-1554, 1994
[24] H. Schuhmacher et al., Dosimetry of low-energy neutrons using low-pressure proportional counters, Radiation Research 111, 1-13, 1987
[25] P. Colautti, et al., Microdosimetric Measurements in the Fast Neutron Therapeutic Beam of Nice, Physica Medica 14, 55-62, 1998
[26] J. Burmeister et al., Characterisation of miniature tissue-equivalent proportional counters for neutron radiotherapy applications. Phys. Med. Biol. 47, 1633-1645, 2002
[27] J. Burmeister et al., Miniature tissue-equivalent proportional counters for BNCT and BNCEFNT. 001 Medical Physics 28, 1911-1925
[28] L. De Nardo, E. Seravalli, G. Rosi, J. Esposito, P. Colautti, V. Conte, G. Tornielli, BNCT microdosimetry at the Tapiro reactor thermal column, Radiat Prot Dos., 110, 579-586, 2004
[29] L. De Nardo, V. Cesari, G. Donà, G. Magrin, P. Colautti, V. Conte, G. Tornelli, Mini-TEPCs for radiation therapy, Radiat Prot Dos., 108, 345-352, 2004
[30] D.Moro e al. Two miniaturised TEPcs in a single detector for BNCT microdosimetry. Rad.Prot.Dosim. 122, 396-400, 2007.
[31] D.Moro. Development of tissue-equivalent proportional counters for BNCT microdosimetry. PhD thesis, physics department of Ferrara University, XIX cycle, March 2007.
[32] Loncol T. et al. Radiobiological effectiveness of radiation beams with broad LET spectra: microdosimetric analysis using biological weighting functions. Radiat.Prot.Dosim. 52, 347-352, 1994.
[33] D.Moro, E.Seravalli, P.Colautti. *Statistical and Overall Uncertainties in BNCT Microdosimetric Measurements.* LNL-INFN(REP)-199/2003
[34] E. Friso et al, A novel 10B-enriched carboranyl-containing phthalocyanine as a radio- and photo-sensitizing agent for boron neutron capture therapy and photodynamic therapy of tumors: in vitro and in vivo studies, Photochemical & Photobiological Sciences, 5(1), 39-50, 2006
[35] J.Esposito, G.Rosi, S.Agosteo. *The New Hybrid Thermal Neutron Facility at Tapiro Reactor for BNCT Radiobiological Experiments.* Radiation Protection Dosimetry (in press) 2007.
[36] Claus E. Rolfs and William S. Rodney: "Cauldrons in the Cosmos". Nuclear Astrophysics, The University of Chicago Press, Chicago and London, 1998.
[37] H. Beer, F. Voss and R. R. Winters: "On the calculation of Maxwellian-averaged capture cross sections". The Astrophysical Journal Supplement Series, 80: 403-424, 1992 May.
[38] Z.Y. Bao, H. Beer, F. Kappeler, F. Voss, K. Wisshak and T. Rauscher: "Neutron cross sections for nucleosynthesis studies". Atomic Data and Nuclear Data Table 76 (2000) 70. Web site:http://nuclear-astrophysics.fzk.de/kadonis/
[39] M. S. Smith et al: "Nuclear data on unstable nuclei for astrophysics". Nuclear Physics A 746 (2004) 569c-572c. Web site: http://www.nucastrodata.org/
[40] P. Corvisiero, D. Frekers, S. Goriely, P. Haensel, W. Hillebrand, J. Kiener, K. Langanke, M. Lattuada and O. Sorlin. NuPECC Liaison: D. Guillemaud-M¨ller , M. Huyse November 30, 2002.
[41] NEA High Priority Nuclear Data Request List, private comunications
[42] IAEA, Reference Neutron Activation Library.

[43] M. Al-Abyad, I. Spahn, S. Suda´ r, M. Morsy, M.N. H. Comsan, J. Csikai, S.M. Qaim, H.H. Coenen, "Nuclear data for production of the therapeutic radionuclides ^{32}P, ^{64}Cu, ^{67}Cu, ^{89}Sr, ^{90}Y and ^{153}Sm via the (n,p) reaction: Evaluation of excitation function and its validation via integral cross-section measurement using a 14MeV d(Be) neutron source "Applied Radiation and Isotopes 64 (2006) 717–724

[44] W.B. Howard, S.M. Grimes, S.I. Al Quarinshi, D. K. Jacobs, C.E. Brient J.C. Yanch, "Measurement of the thick target 9-Be(p,n) Neutron Energy Spectra " Nuclear Science Engineering, 138, 145-160 (2001)

[45] W.B. Howard, et al., " Measurement of the 9Be(p,n) thick target spectra for use in accelerator based neutron capture therapy" , Advances in Neutron Capture Therapy, Vol. 1, (1997) pp 511-515

[46] P.E. Koehler "Comparison of white neutron sources for nuclear astrophysics experiments using very small samples " Nuclear Instruments and Methods in Physics Research A 460 (2001) 352}361

[47] R.C. Mobley, "Proposed Method for Producing Short Intense Monoenergetic Ion Pulses", Phys. Rev.88(2), 360-361, 1951

[48] NSE **138,** 145-160 (2001)

[49] D. Rochman et al. "Characteristics of a lead slowing-down spectrometer coupled to the LANSCE accelerator", Nuclear Instruments and Methods in Physics Research A 550 (2005) 397–41 and references therein

[50] W. Ratynski and F. Käppeler, "Neutron capture cross section of ^{197}Au: A standard for stellar nucleosynthesis "Phys. Rev. C **37**, 595 (1988)

[51] Yu P POPOV "Peculiarities of the modern neutron spectrometry",PRAMANA journal of physic- Indian Academy of Sciences- Vol. 57, Nos 2 & 3 (2001) 601–610

CHAPTER XIII

INFRASTRUCTURES

13.1 Introduction

The SPES project will require a completely new development of buildings and related services. The design will take care of all the needs requested by the safety and radioprotection rules. Specific study will be carried out by a company with expertise in the domain of nuclear safety and the results of this study can modify the present layout of the infrastructures.

LNL has already implemented some preliminary activities to allow the construction.

A new electrical power station is under completion. This will allow a power of 30 MW for the new project and 10 MW for the other activities of LNL The power station has been designed and built in order to give a final power capability of 100 MW. Furthermore the station is linked to the 132 KV RTN in order to reduce the problem of micro interruption (few micro seconds)

A small gulch located in the foreseen site of the building has already been deviated so the continuity with the III experimental hall is already guaranteed.

The main roads around the area are under completion and the access to the new area is already available. Included in this activity the construction of first part of a new technological platform has already been started as well as a tunnel to distribute to new sites all the technical facilities (compressed air, cooling water, cryogenics fluids .....)

13.2 The buildings

The SPES building will be a new construction located west of the third experimental hall, and will house the linac, the production target area and the BNCT facility (Fig. 6.4). The characteristics of this building are mainly dictated by the shielding requirements. The area is located on the other side of an existing catch water drain that has been deviated.

A preliminary study of SPES building was done considering a metallic shed, about 30 m wide and 100 m long. The central strip houses the linac, the strip south houses the linac services (RF systems), the strip north the BNCT and LENOS facility. The east part is dedicated to the production target complex, the hot cells and the system to move the used targets.

A sled with light external structures would be used, but with a floor sitting on a thick concrete bed in the regions where ionizing radiation is produced; the floor must be able to sustain the thick shielding walls, with the possibility to add concrete blocks for example in case of beam

In the north part of the new SPES building the area for a new experimental hall will be left ready for construction for low energy experiments with RIBs and for additional instrumentation upgrade. The characteristics of this building will be very similar to the ones of the existing experimental hall, with the experiment floor 4.35 m below the ground level.

Moreover the building has to guarantee the dimensional stability necessary to maintain the alignment of the linac and beam lines.

In a preliminary study it has been checked the feasibility of this solution, using on purpose an over designed shielding thickness: in the central part of the building a linac tunnel 8 m wide and 4.6 m height is considered, a 4 m thick concrete bed below the linac tunnel, 2 m lateral shielding and 1.5 m concrete roof. A core boring of the ground showed various layers of clay,

silt and sand, with the water layer at –2.5 m from ground level. A specific proposal for the construction of the building under these geological conditions has been done [1].

13.3 Nuclear Waste confinement and management

Special care will be devoted to the construction of the building of the production target. A solution with double containment will be adopted to increase the safety of the system. A bunker will host the target and source platform. The necessary shielding to maintain the dose outside the bunker on the order of 1.5 μSv/h will be used. This requires a concrete thickness of 2-3 m. Two independent production target stations will be constructed with the aim to operate them in alternate way to optimize the capability to supply beam on experimental target.

Due to the problem related to the air activation the bunker will be designed as small as possible and a dedicated nuclear ventilation system will be installed.

The two bunkers will be inside the main target building for which a second nuclear ventilation system will ensure an additional safety wall to the radioactive material release in air.

The storage of used targets will be performed in a special area at low neutron activity. A bunker adjacent to the target building will host the sarcophagus of used targets. This building will be designed to be at high radioprotection level using special concrete for nuclear confinement.

A limited number of targets are expected to be used (2 or 3 per year). The substitution of the target is envisaged in case of internal damage or for different characteristics, mainly related to kind of beam for which the target is optimized, i.e. for the ion source.

The decommissioning of unused targets will be done according to he current safety rules with the transfer to a storage site. The procedure for decommissioning will be part of the radioprotection and safety document as well as the official Memorandum of Understanding with third parts qualified to radioactive material storage.

---

[1] Studio di Fattibilità relativo alle opere stutturali di schermature per il progetto denominato SPES (Relazione illustrativa generale by Ing. E. Centis)

CHAPTER XIV

PROJECT SCHEDULE PERSONNEL AND COSTS

14.1 Schedule

The time schedule for the implementation of the facility is shown in table 14.1. Before starting the construction the R&D program will continue for key development subsystems to receive adequate answers; such items, discussed in the previous chapters, will be completely mature in about one year.

At the same time the detailed design and the procedure needed for the construction authorization will be implemented.

Design and construction of the complete facility will require 4 years, with the installation and commissioning of parts of the machine beginning immediately after the completion of the buildings and related infrastructures. Critical parts as RIB target and high current RFQ are in advanced construction stage and will be ready for laboratory test before the building construction. The implementation of the ALPI re-accelerator is already scheduled starting from the current year.

Table 14.1

	2007	2008	2009	2010	2011	2012	2013
Target prototypes							
Authorization to construction							
Facility Design							
Building Construction							
Completion of driver (1st part-RFQ)							
Installation and commissioning of SPES-1							
Construction of driver (2nd part-DTL)							
Installation and comm. of the full driver							
Installation and comm of the target system							
Alpi preparation for post acceleration							
Installation of RIBs transfer lines and spectrom.							
Complete commissioning							

14.2 Costs

Table 14.2 summarizes the cost breakdown of the entire facility described in the previous chapters; it relates to a 40 MeV 200 μA proton driver linac, to a RIB production section based on UCx direct target and to the reacceleration in ALPI, upgraded in its high beta section. The specific items of the BNCT dedicated line and of an additional neutron production station for material science, are listed separately.

A few remarks on the table of costs are presented in the following.

As for the driver DTL, the proton source, the design, prototyping and mechanical construction of the RFQ structure are not included, since they are funded by the TRASCO-ADS Program.

Moreover, the rf equipment and the power supplies for the injector are loaned from CERN, on the basis of a Memorandum of Understanding.

The costs of the re-accelerator are for an upgrade of the cryogenic system of the present ALPI, for the reallocation of PIAVE and for the construction of the buncher RFQ and the Charge breeder.

Although the costs for the 10 kW proton beam target station are summarized in a limited number of items, they are the result of an extremely detailed analysis and of a close comparison with the cost of similar items at existing facilities (e.g. ORNL, TRIUMF, CERN, GANIL) and the result of the design and test work performed during 2006.

Table 14.3 oes not include a few additional dedicated laboratories and facilities, which are needed for operation of the machine, such as a chemistry laboratory for the synthesis of target materials, a laboratory dedicated to radiation safety, a mechanical workshop of low level radioactivity for assembly of target and ion source. Their total cost is rather marginal, and a precise estimate of it can only be made on the basis of accepted safety procedures.

As for the item "Building and Infrastructures", the updated cost of neutron proof plants, appropriately shielded buildings and accelerator safety and radiation control are considered.

Computer control, following our experience and widely shared practice, is added as a 5% addition to the cost of the facilities.

Laboratory personnel costs are not included in the table.

At the end of table 14.3 dditional costs are added for a dedicated BNCT beam station and the development of a target and a moderator for a neutron facility dedicated to cross section measurements and Material Science.

It is estimated that the running costs will amount to around 10 M€/year.

Table 14.2

Item	Cost (Meuro)
DRIVER Injector completion	**3.3**
DRIVER DTL	**7**
Target (2 target stations)	**5.1**
Beam transport	**4.4**
Reacceleration	**8.2**
Building	**9.3**
Technical plant	**2**
Safety and control	**6**
BNCT	**2.1**
Neutron facility	**1.2**
TOTAL	**48.6**

Table 14.3 Costs breakthrough

Item	Quantity	Unit cost	Partial cost	Total cost
TARGET	2		2,554	5,108
vacuum		0,343		
target cambers		0,330		
special materials		0,112		
source (laser)		0,686		
front end		0,132		
remot handling		0,158		
power supply		0,264		
60KV platform		0,224		
mass selector 1/250		0,132		
sensors and controls		0,132		
services		0,040		
Proton DRIVER				
completion injector				3,300
RFQ support and wave guides			0,500	
klystron 1.3 MW power supply			1,700	
solenoids and power lines			0,300	
MEBT power supply and magnets			0,400	
temperature control system			0,400	
DTL				7,000
rf by ACCEL evaluation			4,500	
klystron	2	0,400	0,800	
pulsed power supply	2	0,500	1,000	
RF components	2	0,200	0,400	
temperature control system			0,200	
vacuum system			0,100	
Reaccelerator				8,200
Upgrade Basso Beta			1	
Criogenia			1,45	
Buncher RFQ			0,5	
PIAVE reallocation			0,3	
Bunchers			0,6	
ECR reallocatrion and new 60 kV platform			0,3	
Diagnostics and controls			0,8	
Charge breeder			1	
Vacuum system			1,35	
Cavity for Pulsed beam			0,5	
RF upgrade			0,4	
Beam transport				4,360
beam identification system			0,360	
detectors		0,040		
electronics		0,020		
transport system		0,300		

isotope separator	2,000	
beam line	2,000	
Building		11,300
reaccelerator	0,300	
target	1,000	
proton driver	8,000	
Techn. Plant	2,000	
Safety & Control		6,000
BNCT		2,100
Trasport lines	1	
BNCT Neutron converter	0,5	
Remote handling	0,3	
Spectrum translator	0,3	
LENOS		1,200
LENOS target	0,1	
irradiation experimental point	0,2	
high resolution neutron TOF	0,4	
dosimetry	0,5	
		48,568

14.3 Personnel

For the development of the project several working groups will be created with defined milestones and operative programs.

The main structure and the working groups are reported in Table14.1.

A strong collaboration with Italian Universities and external companies as well as a synergy with the Laboratori Nazionali del Sud will be of great help in the optimization of the human resources. The personnel organization at LNL will be revised according with the request of the SPES project, nevertheless additional technical competences are required for the project development.

In Table 14.4 s reported the LNL personnel dedicated to the project and the additional recourses

Table 14.4 SPES project organization

International referee panel

Steering committee

radioprotection coordinator

project manager

scientific coordinator

infrastructure	**safety and control**	**accelerator**	**target and beam transfer**	**secretary and administration**
building	control system architecture	proton source	ISOL target & source	project secretary
civil engineering	radiation Protection	proton LEBIT	development Lab	budget monitor
nuclear engineering	shielding	proton RFQ	target production	orders preparation
electric power	radiation safety	proton driver	in-beam and off-line test-bench	
nuclear ventilation	conventional safety	proton diagnostic	1+ beam transport	
fluids	accelerator control	High intensity p transport	n+ charge breeder	
	target control	RIB RFQ reacceleration	high resolution mass spectr.	
	vacuum target and RIB	RIB ALPI reacceleration		
	waste management	RIB diagnostic		

Personnel: Ing= engineers, Phys=physicists, Tec=technicians								
Staff Eng	Staff Tec	Staff Eng -Phys	Staff Tec	Staff Eng-Phys	Staff Tec	Staff Eng - Phys	Staff Tec	Staff secretary
3	4	11	3	14	15	16	2	2
Additional personnel								
		2	2	6	9	3	1	

SPES WORKING GROUP

Editor: G.Prete

Co-authors: A.Andrighetto, C.Antonucci, G.Bassato, L.Biasetto, G.Bisoffi, L.Celona, S.Cevolani, M.Cinausero, M. Comunian, P. Colautti, J.Esposito, E. Fagotti, P.Favaron, P.Finocchiaro, F.Gramegna, P.Mastinu, C.Petrovich, A.Pisent, M.Poggi, A. M. Porcellato, C.Signorini, V.Variale, D.Zafiropoulos.

SPES working group Collaboration

INFN Laboratori Nazionali di Legnaro, Italy:
A.Andrighetto, M.Barbui, G.Bassato, A. Battistella, G.Bisoffi, E.Brezzi, M. Calviani, S. Canella, D. Carlucci, S.Carturan, M. Cavenago, F. Cervellera, M.Cinausero, M.Comunian, P.Colautti, L.Corradi, L.Costa, A.Dainelli, G.de Angelis, A.D'Este, J.Esposito, P.Favaron, E.Fagotti, E.Fioretto, M.Giacchini, F.Gramegna, F. Grespan, P.Ingenito, M.Lollo, G.Maggioni, G. Martin Hernandez, P.Mastinu, P. Modanese, M.F. Moisio, A.Palmieri, R.Pegoraro A.Pisent, M.Poggi, A.Porcellato, P.A. Posocco, J. Praena, G.Prete, G.Puglierin, V.Rizzi, C. Roncolato, Y. Shengquan, S. Stark, A.M.Stefanini, M.Tonezzer, D.Zafiropoulos

INFN Laboratori Nazionali del Sud, Catania, Italy:
L.Celona, F.Chines, L.Cosentino, G.Cuttone, P.Finocchiaro, M.Lattuada, G.E.Messina, M.Re, D.Rizzo

INFN-Dipartimento di Fisica, University of Padova, Italy:
S.Beghini, L. De Nardo, P.Mason, M.Mazzocco G.Montagnoli, F.Scarlassara, G.F. Segato, C.Signorini,

Dipartimento di Ingegneria Meccanica, University of Padova, Italy:
L.Biasetto, P.Colombo, M.Manzolaro, G.Meneghetti,

Dipartimento di Ingegneria delle Costruzioni e Trasporti, University of Padova, Italy:
V. Salomoni, C.Majorana

INFN-Dipartimento di Fisica, University of Torino, Italy:
G.Pollarolo

ENEA, Bologna, Italy:
C.Antonucci, S.Cevolani, C.Petrovich, R.Tinti

Dipartimento di Scienze chimiche, University of Padova, Italy:
P.Di Bernardo, P.Zanonato, L.Piga

INFN-Bari, Italy:
V.Variale

INFN-Pavia and University of Pavia, Italy:
P.Benetti

Politecnico di Milano:
S.Agosteo, F.Campi, M.Ricotti

Dipartimento di Ingegneria Meccanica, University of Trento:
I.Cristofolini, M.DeCecco, R.Oboe

CERN:
J.Lettry, S.Manzari, T.Stora, M. Vretenar

Oak Ridge National Laboratory:
D.Stracener, J.Beene

INFN - Laboratori Nazionali di Legnaro
Annual Report Editors
Viale dell'Università, 2
35020 Legnaro (PD)
Italia

Tel: (+39)0498068311
Fax:- (+39)049641925

Requests for additional copies of the report should be addressed to:

Dr. Anna D'Este
INFN - Laboratori Nazionali di Legnaro
Viale dell'Università 2
35020 Legnaro (PD)
Italy

anna.deste@lnl.infn.it
Fax:: (+39)049 641925

"SPES-Technical Design for an Advanced Exotic Ion Beam Facility at LNL" is also available on CD and at the web site: http://www.lnl.infn.it/~spes/